Vol. 48, No.1 / 2016

e: ISSN 2068 – 2239
p: ISSN 2068 – 4215

INMATEH – AGRICULTURAL ENGINEERING

JANUARY - APRIL

No liability is assumed by the editorial staff for the content of scientific papers and opinions published in this volume. They represent the author's point of views.

Editorial

The National Institute of Research-Development for Machines and Installations designed to Agriculture and Food Industry - INMA Bucharest has the oldest and most prestigious research activity in the field of agricultural machinery and mechanizing technologies in Romania.

Short History

- In 1927, the first research **Center for Agricultural Machinery** in Agricultural Research Institute of Romania - ICAR (Establishing Law was published in O.D. no. 97/05.05.1927) was established;
- In 1930, was founded **The Testing Department of Agricultural Machinery and Tools** by transforming Agricultural Research Centre of ICAR - that founded the science of methodologies and experimental techniques in the field (Decision no. 2000/1930 of ICAR Manager - GHEORGHE IONESCU ŞIŞEŞTI);
- In 1952, was established the Research Institute for Mechanization and Electrification of Agriculture - ICMA Bănească, by transforming the Department of Agricultural Machines and Tools Testing;
- In 1979, the Research Institute of Scientific and Technological Engineering for Agricultural Machinery and Tools – ICSITMUA was founded - subordinated to Ministry of Machine Building Industry - MICM, by unifying ICMA subordinated to MAA with ICPMA subordinated to MICM;
- In 1996 the National Institute of Research-Development for Machines and Installations designed to Agriculture and Food Industry – INMA was founded – according to G.D. no.1308/25.11.1996, by reorganizing ICSITMUA, G.D no. 1308/1996 coordinated by the Ministry of Education and Research G.D. no. 823/2004;
- In 2008 INMA has been accredited to carry out research and developing activities financed from public funds under G.D. no. 551/2007, Decision of the National Authority for Scientific Research - ANCSno. 9634/2008.

As a result of widening the spectrum of communication, dissemination and implementation of scientific research results, in 2000 was founded the institute magazine, issued under the name of SCIENTIFIC PAPERS **(INMATEH),** ISSN 1583 – 1019.

Starting with volume 30, no. 1/2010, the magazine changed its name to **INMATEH - Agricultural Engineering,** appearing both in print format (ISSN 2068 - 4215), and online (ISSN online: 2068 - 2239). The magazine is bilingual,
being published in Romanian and English, with a rhythm of three issues / year: January-April, May-August, September-December and is recognized by CNCSIS – with B^+ category. Published articles are from the field of AGRICULTURAL ENGINEERING: technologies and technical equipment for agriculture and food industry, ecological agriculture, renewable energy, machinery testing, environment, transport in agriculture etc. and are evaluated by specialists inside the country and abroad, in mentioned domains.

Technical level and performance processes, technology and machinery for agriculture and food industry increasing, according to national requirements and European and international regulations , as well as exploitation of renewable resources in terms of efficiency, life, health and environment protection represent referential elements for the magazine „**INMATEH - Agricultural Engineering**".

We are thankful to all readers, publishers and assessors.

Editor in chief,
Ph.D. Eng. Pirnă Ion

Managing Editorial Board - INMA Bucharest

Editor in Chief

Pirnă Ion, General Manager, Prof.Hon.Ph.D.Eng, SR I, Corresponding member of ASAS

Executive Editor	Assistant Editor	Logistic support, database
Vlăduț Valentin, Ph.D.Eng, SR I	**Drâmbei Petronela,** Ph.D.Eng, SR I	**Muraru Virgil,** Ph.D.Eng, SR I
Popa Lucreția, PhD.Eng, SR II	**Cioica Nicolae,** Ph.D.Eng, IDT II	**ȚicuTania,** techn.

Scientific Secretary
Cârdei Petre, math.

Official translators
Barbu Mihaela, Prof.English, French

E-mail: **inmatehjournal@gmail.com**

Editorial Board

- Acad. HERA Cristian - Romania, Honorary President of ASAS - Academy of Agricultural and Forestry Sciences"Gheorghe Ionescu Şişeşti", member of Romanian Academy;
- Acad. Prof. Ph.D. SIN Gheorghe - Romania, President of ASAS - Academy of Agricultural and Forestry Sciences "Gheorghe Ionescu Şişeşti";
- Prof. Ph.D. NICOLESCU I. Mihai - Romania, Vicepresidentof ASAS - Academy of Agricultural and Forestry Sciences "Gheorghe Ionescu Şişeşti";
- Hon.Prof.Ph.D.Eng. GÂNGU Vergil - Romania,President ofthe Department of Agricultural Mechanization of ASAS - Academy of Agricultural and Forestry Sciences "Gheorghe Ionescu Şişeşti";
- Ph.D. Eng. NICOLESCU C. Mihai - Romania, ScientificGeneral Secretary of the ASAS-Academy of Agricultural and Forestry Sciences "Gheorghe Ionescu Şişeşti";
- Assoc.Prof. Ph.D. Eng. BELC Nastasia - Romania, IBA Bucharest;
- Ph.D. Eng. BUȚU Alina - Romania, INSB Bucharest;
- Prof. Ph.D. Eng. PARASCHIV Gigel - Romania, P.U. Bucharest;
- Prof. Ph.D.Eng. BIRIŞ Sorin - Romania, P.U. Bucharest;
- Prof. Ph.D. Eng. NICULIȚĂ Petru - Romania, USAMV Bucharest;
- Prof. Ph.D. Eng. VLASE Sorin - Romania, "Transilvania" University Braşov;
- Prof. Ph.D. Eng. ROŞ Victor - Romania,Technical University Cluj Napoca;
- Prof. Ph.D. Eng. FILIP Nicolae - Romania, Technical University Cluj Napoca;
- Prof. PhD. Eng. VOICU Gheorghe - Romania, P.U. Bucharest;
- Prof. PhD. Eng. GERGEN Iosif - Romania,USAMVB Timişoara;
- Prof. Ph.D. Eng. ȚENU Ioan - Romania, USAMV Iaşi;
- Assoc.Prof.Ph.D.Eng. BUNGESCU Sorin - Romania, USAMVB Timişoara;
- Prof. Ph.D.Eng. FENYVESILászló - Hungary, Hungarian Institute of Agricultural Engineering Godolo;
- Prof.Ph.D.Eng. KOSUTIC Silvio - Croatia, University of Zagreb;
- Ph.D. BIOCCA Marcello - Italy Agricultural Research Council, Agricultural Engineering Research Unit;
- Prof.Ph.D.Eng. MIHAILOV Nikolay - Bulgaria, University of Rousse;
- Assoc.Prof. Ph.D.Eng. ATANASOV At. - Bulgaria, University of Rousse;
- Assoc.Prof. Ph.D. ERTEKIN Can - Turkey, Akdeniz University Antalia;
- Prof. Ph.D.Sc. Eng. VARTUKAPTEINIS Kaspars - Latvia, Latvia University of Agriculture, Institute of Agricultural Machinery;
- ir. HUYGHEBAERT Bruno - Belgium, Walloon Agricultural Research Center CRA-W;
- Prof. Ph.D. Eng. FABBRO Dal Inacio Maria - Brazil, Campinas State University;
- Prof. PhD. Eng. DE WRACHIEN Daniele - Italy, State University of Milan;
- Prof. PhD.Guanxin YAO- P.R.China, Along Agriculture R&DTechnology and Management ConsultingCo., Ltd;
- Prof. PhD. Eng. GONZÁLEZ Omar - Republic of Cuba, Central University "Marta Abreu" de las Villas;
- Assist.Prof.Dr. KABAŞ Önder – Turkey, Akdeniz University.

In the present, *INMATEH - Agricultural Engineering* journalis indexed in the next international databases:
ULRICHSWeb: Global Serials Directory, CABI, SCIPIO, ELSEVIER /SciVerse SCOPUS, Index COPERNICUS International, EBSCO Publishing, Elektronische Zeitschriftenbibliothek

INMATEH - Agricultural Engineering
vol. 48, no.1/ 2016
NATIONAL INSTITUTE OF RESEARCH-DEVELOPMENT FOR MACHINES AND INSTALLATIONS DESIGNED TO AGRICULTURE AND FOOD INDUSTRY - INMA Bucharest
6 Ion Ionescu de la Brad Blvd., sector 1, Bucharest
Three issues per year,
e ISSN: 2068 – 2239
p ISSN: 2068 – 4215
Edited by: INMA Bucharest

Copyright: INMA Bucharest / Romania

CONTENT

SIMULATION OF SOUTHERN POTATO GRADER BASED ON ADAMS
/
基于 ADAMS 的南方马铃薯分级机构仿真研究

Lect. Ph.D.Stud. PingYuan Xiong *), Prof. Ph.D. Xuan Lin, Prof. Ph.D.Yi Wang, Stud. SuBing Shen
Department of Mechanic and Electronic Engineering, Zhongkai University of Agriculture and Engineering, Guangzhou/China
Tel: 008602089003183; E-mail: xpy020@163.com

Keywords: *ADAMS, southern potato, grader, simulation*

ABSTRACT

Based on the analysis of existing grading methods, this study focuses on developing a new grading scheme for southern potato, which can automatically adjust the distance between two rolling bars. Using ADAMS software the dynamic simulation model of potato grader has been established, and the simulation results showed that the little potato P1, middle-sized potato P2 and big potato P3 were separated successively. It could strongly prove that this design is feasible. There was little motion when the potatoes were under grading, which indicated that the device worked smoothly. The analysis results of contact forces showed that as the weight of the potato increases, the force between it and the rolling bars enhances, especially for the force between the potato and the movable bars, as in the experiment the maximum value of the contact force between P4 and moving roll was 813.7N. The conclusions can provide the basic data to the optimum design of sample machine.

摘要

分析已有物料分级方法，设计出一种可自动调节辊杆间距的南方马铃薯机械化分级方案；应用 ADAMS 软件构建马铃薯分级机构动态仿真模型，仿真试验结果表明：小薯 P1、中薯 P2、大薯 P3 先后被分离出来，机构设计方案可行，薯块在辊杆上跳动较小，机构运动较平稳；接触力分析结果表明：薯块与辊杆接触力随薯块质量增大而变大，其中与动辊杆接触力变化最显著，试验中超大薯 P4 与动辊杆的极值接触力达 813.7 N；该研究为样机制作提供了优化设计基础。

INTRODUCTION

China is one of the main potato producing countries in the world. In 2013 its cultivated area reached up to 8421 acres and the yield was more than 19.18 million tons, which ranked first in the world *(MOA Department of Plantation Management, 2014)*. In China, “The major production of potato is in the north, while the economic benefit is in the south ". It is because planting winter potato in the south can take full advantages of the idle paddies after rice harvest. Its planting time is short and can go into the market very soon, which can make up for the shortages of the season-restricted northern potato. With its high economic efficiency, the southern potato is popular with the market and the planting households. At present, potato planting in southern China has gradually transferred to the mechanized production not only in planting, but also in field management and harvesting. But the mechanization in potato grading progresses slowly, people still use manual grading method, which is labour-intensive and inefficient, and at the same time can’t respond quickly to market demands *(PingYuan Xiong et al, 2011)*. Grading equipment imported from abroad are expensive and difficult to maintain, while the domestically developed grading equipment is still in trial stage and of low efficiency, especially when it is faced with the juicy and thin-skinned southern winter potato, they can help to make high injury rate. Grading method is the key of potato grading equipment, so this study focuses on designing a simple and efficient grading mechanism based on the physical properties of southern potato. By using the ADAMS software to make kinematics analysis, this study will verify the correctness of the device design scheme and make clear the kinematic parameters, which can provide designing basis for the prototype production.

MATERIAL AND METHOD

Existing grading methods

There are several methods in fruits grading: mesh screen method, grid cylinder method, weight grading method, optical method and rolling-bars grading method *(Blasco et al, 2009; LiangLong Hu, et al, 2007; LiuFang ShenTu et al, 2014; Mendoza et al, 2014; Riquelme et al, 2008; XiaoPing Yang et al, 2014; YiBin Ying et al, 2014)*.Mesh screen method is a widely used grading method. Its grading accuracy can

reach to 95% within the error range of 12.7mm, but this method can make the fruits wear with the mesh seriously, which will easily harm the skin of fruits. Grid cylinder grading equipment consists of several rollers, each roller has unique gap between its grid bars, and the gap will extend as the roller ranges from the minimum level to the maximum level. When the fruit's size is smaller than the gap, it will fall into the corresponding hopper. This method has high efficiency, but the fruits collide and strike strongly in the equipment, which can make them easily be injured. Weight grading method is based on the principle of leverage. It firstly puts the fruits and the counterweight into two cups at both ends of the stent. When the counterweight is pushed slowly along the stent to the spindle, the trimming moment reduces, which will make the cups lose imbalance and tip over, and the fruits will fall into the appropriate hoppers. Because this method bases solely on weight index, its reliability is mediocre. It requires the fruits put into the cup singly, which will results in low grading efficiency. Optical grading method uses image processing technology to make non-contact measurements. The fruit is irradiated with light of certain wavelength, and the reflecting signals will tell its colour, maturity and size characteristics. When the fruit satisfies the grading conditions, the controlling device will pick it to the corresponding conveyor belt. This method is of innovative technology, high grading accuracy and efficiency, but it requires high level of professional knowledge and high cost. Besides, with its immature technology, optical grading method is difficult to be promoted. The principle of the rolling-bars grading method is equipping a rotating roller to the conveyor. When the size of the fruit is smaller than the gap between two adjacent rollers, it will fall into the corresponding hopper. Such an equipment runs smoothly, but requires that the gap between the rollers should be variable to achieve different size fractions. Southern winter potato with its high moisture, thin skin and crisp pulp, is prone to bruising and skin scratching. The design below takes the rolling-bars grading method. By optimizing the installation of adjacent roll bars, it achieves the goal of automatically adjusting the gap to meet the requirement of grading different sizes of potatoes.

Structure design of the grader

Southern winter potato can be seen approximately as an ellipsoid *(ChunHai Wang, et al, 2008)*. Its grading depends on the minor dimension of the ellipse (d), d ∈(37,100) mm. The potatoes are divided into four levels, grading parameters are listed in Table 1. The process of potato grading is: The potatoes enter from the feed inlet to the conveyor belt and spread out evenly, then they enter the first grade transferring area (level 1 grading area), in this area the potatoes of d∈(37.50) mm fall into the first level discharge port, while the remaining potatoes continue processing on the belt and go into the second grade transferring area (level 2 grading area), in this area the potatoes of d∈ (50.70) mm fall into the second level discharge port, the remaining potatoes then go into the third grade transferring area (level 3 grading area), the potatoes of d∈ (70,100) mm fall into the third level discharge port, and finally the oversized potatoes of d> 100mm are output from the end of the grading equipment. The structure diagram of the southern winter potato grading equipment is shown in Figure 1.The conveyor belt is made up of a series of rolling bars, and the potatoes locate in the gaps of the adjacent bars. The bars are divided into fixed rolling bars and movable rolling bars, and the fixed roll bars are installed into the fixed chain plate while the movable rolling bars are installed into the chain plate with a sliding chute in the middle and the bars can move up and down in the chute. The movable rolling bars are placed upon the grading baffles whose distribution is a ladder-like shape. When the movable rolling bars fall from one grading area to the next, with their own gravity and the extrusion of the potatoes, they will drop into the next baffle, and the gap between the bars becomes larger, resulting in the separation of the potatoes whose sizes are accord with this gap. The grading levels are shown in Figure 2, where δ1=36.2mm, δ2=50mm, δ3=70mm, δ4=100mm.

Table 1

Potato grading parameters

Level	Minor dimension, d [mm]	Mass, m [kg]
1	37 < d < 50	0.029 < m < 0.071
2	50 < d < 70	0.071 < m < 0.19
3	70 < d < 100	0.19 < m < 0.57
4	d＞100	m＞0.57

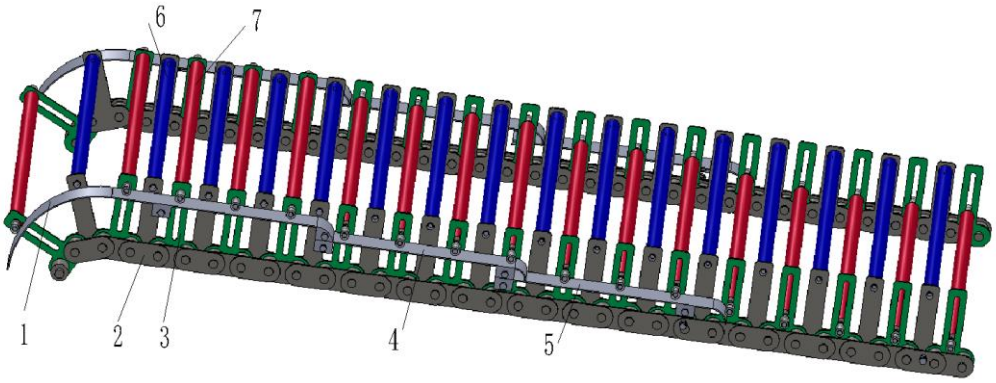

Fig.1 – Schematic on the structure of the Grader

1 – The grade 0 baffle; 2 – The fixed chain plate; 3 – The movable chain plate; 4 – The first level baffle; 5 – The second level baffle; 6 – The fixed rolling bar; 7 – The movable rolling bar

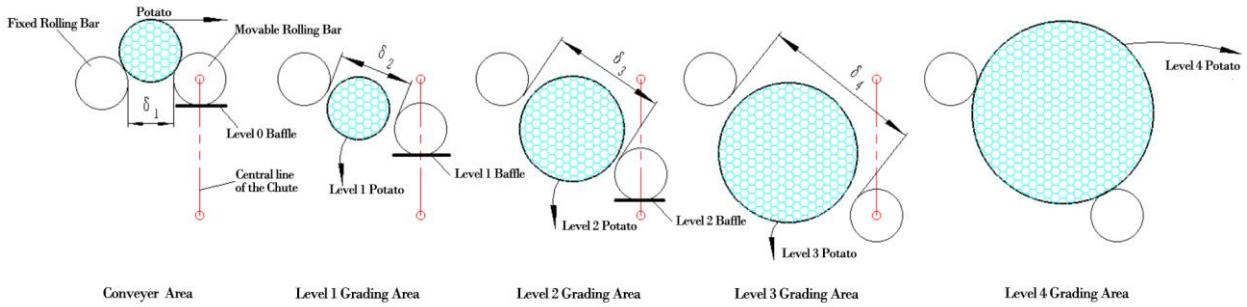

Fig.2 – Schematic on potato grading

Equipment modelling

This study used the 3-D designing software SolidWorks to construct the three-dimensional model of potato grading mechanism. To simplify the model and reduce the software loading time, this model had omitted the nuts, bolts, pins, washers and other fasteners. As the final ADAMS model is made up of basic components, such an ellipsis would not affect the simulation result. Exporting the 3-D model into Parasolid format (extension as * .x_t), then putting into the ADAMS software, setting the properties of the components and the kinematic pair, eventually the final simulation model is shown in Figure 3. The geometry dimensions and physical parameters were measured in this research. Based on measurement results, this study defined 4 potato levels P1, P2, P3, P4 as the test samples, the modelling parameters are shown in Table 2.

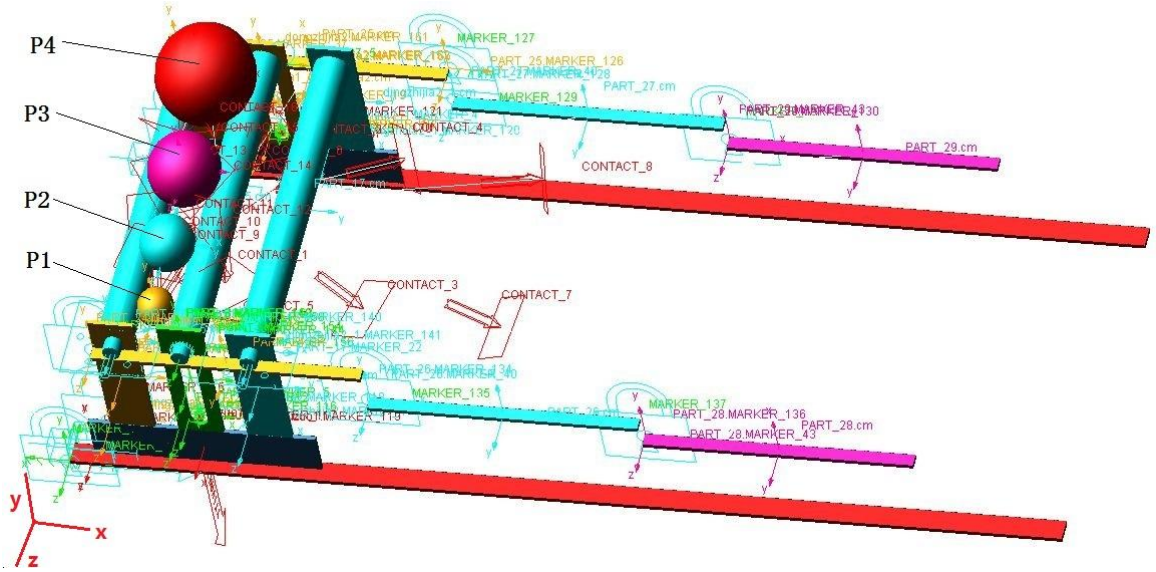

Fig.3 – Simulation model

Table 2

Parameters of the potato model

Type	Minor axis, b [mm]	Major axis, a [mm]	Density [kg/m3]	Mass, m [kg]	Center coordinates [mm]
P1	40	45	1.08×103	0.041	(-38.1, 200.18, -39.5)
P2	60	65	1.08×103	0.130	(-38.1, 220.38, -111.5)
P3	80	80	1.08×103	0.307	(-38.1, 234.35, -203.5)
P4	110	115	1.08×103	0.787	(-38.1, 252.60, -320.5)

There is contact impact force between the potato and the rolling bar, and its function can be represented by the spring-damping model *(XueBin An, ShangFeng Pan, 2014)*. The contact impact force *F,* is defined as:

$$F = k \cdot g^{e} + step\left(g, d_0, c_0, d_{\max}, c_{\max}\right) \cdot \frac{dg}{dt}, \text{ [N]} \quad (1)$$

where:

k represents stiffness of the spring; *g* is the penetration depth between potato and rolling bar; *e* represents shape index which determines the shape of the force- displacement curve; d_0 is the starting value of *g*, which in this case is 0; c_0 is the initial value of *step()* function, when d_0 is 0, c_0 will be 0;d_{max} is the maximum allowable penetration depth; c_{max} is the maximum damping value adopted when it reaches the maximum allowable penetration depth; *step()* represents step function.

It also set the material of the potatoes, the material of the rolling bars, and the Impact parameters between potato and the bars as shown in Figure 4.

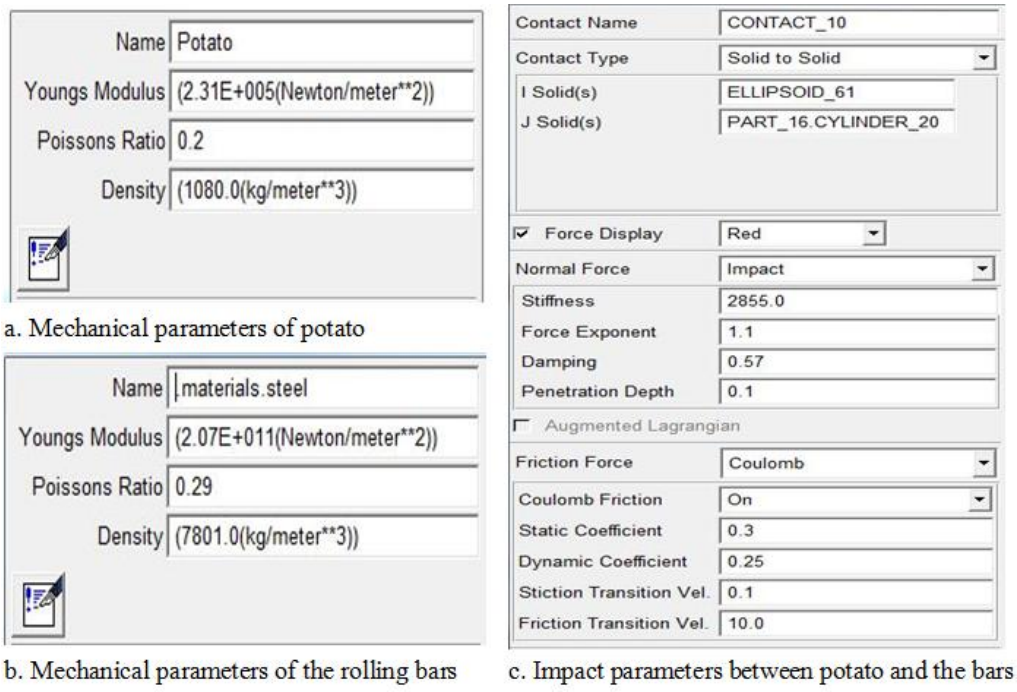

Fig.4 – Mechanics parameter settings of potato and the bars

RESULTS

Motion simulation

Setting the forward velocity of the initial conveyor as 200 mm/s, the simulation time as 4s, the steps of simulation as 120, this study respectively has measured the displacements in the Y direction, velocities in the X direction and the accelerated velocities in the Y direction of the centroids of potato P1, P2, P3 and P4. The results are shown in Figures 5-7.

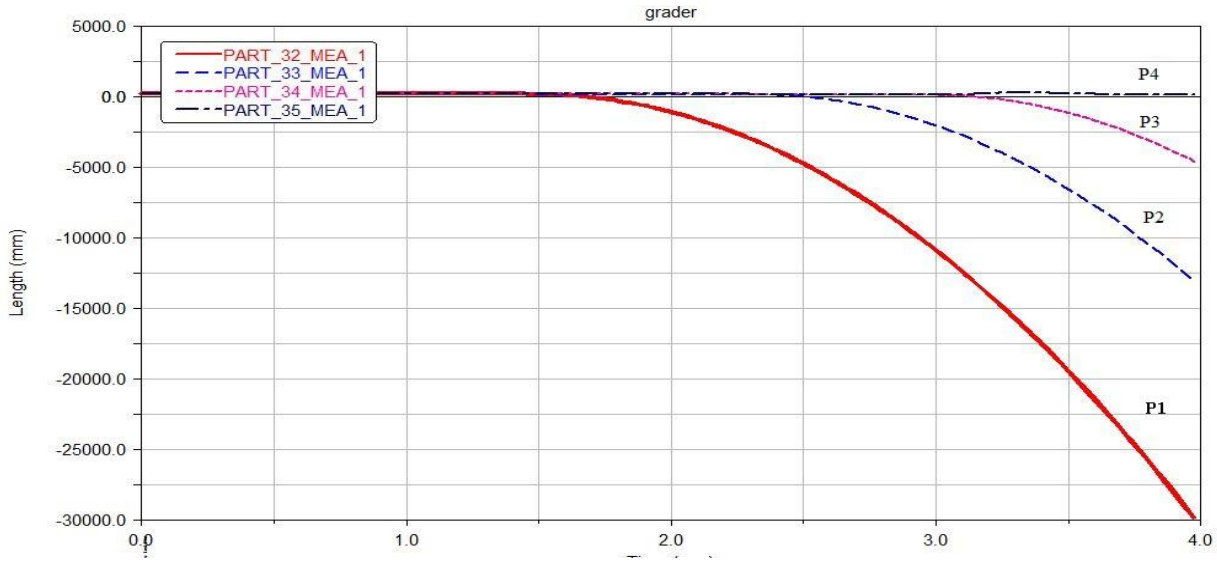

Fig.5 – The displacements of potatoes' centroids in the Y direction

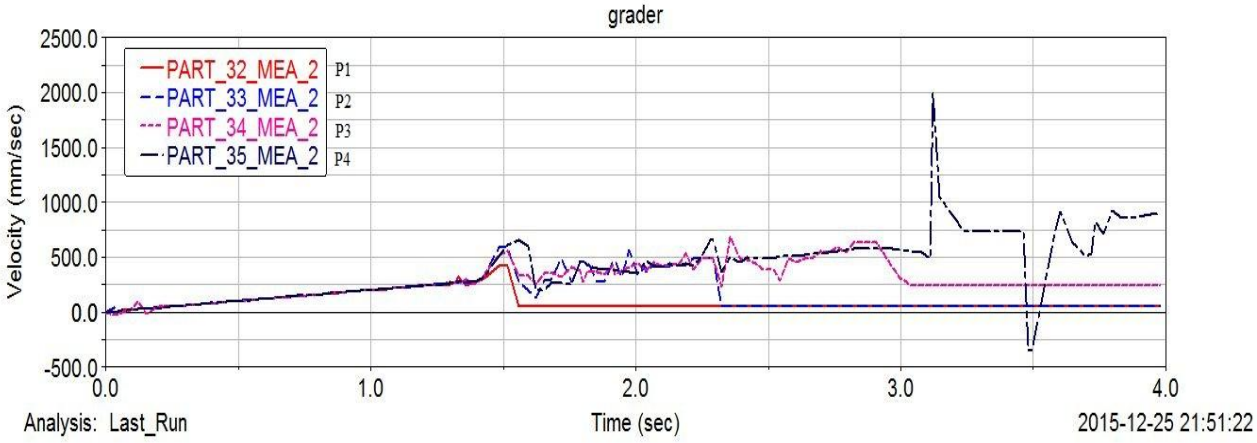

Fig.6 – The velocities of potatoes' centroids in the X direction

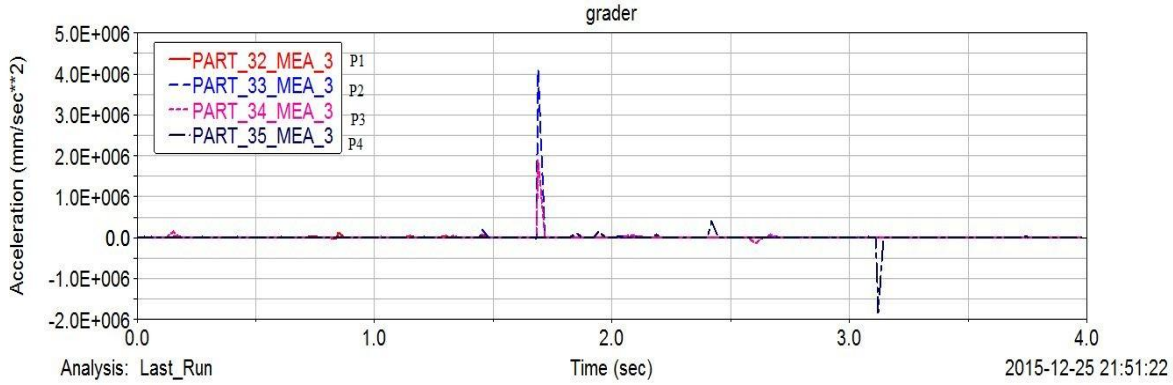

Fig.7 – The accelerated velocities of potatoes' centroids in the Y direction

As shown in Figure 5, when the simulation time was 1.6s, 2.4s, 3.1s, the displacements in the Y direction of potato P1, P2, P3 turned from 0 to negative values, and continued to decline in parabolic forms, indicating that the potatoes had been separated through the gaps. The little potato P1 was the first to be separated, then the middle-sized potato P2 was separated, and finally the big potato P3 was separated, the oversized potato P4 still moved along to the end of the conveyor. The simulation results were consistent with the mechanism designing theory, which proved the correctness of the designing scheme.

As shown in Figure 6, the forward velocities of potato P1, P2, P3 in the X direction fluctuated slightly, but they were basically stabilized. The main reason of the speed fluctuations was that, the potatoes collided

constantly with the fixed rolling bars in front and back of them when moving forward, which generated accelerated velocities in the corresponding directions and thus affected the velocity value in the X direction. After potato P3 was separated, the potato P4 was observed an instantaneous speed fluctuation, but it still remained in a stable value range.

Figure 7 shows that the accelerated velocities along the Y-direction of potato P1, P2, P3, P4 were relatively flat in the whole process, indicating that the potatoes moved fairly slightly in the Y direction, which proved that the equipment worked relatively stable. However, when the movable rolling bars moved from one baffle to the next, the potatoes jumped fairly strong in the Y direction. The situation was: In the first grading, the potato P2 made the maximum movement while the P4 made the minimum; in the second grading, the potato P4 made the maximum movement while the P3 almost remained still; in the third grading, P4 made the maximum movement in the negative Y direction.

Analysis of contact force

Southern potato is tender and has thin skin, which makes it easily injured when colliding with the rolling bars in the grading process. Literatures and experiments show *(Bentini et al, 2006; YongYing Sang et al, 2008)*, the force to ruin a potato is 251.6N. To make a comparative analysis of the contact forces, this study respectively have measured the contact force of P4 with two fixed rolling bars and a movable rolling bars, the contact force of P1 with the rear fixed rolling bars and the movable rolling bars. The results are shown in Figure 8 and Figure 9.

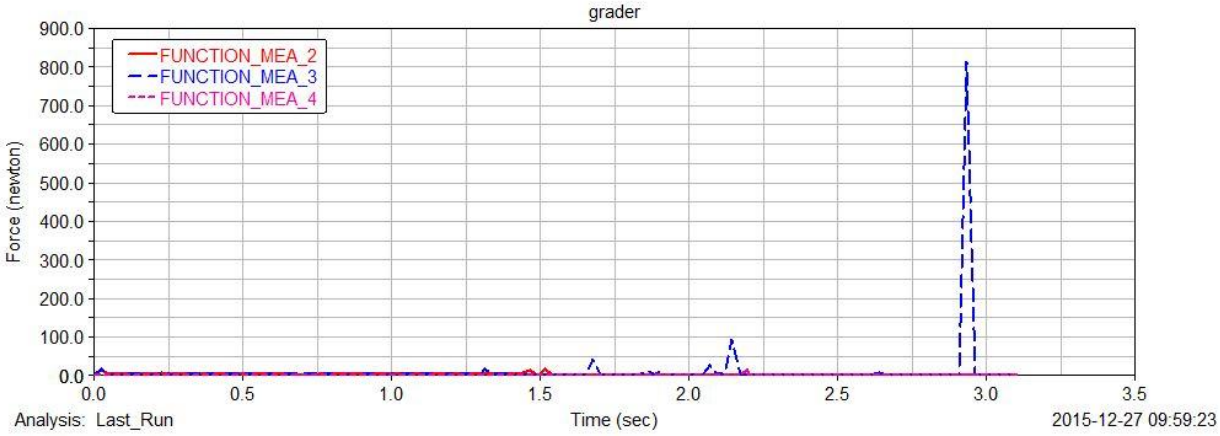

Fig.8 – The contact force of P4 with fixed/ movable rolling bars

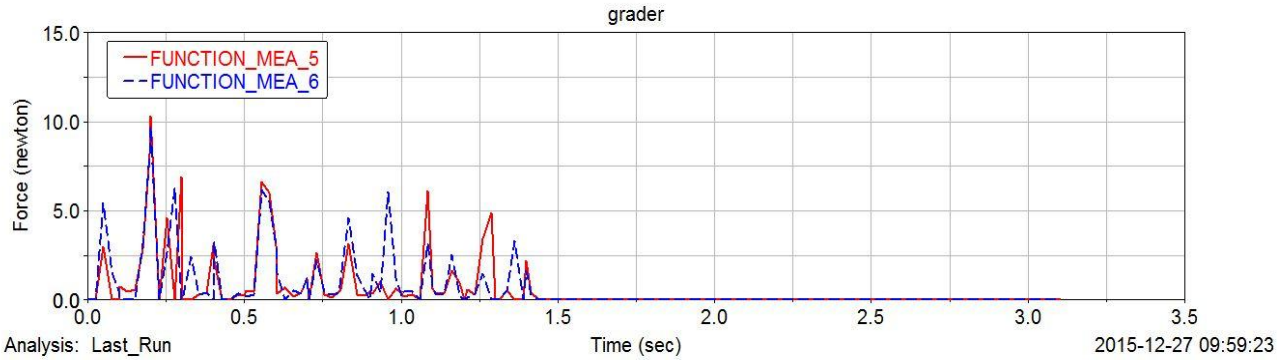

Fig.9 – The contact force of P1 with fixed/ movable rolling bars

As shown in Figure 8, the contact force between P4 and the fixed rolling bars was relatively small, which was not more than 20N. The contact force between P4 and the movable rolling bars rose to its maximum value when movable rolling bars falling into the lower baffle, the maximum values shown respectively as 42.68 N, 92.51 N, 813.7 N. Obviously the contact force between P4 and the movable rolling bars in the third grading was larger than the maximum destructive force of potato. While optimizing the design, a layer of rubber should be wrapped to the movable rolling bars to reduce the contact force.

As shown in Figure 8-9, in 0-1.5s, the average contact force between P1 and the fixed rolling bars was 3 N, only about 50% of the P4's, the extreme contact force between P1 and the movable rolling bars was 11 N, about 26% of the P4's. It indicated that the contact force increased as the quality of the potato increased, which was most significant in the extreme contact force.

CONCLUSIONS

- This study used the software of SolidWorks to establish a three-dimensional model for potato grading, and imported the model into the ADAMS, set the properties of the components, materials, the kinematic pairs and the Impact parameters, and finally built a dynamic mechanical model.
- Simulation analysis showed that, P1, P2, P3 were isolated successively, which means that the mechanism design is correct. The potatoes jumped only slightly upon the rolling bars, which indicates that the device works steadily.
- The analysis of contact force showed that the bigger the quality of the potato was, the greater the contact force between it and the rolling bars was. Such a principle was most significant in the extreme contact force between the potato and the movable rolling bars. In the experiment, the maximum contact force between P4 and the movable rolling bars was 813.7 N. The study can provide a basis for optimizing the design of prototype production.
- The further research is in progress to add a conveyor belt, potatoes will be transported to grading mechanism automatically. Conveying speed and grading speed are very important motion parameters for grader, so this study will focus on the effect on grading quality and efficiency under different conveying speed and grading speed, also analyze the variation of impact force between potatoes and bars, two adjacent potatoes, aiming to get the best motion parameters.

ACKNOWLEDGEMENT

This work is carried out with financial support from science and technology department of Guangdong province in China, science and technology program (No. 2015A030401097), and reform project of higher education teaching and research in Guangdong province "Mechanical innovation experimental platform building based on virtual experiment".

REFERENCES

[1] Bentini M., Caprara C., Martelli R, (2006), Harvesting damage to potato tubers by analysis of impacts recorded with an instrumented sphere, *Biosystems Engineering*, Vol.94, Issue 1, pp.75-85;

[2] Blasco J., Cubero S., Gómez-Sanchís J. et al., (2009), Development of a machine for the automatic sorting of pomegranate (*Punica Granatum*) arils based on computer vision, *Journal of Food Engineering*, Vol.90, Issue 1, pp.27-34;

[3] ChunHai Wang, QingYu Ding et al., (2008), Determination on the Parameters of the Potato Grading Devices (马铃薯分级机构参数的确定), *Agricultural Mechanization Research*, Issue 9, pp.103-107;

[4] LiangLong Hu, LiJia Tian et al., (2007), Design of 5XY-5 cylinder screen grader (5XY-5 型种子圆筒筛分级设备的研制), *Journal of Agricultural Mechanization Research*, Issue 2, pp.90-96;

[5] LiuFang ShenTu, Qi Wei, ZunGuo Gong et al., (2014), Design of potato sorter (马铃薯分选机的设计), *Journal of Agricultural Mechanization Research*, Issue 2, pp.114-115;

[6] Mendoza F., Lu R., Cen H., (2014), Grading of apples based on firmness and soluble solids content using Vis/SWNIR spectroscopy and spectral scattering techniques, *Journal of Food Engineering*, Vol.125, pp.59-68;

[7] MOA Department of Plantation Management, (2014), *Crops Database*, http: //202.127.42.157/ moazzys/nongqing.aspx;

[8] PingYuan Xiong, JiPing Yuan, JunWei Xiao et al., (2011), Structural design of the grader of winterplanting potato in south China (南方冬种马铃薯分级机结构设计), *Journal of Zhongkai College of Agricultural Engineering*, Vol.24, Issue 2, pp.61-63;

[9] Riquelme M.T., Barreiro P., Ruiz-Altisent M. et al., (2008), Olive classification according to external damage using image analysis, *Journal of Food Engineering*, Vol.87, Issue 3, pp.371-379;

[10] XiaoPing Yang, MingMing Shi, HongAn Wei et al., (2014), Design and simulation of grading device on potato combine harvester (马铃薯联合收获机分级装置的设计与仿真), *Journal of Shenyang Agricultural University*, Vol.45, Issue 2, pp.241-244;

[11] XueBin An, ShangFeng Pan, (2014), Analysis of contact model in multi-body system dynamic simulation (多体系统动力学仿真中的接触碰撞模型分析), *Computer Simulation*, Vol.25, Issue 10, pp.98-101.
[12] YiBin Ying, JiangSheng Gui, XiuQin Rao, (2014), Fruit shape classification based on Zernike moments (基于 Zernike 矩的水果形状分类), *Journal of Jiangsu University*, Vol.28, Issue 1, pp.1-4;
[13] YongYing Sang, DongXing Zhang, MeiMei Zhang, et al. (2008), Experimental research on potato crashing injury and finite element analysis, *Journal of China Agricultural University*, Vol.13, Issue 1, pp.81-84.

STUDIES OF PNEUMATIC COLLECTOR OF GRAIN KNOCKED OUT BY REEL BATS
/
РЕЗУЛЬТАТИ ДОСЛІДЖЕНЬ ПНЕВМОВЛОВЛЮВАЧА ЗЕРНА, ЩО ВИБИВАЄТЬСЯ ПЛАНКАМИ МОТОВИЛА

Ph.D. Eng. Shvedyk M.
Lutsk National Technical University / Ukraine
Tel: +38(0332)74-61-32; Fax: +38(0332)74-61-03; E-mail: lab-amb@ukr.net

Keywords: *reel, grain, impact, pneumatic collector, cyclone, pipeline, pressure*

ABSTRACT

In the article the studies of crop losses causes during harvest are presented. It is established that a significant cause of grain loss is a non-simultaneous ripening in the wheat. Thus, during reel bats impacts on stalks, the largest and most valuable grains that ripen earliest are knocked out of the wheat and fall to the ground. It is established that these losses are significant and irreversible. The current technical condition of combine harvesters cannot eliminate these losses. To eliminate these losses, a new design of pneumatic collector has been proposed in the article. The principle of its work is based on the vacuum created. Due to the vacuum, the grains that were knocked out from the wheat by reel bats are sucked and sent into the cyclone.

РЕЗЮМЕ

В статті наведено результати досліджень причин недобору врожаю під час його збирання. Встановлено, що істотною причиною втрати зерна є неодночасне його дозрівання в колосі. Як наслідок під час ударів планок мотовила по стеблах, найбільш крупні і найцінніші зернівки, які найпершими дозрівають, вибиваються з колоса і падають на землю. Встановлено, що ці втрати є значними і незворотними. Сучасний технічний стане зернозбиральних комбайнів не дозволяє усунути ці втрати. Для усунення цього недоліку в статті запропоновано конструкцію пневмовловлювача. Принцип його роботи ґрунтується на розрідженні, що створюється в конфузорі. Завдяки розрідженню все зерно, що вибивається з колоса планками мотовила, засмоктується і спрямовується в циклон.

INTRODUCTION

In the structure acreage of world agriculture the cereal crops occupy more than half. Its main areas are in Asia, North America, Europe, Australia and Africa. Over the past five years, Ukraine increased its grain production at a rapid pace and proved its total yield more than 60 million tons, which gave it the opportunity to take the second place on the world market among the countries-exporters of grain.

However, in order to stay on the market and among the world leaders it's necessary to continue to increase the volume of its production. But given the fact that in the structure of grain production in Ukraine about of 50% are the cereal crops, almost two-thirds of which prone to lodging, the timing of the harvest increased, and the process of machines operation is much more complicated. As a result, it leads to losses of grain which reaches 10-30%, and sometimes more, as the lodged grain stay below the headers cutting height *(Hrechkosiy V. et al, 1991)*.

To prevent the lodged grain currently used two methods - chemical and biological. The main point of the first method is that plants are treated with special chemicals that inhibit the plants growth and favor to thickening of the stalk, root development and make it resistant to lodging of cereals *(Alferov S. et al, 1981; Hrechkosiy V. et al, 1991)*. However, this method is not always effective. More promising is the use of short stalked, dwarf varieties which are characterized by high resistance to lodging of cereals and high yield. However, these varieties require shallow depth of seed placement - not more than 2 cm *(Shmat I. et al, 2009; Sysolin P. et al, 2001),* because they cannot grow in all areas.

Another cause of significant losses of grain is the ripening heterogeneity of grain in the wheat. Thus, at the time of harvest ripens earliest and lose contact with the wheat the largest and most valuable grains, which are located in its upper part. As a result, during the impacts on the stalk of the reel bats these grains are knocked out of the wheat and fall to the ground. Simple calculations show if of each wheat is knocked out of 2 grain, and in the time of harvest on fields of 1 m^2 on the average there are 500-600 stalks (*Hrechkosiy V. et al, 1991*), then on each hectare of at 6-8 hundredweight of grains are knocked out. Practically, these losses are irreversible, because the current technical condition of combine harvesters does not permit to eliminate it.

The conducted structural and biological analysis of standing crop of cereal crops shows that 70% of full grain is stored in 30-centimeter layer of wheat, and the rest - in the low-growing stalks, called undergrowth, where the grain by its properties is small, feeble and useful only to feed *(Dubrovin V., Shvedik N., 2014)*. It is obvious that these biological characteristics of cereal crops should form the basis for developing a new principle of its harvesting - namely, the volume reduction of biological mass that is feed for the threshing and for the cleaning.

Therefore there is a need to develop new working bodies that could fully ensure the effective harvesting not only of erect and lodged grain but also collect the grain knocked out by reel bats and would create conditions for a sharp increase of the productivity of combine harvesters.

MATERIAL AND METHOD

The effectiveness of the harvest in different countries is solved in different ways *(Ivan Gh., Usenko M., 2014; Ivan Gh., Vladut V.N, 2014; Moiceanu G. et al, 2015; Xiaoning Zhu et al, 2015)*. But we believe the most effective way to defect correction is the use of two-tier cutting of grain with separate threshing of the upper and lower tiers of wheat part and pneumatic lifting of the lodged grain and pneumatic collecting of the grain knocked out by the reel bats, based on creating of a vacuum in the area of reel. Process scheme of pneumatic collector of grain knocked out by combine harvesters reel bats is shown in Fig.1.

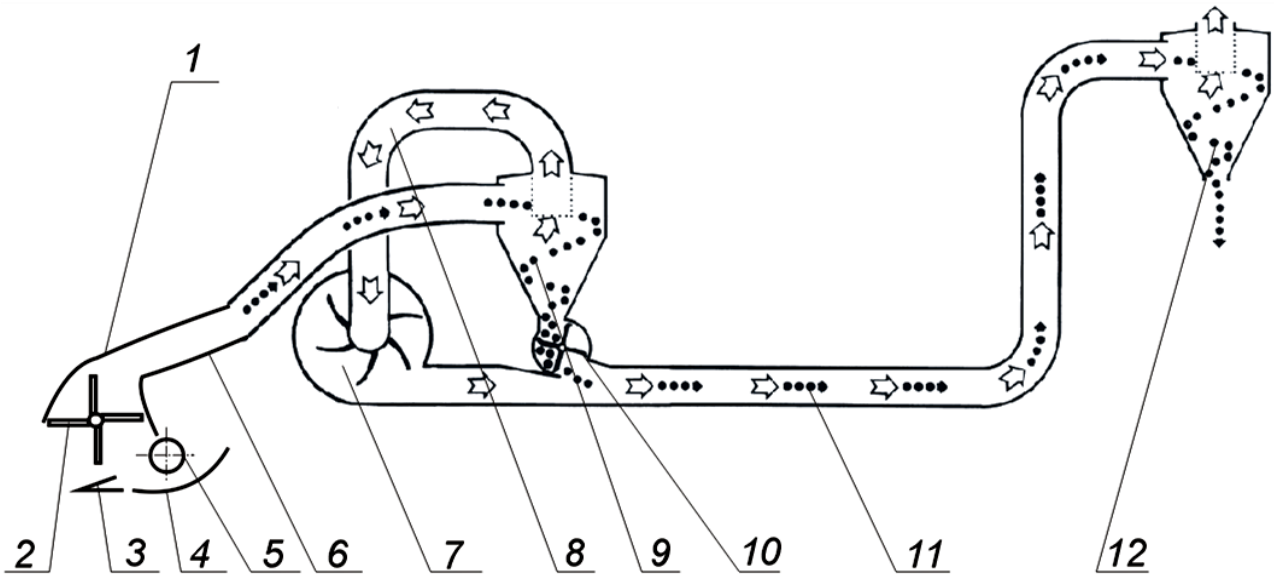

Fig.1 - Process scheme of pneumatic collector of grain knocked out by combine harvesters reel bats
1 – pneumatic collector; 2 – reel; 3 – cutter bar; 4 – header gutter; 5 – header auger; 6 – pneumatic pipeline; 7 – extractor-type fan; 8 – suction pipe; 9 – suction cyclone; 10 – rotor valve; 11 – transport line; 12 – offloading cyclone

The technological process of grain collecting is as it follows. When driving a combine harvester in the field, the extractor-type fan *7* through the pipe *8* sucks the air from the suction cyclone *9* and creates a vacuum in it, which through flexible pneumatic pipeline *6* extends to pneumatic collector *1*. Due to the vacuum, the lodged grain rise and enter the zone of the reel, which leads it to the cutter bar *3*.

After cutting, the wheat part of grain placed on the header gutter *4* upper tier and then by header auger *5* is supplied in inclined camera. This grain that falls out of the wheat during the lifting of stalks and by the reel bats *2* impacts sucked by the flow of air into the cyclone *9* where the grains and air are shared. Extractor-type fan accelerate the air to the speed of $v \approx 25$ m/s while the rotor valve *10* provides a uniform grain supply into the transport line *11* and it is transported to the offloading cyclone *12*. There, the exhaust air with light mixture removed through the top hole of the cyclone in the atmosphere, and the grain is emptied into a special tank for its accumulation.

Expediency of pneumatic collector using will depend primarily on the ratio of the additional cost of diesel oil necessary to drive the fan and the market value of collected grain. Consumption of diesel fuel depends on the pressure losses in the suction path of pneumatic collector. To determine these losses it must first make a pneumatic scheme of pneumatic collector that shown in Fig.2.

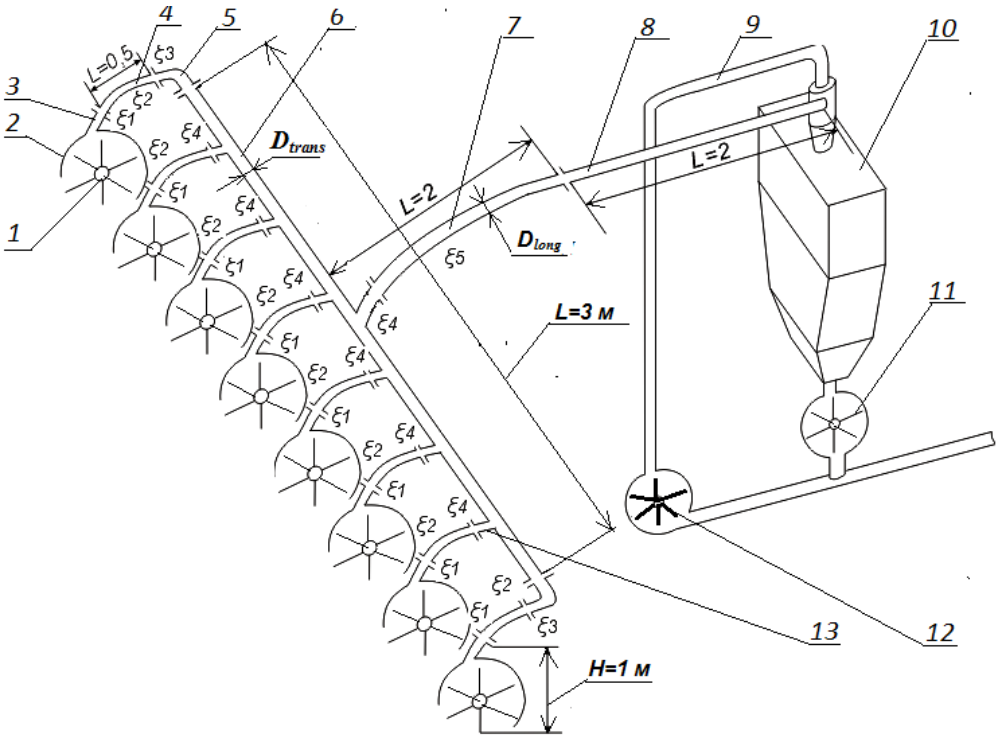

Fig.2 – Pneumatic pipeline layout scheme and placement of design elements, in which the local resistances results

1 – reel; 2 – fan; 3 – fan branch pipe; 4 – connecting branch pipe; 5 – knee; 6 - transverse pipeline; 7 – flexible pipeline; 8 - horizontal pipeline; 9 - suction pipeline; 10 – cyclone; 11 - rotor valve; 12 – fan; 13 – branch tube

Cutter bar does not effect virtually on the process of grain knocking out. Therefore, it is not considered in researches and not included in the scheme. On this scheme all fans and pipelines and branch pipes that connect them are shown. It also noted all the local resistances where pressure losses occurring (knees and narrowing of the pipeline, unloaders, etc.). The above scheme shows that the static pressure is spent to overcome friction in the pipeline, local resistances (knee, deflectors, discharger and flexible pipeline) and to lift the grain. That is, the total pressure losses $\sum h$ in suction path can be defined by the formula:

$$\sum h = h_1 + h_2 + h_3 + h_4 + h_5, \text{ [Pa]} \quad (1)$$

where:

h_1 - pressure loss from friction when clean air moving along the pipeline, [Pa];
h_2 - pressure loss from friction when the mixture of air and grain moving through the pipeline, [Pa];
h_3 - pressure loss in local resistances (knees and narrowing of the pipeline, unloaders, etc.), [Pa];
h_4 - pressure loss in fan to lift the grain, [Pa];
h_5 - pressure loss in the unloaders (cyclone), [Pa].

To check the accepted hypothesis authenticity can be conducted an experimental research. The main material that was studied in this paper was the haulm stand of the wheat and its grain. Research conducted in the field in the three replications according to developed methods using the experimental device.

Experimental device for pneumatic collecting of the grain knocked out by reel bats during its movement over the haulm stand of cereal crops is shown in Fig.3.

The device consists of pneumatic collector *11* and the cyclone *5*, which are installed on the self-propelled chassis *1* and connected to each other by flexible pneumatic pipeline *8*. This pneumatic collector is installed on the side of the self-propelled chassis on the rectangular frame (console) which is attached to adjustable risers which are installed on the frame and the cyclone is installed directly on three pillars. To the cyclones upper flange is attached the branch pipe with a hole that is cut off by the support *7*, and at the end of the branch pipe the fan *6* is installed. To lower cyclones flange is attached the transparent cone which is closed at the bottom by the cover.

Devices movement is carried out by using of winch *3*, which is driven by the electric motor *2*, which is powered by a battery 4.

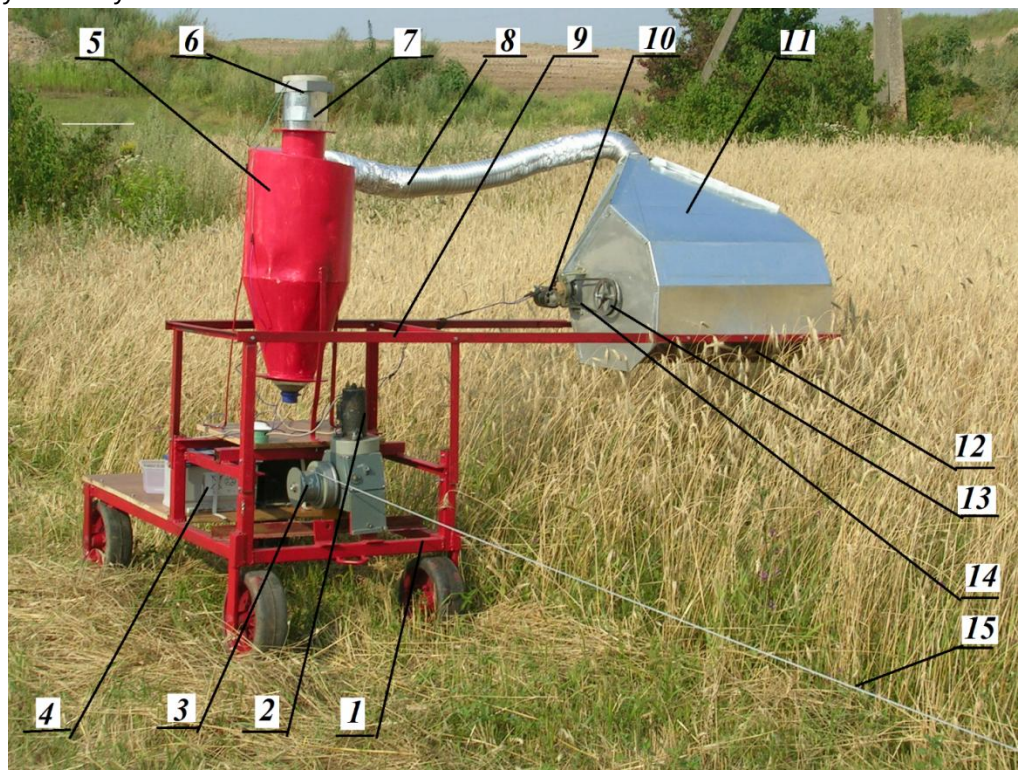

Fig.3 - Experimental device for collectiing of the grain knocked out by reel bats
1 – self-propelled chassis; 2 – electric motor; 3 – winch; 4 – batteries; 5 – cyclone; 6 – fan; 7 – support; 8 – pneumatic pipeline; 9 – console; 10 – electric motor; 11 – pneumatic collector; 12 – reel; 13 – pulley; 14 – belt; 15 – rope

For this, the rope *15* unwound from the winches drum and by free end with the hook is attached to a metal rod that is rammed into the ground.

The drive of the reel *12* is carried out by the V-belt drive *14* from the electric motor *10* through a worm reducer and the cyclones *5* fan *6* is driven by its own electric motor. All DC motors are powered by batteries with a voltage of 12 V.

Given that the reels and fans, the electric motor is powered by one battery and the chassis electric motor - by the other. Start the electric motors by using of individual switches.

The process passes as follows. At first turns on the fan *6* of the cyclone *5* and makes the vacuum in it, the depth of which is regulated by the change of the size of the inlet hole on branch pipe by moving of the support *7*. Then, turns on the electric motor *10* of the reels *12* drive and then the electric motor *2* of the winch *3*. When reeling the rope *15* on the winches drum the wagon *1* moves along the standing crop on the edge of fields or stubble and the pneumatic collector *11* moves over the layer of ears of wheat of the standing crop. Given that the reel bats separate the portion of the stalks from the main standing crop and incline it inside the pneumatic collector reproducing the same work process of the combine harvester header. Because of the vacuum from the cyclone *5* through the pneumatic pipeline *8* extends inside the pneumatic collector *11*, the grain knocked out from the wheat by the reel bats is sucked and transported by air flow in the cyclone. Here the air is separated from the grain and through the top branch pipe by the fan *6* is thrown out into the atmosphere, and the grain falls into the bottom of the cyclone and is collected in a transparent cone.

After passing by self-propelled chassis of a test length equal to 12.5 m the electric drives of winches, reel and fan are turned off and at the bottom of the cyclone where the box is placed, then the cover unscrewed and the grain by gravity emptied from the cone into the box. Then this grain from the box emptied into a plastic bag, putted in it the label prepared beforehand, in which indicated a sort, experiment # and replication #, then closed it tightly and emptied into a separate box for further processing in steady state conditions.

On the pneumatic collector was installed the reel with five bats of the diameter of 0.5 m and the length of 0.75 m. The width *a* and the length *b* of the inlet port at the bottom of pneumatic collector are equal accordingly to 0.8 m and 0.5 m.

Since the test length of the standing crops field in each experiment was similar to 12.5 m, so the area of layer of wheat ear, which is processed by reel bats is also was similar to 10 m^2.

RESULTS

Components of pressure losses in the suction path of pneumatic collector can be defined as follows.

1. Pressure losses *h* of friction when moving clean air along the pipeline can be defined by the Darcy formula *(Kondakov V. et al, 1973)*:

$$h = \lambda \frac{L \rho v^2}{2gD} \quad [\text{Pa}] \tag{2}$$

where:

λ - friction resistance coefficient;
L - length of pipeline, [m];
ρ - air density, [kg/m^3];
v - air speed, [m/s];
g - gravitational acceleration, [m/s^2];
D – diameter of pipeline, [m].

Friction resistance coefficient can be defined by the Brazius formula (*Krasnikov V., 1981*):

$$\lambda = \frac{0.3164}{R_e^{0.25}} \tag{3}$$

here:

R_e - Reynolds number, which is defined as *(Kondakov V. et al, 1973)*:

$$R_e = \frac{v \cdot D}{\upsilon} \tag{4}$$

here:

υ - air kinematic density, [m^2/s].

By the air temperature of $t = 30°$ C, which mainly corresponds to actual conditions of harvesting $\upsilon = 16.6 \cdot 10^6$ m^2/s.

Effective calculated length of the pipeline can be determined taking into account its piping layout, Fig.1. The scheme is shown that the total length of the suction pipeline consists of two parts. To the first part $\sum L_{p1}$ belong the branch pipes that connect the fans with transverse pipeline with diameter D_{trans}, i.e.:

$$\sum L_{p1} = 8 \sum L_{conf} + \sum L_{bp} + \sum L_{kn} \quad [\text{m}] \tag{5}$$

and to the second part $\sum L_{p2}$ belongs the transverse pipeline and two areas of longitudinal pipelines with diameter D_{long}, i.e.:

$$\sum L_{p2} = 8 \sum L_{tc} + \sum L_{fp} + \sum L_{hp} \quad [\text{m}] \tag{6}$$

where:

L_{conf} - fan length (vertical part of pipeline), [m];
L_{bp} - length of the connecting branch pipes, [m];
L_{kn} - knee length, [m];
L_{tc} - length of transverse collector, [m];
L_{fp} - length of flexible pipeline, [m];
L_{hp} - length of horizontal pipeline, [m].

Now by the formulas (3) and (4) can be defined the Reynolds number and friction resistance coefficient for each of the pipelines part.

Using the formula (1) can be defined the pressure loss h_{trans} of air friction during its movement in area of transverse pipeline with diameter D_{trans} having a total length $\sum L_{trans}$ and h_{long} for longitudinal pipeline with diameter D_{long} having a total length $\sum L_{long}$.

Therefore

$$h_1 = h_{trans} + h_{long}. \text{ [m]} \quad (7)$$

2. Pressure loss h_2 of friction when moving through pipelines of mixture of air and grain can be defined by the formula *(Krasnikov V., 1981)*:

$$h_2 = h_1(1 + c \cdot \mu) \text{ [m]} \quad (8)$$

where:

c - coefficient that depends on the concentration of the mixture, speed and physical and mechanical properties of grain. When v_p = 13-26 m/s the value of the coefficient is in the range of c = 0.83-0.31;

μ - coefficient of weight concentration of the mixture.

3. Pressure losses h_3 in local bearings (knees, by narrowing of the pipeline, unloaders, etc.) can be determined by the formula (*Kondakov V. et al, 1973*):

$$h_3 = \sum \xi \frac{\rho v^2}{2g} \text{ [m]} \quad (9)$$

where:

ρ - air density, [kg/m^3];
v - air speed, [m/s];
g - gravitational acceleration, [m/s^2];
ξ - sum of the coefficients of local resistance.

According to the pneumatic diagram of the grain pneumatic collector:

$$\sum \xi = 8\xi_1 + 8\xi_2 + 2\xi_3 + 3\xi_4 + \xi_5 \quad (10)$$

here:

ξ_1 - coefficient of local resistance of unexpected narrowing that occurs in fan.

The value of this coefficient can be determined by the formula *(Krasnikov V., 1981)*:

$$\xi_1 = 0,5\left(1 - \frac{F_{ap}}{F_{ac}}\right) \quad (11)$$

here:

F_{ap} – area of the pipeline, [m^2]: $F_{ap} = \frac{\pi D^2}{4}$;

F_{ac} – area of open hole of fan, [m^2]: $F_{ac} = a \cdot b$;

a and b - width and length of fan hole, [m^2];

$\xi_2 \dots \xi_5$ - coefficient of local resistance that occurs accordingly in connecting branch pipe, connected knees, branches and flexible pipeline and is determined by the formula (*Potapov G., 1990*):

$$\xi_2 = \sqrt{\frac{\delta}{90^\circ}} \quad (12)$$

here:

δ - angle of branch pipe, knee, branch of flexible pipeline, [deg.]. For pneumatic collector these angles are accordingly 60°, 90°, 90°, 45°;

ξ_3 - coefficient of local resistance that occurs in connection knees with angle of knee 90°. Its value can be determined by the formula (12);

ξ_4 - coefficient of local resistance that occurs in branches. As branches are mounted on the pipe at the angle 90°, its value is also can be determined by the formula (12);

ξ_5 - coefficient of local resistance that occurs in the flexible pipeline with the angle 45°.

4. Loss of pressure h_4 in fan for lifting the grain can be determined by the formula *(Krasnikov V., 1981)*:

$$h_4 = g \cdot \mu \cdot \rho \cdot H \text{ [Pa]} \quad (13)$$

where:

g – gravitational acceleration, [m/s^2];
μ - concentration factor of air mixture;
ρ - air density, [kg/m^3];
H - height of grain lifting, [m]. It is determined by the size of pneumatic collector (Fig.2) and is 1 m.

5. Pressure loss h_5 in unloader (cyclone) can be determined by the formula *(Kondakov V. et al, 1973*):

$$h_5 = \xi \frac{\rho v^2}{2g} \text{ [Pa]} \quad (14)$$

where:

ξ = 2.5 - coefficient of local resistance that occurs when the air-grain mixture inlet in the cyclone;
ρ - air density, [kg/m^3];
v - air speed, [m/s];
g - gravity acceleration, [m/s^2].

For example is taken a 4-meter harvester-threshers header and by the present methods can be determined the total pressure losses. Σh in the suction path of pneumatic collector consists of eight fans. Height of grain lifting in each fan is H = 1.0 m and the width and the length of its inlet hole are a = 0.7 m and b = 0.5 m. The total length of pipelines in accordance with the scheme (Fig.2) are ΣL_{trans} = 13.0 m and ΣL_{long} = 7.0 m.

For calculations is taken the transverse pipeline diameter D_{trans} = 0.078 m and longitudinal pipeline diameter D_{long} = 0.150 m *(Dubrovin V., Shvedik N., 2014*). Can be accepted also v = 25.0 m/s, μ = 3...5, c = 0.31...0.35 *(Krasnikov V., 1981*). Thus, under these conditions the total pressure losses Σh in the suction path according to calculations from the formula (1) can vary from 0.6 kPa to 1.2 kPa.

6. After determining of the air total losses can be determined the inputs of air power N to drive the fan, which creates a vacuum in fan needed for collecting (suctioning) of grain knocked out by reel bats and its supplying to the cyclone by the formula (*Krasnikov V., 1981*):

$$N = \frac{\sum h \cdot v}{3600 \cdot \eta_{be} \cdot \eta_{te} \cdot \eta_{fe}}, \text{ [kW]} \quad (15)$$

where:

v - air velocity, [m/s];
η_{be} - bearing efficiency;
η_{te} - transmission efficiency;
η_{fe} - fan efficiency.

After applying in the formula (15) the data v = 25.0 m/s, η_{be} = 0.97, η_{te} = 0.99 i η_{fe} = 0.8 the power losses required to drive the fan, which creates a vacuum in pneumatic collectors fans (total pressure losses Σh in the suction path defined by the formula (1) and are 0.6 kPa and 1.2 kPa) are accordingly N_1 = 5.42 kW and N_2 = 10.84 kW.

The experimental research results by using of pneumatic collector device (Fig. 3) showed that by reel speed increasing from 50 rpm to 75 rpm when the self-propelled chassis moving with the speed of 1.5 m/s which corresponds to the combine harvesters operating regime the knocked out grain mass increased from 277 g to 330 g, and while moving the self-propelled chassis with the speed of 2.5 m/s the knocked out grain mass increased from 293 g to 365 g. These losses show that in real conditions of work of combine harvesters on each fields hectare it can be knocked out by the reel bats from 460 kg to 600 kg of grain. The nature of grain (1000 pcs. of grains) on discount area was 60 g. Analysis of the studies showed that analytically determined by the formula (1) the total pressure losses Σh in the suction path ranges from 0.6 kPa to 1.2 kPa and coincide with the experimental data. In accordance with the vacuum gauge readings the vacuum in the fan in the first case was 0.75 kPa and in the second - 1.32 kPa. Thus, given in the article the analytical dependencies make it possible to determine with sufficient precision the pressure losses in the suction path of pneumatic collector and the power necessary to drive its fan. The studies will be useful in the development and design of pneumatic collector, which will be installed on production combine harvesters.

CONCLUSIONS

1. By reel speed increasing from 50 rpm to 75 rpm when the self-propelled chassis moving with the speed of 1.5 m/s which corresponds to the combine harvesters operating regime the knocked out grain mass from layer of ears of wheat on each area of 10 m^2 increased from 277 g to 330 g and by the self-propelled chassis moving with the speed of 2.5 m/s – increased from 293 g to 365 g.
2. In real conditions of work of combine harvesters on each field hectare it can knocked out by the reel bats from 460 kg to 600 kg of grain.
3. In order to provide 100% of grain collecting knocked out by reel bats when the combine harvester moves at a speed of 1.5 m/s and 2.5 m/s in fan must be created the vacuum accordingly 0.75 kPa and 1.32 kPa. The power needed to drive the fan can range from 5.42 kW to 10.84 kW.

REFERENCES

[1] Alferov S.A., Kaloshin A.I., Ugarov A.D., (1981), *How a harvester-thresher works (Как работает зерноуборочный комбайн),* p.190, Ed. Mechanical Engineering, Moscow/Russia;

[2] Dubrovin V., Shvedik N., (2014), Analysis of the proses of interaction of the reel bat with layer of ear of wheat (Анализ процесса взаимодействия планки мотовила с колосоносным слоем)*, MOTROL. Commission of Motorization and Energetics in Agriculture*, Vol.16, no.3, pp.273-278, Lublin/Poland,;

[3] Hrechkosiy V.D., Alimov D.M., Kyforenko V.I., ed al., (1991), *Overall mechanization of grain production (Комплексна механізація виробництва зерна),* p.216, Ed. Harvest, Kiev/Ukraine,;

[4] Ivan Gh., Usenko M., (2014), Theoretical study on feeding the tangential threshing system of conventional combine harvesters (Studiu teoretic privind alimentarea cu masa vegetala a aparatului de treier tangential all combinelor de recoltat cereale), *INMATEH. Agricultural Engineering Journal,* Vol.42, no.1, pp.33-40, Bucharest/Romania,;

[5] Ivan Gh., Vladut V.N., (2014), Kinematic study of threshing process conducted by tangential threshing system of conventional cereal harvesting combines (Studiul cinematic al procesului de treier realizat de aparatul de treier tangentiual al combinelor conventionale de recoltat cereale), *INMATEH. Agricultural Engineering Journal,* Vol.44, no.3, pp.59-68, Bucharest/Romania,;

[6] Kondakov V.N., Korobov M.M., Gritsyuk I.G., et al., (197 (3), *Pneumatic and hydraulic transport in the food industry (Пневматический и гидравлический транспорт в пищевой промышлености),* p.182, Ed. Food Industry, Moscow/Russia;

[7] Krasnikov V.V., (1981), *Carrying and lifting machines (Подьемно-транспортные машины),* p.263, Ed. Kolos, Moscow/Russia;

[8] Moiceanu G., Voicu Gh., Paraschiv G. et al, (2015), Mechanical properties of energetic plant stems - review (Proprietatile mecanice ale tulpinilor plantelor energetice-review)*, INMATEH. Agricultural Engineering Journal,* Vol.45, no.1, pp.149-156, Bucharest/Romania;

[9] Potapov G.P., (1990), *Load-haul-dump machine for livestock farming. Handbook (Погрузочно-транспортные машины для животноводства. Справочник)*, p.239, Ed. Agropromizdat, Moscow/Russia;

[10] Shmat I.K., Sysolin P.V., Samarin O.E., et al., (2009), *Methods and design principles of agricultural machines and units. Manual (Методи і принципи проектування сільськогосподарських машин і агрегатів. Навчальний посібник),* p.132, Ed. Oldie-plus, Kherson/Ukraine;

[11] Sysolin P.V., Salo V.M., Kropivny V.M., (2001), *Agricultural machines: theoretical foundations, construction, design. Arable farming machines (Сільськогосподарські машини: теоретичні основи, конструкція, проектування. Машини для рільництва),* Vol.1, p.384, Ed.Harvest Kiev/Ukraine;

[12] Xiaoning Zhu, Rui Yan, Hongli Wang, (2015), Harvesting scheduling operations for the machinery owners under multi-farming, multi-type situation with time window – an empirical study arising in agricultural context in China（基于时间窗的多农机点、 多农田作业点、 多机型的混合农机资源调度问题研究）, *INMATEH. Agricultural Engineering Journal,* Vol.46, no.2, pp.175-182, Bucharest/Romania.

COMPARATIVE STUDY REGARDING THE WORK PERFORMANCES FOR TWO TYPES OF FORAGE DISTRIBUTING MACHINES
/
STUDIU COMPARATIV PRIVIND PERFORMANȚELE DE EXPLOATARE A DOUĂ TIPURI DE MAŞINI PENTRU DISTRIBUIT FURAJE

PhD. Eng.Nedelcu A.*[1)], PhD. Eng. Popa L.[1)], Prof. Ph.D. Eng. Voicu Gh.[2)], PhD.Stud.Eng. Andrei S.[1)], PhD.Stud.Eng. Zaica A[1)]., PhD. Stud. Eng. Lazar G.[1)], PhD. Stud. Eng. Petcu A.[1)]
[1)]*INMA Bucharest*
[2)] University POLITEHNICA of Bucharest, Faculty of Biotechnical Systems Engineering / Romania
Tel: 0212693255.; E-mail: anedelcu@inma.ro

Keywords: *livestock, cattle, equipment for forage distribution*

ABSTRACT

For the study of methods and means to achieve a high performance technology for the distribution of forage, two different machines have been built and investigated, capable to perform several activities within the technology for preparing and distributing forage to cattle. In this article are presented the results of experimental researches carried out at a livestock farm, on a lot of milk cows, in similar working conditions, emphasizing the technical performances, the structure of working times, the working capacity of machines, important indicators for obtaining high production and increasing work productivity.

REZUMAT

Pentru studierea metodelor şi mijloacelor de realizarea a unei tehnologii performante de distribuire a furajelor s-au realizat şi cercetat doua maşini deosebite constructiv, capabile să execute mai multe activități din cadrul tehnologiei de pregătire şi distribuire a nutreților la bovine. În cadrul acestui articol sunt prezentate rezultate ale cercetărilor experimentale desfăşurate la o fermă zootehnică, pe un lot de vaci de lapte şi în condiții asemănătoare de lucru, cu accent pe performanțele tehnice, structura timpilor de lucru, capacitatea de lucru a maşinilor, indicatori importanți pentru obținerea de producții ridicate şi creşterea productivității muncii.

INTRODUCTION

Agricultural scientific research, by its research object - soil, plant, animal – aims to offer high quality biological products, raw material, technologies, appropriate knowledge that should contribute to promotion of sustainable agriculture and rural development, increase food security and safety according to general and specific requirements of the market.

For the economy, the agriculture can represent an opportunity, in recent years, being manifest trends of its diversification and consolidation, farming becoming more attractive to investors, (*Ciupercă et al., 2015; Eurostat, 2011; MADR, 2014*). In Romania, almost all the species from animal farms are being breeding, assuring the whole variety of agro-food products of animal origin of natural and cultivated grasslands, as well as the outstanding potential of cereal and fodder vegetable production can help to obtain important animal origin products for exportation, as “organic or ecological product”.

Cattle’s growing is a traditional activity in rural and especially mountain and hill area of Romania. Diversity of productions achieved, reduced energy consumption and type of fodder used make from cattle breeding a sustainable and perspective activity.

In 2011, the value of animal production represented 28% out of agricultural production amount (*Eurostat, 2011*), severely decreasing from 44%, as was registered in 1998. Cattle population (approximately 2 millions of heads in 2012, used especially for milk production) is mainly concentrated in North and North-Eastern of Southern Plain.

Cattle food has a specific structure, being based on producing high quality forage in sufficient quantity able to ensure balanced ratios for animal daily necessity, especially volume forage (hay juicy fodder, green matter) and concentrated fodder. Ensiling represents one of the three methods of current use of fodder plants in animal feeding, the other two being grazing and hay production, (*R. Jarrige et al., 1993; Mocanu and Hermeneanu, 2013; Voicu E. et al. 2007*).

Quality of food designed to animals must have an appropriate quality and be in suitable quantity with a nutritive value appropriate to physiological requirements of each breed, age or weight category, absence

of contaminants, as important values of free access to food and water, depending on feeding, number of daily portions correlated to growing and maintenance system, *(Pintea I., 2015*). The feeding technique is characteristic on categories of animals and ecological areas, depending on variety and quality of fodder produced, specialty and endowment level of respective units and even on area tradition, *(Mănişor P., 1994; Mănişor P., 1991)*.

Fodder UNIC corresponds to method of feeding with balanced ratios made of several types of forages (fibrous, raw, root and concentrated) mixed in a technological trailer. Quality of UNIC fodder depends on components quality and mincing and mixing processes quality, for homogenizing it in machines storage hopper, (*Dărăban S., 2010; Mănişor P., 1991*).

In recent years, the modern technique has highly developed in this field, being manufactured mobile or fixed machines which perform several operations (dosing, mixing and distributing food to stables or paddock), (*Mănişor P., 1994; Mocanu and Hermeneanu., 2013*)

Working systems of foddering machines are known as tillage cutter which breaks and loads into the silage, rotor with blades or spires for mincing and mixing the forage, conveyor that distributes the fodder mixture to animals. For reducing the manpower and especially for obtaining high quality works, scientific studies and researches on this equipment working processes, have been achieved, (*Nedelcu A et al., 2007 Nedelcu A. et al., 2012*).

MATERIAL AND METHOD

For studying the methods of achieving a state-of-the art technology for fodder distribution, within INMA, two variants of machines designed to prepare and distribute food to farm animals, were designed, manufactured and tested, namely: *Technological trailer for chopping, mixing and distributing the forage, RTF* (fig.1), *Fodder machine, MF8* (fig.2), having specific technical and functional characteristics each, determined by the constructive requirements of main technical equipment designed to loading, , chopping, mixing and distributing the fodder.

The technological sequences within the technology of distribution of fodder, which were analyzed, are the following:

- movement of tractor-machine aggregate to feeding points;
- dislodging from the store and loading into the body of fibrous forages;
- automated weighing or special platform of fodder weighed;
- chopping and homogenizing the fodder mixing;
- aggregate movement to distribution points;
- distribution of fodder to animals.

Fig.1 – Technological trailer for chopping, transporting and distributing the forage, RTF

Fig.2 – Fodder machine, MF8

With *Technological trailer for chopping, mixing and distributing the forage, RTF*, that is simpler as construction, the technological processes of chopping and mixing the fodder loaded into the body, transport and distribution of fodder to animals, were performed; with *Fodder machine* F8, a real domestic kitchen, the technological processes of silage forage dislodging and loading, chopping and mixing of fodder ensilaged, straw or hay bales chopping, automated weighing of recipe fodder, homogenization and distribution of resulted fodder mixture, were performed.

The two machines were tested at a livestock farm for cattle growing from S.C. AGROINDUSTRIALA Pantelimon S.A./Ilfov/Romania.

In figure 3, are shown the technological variants achieved by the two types of technical equipment, emphasizing the working processes and methods of achieving them.

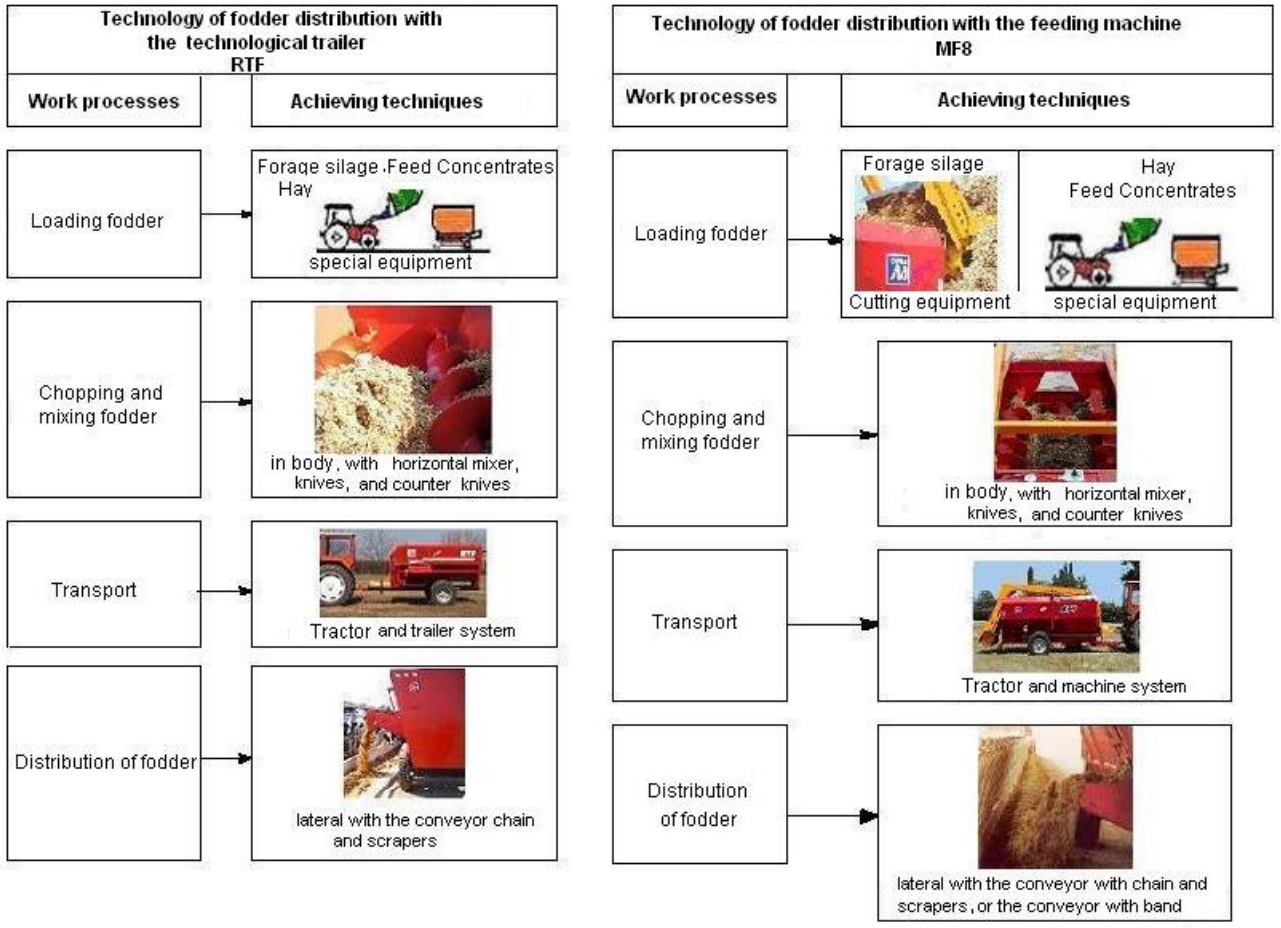

Fig.3 – Scheme of foraging technology with achieving variants according to equipment used

Within the technology of preparing and distributing the fodder to cattle, measurements for determining the working parameters of equipment loaded, were achieved, namely: moments, distribution height, time and qualitative working and exploitation indexes *(Nedelcu A., 2012)*.

The tests were made with wheeled tractor U 650, suitably equipped with lower traction coupler and system of taking over the vertical loads, independent PTO with rotating speed of n=540 rot/min; storage battery 12 V; 12/150 Ah, tensiometer plug with moment transducer HBMT4Wa-S3, centrifugal tachometer 40 - 48000 rot/min, mechanical chronometer, weighing lever 250 - 10000 kg and other specific measuring instruments.

In the machine body were loaded especially the ensiled material and different proportions of hay and straw bales, according to recipe established by the specialist.

Corn silage loading was made in a silage cell where the material density per worked surface has varied from upper to lower part ranging between: 520…756 kg/m^3 .

Material ensilaged was dislodged and loaded with fodder machine cutter MF8, and in technological trailer RTF with special equipment of IFRON type.

Power, *P*, necessary for driving each working equipment was calculated with relation (1) *(Şandru A. et al. 1983, Tecuşan N. et al., 1982*):

$$P = \frac{M \cdot n}{9550} \quad [\text{kW}] \qquad (1)$$

where:

M – moment measured [Nm];

n – rotating speed [rot/min];

Aggregate moving to loading or distribution points has been done with constant speed in a horizontal road and that is why the traction force and traction power are calculated with relations (2).

$$F_t = f \cdot Q \quad [N] \tag{2}$$

$$P = \frac{F_t \cdot v_l}{1000} \quad [kW]$$

where:

F_t - traction force in towing point, [N];

f – coefficient of resistance to running;

f = 0.018 - 0.020, on worn asphalt or concrete road, (*Tecuşan N. et al., 1982*).

Q – machine's weight including the load, [N].

V_l – rate of travel, [m/s];

Performing the operations with mechanized methods greatly contributes to increasing work productivity, due to the quality of work.

Working capacity of aggregate, W, represents the average volume of suitable quality operations, U, achieved in time unit T_i, according to relation (3).

Structure of working time represents the group of elements belonging to a shift time, being calculated with relation (4) *(Şandru A. et al., 1983*).

$$W = \frac{60 \cdot U}{T_i} \quad [UM/h] \tag{3}$$

$$\begin{aligned} T_{02} &= T_1 + T_2 \\ T_{03} &= T_{02} + T_3 \\ T_{04} &= T_{03} + T_4 \\ T_{07} &= T_{04} + T_5 + T_6 + T_7 \\ T_{08} &= T_{07} + T_8 \end{aligned} \quad [min] \tag{4}$$

where:

T_1 – working time; T_2 – additional time, T_3 – time designed to technical service of the machine; T_4 – time for remediation of technological failures, T_5 – time for personal rest; T_6 – time for changing the workplaces; T_7 – time for technical maintenance, T_8 – total working time.

Knowing the structure of time the coefficients of time utilization are calculated, as well as the exploitation indexes characterizing the working time and contribute to estimation of technological and technical deficiencies.

RESULTS

Within the tests, measurements were made for determining the dimensional characteristics shown in table 1.

During the basis operations of the technology one or several main assemblies will be put in function, depending on variant of machine used; when measuring the moments and analyze the power consumption one will take into account all these.

Table1

Main technical characteristics of equipment tested

Technical characteristics	MU	Technical equipment	
		Technological trailer for chopping, transporting and distributing fodder RTF	Fodder machine MF 8
Category	-	Machine for works	Machine for works
Type	-	uniaxial	uniaxial

Technical characteristics	MU	Technical equipment	
		Technological trailer for chopping, transporting and distributing fodder RTF	Fodder machine MF 8
Overall dimensions: - length - width - height	 mm mm mm	 4280 2860-2550 2275	 6250 2350 2445
Distribution height	mm	600 -1340 (depending on conveyor type)	400-630 (adjustable working position)
Wheel track	mm	1600	1800
Useful volume	m^3	3.5	8
Own mass	kg	2000	3650
Loading equipment	-	-	Cutter type
Type of distributing conveyor	-	With chain and blades	With chain and blades
Working speed	km/h	2-4	2-4

In table 2 were comparatively identified the assemblies which participate in performing the working processes appropriate to technology of foraging.

During forage loading into the machine body, the mixing worms are permanently operating, being driven from tractor's PTO through the mechanical transmission; at the same time, if the body is loaded with fodder and moves to the distribution points, the worms will be driven for chopping and mixing in order to homogenize the matter.

In table 3 are given the average values of rotating speed and moments measured at the main axle driving the working parts for loading, mincing, mixing and distributing the fodder.

Table 2

Table of consumers of power developed by tractor from the PTO

Working process	Operating assemblies				
	Technological trailer, RTF		Fodder machine, MF8		
	Mixing worms	Conveyor	Mixing worms	Cutter	Conveyor
Motion of unloaded machine	-	-	-	-	-
Loading of fibrous ensilaged fodder	X	-	X	X	-
Loading of concentrated or other types of forage	X	-	X	-	-
Movement to points of fodder feeding	X	-	X	-	-
Chopping, mixing and travel to distribution points	X	-	X	-	-
Distribution of forage mixture	X	X	X	-	X

PTO's rotating speed when the machine is unloaded has had values ranging within 500-540 rot/min

Table 3

Determinations per different working stages

Working process	Technological trailer - RTF			Fodder machine - MF 8		
	Operating assemblies	Moment [N m]	Power necessary [kW]	Operating assemblies	Moment [N m]	Power necessary [kW]
Silage fodder loading	Mixing worms	200-230	11.31-13.1	Worms and cutter	330-400	18.7-22.6
Other fodder loading according to recipe	Mixing worms	200-250	11.31-14.2	Mixing worms	300-350	17-19.8
Blending and grinding	Mixing worms	220-280	12.5-15.8	Mixing worms	320-390	18-21.5
Fodder distribution	Mixing worms and conveyor	260-290	14.70-16.4	Mixing worms and conveyor	340-400	19.2-22.6

Power necessary to drive the working systems for the main working processes within the technology studied, were calculated with relation (1), where the rotating speed n=540 rot/min (according to Tractor technical book), results being synthesized in table 4.

In order to test the machine operation and determine their functional characteristics, different types of silage fodder were loaded in machines body: silage corn, hay and straw bales, fodder combined in different proportions according to recipe.

Fodder matter loaded in machine body during works:

- technological trailer, RTF, *m* = 1000 kg
- fodder machine, MF 8, *m* = 2000 kg

During the experiments, it has been found that for machines good operation, the humidity of fodder used should not surpass 70%. Using appropriate humidity forage, the processes of mixing, homogenization and distribution are continuously run and the material adhesion and settlement phenomena on the bottom of the body, as well as an excessive shredding or a pasty mixture, are avoided.

Measurements for finding out the characteristics of ensiled fodder used were made on 500 g samples of silage maize with husk, taken during two different stages of technology:

1. from the silage cell, before dislodging and charging into the machine body;
2. from the layer of chopped material in the machine body and distributed to animals.

Time of mixing and shredding was of 20 min.

Table 4 comparatively shows the characteristics of silage fodder before and after processing it in the body of fodder distribution machines RTF and MF 8. Values indicated represent the average of two material samples taken for each machine and are valid for both machines, because of the mixing worms identical constructive solutions and their endowment with notched knives.

Table 4

Silage material characteristics before and after the processing in distribution machines

Fragments length [mm]	Characteristics of material loaded in machines body			Characteristics of material after the processes of shredding and mixing		
	Humidity [%]	Quantity [g]	Shredding level [%]	Humidity [%]	Quantity [g]	Percentage in fodder mass [%]
l<50	31.82	241.6	48.34	37.54	433.5	86.7
l=50-100		70.8	14.16		66.5	13.3
l=101-150		54.1	10.82		-	-
l=151-250		133.4	26.61		-	-

For *f*=0.02, the working speed *v*=2…4 km/h and fodder mass loaded, the following values for traction force and power necessary to traction, were registered:

- technological trailer RTF, F_t = 600 N; P_t =0.36…0.66 kW
- fodder machine, MF 8 , F_t = 1130 N, P_t =0.63-1.25 kW

Wheeled tractor U 650 with which tests were performed, is an average power tractor, equipped with Diesel engine of 47.8 kW (65 HP) at 1800 rot/min. In table 5 are shown the values for power stock in different stages of technology, calculated for the working speed v = 4km/h.

Within the technology for preparing and distributing fodder to cattle, performed with the machine studied, besides the functional characteristics were determined also the working time, working capacity and the results obtained were analyzed and a series of exploitation indexes shown in testing reports according, were established.

Table 5

Power consumption during different working stages [kW]

Operation	Technological trailer - RTF		Forage machine - MF 8	
	Max. power consumed	Power stock	Power necessary	Power stock
Silage forage loading (stationary)	13.10	34.70	22.60	25.20
Other fodder loading according to recipe (stationary)	14.20	33.60	19.80	28.00
Mixing and grinding (stationary)	15.80	32.00	21.50	26.30
Mixing, grinding and travel to distribution point	16.46	31.34	22.75	25.05
Forage distribution	17.10	30.70	23.85	23.95

Structure of working time was estimated when the forage was distributed to 100 milk cows, and the feeding portion was of 35-40 kg/day *(Şandru A et al, 1983*).

Table 5

Structure of working time

Parameter	Symbol	Technological trailer, RTF	Fodder machine, MF 8
		Values measured	Values measured
Working hours for one charge [min	T1	36	28.5
Number of charges per day [min]	N_S	4	4
Additional time (unloaded machine movement) [min]	T2	5	3
Time for machine technical service (preparation of working machine) [min]	T3	5	5
Time for remedying the deficiencies {min]	T4	6	4
Operating time [min]	T_{02}	41	31.5
Total operating time, [min]	T_{03}	46	36.5
Time of production [min]	T_{04}	52	40.5
Working hours per day [min]	$T_{zi} = N_S$ xT1	144	57
Total working time (one day) [min]	$T_{08}=N_S$ x T_{04}	208	114
Hourly working capacity appropriate to one charge production time [kg/h]	W_{04}	1154	2963
Coefficient of utilization of operating time for one charge	K_{04}	0.69	0.70
Coefficient of safety operation	$k_4 = \frac{T_1}{T_1 + T_4}$	0.86	0.88

CONCLUSIONS

The both machines differ from constructive point of view, which resulted in specific characteristics for each of them, according to table 1, as well as different involvement in achieving technological sequences within the technology;

After the analysis of moments measured and power driving the working parts, the following have been found:

- for technological trailer RTF, loaded with 1000kg forage, the max. necessary power is of 16.46kW suitable to transport and distribution processes (the mixing worms operate simultaneously with chain and rake conveyor);
- for fodder machine MF8, loaded with 2000kg of forage, the maximum necessary power is of 23.85kW corresponding to forage transport and distribution the (mixing worms operate simultaneously with chain and rake conveyor);
- for both variants of machines, a power stock has remained during operations performing;

Endowment of fodder machine, MF 8 with own dislodging and loading equipment and weighing installation has led to obtaining smaller time of loading and movement, thus, resulting smaller working hours: T1=28.5min for the machine MF8, instead of T1=36min for trailer RTF, influencing also the other components of time structure and hourly working capacity.

Operation safety coefficient, K_4 , calculated for the two variants of machines are very close.

Utilization of fodder machine, MF8, has been more advantageous than the technological trailer, RTF, because it performs with its own equipment the silage forage dislodging and loading in its own body.

REFERENCES

[1] Ciupercă R., Lazăr G., Popa L., Nedelcu A., Ştefan V., Zaica A, Petcu A., (2015), Organic plant and animal waste management system (Sistem ecologic de gestionare a deşeurilor vegetale şi animale), *INMATEH-Agricultural Engineering Journal,* Vol.46, No.2, pp.69-76, ISSN: 2068–2239, Bucharest/Romania;

[2] Dărăban S., (2010), Sheep feeding during the stable feeding, (Hrănirea ovinelor în perioada de stabulație), *The Village World* Journal Publishing, No.1, 1-15 January;

[3] Jarrige R. et al, (1993), *Cattle, sheep and goats feeding*, INRA, ISBN 2-7380-0563-2, Paris/France;

[4] Mănişor P., (1994), *Mechanization and automation of livestock works (Mecanizarea şi automatizarea lucrărilor în zootehnie)*, CERES Publishing, ISBN 973-40-0304-6, Bucharest/Romania;

[5] Manişor P., (1991), *Technologies and equipment for valorisation of volume forage in industrial flow (Tehnologii şi utilaje pentru producerea şi valorificarea furajelor)*, CERES Publishing, ISBN 973-40-0156-6, Bucharest/Romania;

[6] Mocanu V, Hermeneanu I., (2013), *Mechanization of agricultural works on lawns. Technologies, machines and equipment (Mecanizarea lucrărilor agricole pe pajişti. Tehnologii, maşini şi echipamente),* Ed. Universitatea Transilvania Braşov Publishing, ISBN 978-606-19-0237-8, Braşov / Romania;

[7] Nedelcu A., Popa L., Cojocaru I., Ciupercă R., (2007), Modern technologies for forage distributing in cattle farms (Tehnologii moderne pentru distribuirea furajelor in fermele de bovine), *INMATEH Scientific Works (INMATEH -Lucrări ştiințifice)*, vol. 20, no. 2/2007, ISSN 1583–1019, pp.61-66;

[8] Nedelcu A. Ciuperca R., Popa L., Bodea C., (2012), Researches Regarding the Shredding, Mixing and Distribution Processes within Foddering Technology of the Cattle (Cercetări asupra proceselor de mărunțire, amestecare, distribuție din cadrul tehnologiei de furajare a bovinelor), *The 4th International Conference "Advanced Composite Materials Engineering" COMAT 2012,* ISBN 978-973-131-162-3, pp. 838-842, Brasov/Romania;

[9] Pintea I., (2015) Recommendations regarding the production, storage and foraging to animals (Recomandari privind producerea depozitarea si distribuirea furajelor pentru animale), *Gazeta Agricolă*, http://www.gazetadeagricultura.info;

[10] Şandru A., Popescu S., Cristea I., Neculaiasă V., (1983), *Exploitation of agricultural equipment (Exploatarea utilajelor agricole)*, Ed. Didactica şi Pedagogică Publishing House, Bucharest / Romania;

[11] Tecuşan N., Ionescu E., (1982), *Tractors and motor cars (Tractoare şi automobile),* Ed. Didactică şi Pedagogică Publishing House, Bucharest/Romania;

[12] Voicu E., Gângu V., Ciure G., Tican N., (2007) Machine for green fodder ensiling in polyethylene bags, (Maşina pentru însilozat furaje verzi în sac de polietilena), *INMATEH Scientific Works (INMATEH - Lucrări ştiințifice)*, vol.23, no.5/2007, ISSN 1583–1019, pp.33-38, Bucharest/Romania;

[13] *** EUROSTAT - http://ec.europa.eu/eurostat/data/browse-statistics-by-theme;

[14] *** MADR - (2014) *Strategy for long and average term development of agro-food sector-Horizon 2020-2030, (Strategia pentru dezvoltarea sectorului agroalimentar pe termen mediu şi lung orizont 2020-2030),* Romania, http://www.madr.ro/proiecte-de-acte-normative/1291-proiect-1-25-06-2014.html.

INVESTIGATION OF A TRANSFER BRANCH OF A FLEXIBLE SCREW CONVEYER
/
ДОСЛІДЖЕННЯ ПЕРЕВАНТАЖУВАЛЬНОГО ПАТРУБКА ГНУЧКОГО ГВИНТОВОГО КОНВЕЄРА

Prof. Ph.D. Eng Hevko R.B.[1)], Lect. Ph.D. Eng. Klendii M.B.[2)], Ph.D. Eng. Klendii O.M.[2)]
[1)]Ternopil National Economical University / Ukraine; [2)] Separated Subdivision of National University of Life and Environmental Sciences of Ukraine Berezhany Agrotechnical Institute / Ukraine
E-mail: alex_ks@mail.ru

Keywords: *screw conveyer, transfer branch, screw, technological line*

ABSTRACT

Having analysed the researches on the operating process of screw conveyers, a transfer branch with a central drive has been offered to be mounted between uploading and unloading pipe lines. This helps to increase the length of bulk load conveying and to decrease power load on helixes at the point of their attaching to drive shafts. Process flow sheets of possible ways of conveying bulk load in a transfer branch have been developed and its experimental sample has been made. Theoretical and experimental investigations of the process of conveying bulk load between operating devices in a transfer branch have been conducted.

РЕЗЮМЕ

На основі аналізу результатів досліджень процесів роботи гвинтових конвеєрів запропоновано між завантажувальною та вивантажувальною магістралями встановити перевантажувальний патрубок з центральним приводом. Це дозволяє збільшити довжину транспортування сипких матеріалів, а також знизити силові навантаження на спіралі в зоні їх кріплення до привідних валів. Розроблено технологічні схеми можливих варіантів переміщення сипкого матеріалу в перевантажувальному патрубку та виготовлено його експериментальний зразок. Проведено теоретичне дослідження процесу переведення сипкого матеріалу між робочими органами в перевантажувальному патрубку та проведено експериментальні дослідження.

INTRODUCTION

Transfer branches in flexible screw conveyers are widely used for uploading and unloading process operations. However, the existing designs of transfer branches do not meet exploitation requirements in full measure. Main disadvantages are the following: an increased energy consumption, which is connected with the need of lifting the material at the point of its transfer in order to provide a gravity flow from a loading pipe line to an unloading one; the increased damage of grain material and the complexity of branch designs, especially at their considerable overall size.

In the familiar designs of transfer branches *(Boyko A.I. and Kulikiskiy V.L., 2011; Hevko R.B. and Klendiy O.M., 2013; Klendiy M.B., 2006; Klendiy M.B. and Hevko R.B., 2005; Klendiy M.B., 2007)*, in which the above mentioned problems are partially solved, the process of bulk load transfer becomes more complicated and under some operating conditions there is an increased possibility of congestion, which can cause a crash of a flexible screw conveyer.

MATERIAL AND METHOD

In order to improve the performance criteria of flexible screw conveyers, diagrams of the directions of bulk load transfer from a loading pipe line to an unloading one have been suggested, and the design of a transfer branch with a central drive and a safety device with unloading of screw operating devices in a horizontal plane has been designed *(Hevko R.B. and Klendiy O.M., 2014; Hevko R.B. et al., 2014; Hevko R.B. et al., 2015; Hevko R.B. et al., 2012; Hevko R.B. et. al., 2014)*. In order to choose the optimal design of a transfer branch of a screw conveyer, let us consider various directions of bulk load transfer by operating devices from an uploading pipe line to an unloading one *(Klendiy M.B., 2006)* (Fig.1).

In the first alternative, when using a leftward helical spiral with screw operating devices turning in the same counterclockwise direction (Fig.1, a), bulk load is transferred along the bottom horizontal surface of a transfer branch. When using a rightward helical spiral with screw operating devices turning in the same clockwise direction (Fig.1,b), bulk load is transferred along the upper horizontal surface of a transfer branch.

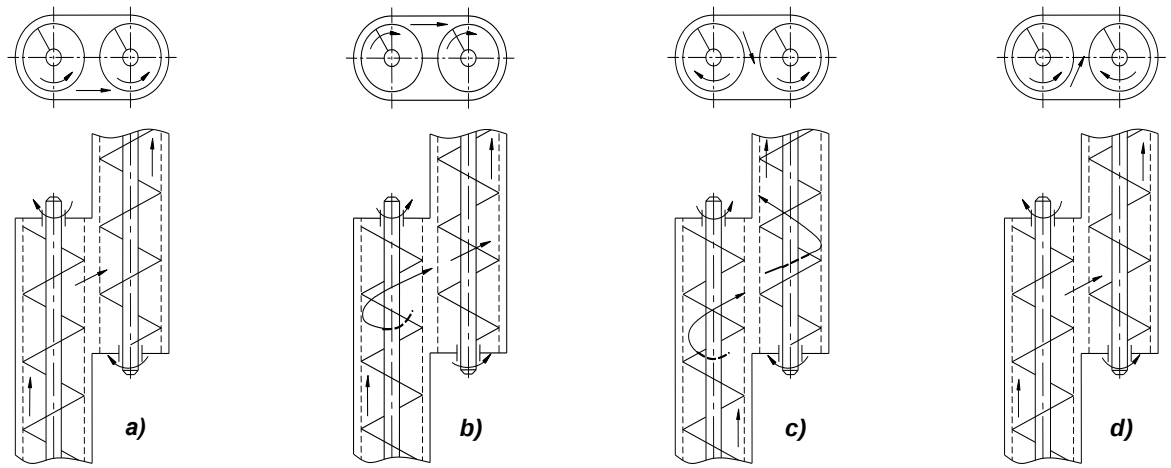

Fig.1 - Diagrams of the directions of bulk load transfer from an uploading pipe line to an unloading one

In the other alternative, bulk load transfer in a transfer branch can be provided by spirals turning in different directions for transferring from a loading pipe line to an unloading one at the point of transfer (Fig.1, c, d).

Design concept and overview of a transfer branch of a screw conveyer are represented in Fig.2.

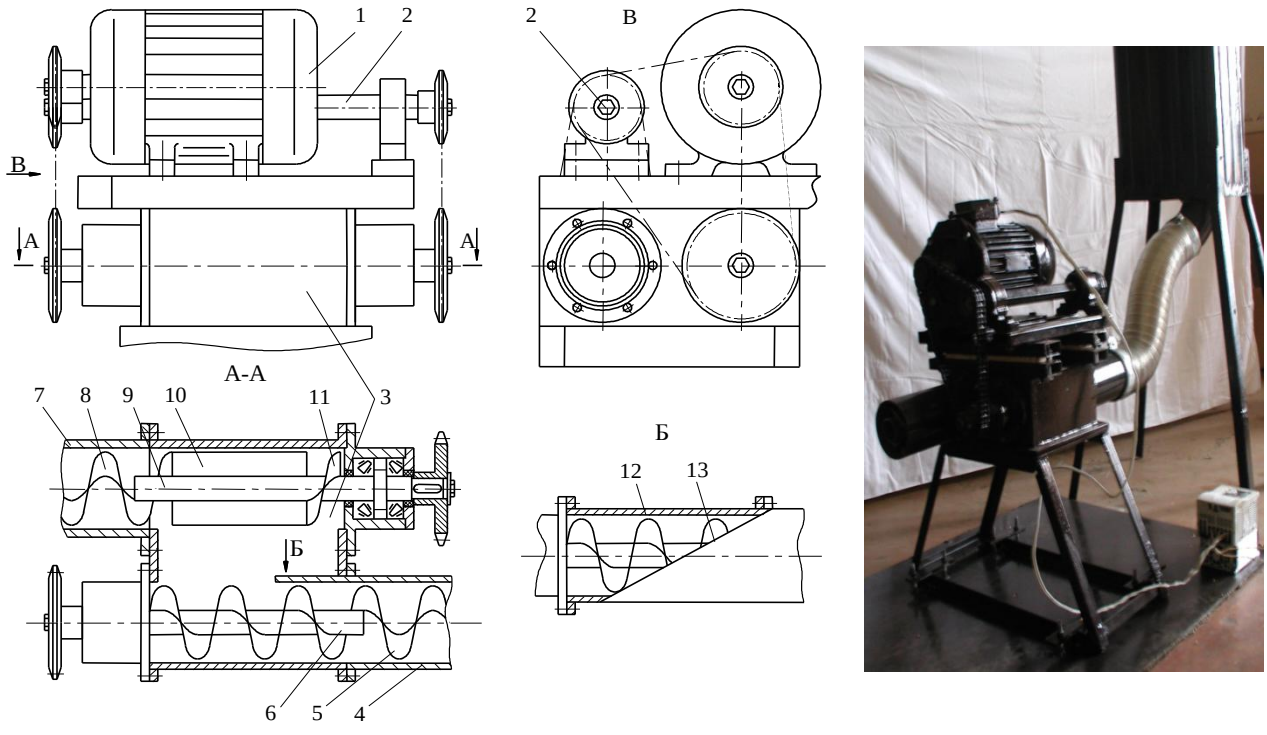

Fig.2 – Design concept (a) and overview (b) of a transfer branch of a flexible screw conveyer

It contains uploading and unloading pipe lines, which are made in the form of casings *7* and *4* and uploading *8* and unloading *5* operating screw helixes mounted in parallel, which are attached on driving shafts *9* and *6* respectively. A countershaft *2* is arranged in parallel with driving shafts fixed on a transfer branch *3*; driving and counter shafts outside a transfer branch are joined in kinematics terms with an electric motor shaft *1* and placed in a horizontal plane. Radial plates *10* are attached on a shaft *9*, and on the other side there is a sector of a screw helix *11*, which coiling direction is the opposite of the one of an operating loading screw helix *8*. An unloading screw helix *5* in a transfer branch is arranged in a conductor cylindrical tube *12*, where there is a wedge-shaped cut out *13* made on the side of radial flat plates.

While in operation, kinematically joined driving shafts, a counter shaft and an electric motor shaft provide the rotation of operating screw helixes. While feeding bulk load, a helix *8* transfers it in a casing towards a transfer branch. Since driving shafts are arranged in a horizontal plane, material feeding on an unloading pipe line is carried out by radial flat plates. A sector of a screw helix *11* provides bringing of the whole bulk load mass together on radial flat plates in order to avoid congestion. Further, bulk load gets onto an unloading operating screw helix, which draws it into a wedge-shaped cut out in a tube *12* and moves it in a casing towards the unloading area. Availability of a wedge-shaped cut out provides gradual input of material into a cylindrical tube that changes into a casing *4*, which facilitates the decrease in damaging bulk load.

Arrangement of shafts in a horizontal plane with the use of radial plates and a conductor cylindrical tube with a wedge-shaped cut out provides the transfer of bulk load from an uploading pipe line to an unloading one in a horizontal plane, which facilitates the increase in operational reliability of a conveyer at general decrease in energy consumption. In addition, torque, which acts upon every operating device, is reduced, which enables proportional increase of the length of transportation.

In order to investigate the conveying of material, a mathematical model of the process of bulk load transfer in a transfer branch has been developed as:

$$\omega_B = \frac{\omega T\left(T - \mu\pi D \operatorname{sgn}\omega\right)}{\left(\pi D\right)^2 + T^2}$$

$$T_B = T\left(1 - \frac{\omega}{\omega_B}\right) \qquad (1)$$

$$v_0 = \frac{\omega T T_B}{2\pi\left(T - T_B\right)}$$

where ω_B - angular velocity of the rotation of the material transported; T - pitch of a screw; T_B - pitch of a helical line of load conveying; ω - angular velocity of screw rotation; μ - friction coefficient of the material conveying along the screw surface taking into consideration capillary phenomena; D - screw diameter; v_0 - axial velocity of load conveying.

In the system (1) it is customary, that the value for leftward screws is $\operatorname{sgn}\omega = -1$, and for rightward ones it is $\operatorname{sgn}\omega = 1$. The determined mathematical model is applicable for high-speed screws, which specific speed is $\frac{\omega^2 D}{2g} > 1$.

Suppose, the entry of a screw into a transfer branch is perpendicular to the axis of a screw and load throwing is carried out on the half of an open flight rightwards in case of axial feeding of an observer, as it is shown in Fig.3.

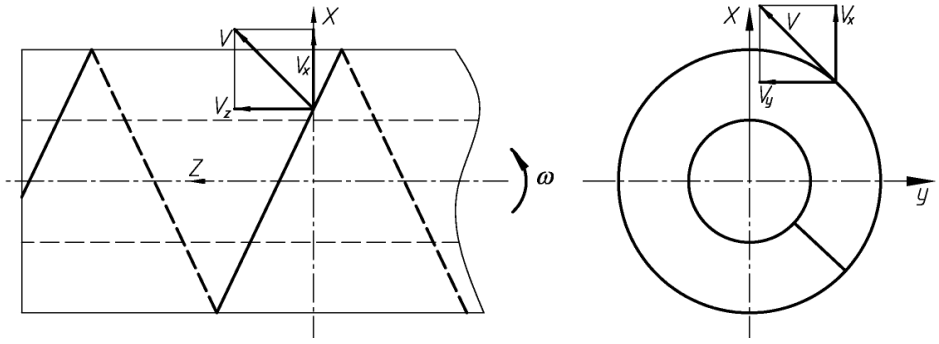

Fig.3 – Design diagram for determination of bulk load movement

In case of a rightward screw, which turns in counter clockwise direction, load throwing is done at a screw entry from below a screw; in case of a leftward screw load throwing in carried out from above.

For both of the cases mentioned, dependencies to determine the points of throwing and escaping velocity of load particles have been deduced:

In case of a rightward helical spiral:

$$\begin{aligned} X_B &= R\sin\omega t;\\ Y_B &= R(1-\cos\omega t);\\ Z_B &= 0;\\ v_x &= \omega_B R\cos\omega t;\\ v_y &= \omega_B R\sin\omega t;\\ v_z &= v_0; \end{aligned} \tag{2}$$

In case of leftward helical spiral (suppose $\omega > 0$, however, turning is in clockwise direction):

$$\begin{aligned} X_B &= R\sin\omega t;\\ Y_B &= R(1+\cos\omega t);\\ Z_B &= 0;\\ v_x &= \omega_B R\cos\omega t;\\ v_y &= -\omega_B R\sin\omega t;\\ v_z &= v_0, \end{aligned} \tag{3}$$

where X_B, Y_B, Z_B – coordinates of a point of separation of a particle from a screw; v_x, v_y, v_z - components of particle velocity along corresponding axis; $R = D/2$ - radius of a screw.

A particle moves under predetermined starting conditions until its interaction with the bottom surface of a screw for the time, which is determined under free fall under the influence of gravity acceleration:

$$t = \frac{\sqrt{v_y^2 + 2gY_B} + v_y}{g} \tag{4}$$

Coordinates of a particle fall point are calculated according to the following dependencies:

$$\begin{aligned} X_P &= X_B + v_x t\\ Z_P &= Z_B + v_z t. \end{aligned} \tag{5}$$

RESULTS

Dependency of coordinates of a conveying load fall point on a change of various parameters of operating devices has been investigated with the help of a Delphi program with graphical presentation of results. The results of the analysis are represented in the form of graphical dependencies (Fig.4).

Having analysed graphical dependencies (Fig.4, a), it has been stated that particles of conveying material are thrown at a distance of 40–60 mm (parameter XP), which provides their reaching a receiving (unloading) screw without causing congestion. Positive value of ZP shows, that longitudinal direction of particle flow takes place in the direction of the conveying material; that is why, mutual axial displacement of feeding and receiving screws by the amount, which is approximate to that of a half pitch of a screw, is reasonable.

As a result of the investigation, it has been determined, that inside a transfer branch there should be about two flights of each screw in order to provide load transfer without causing congestion and damage.

In order to have reliable transfer of bulk load, which gets from a leftward screw to a receiving one, the latter should be made in such a way as to capture material inside an operating device of a bottom surface of a branch, that is to say, this screw needs to be rightward.

As a result of the analysis of graphical dependencies (Fig.4, b, c, d), it has been stated that for the improvement of transfer process a pitch of a screw and a friction coefficient of material are of importance. Minor dependence of the distance of throwing on the diameter of a screw can be explained by the fact, that for a stable pitch, an increase in the diameter results in an increase in the helix angle of a screw.

Having analysed graphical dependencies (Fig.4, a), it has been stated that particles of conveying material are thrown at a distance of 40–60 mm (parameter X_P), which provides their reaching a receiving (unloading) screw without causing congestion. Positive value of Z_P shows, that longitudinal direction of particle flow takes place in the direction of the conveying material; that is why, mutual axial displacement of feeding and receiving screws by the amount, which is approximate to that of a half pitch of a screw, is reasonable.

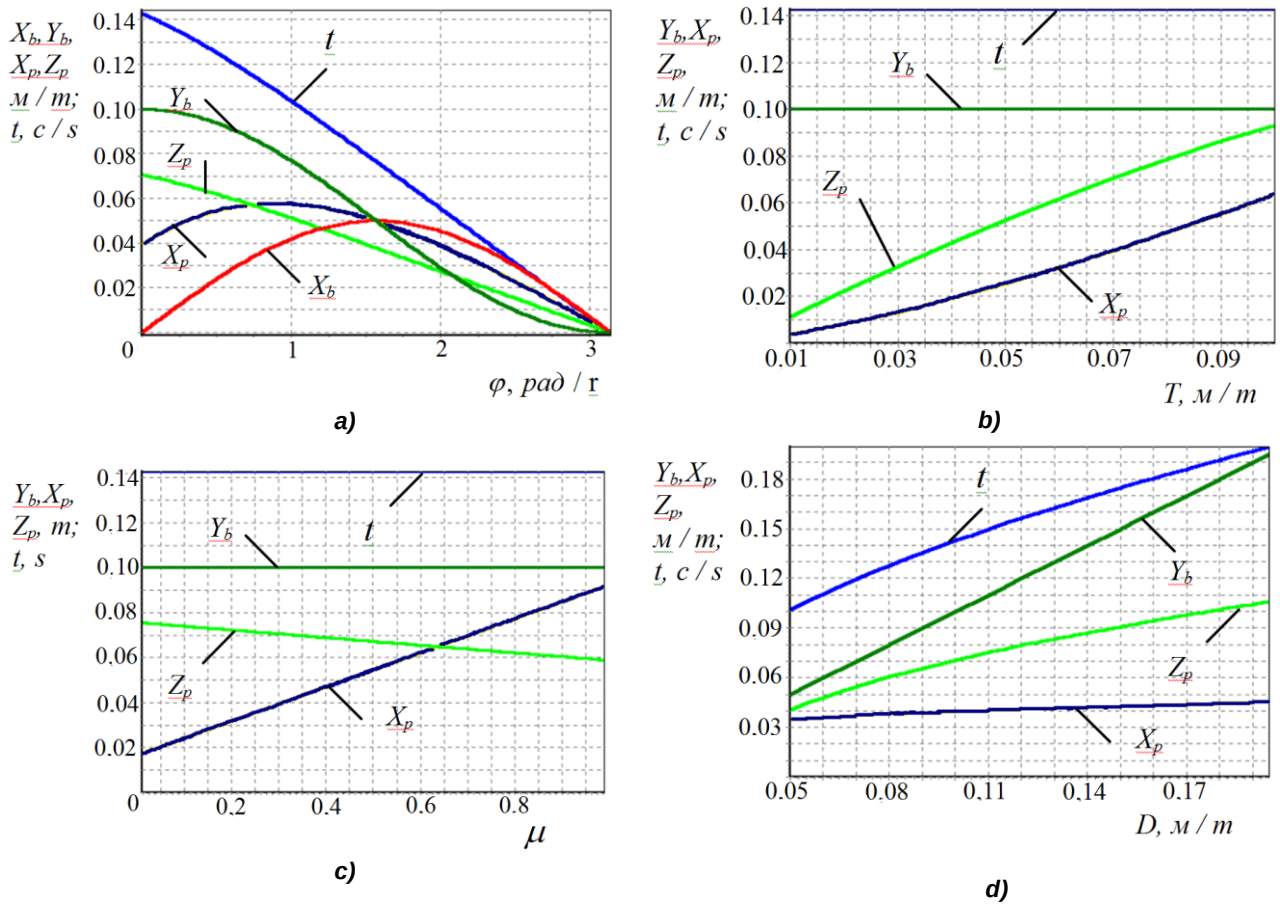

Fig.4 – Dependency of a point of separation of material from an operating surface and a point of its fall on the surface of a screw when being thrown by a leftward screw

a) on an angular velocity; b) on a pitch; c) on a friction coefficient; d) on a diameter

As a result of the investigation, it has been determined, that inside a transfer branch there should be about two flights of each screw in order to provide load transfer without causing congestion and damage.

In order to have reliable transfer of bulk load, which gets from a leftward screw to a receiving one, the latter should be made in such a way as to capture material inside an operating device of a bottom surface of a branch, that is to say, this screw needs to be rightward.

As a result of the analysis of graphical dependencies (Fig.4, b, c, d), it has been stated that for the improvement of transfer process a pitch of a screw and a friction coefficient of material are of importance. Minor dependence of the distance of throwing on the diameter of a screw can be explained by the fact, that for a stable pitch, an increase in the diameter results in an increase in the helix angle of a screw.

As a result of the experimental investigations conducted, it has been stated, that the productivity of a transfer branch Q increases proportionally to an increase in the frequency of the rotation of operating devices n and decreases with an increase of a slope angle of a screw body to the horizon. Over the range of n changing from 300 RPM to 800 RPM Q increases in 2-2.4 times, while as changes from 0º to 30º Q decreases in 45-55%.

As a result of a multiple-factor experiment, regression equation has been obtained; after its analysis it has been determined, that for the designed transfer branch, over the range of the parameter change of $96 < D < 98$ (mm); $300 < n < 700$ (RPM) and $0 < \alpha < 30$ (degrees) the dominant factor, which influences the degree of grain material damage is the value of clearance between the rotating surface of an operating device and a casing, next it is the frequency of its rotation and a slope angle of a transfer branch to the horizon.

CONCLUSIONS

Having reviewed patents and existing research works on the operation of transfer branches in screw conveyers, a new design of a transfer branch has been suggested, which enables to increase the length of material conveyance at generally lower energy consumption. Having analysed process flow sheets of the

possible options of bulk load conveying, a transfer branch has been developed and made.

Theoretical investigation of the process of bulk load transfer with the help of a screw operating device of a conveyer in a horizontal transfer branch has been carried out.

It has been stated that feed particles are thrown by a feeding screw at a distance of 40-60 mm in the axial direction, that is why, mutual axial displacement of feeding and receiving screws by the amount, which is a half pitch of a screw, is reasonable. From analysis of graphical dependencies it follows, that in the middle of a transfer branch there should be about two flights of each screw in order to provide material transfer without congestions and damage. In addition, it has been determined, that a pitch of a screw and a friction coefficient of material are of importance and a screw diameter counts little. That is why, it is reasonable to choose the diameter of a screw according to the productivity, and a pitch value as T = (0.6-0.8) D.

The results represented in the article may be used for engineering design of a transfer branch of a flexible screw conveyer.

REFERENCES

[1] Boyko A.I., Kulikiskiy V.L., (2011), Investigation of contact grain interaction in gap “coil-jacket” of screw feeders grain cleaning machines (Дослідження контактної взаємодії зерна в зазорі “виток-кожух” шнекових живильників зерноочисних машин). *Scientific Bulletin of NUBiP-K.: Red species*. Department NUBiP 201, Vol.166, Engineering and Energy AIC, P.1, pp.267-274;

[2] Hevko R.B., Klendiy O.M., (2014), The investigation of the process of a screw conveyer safety device actuation, *INMATEH - Agricultural Engineering Journal*, vol.42, no.1, pp.55-60, Bucharest/Romania;

[3] Hevko R.B., Dzyura V.O., Romanovsky R.M., (2014), Mathematical model of the pneumatic-screw conveyor mechanism operation, *INMATEH-Agricultural Engineering Journal*, vol.44, no.3, pp.103-110, Bucharest/Romania;

[4] Hevko R.B., Zalutskyi S.Z., Tkachenko I.G., Klendiy O.M., (2015), Development and investigation of reciprocating screw with flexible helical surface, *INMATEH - Agricultural Engineering Journal*, vol. 46, no.2, pp.133-138, Bucharest/Romania;

[5] Hevko R.B., Vitrovyi A.O., Pik A.I., (2012), Advance in technology of flexible screw conveyers: monograph *(Підвищення технічного рівня гнучких гвинтових конвеєрів: монографія)*, p.204, Aston, Ternopil;

[6] Hevko R.B., Klendiy O.M., (2013), Methodology of investigation of a screw conveyer with a safety device (Методика проведення досліджень шнекового транспортера із запобіжним пристроєм), *Agricultural Machinery: Scientific works. (Сільськогосподарські машини: Збірник наукових статей)*, no.24, Edition of Lutsk NTU, pp.67–75, Lutsk;

[7] Hevko R.B., Hlado U.B., Shynkaryk M.I., Klendiy O.M., (2014), Dynamic calculation of a safety device of a screw conveyer (Динамічний розрахунок запобіжного пристрою шнекового транспортера), *Bulletin of Engineering Academy of Ukraine (Вісник інженерної академії України),* no.2, pp.163–168, Kyiv;

[8] Klendiy M.B., (2006), Investigation of transfer process of bilk load by screw operating devices (Дослідження процесу перевантаження сипкого вантажу гвинтовими робочими органами), *Bulletin of Ternopil Ivan Puliui State Technical University (Вісник Тернопільського державного технічного університету імені Івана Пулюя),* Vol.3, pp.92-100, Ternopil;

[9] Klendiy M.B., Hevko R.B., (2005), Methodology of investigation of new types of transfer branches of screw conveyers (Методика досліджень нових типів перевантажувальних патрубків гвинтових конвеєрів), *Scientific Works of Vinnytsia State Agrarian University (Збірник наукових праць Вінницького державного аграрного університету),* Vol.20, pp.190–195, Vinnytsia;

[10] Klendiy M.B., (2007), Development and parameters validation of paddle conveyor-mixer design (Розробка конструкції та обґрунтування параметрів лопатевого транспортера-змішувача), *Scientific Bulletin of National Agricultural University,* Vol.92, P.2, pp.533-540.

INVESTIGATION OF THE RADIUS OF BENDING FOR FLEXIBLE SCREW SECTIONAL CONVEYERS
/
ДОСЛІДЖЕННЯ РАДІУСА ЗГИНУ ГНУЧКИХ ГВИНТОВИХ КОНВЕЄРІВ З СЕКЦІЙНИМИ ЕЛЕМЕНТАМИ

Prof. PhD. Eng. Hevko Iv.B., Prof. Ph.D. Eng. Lyashuk O.L., Lect. Ph.D. Eng. Leshchuk R.Y., Rogatinska L.R., Melnychuk A.L.
Ternopil Ivan Pul'uj National Technical University /Ukraine
E-mail: Oleg-lashyk@rambler.ru

***Keywords**: screw operating member (SOE), transportation, minimum radius of bending, angle of twist*

ABSTRACT

Method of calculation of radius of bending for the flexible screw sectional conveyer was presented. Analytical dependencies for finding maximal turning radius in order to provide the reliable operation of the mechanism were defined. The stand construction for investigation of the angle of twist of the sectional operating members was developed. The effect of different construction parameters (section length, diameter) on their operating life characteristics as well as the comparative testing of different types screw operating elements (SOE) samples, were found. The technique of testing the working bodies of flexible screw conveyor sections for manufacturability of a construction, which provides a minimum bend radius of track transportation, was presented.

РЕЗЮМЕ

Наведено методику розрахунку радіуса згину гнучкого гвинтового конвеєра з секційними елемента. Виведено аналітичні залежності для визначення оптимального значення радіуса повороту з метою забезпечення надійної роботи механізму. Розроблена конструкція стенд для дослідження кута закручування секційних робочих органів і встановлено вплив різних конструктивних параметрів (довжина секції, діаметр) на їх ресурсні характеристики, а також порівняльні випробування різних типів дослідних взірців гвинтових робочих органів ГРО. Наведено методику відпрацювання робочих органів гнучких гвинтових секцій конвеєрів на технологічність конструкції, яка забезпечує мінімальний радіус згину траси транспортування.

INTRODUCTION

In modern agricultural mechanical engineering, elevating-transporting and other vehicles screw transporting-technological systems (STTS), the principle of operating members such as flexible screw mechanisms, are of great importance, high requirement being held for the reliability and durability of these mechanisms operation, providing high engineering-economic indices and low expenditures for operation and maintenance of the agricultural machine. From the point of view of mechanism operation reliability, determination of the acceptable and maximal radius of the operating member bending is of importance while using flexible screw conveyer sectional operating member.

The objective of the work is to develop the method for finding the radius of bending for the sectional operating member in order to provide its operational and technological parameters.

The papers by A.M. Grygoriev, S.M. Mykhailov, K.D. Vaschagin, B.M. Gevko, R.M. Rogatynsky, O.Trufanov, H. German, M.I. Pylypets etc., are devoted to the theoretical interpreting of the flexible screw transshipment mechanisms operation, methods of calculation of their basic parameters, development of advanced constructions of such means of bulk materials mechanized transporting along the curved routes. There are also other important authors works which include preoccupations in this research field *(Hevko R.B. et al., 2012; Hevko B.M., 1993; Hevko B.M., Rohatynsky R.M., 1989; Hevko I.B., 2008; Hevko B.M., et al, 2008)*. In many works are developed the main principles of construction and modelling of screw conveyors, such as *(Fernandez J.W. et al, 2009; Hu G. et al, 2010; Owen P.J. and Cleary P.W., 2009; Zareiforoush H. et al, 2010)*.

Analysis of key principles in the design of flexible screw conveyers (FSC) testifies that the single point of view on the essence of the phenomena observed during operation of such means of mechanization is not available. Special attention in the analysis of the previous investigations is paid to

those papers, in which the problem of the choose of operating members parameters and the processes of transporting grain, granular fertilizers, etc., are analysed, as the problem of the bulk materials damage has not been studied enough yet.

MATERIAL AND METHODS

Stand for investigation of the STTS sectional operating member angle of twist is presented in Fig. 1. It consists of the body *1*, to which the stick *2* is mounted rigidly and on which operating member *3* is fixed, which is freely set in the U-shaped box. The box is fixed on the base *5* with supporting elements *6*. Free end of the sectional operating member is inserted into the holder hole *7*, on the right end of which the Nonius scale is made. In order to investigate different length operating members the holder is located on the guides, which make possible to change its position. On the free end of the operating member, which overhands from the holder hole, the bush with the arrow *10*, which has the ability of angle displacement while screw tightening, and calibrated level *12*, the size of which is determined by the loading capacity of the operating member, is fixed rigidly.

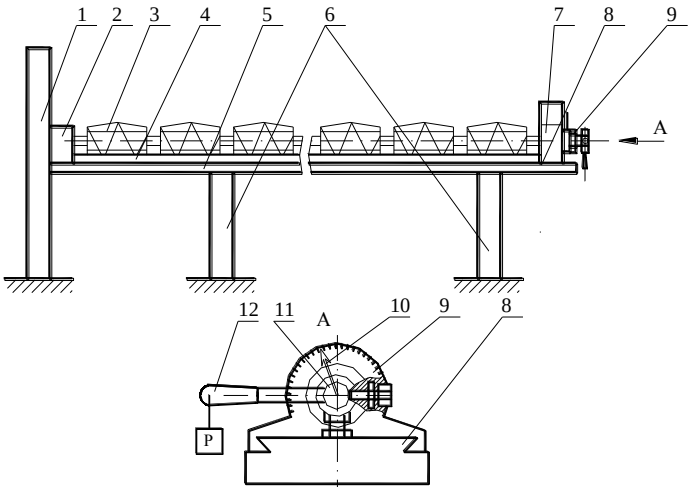

Fig.1 – Stand for investigation of the sectional operating member angle of twist

Rigidity of the screw operating member as well as the SOE sectional elements wear are found according to the angle of twist value. To find the screw spirals torsion rigidity, the curvature radius effect on the spirals operation reliability, to determine the most dangerous areas in the SOE constructions elements under overloading, experimental stand presented in Fig.2 was used. It is designed for static, dynamic and operating life testing and comparative estimation of different construction parameters operating member's structures. The stand consists of the frame *7*, on which the generator *1* (namely, engine 4PF112LVB04) is mounted on the turning plate *3*, which is bolted by the screw joints *2* and *4* to the guiding channel *6*. The guiding channel is fixed to the frame *7* and its fitting in the given position is provided by the bolt joint *5*. Besides, the stand is provided with the three-phase induction asynchronous motor *10* (AIP90L4Y3), which is mounted on the displaceable plate. Investigated SOE *8* is fixed on the motor output shafts *1* and *10* by means of either the flanged joints or the flanged joints and the safety clutch *9*.

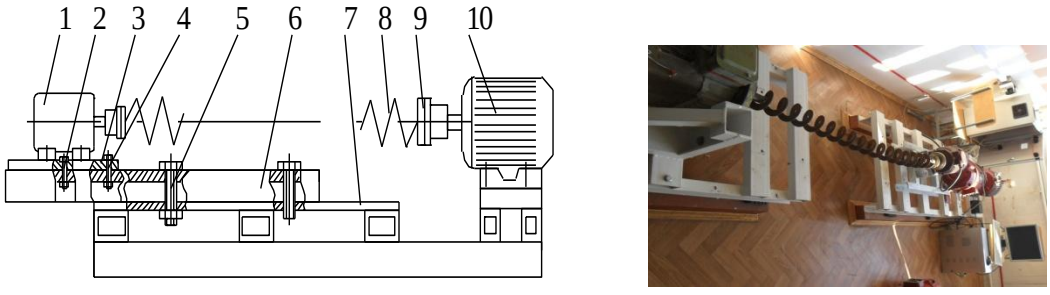

a) **b)**

Fig.2 - Stand for investigations of the screw spirals tortion rigidity: a) scheme; b) general view

Investigations of the screw spirals torsion rigidity, taking advantage of this stand, are carried out as follows. The investigated object *8* is placed on the generator *1* and motor *10* shafts and the necessary spiral curvature radius is set with the help of the displaceable plate. As the motor can be displaced in the longitudinal and transversal directions, different length and configuration spirals can be tested on this stand. Then, is run following PC connection to the power supply source (Fig.2) and software PowerSuit for tuning of Altivar 7.1 series transformers frequency. Frequency of the motor rotation was controlled automatically from 0 till 1460 rev/min. Besides, smooth and sharp starting and reversing were performed, if needed. The generator (d.c. motor 4PF112LVB04) worked as brake, which was operating with the separate excitation to make the required loading on the investigated object possible. That is why the current comes from the stabilizer to the (laboratory automatic transformer), where its regulation (U-const) to the required value (I=0…4A) is carried out and then through the rectifier (diode bridge) it is transferred to the generator stator excitation winding. Accordingly, the excitation winding current changes the generator loading current (resultant generator magnetic field) and, thus, the generator consumption power is changed. Exact data on the rotation frequency on the motor shaft (error within ± 1.5 %) is recorded, taking advantage of the motor shaft rotation frequency meter (E40S6-10Z4-6L-5), which is connected to the motor rotor.

Since operation characteristics of any elevator flexible operating member are determined by the radius of its bending, this parameter specifies the level of the production effectiveness of such transporting member. The value of the radius of bending is to be known while their designing for the loads transporting along the curvilinear routes, the designer being able to provide required technological capabilities of the device and purposefulness of its application. To find this parameter one should follow the calculation scheme presented in Fig.3.

The value of bending of the screw operating member under absolute rigidity according to the required linear sizes is equal to its general linear length. According to the calculation scheme the relation between the bending length and the screw element radius is:

$$l_{bend} = \frac{2\alpha \cdot \pi R_{bend}}{180^{\circ}} \tag{1}$$

The radius of bending can be expressed by the distance between the device bended operating member ends due to L parameter. According to the calculation scheme the radius of bending equals (*Leschuk R.Y., 2003*):

$$R_{bend} = \frac{L}{2 \cdot \sin \alpha}, \tag{2}$$

where:

L – linear distance between the screw elements ends;

α – angle of bending of the screw element sections.

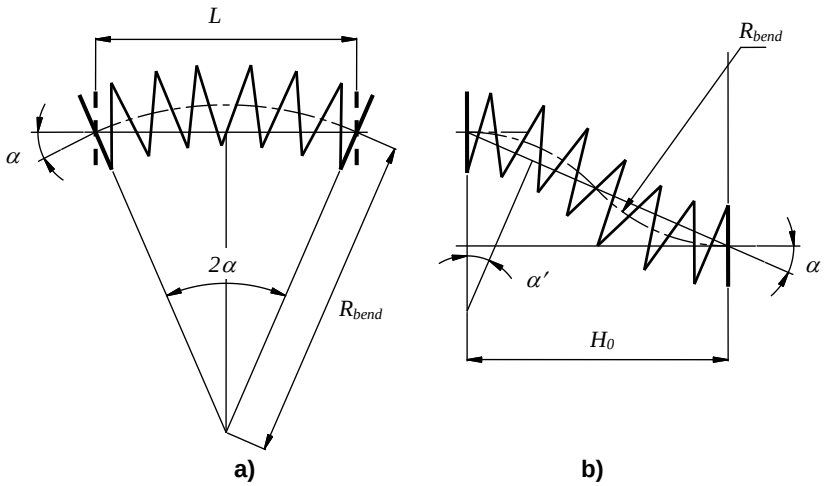

Fig.3 - Calculation scheme for finding the radius of bending for the elevator flexible screw member:

a) bending rout along the radius; b) bending rout along the curve

Having substituted the values of equality (2) in the dependence (1), the value of the elevator screw operating member bending length will be obtained:

$$l_{bend} = \frac{\pi L \alpha}{180^{\circ} \sin \alpha} = \frac{\alpha \cdot L}{\sin \alpha}. \quad (3)$$

In the case of two bending paths, the radius of bending is worthy being determined from the dependence:

$$R_{sr.p} = \frac{L \cdot \sin \alpha}{4 \cdot \cos \alpha} = 0{,}25 \cdot L \cdot \mathrm{tg}\alpha. \quad (4)$$

The length of bending (linear length of the screw operating member) is found from the dependence:

$$l_{bend} = 0{,}5L \cdot \mathrm{tg}\alpha \cdot \pi \cdot 2\alpha. \quad (5)$$

However, such important parameter as the angle of bending of the elevator sections α is still unknown. To find this parameter and the dependence of the angle of bending of the flexible screw operating member on the other structural parameters, one should take advantage of the calculation scheme presented in Fig.4. Thus, to find the analytical dependencies, which are used to calculate the angle of bending of one section relatively the other one, we should consider triangle Δ abc, according to which (*Hevko B.M. and other, 2008; Leschuk R.Y., 2003)*:

$$\mathrm{tg}\alpha = \frac{cb}{ac} = \frac{D_B - d_B - 2s}{B} \quad (6)$$

where:

D_B – outer diameter of the elevator sections bushes;

d_B – diameter of the joint rolls;

s – thickness of bushes;

B – width of bushes.

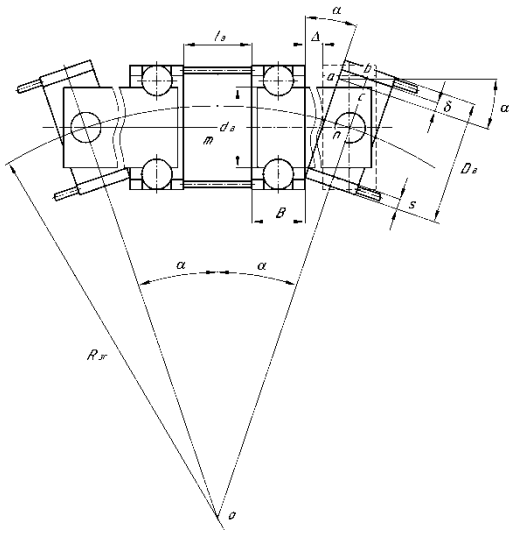

Fig.4 - Calculation scheme for finding the minimal radius of bending for the screw sectional operating members elevator

To find the angle of bending let us consider triangle Δ omn. According to the calculation scheme, presented in Fig. 4, the radius of bending Rbend will equal:

$$R_{bend} = on = \frac{mn}{\sin \alpha}. \quad (7)$$

According to the calculation scheme the value *mn* equals:

$$mn = l_B/2 + B + \Delta + B/2, \quad (8)$$

where:

l_B – distance between the bushes in one section,

Δ – gap between the adjacent sections

Taking into account equations (6) and (8), the dependence (7), which determines the minimal radius of bending of the sectional elements elevator operating members, will look like:

$$R_{bend} = \frac{1{,}5B + l_B + \Delta}{2\sin\left(\text{arctg}\left(\frac{D_B - d_B - 2s}{B}\right)\right)}. \quad (9)$$

RESULTS

Special stand equipment was used for the operating life testing of the strain-strength characteristics of the flexible sectional SOE (Fig.2). At the beginning of the operating life testing measuring of the angle twist of the sectional SOE with the hinged joint (Fig.9, a) and safety joint (Fig.9, b) on the stand for testing the angle of twisting of sectional SOE, were carried out. The next stage was operating life testing (under loading) on the stand for investigation of the strain-strength characteristics of the screw spirals (Fig.6). Then, equal periods of time (10 hours) repeated for measuring of the angle of twisting of the sectional SOE on the stand were carried out to investigate the angle of twisting of sectional SOE. In Fig.5 graphic dependencies of the radius of bending value change of the screw conveyer on the construction parameters of the sectional elements, are presented.

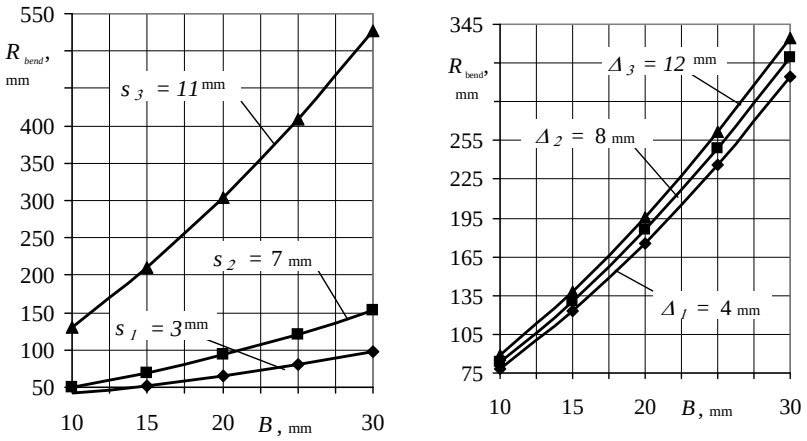

Fig.5 - Graphical dependences of the radius of bending value change of the screw conveyer on the construction parameters of the sectional elements

According to the embodiment of the working body of the ratio between the angular velocities master and slave sections for a full rotation will be:

$$\frac{\omega_2}{\omega_1} = \frac{\cos(arctg(D_B - d_B - 2s)/B}{1 - \sin^2(D_B - d_B - 2s)/B} \quad (10)$$

Analyzing the obtained graphical dependencies (Fig.5) of the flexible screw conveyer radius of bending change on the construction parameters of the operating members sections, one can conclude, that the thickness of the bush S together with the width of the bushes B are sufficient to influence this value. Thus, when the value S is increased within 3...11 mm and B equals 10; 15; 20; 25; 30 mm under constant value D_B=60mm; d_B=45mm; l_B=50mm; Δ=10mm, the radius of curvature increases within 41.4…125.5 mm and 95.1…531.6 mm, that is, in 3.2…5.8 times. Thus, sufficient limitation of the device technological capabilities occurs, as the radius of bending must be minimal. Under similar data of these construction parameters, but while changing the gap size between the adjacent sections Δ within 4…12 mm, the radius of bending varies within 76.3…314.1; 90.4...336.5 mm. According to the investigations the device with the less width of the bush sections will be more production effective, as under similar productivity and operating life time of operation will take less manufacturing areas.

As the result of the carried out investigations it was found that the angle of twist for the sectional SOE with the hinged and safety joints (SOE length L=2m) did not exceed 9°. Before the operating life testing the angle of twist for the investigated sectional SOE did not exceed 3.2°. At the initial stage of the operating life testing (after 10 hours of operation) the angle of twist for both sectional SOE has increased sharply, which can be caused by the wearing out of SOEe screw construction elements. Further its increase was slowed down and stabilization was observed.

In Fig.6 dependencies of the sectional SOE angle of twist on the operating time are presented (turning diameter–96 mm, section length–130 mm, SOE length–2 m, loading on SOE–12 Hm, frequency of rotation–426 rev/min under radius of bending – R_{bend} = min and under the straight SOE – R_{bend} = 0).

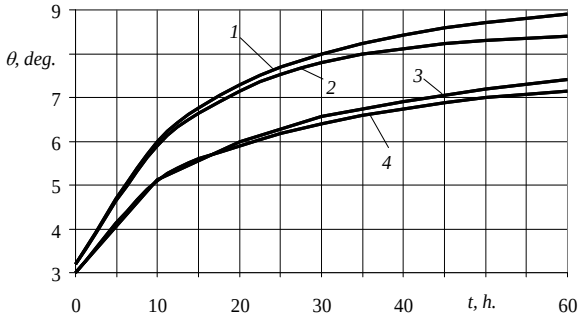

Fig.6 - Dependence of the sectional SOE angle of twist on the operating time:
1 – with the hinged joint under R_{bend} = min; 2 – with the safety joint under R_{bend} = min; 3 – with the hinged joint under R_{bend} = 0; 4 – with the safety joint under R_{bend} = 0

Angular acceleration of the master section for a uniform rotation of the slave unit is expressed by:

$$\beta_2 = \omega_1^2 \frac{\sin^2(arctg\frac{D_B - d_B - 2s}{B})\cos(arctg\frac{D_B - d_B - 2s}{B})\sin 2\alpha}{(1-\sin^2(\frac{D_B - d_B - 2s}{B})\sin^2\alpha)^2} \quad (11)$$

Accordingly, coefficient of irregularity rotation of the slave section:

$$k = tg(arctg(\frac{D_B - d_B - 2s}{B}))\sin(arctg(\frac{D_B - d_B - 2s}{B})) \quad (12)$$

Torque at an intermediate section is determined from the relationship:

$$T_{n.c.} = T\sqrt{1+tg^2(arctg(\frac{D_B - d_B - 2s}{B}))\cos^2\alpha} \quad (13)$$

where:

T – torque that acts on slave section.

As a result was built graphical dependence (Fig.7, Fig.8) in analysis of which we can conclude that they are close to the straight line of law distribution.

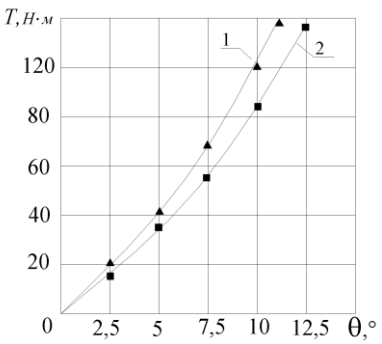

Fig.7 - The dependence of the torque T from the angle of twisting θ working unit for one section:
1 - l = 100 mm, 2 - l = 130 mm

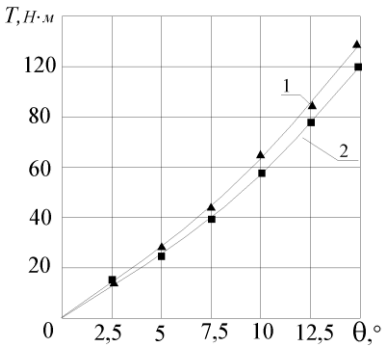

Fig.8 - The dependence of the torque T from the angle of twisting θ working unit for two section:
1 - l = 100 mm, 2 - l = 130 mm

As seen from (Fig.7 and Fig.8.) the increase of the length of the section naturally leads to a proportional increase in the maximum angle of twist and hinge joint almost has no effect on the amount of strain, as its stiffness is much higher than the stiffness of the section. It has been found that maximum torque T_{max} that results in a breakdown of the section of working unit is much larger than the torque required for handling bulk cargo by designed working unit at maximum working height of handling and minimal radius of curvature of pipeline.

Basing on the presented calculations screw sectional elements operating members were designed and manufactured, which are presented in Fig. 9. The results of the carried out investigations testify that the period of running-in in the idle regime of the sectional SOE must be carried out in order to provide the fitting of SOEe construction elements, which should be followed by the maintenance inspection. However, existing screw operating members (SOE) constructions are often exposed to dynamic loadings in starting and operating conditions during the operation. Therefore, we have developed a number of advanced constructions with elastic and safety connections that help us to improve the reliability and durability of flexible screw conveyers (FSC) and also help to avoid their failures. They allow to ensure a smooth launching of screw operating members (SOE) during starting an engine and during operation and also they avoid failures from dynamic loadings. Flexible screw conveyers (FSC) as shown in the image 10.a, allow us to compensate for starting loadings on screw operating members (SOE) by using compensation connection. The image 10.b shows us a flexible helical spring working body which provides compensation starting loads as well as those that arise in the process of transporting the material *(Hevko I.B., Melnychuk A.L., Shust I.M., 2015; Hevko I.B., Komar R.B., Leschuk R.Y., Novosad I.Y., 2005)*. Fig.10.c shows a helical spiral with safety cone-shaped cam connection sections, which provides separate sections of screw operating members (SOE) during the critical loadings, that helps us to avoid faults of elements of flexible screw conveyers (FSC).

The developed models of the screw operating members (SOE) and flexible screw conveyers (FSC) with sectional elements can be widely used in the food processing branches of industry, agriculture, as well as in technological processes of mechanized loading of mineral fertilizers, seeds and grains due to the improved technological capabilities while decreasing the radius of its bending and raising reliability as the result of the improved construction.

a) b)

Fig.9 - Sectional screw operating members with a) hinged joints; b) safety joints

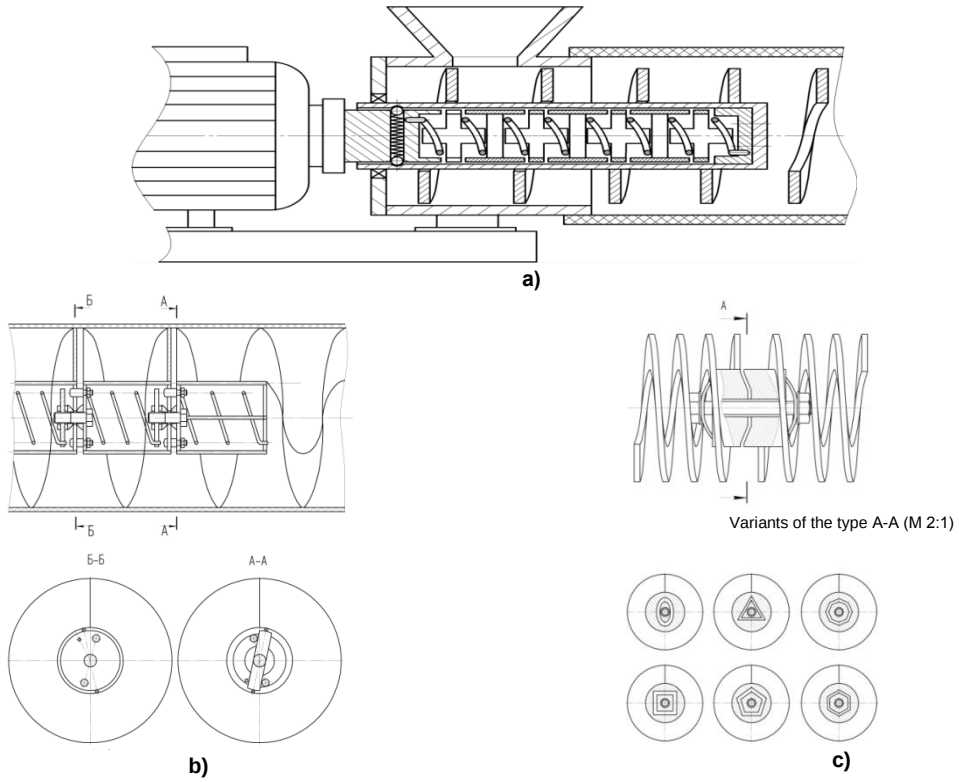

a) b) c)

Fig.10 - Flexible screw conveyers:

a) connection with compensation; b) elastic flexible screw working body;
c) flexible screw working body with conical cam precautionary connection sections

CONCLUSIONS

1. The developed models of the screw operating members (SOE) and flexible screw conveyers (FSC) with sectional elements can be widely used in the food processing branches of industry, agriculture, as well as in technological processes of mechanized loading of mineral fertilizers, seeds and grains due to the improved technological capabilities while decreasing the radius of bending and raising reliability as the result of the improved construction

2. Construction stand for investigation of the sectional operating member angle of twist has been developed. Dangerous radii of the spiral curvature and critical loadings, which cause the SOE fracture, have been found. The effect of different construction parameters (section length and diameter) on their operating life characteristics has been determined. Comparative testing of different types SOE samples, have been carried out.

3. Basing on the carried out investigations analytical dependencies for finding the radius of bending of the sectional flexible screw conveyer, depending on the sections construction parameters, have been derived. Graphical dependencies of the change of radius of bending value of the sectional operating member on the sectional elements construction parameters have been found. The change of the minimal radius bending is affected by the turn thickness comparatively with its width, the angle of bending for the sectional SOE with hinged and safety joints (SOE length = 2m) not exceeding 90°.

REFERENCES

[1] Hevko R.B., Vitrovyi A.O., Pik A.I., (2012), *Advance in technology of flexible screw conveyers: monograph (Підвищення технічного рівня гнучких гвинтових конвеєрів: монографія)*, p.204, Aston, Ternopil;

[2] Hevko B.M., (1993), *Mechanisms with screw devices. High school* (*Механізми з гвинтовими пристроями. Вища школа*), p.205, Lviv;

[3] Hevko B.M. Rohatynsky R.M., (1989), *Screw feeding mechanisms of agricultural machines. High school* (*Винтовые подающие механизмы сельскохозяйственных машин. Вища школа*), p.175, Lviv;

[4] Hevko I.B., (2008), *Screw transporting-technological mechanisms. Calculation and designing (Гвинтові транспортно-технологічні механізми. Розрахунок і конструювання),* TNTU, p.307, Ternopil;

[5] Hevko B.M. et al., (2008), *Technological bases of special profile screw parts shaping (Технологічні основи формоутворення спеціальних профільних гвинтових деталей),* SMP “Tajp”, p.367, Ternopil;

[6] Hevko I.B. et al., (2005), Patent №18401. Ukraine. *Screw operating member of juice-extruder (Гвинтовий робочий орган соковитискача),* Digest №7, p.4;

[7] Hevko I.B. et al., (2015), Patent № 103550. Ukraine, *Elastic flexible screw working body (Пружний гнучкий гвинтовий робочий орган),* Digest №24, p.2;

[8] Hu G., Chen J., Jian B., Wan H., Liu L., (2010), Modelling and simulation of transportation system of screw conveyors by the discrete element method, *International Conference on Mechanic Automation and Control Engineering*, *MACE2010*, Article number 5536244, pp.927-930;

[9] *Fernandez J.W, Cleary P.W., Bride W.,* (2009), Effect of screw design on hopper draw down by a horizontal screw feeder, *Seventh international conference on CFD in the minerals and process industries CSIRO*, Melbourne/Australia;

[10] Leschuk R.Y., (2003), Interpreting of design-power parameters of the sectional screw mechanisms operating members. *Dissertation for the scientific degree of Candidate of sciences (Engineering)*, p.19, Lviv;

[11] Owen P.J., Cleary P.W., (2009), Prediction of screw conveyor performance using the Discrete Element Method (DEM), *Powder Technology*, 193(3), pp.274-288;

[12] Zareiforoush, H., Komarizadeh, M.H., Alizadeh, M.R., (2010), Effect of crop-screw parameters on rough rice grain damage in handling with a horizontal screw conveyor*. Journal of Food, Agriculture and Environment* Volume 8, Issue 3-4, Part 1, pp.494-499.

THEORETICAL STUDIES ON THE WORKING CAPACITY OF DISK DEVICES FOR GRINDING AGRICULTURAL CROP SEEDS
/
ТЕОРЕТИЧНІ ДОСЛІДЖЕННЯ ПРОДУКТИВНОСТІ ДИСКОВОГО ТЕРКОВОГО ПРИСТРОЮ ДЛЯ ВИТИРАННЯ НАСІННЯ СІЛЬСЬКОГОСПОДАРСЬКИХ КУЛЬТУР

Assist. Tverdokhlib I.V., Ph.D. Spirin A.V.
Vinnitsa National Agrarian University
Tel: +380672152088; E-mail: igor_tverdokhlib@yahoo.com

Keywords: *legume grasses, technological process, disc grating apparatus*

ABSTRACT

The article describes the technological process of operation of the improved disc grating apparatus aimed to grate seed of legume grasses and presents the results of analytical studies of its performance.

РЕЗЮМЕ

У статті наведено опис технологічного процесу роботи удосконаленого дискового теркового пристрою, призначеного для витирання насіння бобових трав і результати аналітичних досліджень продуктивності його роботи

INTRODUCTION

Sustainable development of agricultural production in Ukraine is possible on the basis of further modern mechanization of all production processes through the development and introduction of highly efficient technologies of crop harvesting, including perennial legume grasses *(Grynyk I. et al, 2014)*.

Sharp decrease of livestock population in Ukraine in recent years has led to the decline of such industry as seed production of perennial legume grasses (clover, alfalfa, sweet clover). Researches on the development of technologies and means of mechanization that would improve quality indicators of machines aimed to harvest seed of perennial legume grasses practically have not been carried out in recent years. Recently there has been observed a trend towards the intensification of production of animal products, so there is a need to develop feed base of farms and to provide these farms with seed of such crops as perennial legume grasses (clover, alfalfa, sweet clover) *(Burkov A. et al, 2008)*.

Operational process of treatment or wiping of alfalfa seed from a pile that is threshed by the working bodies of harvesting machines and then goes to the separating transporting and technological systems is one of the most important and complex technological operations in the scope of the technological process of operation of combine harvesters. Growth of the degree of seed wiping, reduction of seed damage and losses are priority goals in terms of meeting agricultural and technical requirements for seed processing, i.e. seed quality *(Adamchuk V. and Bulgakov V., 2010)*.

The problem of improvement of the technological level of grating modules, which are assessed by the seed quality indicators remains particularly relevant in terms of further development of stationary threshing machines and combine harvesters in general.

There is a great variety of construction and layout schemes of the stationary threshing machines and working bodies of grating devices. This is related to both harvesting technologies and agro-technical requirements for quality indicators of grating legume grass seed *(Antipin V. and Erk F., 2006; Burkov A., et al, 2008)*. Since the development and application of the first technical devices and facilities for mechanical harvesting of legume grasses an extensive experience in the establishment of relevant working bodies and machines has been gained in the world practice. Agro-biological and mechanical properties of the grass seeds have a great influence on working conditions of grating modules and regulate construction features of working bodies for grating off legume grass seed *(Grynyk I. et al, 2014)*.

Taking into account specific mechanical and technological properties of seed inside the pod and world tendencies of harvesting legume grasses it can be concluded that the technological process of grass seed grating should be performed by the working bodies of stationary machines according to the principle of seed grating off from the pods *(Burkov A. et al, 2008)*

Therefore, improvement of construction and layout schemes and working bodies of machines for grating legume grass seed and substantiation of parameters of their working bodies should be carried out taking into account specific properties of this process. This is particularly important and actual to provide necessary quality indicators of work according to agro-technical requirements *(Antipin V. and Erk F., 2006)*.

The objective of the study is to increase technological process indicators of harvesting of legume grasses through the development and substantiation of working parameters of the discs grating device.

MATERIAL AND METHOD

In general, the object of research of the discs grating device (DGD) is a technological process of treatment (wiping) of the prepared material (pile of alfalfa). The integral component of the technological process of lucerne pile treatment is the study of changes of the technological parameters or changes of DGD performance depending on the construction and technological parameters of its structural elements.

The subject of research is construction and kinematic parameters of the working bodies of DGD that perform technological process of seed removal from alfalfa pile, and performance parameters.

Methodology of the theoretical research was based on the mathematical modelling of the technological process of DGD operation in order to construct determinate mathematical models that characterize basic technological parameters.

Development of modern advanced layout schemes and new constructions of working bodies of the threshing-separating devices and their modules must be based on the international experience, taking into account peculiarities of local agricultural, technical, economic, and environmental requirements.

Based on the analysis of the obtained quality indicators and technological indicators of harvesting legume grasses we have proposed an improved design of DGD ДТП *(Tverdokhlib I. and Anelyak M., 2013; Tverdokhlib I. et al, 2014)*

Construction scheme of DGD is shown in Fig.1.

Grinding disc device DGD includes the body 6, where the tank is set 1, which has a loading mouth feed 2 and loading opening 3. In the tank space pin activator is installed 4, which has boards 5. Activator is fixed on top of the shaft 9, and on the lower part of the shaft moving grinding disc is fixed 8. In the body it is set a fixed disk 7, which has a glass, the hole of which follows loading mouth feed. Glass is designed as a hollow cylinder on the outside of which the threaded bushing is twirled. To the bottom surface of fixed disk are the beaters, installed on the disk in the form of rays. Beaters are made from steel in the reef form which has a notch. In the intervals between beaters concentric to the axis of the disc are placed ring lugs. At the bottom of tank there is the output channel 10.

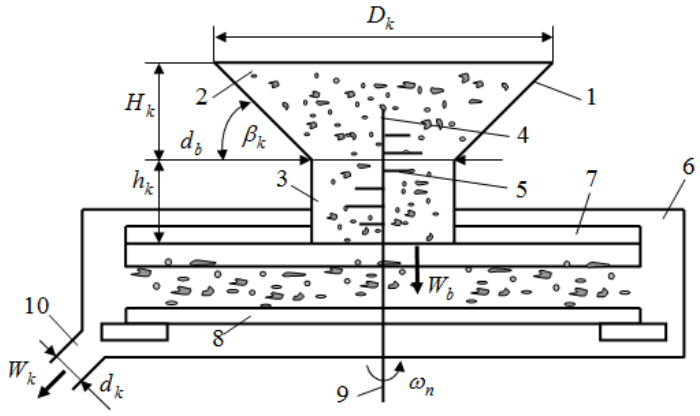

Fig.1 – Constructional scheme DGD:
1 – tank; 2 – loading mouth feed; 3 loading hollow; 4 – activator; 5 – blade; 6 – body; 7, 8 – stationary and moving disc; 9 – driving shaft; 10 – output channel

RESULTS

In addition to the ability to grind seeds, grinding device is also characterized by operational and technological criteria, including technological capacity. *(Antipin V., Erk F., 2006)* regulates the productivity of grinding devices and, ultimately, productivity of harvesting machines, or the ability to handle pile constituents without their 'download' on working surfaces for minimizing damage and loss of seeds.

To sustain the rational constructive-kinematic parameters DGD that meet the technical data of the machine, first is theoretical foundation of DGD band width or performance *(Tverdokhlib I., Spirin A. 2015)*.

The basis of the criterion foundation process work DGD is that the capacity of its working bodies within interval $t = 1$ C, or productivity must be equal or higher than the total of per second filing alfalfa pile that comes to them from previous transport and technological systems of harvesting machines, so the condition shall be fulfilled:

$$dQ_n / dt \geq dW_b / dt \text{ , or } Q_n \geq W_b \text{ ,} \quad (1)$$

where: Q_n – capacity (or productivity) accident DGD, kg/s;

W_b – general pile loading seconds transferred to DGD, kg/s.

In order to formalize alfalfa pile processing by DGD and to further study of the parameters of its working bodies, let`s consider the design scheme of the internal working space surround channel, shown in Fig.2 and workflow of DGD.

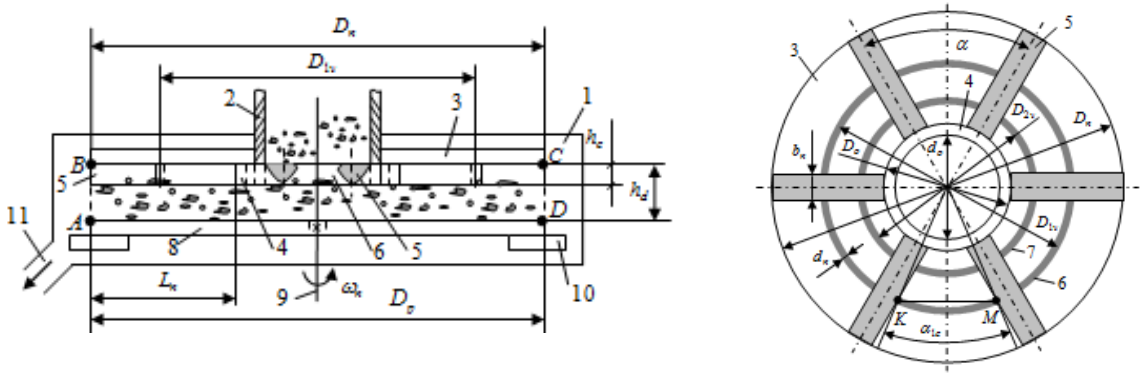

Fig.2 – Design scheme of the internal working space surround channel of DGD

1 – body; 2 – bushing; 3, 8 – stationary and moving disc; 4 – clip; 5 – beater; 6, 7 – ring lugs, 9 –shaft; 10 – blade; 11 – output channel

The internal volume of the working space of DGD is formed by adjacent - vertical position of stationary *3* (Fig.2) and *8* movable discs placed in the body *1* with the clearance, the height of which is h_d, with the outer diameter of the disk D_n and moving D_p that installed on the shaft *9* rotating with angular speed ω_n. In worktop of the stationary disk perpendicular and concentric to it is fixed holder *4*, made in the form of bushings, outer diameter of which is D_o as mid – d_o and are installed in form of rays- beaters *5* the number of which is k_n, made in the form of rays (reefs) with the width b_n, length L_n and height h_c, which are enshrined to the hub. There are also on the working surface of the stationary disk in between beaters concentric to the axis of the disc ring lugs *6*, *7* of total number k_v formed as a round rod; the average diameter is from the centre of the disk at a distance of 0.5 D_{1v} and 0.5 D_{2v}.

For further analysis and description of the formalized process of wiping alfalfa seeds in the context of the scheme we accept the following assumptions:

- the working space is a rectangle ABCD in section, that is why the working surfaces of the stationary *3* and the movable disks *8* are parallel to each other, so $D_n = D_p$;

- the cross section of beaters *5*, which is fixed to the radial inner surface of the stationary disk is a segment of a cylinder with equal height segment h_c;

- diameter ring lugs *6*, *7* which are concentric to the axis stationary disk and is the same d_n as the height of the sleeve *4* is cross-sectional height of *5* and beaters totals h_c.

Pile with non - grind alfalfa seeds enters through the loading channel *2* the internal volume space of the working channel of an DGD, where the centrifugal force shifts it from the centre axis of the movable disk *8* and from the axis centre of rotation of disc *3* fixed to their periphery. In the process of its motion in space working channel the process of grinding alfalfa seeds takes place, and further processed alfalfa pile is taken by blades *10* which direct it to the output channel 11, through which it leaves GDD.

Productivity of DGD, Q_n , according to *(Bronstein I. and Semendyaev K., 2009; Gorbert Goldeteyn et al, 2012)* can be calculated by a common formula which determines the performance of machines of continuous action.

$$Q_n = F_p \rho_v \varphi_n V_c ;\ F_p = 0{,}25\pi\left(D^2 - d_v^2\right);\ \varphi_n = V_v / V_n ;\ V_n = 0{,}25\pi D^2 h_d \quad (2)$$

where:

F_p – the working area of basic (moving) disk, m^2;

ρ_v – Bulk alfalfa pile density, kg/m^3;

φ_n – Filling factor of internal working space formed by figure $ABCD$;

V_c – the average speed of the processed pile towards the periphery of the disc, m/s;

V_v – the amount of space pile alfalfa working channel, m^3;

V_n – The total amount of space inside the working channel, m^3;

V_n – Diameter and height of the cylinder, m.

The maximum possible volume $V_{v.max}$ of alfalfa pile that fills the space of the working channel of an DGD will consist of the difference of the total internal volume V_n of the working space of the channel and the total volume $\sum V_e$ of structural elements that are installed on the inner surface of the fixed disk and which hold a certain amount volume, i.e.

$$V_{v.max} = V_n - \sum V_e = V_n - \left(V_w + \sum_{i=1}^{k_n} V_{b_j} + \sum_{i=1}^{k_v} V_{k_i} + V_d \right) \quad (3)$$

where: V_w , $\sum_{j=1}^{k_n} V_{b_j}$, $\sum_{i=1}^{k_v} V_{k_i}$, V_d – accordingly, bushings volume, the total volume of the beaters ring inserts and drive shaft volume, m^3.

This amounts corresponding figures that adopted the design elements found on the inner surface of the real disk are determined by formulas

$$V_w = 0{,}25\pi h_c\left(D_o^2 - d_o^2\right);\ \sum_{j=1}^{k_n} V_{b_j} = F_c L_n k_n = 0{,}5 r_b^2 \left[\left(\pi\alpha_b / 180\right) - \sin\alpha_b\right] L_n k_n \quad (4)$$

$$\sum_{i=1}^{k_v} V_{k_i} = \sum V_{1v} + \sum V_{2v} + ... + \sum V_{iv} ;\ V_d = 0{,}25\pi d_v^2 h_d ;\ i = 1, 2, \ldots, k_v \quad (5)$$

$$\sum_{i=1}^{k_v} V_{k_i} = \left(V_1 + V_2 + ... + V_i\right) - V'_{k_n} k_n k_v \quad (6)$$

where:

D_o , d_o – outer and inner diameter of bushing, m;

h_c – height of bushings, m;

F_c – beaters cross-sectional area or segment, m^2;

α_b – central angle, tightening beater chord, grade;

k_n – total number of installed beaters, pcs.;

L_n , r_b – beat length and radius of the arc segment beat, m;

$\sum V_{1v}$, $\sum V_{2v}$,..., $\sum V_{iv}$ – the total volume of one of the ring insert, which is placed concentrically at a distance from the centre of the stationary disc is equal, respectively, to 0.5 D_{1v} , 0.5 D_{2v} ,..., 0.5 D_{iv} , m^3;

V_1 , V_2 ,..., V_i – respectively, the total volume of each i of ring insert, which is placed concentrically at a distance from the centre of the stationary disc is equal, respectively, to 0.5 D_{1v} , 0.5 D_{2v} ,...,0.5 D_{iv} , m^3;

V'_{k_n} – the amount of each i ring insert, placed across the width b_n of each set on a fixed disk beater, m^3.

On the other hand the difference between the constituent right side of equation (6) can be written in the form $V_1 - V'_{1k_n} = V_{1k_n}$, $V_2 - V'_{2k_n} = V_{2k_n}$, $V_i - V'_{ik_n} = V_{ik_n}$, where V_{1k_n}, V_{2k_n},…, V_{ik_n} – the amount of each i ring insert, which is placed between two adjacent concentric beaters away from the centre of the real disk is equal, respectively, to 0.5 D_{1v}, 0.5 D_{2v},…,0.5 D_{iv}, m^3.

Then the total volume of each i ring insert which is placed concentrically at a distance from the centre of the real disk, which is equal to, respectively, 0.5 D_{1v}, 0.5 D_{2v},…,0.5 D_{iv} will be determined by the formula:

$$\sum V_{1v} = V_{1k_n} k_n;\ \sum V_{2v} = V_{2k_n} k_n;\ \sum V_{iv} = V_{ik_n} k_n, \text{ a } V_1 = 0{,}25\pi^2 D_{1v} d_n^2;\ V_2 = 0{,}25\pi^2 D_{2v} d_n^2;\ V_i = 0{,}25\pi^2 D_{iv} d_n^2 \quad (7)$$

where: D_{1v}, D_{2v},…, D_{iv} – the diameter of the centre section of the centre ring of the torus, m;

d_n – diameter of circular section torus, m.

Volume of each sector i ring insert, which is placed between two adjacent concentric beaters away from the centre of the stationary disk is equal to, respectively, 0,5 D_{1v}, 0,5 D_{2v},…,0,5 D_{iv} and angle between the central part of i torus with (7) will be determined by the formula

$$\left.\begin{aligned} V_{1k_n} &= 0{,}25\pi^2 D_{1v} d_n^2 \alpha_{1c} / 360^0; \\ V_{2k_n} &= 0{,}25\pi^2 D_{2v} d_n^2 \alpha_{2c} / 360^0; \\ &\cdots\cdots\cdots\cdots\cdots\cdots\cdots\cdots; \\ V_{ik_n} &= 0{,}25\pi^2 D_{iv} d_n^2 \alpha_{ic} / 360^0 \end{aligned}\right\} \quad (8)$$

where: α_{1c}, α_{2c},…, α_{ic} – central angle that tights a chord of each sectorial i ring insert, which is placed at a distance from the centre of stationary disk at 0.5 D_{1v}, 0.5 D_{2v},…,0.5 D_{iv}, rad.

Central angle that tights a chord of each sectorial share of i ring insert, which is placed at a distance from the centre of the disc real is equal, respectively, to 0.5 D_{1v}, 0.5 D_{2v},…,0.5 D_{iv} according to *(Grynyk I. et al, 2014)* and is given by formula:

$$\alpha_{1c} = 2arcsin(a_{1v} / D_{1v});\ \alpha_{2c} = 2arcsin(a_{2v} / D_{2v});\ \alpha_{ic} = 2arcsin(a_{iv} / D_{iv}) \quad (9)$$

where: a_{1v}, a_{2v},…, a_{iv} – a chord length of each sectorial share of i ring insert, which is placed between two adjacent concentric beaters away from the centre of the real disk is equal, respectively, to 0.5 D_{1v}, 0.5 D_{2v},…,0.5 D_{iv}, charged by corresponding central angle, α_{1c}, α_{2c},…, α_{ic}, m.

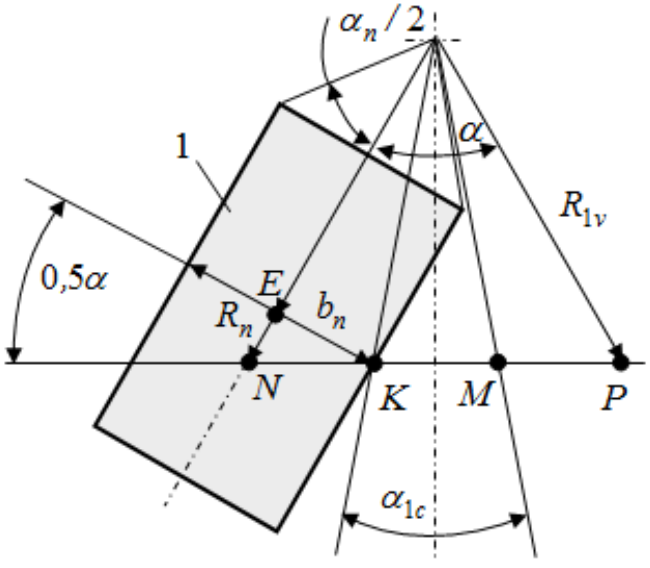

Fig. 3 – Scheme to determine the length of the chord:
1 – beater

To determine the length of the chord a_{1v}, a_{2v},…, a_{iv}, consider the composite scheme (Fig.3), while:

$$a_{KM} = 2\left(R_{1v} + 0{,}5b_n / sin(\alpha/2)\right) - 2\cdot 0{,}5b_n / cos(\alpha/2) = D_{1v} + \frac{b_n}{2}\left(\frac{1}{sin(\alpha/2)} - \frac{1}{cos(\alpha/2)}\right) = a_{1v} \quad (10)$$

$$a_{2v} = D_{2v} + \frac{b_n}{2}\left(\frac{1}{sin(\alpha/2)} - \frac{1}{cos(\alpha/2)}\right);\ \ a_{iv} = D_{iv} + \frac{b_n}{2}\left(\frac{1}{sin(\alpha/2)} - \frac{1}{cos(\alpha/2)}\right) \quad (11)$$

Then, according to (9) and (10) we have

$$\left.\begin{aligned} &\alpha_{1c} = 2\,arcsin\left(1 + \frac{b_n}{2D_{1v}}\left(\frac{1}{sin(\pi/k_n)} - \frac{1}{cos(\pi/k_n)}\right)\right);\\ &\alpha_{2c} = 2\,arcsin\left(1 + \frac{b_n}{2D_{2v}}\left(\frac{1}{sin(\pi/k_n)} - \frac{1}{cos(\pi/k_n)}\right)\right);\\ &\ldots\ldots\ldots\ldots\ldots\ldots\ldots\ldots\ldots\ldots\ldots\ldots\ldots\ldots\ldots\ldots\ldots\ldots;\\ &\alpha_{ic} = 2\,arcsin\left(1 + \frac{b_n}{2D_{iv}}\left(\frac{1}{sin(\pi/k_n)} - \frac{1}{cos(\pi/k_n)}\right)\right) \end{aligned}\right\} \quad (12)$$

Then, substituting the values (12) to (9), and subsequently (9) (8) and according to (7), we obtain the formula for determining the total volume of each i ring insert, which is placed between two adjacent beaters and between beater central angle α_{1c}, α_{2c},…, α_{ic}, a sector of a torus of i.

$$\left.\begin{aligned} &\sum V_{1v} = 0{,}5\pi^2 D_{1v} d_n^2 k_n\, arcsin\left(1 + \frac{b_n}{2D_{1v}}\left(\frac{1}{sin(\pi/k_n)} - \frac{1}{cos(\pi/k_n)}\right)\right)/360^0;\\ &\sum V_{2v} = 0{,}5\pi^2 D_{2v} d_n^2 k_n\, arcsin\left(1 + \frac{b_n}{2D_{2v}}\left(\frac{1}{sin(\pi/k_n)} - \frac{1}{cos(\pi/k_n)}\right)\right)/360^0;\\ &\ldots\ldots\ldots\ldots\ldots\ldots\ldots\ldots\ldots\ldots\ldots\ldots\ldots\ldots\ldots\ldots\ldots\ldots;\\ &\sum V_{iv} = 0{,}5\pi^2 D_{iv} d_n^2 k_n\, arcsin\left(1 + \frac{b_n}{2D_{iv}}\left(\frac{1}{sin(\pi/k_n)} - \frac{1}{cos(\pi/k_n)}\right)\right)/360^0 \end{aligned}\right\} \quad (13)$$

where:

V_w, $\sum V_b$, $\sum_{i=1}^{k_v} V_{k_i}$, V_d, – bushings volume, the total volume of the beater inserts and ring volume drive shaft m^3.

Substituting the value of the total volume of each of i ring inserts with (13) in the first equation (5) we obtain the formula for determining the total beater volume k_n the total of which occupies the space of the working channel of DGD:

$$\sum_{i=1}^{k_v} V_{k_i} = \frac{0{,}5\pi^2 d_n^2 k_n}{360^0}\left\{\begin{aligned} &D_{1v}\, arcsin\left[1 + \frac{b_n}{2D_{1v}}\left(\frac{1}{sin(\pi/k_n)} - \frac{1}{cos(\pi/k_n)}\right)\right] +\\ &+ D_{2v}\, arcsin\left[1 + \frac{b_n}{2D_{2v}}\left(\frac{1}{sin(\pi/k_n)} - \frac{1}{cos(\pi/k_n)}\right)\right] + \ldots +\\ &+ D_{iv}\, arcsin\left[1 + \frac{b_n}{2D_{iv}}\left(\frac{1}{sin(\pi/k_n)} - \frac{1}{cos(\pi/k_n)}\right)\right] \end{aligned}\right\}. \quad (14)$$

The total volume $\sum V_e$ of structural elements that take a certain amount of the total internal volume V_n of the working space bed according to (3), (4) and (14) will be determined by the formula:

$$\sum V_e = 0{,}25\pi h_c\left(D_o^2 - d_o^2\right) + 0{,}5r_b^2\left[\left(\pi\alpha_b/180\right) - \sin\alpha_b\right]L_n k_n + 0{,}25\pi d_v^2 h_d + \\ + \frac{0{,}5\pi^2 d_n^2 k_n}{360^0}\left\{\begin{array}{l} D_{1v}\,arcsin\left[1 + \frac{b_n}{2D_{1v}}\left(\frac{1}{\sin(\pi/k_n)} - \frac{1}{\cos(\pi/k_n)}\right)\right] + \\ + D_{2v}\,arcsin\left[1 + \frac{b_n}{2D_{2v}}\left(\frac{1}{\sin(\pi/k_n)} - \frac{1}{\cos(\pi/k_n)}\right)\right] + \ldots + \\ + D_{iv}\,arcsin\left[1 + \frac{b_n}{2D_{iv}}\left(\frac{1}{\sin(\pi/k_n)} - \frac{1}{\cos(\pi/k_n)}\right)\right] \end{array}\right\}. \quad (15)$$

At maximum volume $V_{v.max}$ alfalfa pile that fills the space of the working channel of the DGD according to (3)–(5) and (14) is determined:

$$V_{v.max} = 0{,}25\pi D^2 h_d - 0{,}25\pi h_c\left(D_o^2 - d_o^2\right) + 0{,}5r_b^2\left[\left(\pi\alpha_b/180\right) - \sin\alpha_b\right]L_n k_n + \\ + \frac{0{,}5\pi^2 d_n^2 k_n}{360^0}\left\{\begin{array}{l} D_{1v}\,arcsin\left[1 + \frac{b_n}{2D_{1v}}\left(\frac{1}{\sin(\pi/k_n)} - \frac{1}{\cos(\pi/k_n)}\right)\right] + \\ + D_{2v}\,arcsin\left[1 + \frac{b_n}{2D_{2v}}\left(\frac{1}{\sin(\pi/k_n)} - \frac{1}{\cos(\pi/k_n)}\right)\right] + \ldots + \\ + D_{iv}\,arcsin\left[1 + \frac{b_n}{2D_{iv}}\left(\frac{1}{\sin(\pi/k_n)} - \frac{1}{\cos(\pi/k_n)}\right)\right] \end{array}\right\} + \\ + 0{,}25\pi d_v^2 h_d \quad (16)$$

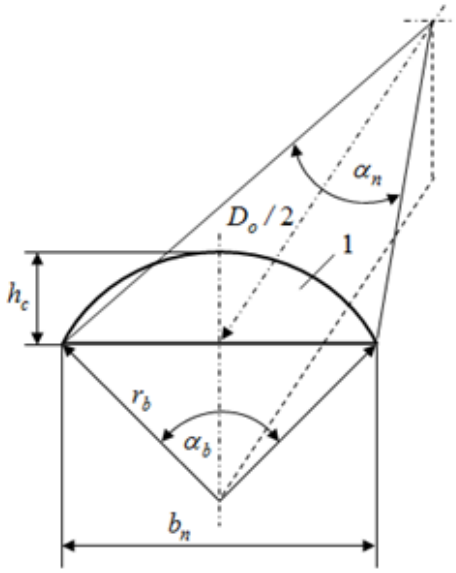

Fig. 4 – Scheme for definition of central angle α_b and radius r_b:

1 – beater

To determine the central angle α_b, tightening chord b_n of beater 1 and radius r_b we consider the composite circuit shown in Fig. 4.

According to Fig.4 and identities that are given in *(Fedorenko V., et al., 2009)*, we have

$$b_n = 2\sqrt{2h_c r_b - h_c^2} = 2r_b\,sin\left(\alpha_b/2\right), \text{ or } b_n^2 = 4\left(2h_c r_b - h_c^2\right),\ sin\left(\alpha/2\right) = b_n/2r_b.$$

Where:

$$r_b = \left(b_n^2/8h_c\right) + 0{,}5h_c;\ \ \alpha_b = 2\,arcsin\left(\frac{b_n h_c}{0{,}125b_n^2 + h_c^2}\right) \quad (17)$$

Maximum coefficient of filling $\varphi_{n.max}$ the internal space of the working channel of the DGD according to (2), (3) and (16), (17) is determined:

$$\varphi_{n.max} = 1 - \frac{\begin{array}{l} h_c\left(D_o^2 - d_o^2\right) + \frac{4}{\pi}\left[\left(b_n^2 / 8h_c\right) + 0{,}5h_c\right]^2 \times \\ \times\left[\left(\pi\, arcsin\, b_n h_c / 180 \cdot \left(0{,}125b_n^2 + h_c\right)\right) - sin\frac{b_n h_c}{0{,}125b_n^2 + h_c^2}\right] L_n k_n + d_v^2 h_d + \\ + \frac{\pi d_n^2 k_n}{180^0}\left\{\begin{array}{l} D_{1v}\, arcsin\left[1 + \frac{b_n}{2D_{1v}}\left(\frac{1}{sin(\pi / k_n)} - \frac{1}{cos(\pi / k_n)}\right)\right] + \\ + D_{2v}\, arcsin\left[1 + \frac{b_n}{2D_{2v}}\left(\frac{1}{sin(\pi / k_n)} - \frac{1}{cos(\pi / k_n)}\right)\right] + \ldots + \\ + D_{iv}\, arcsin\left[1 + \frac{b_n}{2D_{iv}}\left(\frac{1}{sin(\pi / k_n)} - \frac{1}{cos(\pi / k_n)}\right)\right] \end{array}\right. \end{array}}{D^2 h_d} \quad (18)$$

The average speed V_c of pile processed towards the periphery of the movable and immovable discs will be determined:

$$V_c = V_m \lambda_V = 0{,}5(d\varphi / dt) D\lambda_V = 0{,}5\omega_n D\lambda_V\,, \quad (19)$$

where:

V_m – the theoretical speed of the material, [m/s];

λ_V – factor for the decline rate V_m relative to the theoretical average speed V_c;

φ – rolling disk angle, [grd];

ω_n – angular velocity of a moving disk, [rad/s].

Thus, maximum productivity of DGD $Q_{n.max}$ according to (2), (18) and (19) is determined by dependence:

$$Q_{n.max} = \pi\omega_n \lambda_V \rho_v \left(D^2 - d_v^2\right)\left(1 - \frac{h_c\left(D_o^2 - d_o^2\right) + \left(4\Theta L_n k_n / \pi\right) + d_v^2 h_d + \Omega\pi d_n^2 k_n / 180}{8Dh_d}\right) \quad (20)$$

Where: $\Theta = \left[\left(b_n^2 / 8h_c\right) + 0{,}5h_c\right]^2 \times \left[\left(\pi\, arcsin\left(b_n h_c / 180\right) \cdot \left(0{,}125b_n^2 + h_c\right)\right) - sin\frac{b_n h_c}{0{,}125b_n^2 + h_c^2}\right]$

$$\Omega = D_{1v}\, arcsin\left[1 + \frac{b_n}{2D_{1v}}\left(\frac{1}{sin(\pi / k_n)} - \frac{1}{cos(\pi / k_n)}\right)\right] +$$

$$+ D_{2v}\, arcsin\left[1 + \frac{b_n}{2D_{2v}}\left(\frac{1}{sin(\pi / k_n)} - \frac{1}{cos(\pi / k_n)}\right)\right] + \ldots +$$

$$+ D_{iv}\, arcsin\left[1 + \frac{b_n}{2D_{iv}}\left(\frac{1}{sin(\pi / k_n)} - \frac{1}{cos(\pi / k_n)}\right)\right]$$

For practical use of the dependence (20), which is cumbersome, based on further analysis will hold its simplification based on the following considerations.

Maximum meaning of filling factor $\varphi_{n.max}$ the space working channel of DGD can be represented as a product useful volume φ_n' and the working space entered factor φ_e for the volume that is occupied by the structural elements installed on the inner surface of the stationary disc. This meaning is defined as the ratio of the total amount $\sum V_e$ of structural elements that are installed on the inner surface of the

stationary disk to the total internal volume V_n space of the working channel of DGD or:

$$\varphi_e = \sum V_v / V_n = \frac{h_c\left(D_o^2 - d_o^2\right) + 4\Theta L_n k_n / \pi + d_v^2 h_d + \frac{\pi d_n^2 k_n}{180^0}\Omega}{8Dh_d} \tag{21}$$

Then, taking into account the factor φ_e, the actual meanings of filling $\varphi_{n.max}$ the space of the working channel of the DGD will be determined:

$$\varphi_{n.max} = \varphi'_{n.max}\varphi_e = \left(\varphi'_{n.max} h_c\left(D_o^2 - d_o^2\right) + 4\Theta L_n k_n / \pi + d_v^2 h_d + \frac{\pi d_n^2 k_n}{180^0}\Omega\right) / 8Dh_d \tag{22}$$

In this case, the maximum productivity of DGD $Q_{n.max}$ according to (22) will be determined by dependence:

$$\begin{aligned} Q_{n.max} &= 0{,}125\pi D\left(D^2 - d_v^2\right)\rho_v \varphi'_{n.max}\varphi_e \lambda_v \frac{d\varphi}{dt} = \\ &= 0{,}125\pi D\left(D^2 - d_v^2\right)\rho_v \varphi'_{n.max}\lambda_v \frac{h_c\left(D_o^2 - d_o^2\right) + 4\Theta L_n k_n / \pi + d_v^2 h_d + \frac{\pi d_n^2 k_n}{180^0}\Omega}{8Dh_d}\frac{d\varphi}{dt} \end{aligned} \tag{23}$$

Or:
$$Q_{n.max} = \frac{\pi^2 n_n D\left(D^2 - d_v^2\right)\rho_v \varphi'_{n.max}\varphi_e \lambda_v}{120}, \tag{24}$$

where: n_n – fixed speed [rot/min].

The resultant dependence (24) characterizes the change in productivity of DGD depending on its structural and kinematic parameters.

According to the dependence (24) constructed are image reproductions $Q_{n.max}$ as functional changes: Fig. 5 – $Q_{n.max} = f(D,n)$, Fig. 6a – $Q_{n.max} = f(n)$; Fig. 6b – $Q_{n.max} = f(\varphi'_n)$.

Analysis of dependence $Q_n = f(D,n)$ (Fig. 5) shows that productivity of DGD varies approximately in the range of 0.2 to 1.3 kg/s, depending on the meaning of the diameter D and rotational speed n_n of moving disc by linear variation of Q_n, with increased productivity n_n and unit growing D, which is also characteristic for dependencies that are shown in Fig. 6.

Significant productivity growth Q_n is observed in the meaning of movable disk diameter of $D \geq$ 0.5 m, with a range of changes 400 $\leq n_n \leq$ 1000 rot/min for the moving diameter of $D =$ 0.6 m, drive productivity Q_n increases by about 0.65...0.7 kg/s (Fig. 6a) and a significant increase in productivity Q_n, depending on changes in fill factor φ'_n working space channel of GDD (about 0.2...0.25 kg/s) is the meaning of $\varphi'_n \geq$ 0.5 (Fig. 6b).

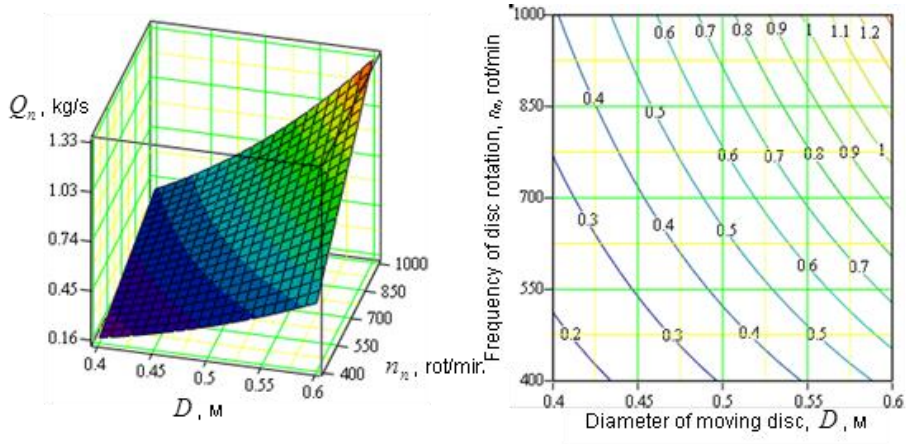

Fig.5 – Dependance of change Q_n as functional: $Q_{n.\max} = f(D,n)$

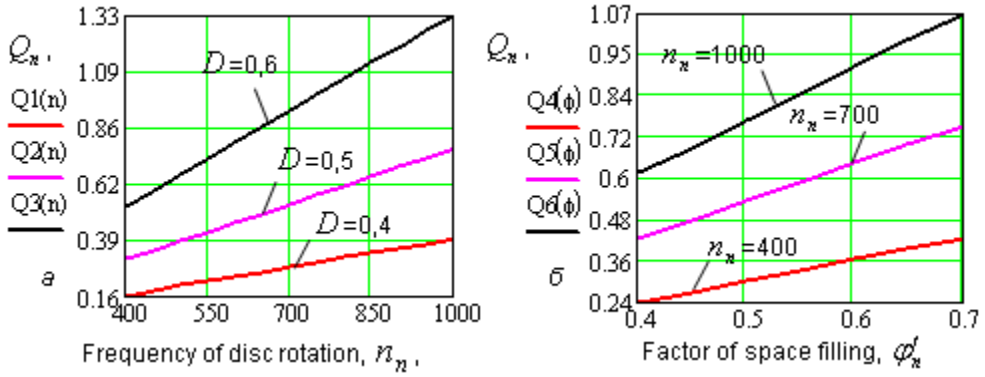

Fig.6 – Dependance of change Q_n as functional: *а* – $Q_{n.max} = f(n)$; *б* – $Q_{n.max} = f(\varphi'_n)$

CONCLUSIONS

Thus, the developed analytical model of DGD productivity allows to theoretically support structural and kinematic parameters and modes of grinding device.

REFERENCES

[1] Adamchuk, V., Bulgakov, V., (2010), The current state of scientific support of agricultural mechanization (Сучасний стан наукового забезпечення механізації сільського господарства), *Scientific Journal NUBiP Ukraine* (*Науковий вісник НУБіП України*), pp.144;

[2] Antipin V., Erk F., (2006), *Production of perennial grass seeds (Производство семян многолетних трав,* Rosselkhozizdat, p.191, Moscow/Russia;

[3] Bronstein, I., Semendyaev K., (2009), *Mathematical Handbook* (*Справочник по математике*), Ed. physical and mathematical literature, pp.608, Moscow/Russia;

[4] Bugaev V., Kolesnik S., Anthony S., (2008), *Technology of growing perennial grasses for seed: recommendations (Технології вирощування багаторічних трав на насіння*: рекомендації). Vinnitsa/Institute of feed UAAS, p.48, Ukraine;

[5] Burkov A., Smirnov M., Mashkovtsev M., (2008), Definition of quality indicators of operation of the device for wiping grass seed (Определение показателей качества работы устройства для вытирания семян трав). *Mechanization and electrification of agriculture (Механизация и электрификация сельского хозяйства)*, Issue number 12, pp.18-19, Moscow/Russia;

[6] Fedorenko V., Buklagin D., Kostina L., (2009), For the selection of machines, variety trials and initial seed field crops (Машины для селекции, сортоиспытания и первичного семеноводства полевых культур : каталог), Katalog: FGBNU "Rosinformagroteh", pp.224, Moscow/Russia;

[7] Gorbert Goldeteyn, Charles Poole, Dzhon Safko, (2012), *Classical Mechanics (Классическая механика)*, Institute computer isledovany, p.367;

[8] Grynyk I., Adamchuk V., Kaletnik G., Bulgakov, V., (2014), The state of design and production of agricultural machinery modern technical level in Ukraine (Стан проектування і виготовлення в Україні сільськогосподарських машин сучасного технічного рівня), *Mechanization and electrification of agriculture (Механізація і електрифікація сільського господарства)*, no.99 (1), pp.34-39;

[9] Gukov Y., Grytsyshyn M., (2008), State of mechanization of agricultural production in Ukraine (Стан механізації сільськогосподарського виробництва в Україні), *Mechanization of agricultural production (Механізація сільськогосподарського виробництва)*, Vol.XIV, pp.64-70, Kyiv;

[10] Tverdokhlib I., Anelyak M., Kuzmich A., Kustov S., (2013), *Threshing-separating device* (*Молотильно-сепаруючий пристрій*), Patent № 101449, Ukraine;

[11] Tverdokhlib I., Anelyak M., Kuzmich A., Kustov S., (2014), *Device for friction* (*Терковий пристрій*), Patent № 105114, Ukraine;

[12] Tverdokhlib I, Spirin A (2015), The results of experimental studies of seed wiping by disk-grinding device (Результати експериментальних досліджень витирання насіння дисково-терковим пристроєм), *Engineering, Energy, Transport, Agriculture (Техніка, енергетика, транспорт АПК)*, Vol.92 (3), pp.28-36, Vinnitsa/Ukraine.

STUDY OF LABORATORY GERMINATION OF SEEDS FROM MILYANA TOMATO VARIETY AFTER ELECTROMAGNETIC TREATMENT
/
ИЗСЛЕДВАНЕ НА ЛАБОРАТОРНАТА КЪЛНЯЕМОСТ НА СЕМЕНА ОТ ДОМАТИ, СОРТ МИЛЯНА, СЛЕД ПРЕДСЕИТБЕНИ ЕЛЕКТРОМАГНИТНИ ОБРАБОТКИ

Assoc. Prof. PhD Eng. Sirakov K.[1)], Assoc. Prof. PhD Ganeva D.[2)], PhD Eng. Zahariev S.[1)], Prof. PhD Eng. Palov I.[1)], Prof. PhD Eng. Mihov M.[2)]
[1)]Angel Kanchev University of Ruse, Bulgaria; [2)]Maritsa Vegetable Crops Research Institute, Plovdiv, Bulgaria
Tel: +359 88 888 264; E-mail: csirakov@uni-ruse.bg

***Keywords**: seeds, electromagnetic treatment, laboratory germination, surfaces and lines of response*

ABSTRACT

After pre-sowing electromagnetic treatments by expanded experimental plan from B_3 type and after theoretical studies of the constructed response surfaces and lines of the response – laboratory germination of the seeds from tomato variety Milyana it was theoretically confirmed that the positive results are obtained in the following values of the controlled factors: voltage of treatments U=12 kV, duration of treatment τ=35 s and length of stay to sowing T=12 days. It is proven that an effective impact could be obtained in combined increase of the controlled factor voltage of treatment and shortening of the duration of treatment τ=2 s.

РЕЗЮМЕ

След предсеитбени електромагнитни обработки по разширен план на експеримента от типа B_3 и теоретични изследвания на построените повърхнини и линии на отклика – лабораторна кълняемост на семена от домати сорт Миляна, теоретично е потвърдено, че положителни резултати се получават при стойности на управляемите фактори: напрежение на обработка U=12 kV, продължителност на въздействие τ=35 s и продължителност на престоя от обработката до засяването T=12 денонощия. Доказано е, че ефективно въздействие може да се получи и при съчетано увеличаване стойността на управляемия фактор напрежение на обработка и съкращаване продължителността на въздействие τ=2 s.

INTRODUCTION

The seeds are carriers of morphological, biological and economical characters and properties of the plants and their quality reflects in a great degree on the productivity and quality of the variety produce. (*Danailov, 2012*). High quality of the seeds is a base for development of normal plants (*Poryazov I. et al., 2013*). The growth power of the seeds influences the further development of the new grown plants and has particularly strong effect on their vegetative growth and, therefore on the productivity (*TeKrony and Egli, 1991*). The seeds with greater germination energy and germination give quick and total germination, faster development, and smaller susceptibility to the unfavourable conditions. The competence and correct application of the pre sowing treatment of the seed could be an efficient mean for increasing the sowing qualities of the cereal, technical and vegetable crops seeds (*Sirakov, 2006; Radevska M. et al., 2012*).

The results from study, the effect of pre-sowing electromagnetic treatments on the laboratory properties of seeds from tomato variety Milyana are shown in (*Ganeva D. et al., 2014*). A stimulation effect of parameters of the electromagnetic treatment, namely voltage of treatments U=12 kV, duration of treatment τ=35 s and length of seed stay from treatment to sowing T=12 days were established. It was achieved an increase of germination energy with 103.60%/c, laboratory germination with 104.60%/c, hypocotyls length with 15.73%, cotyledons length – with 21.88%, root length with 24.41% as well as an increase of the plant fresh weight – with 25.00% towards the control (untreated) seeds.

In other parameters of the pre-sowing treatment (U=6 kV, τ=5 s and stay to seed set for germination T=4 days) was established a depressive effect on the seed development – the length of the roots, hypocotyls and cotyledons were by (16…20)% smaller compared to the control and the plant fresh weight has been increased with over 22%.

According to the above considerations, the investigations were continued and the seed laboratory germination was established after conducting of pre-sowing electromagnetic treatment of the seeds by extended plan B^3 (*Mitkov, 2011*), and the response surface and lines of response were obtained.

The purpose of the study was the probable values of the controlled factors stimulating more effectively the laboratory germination of tomato seeds from Variety Milyana to be established by means of the extended plan of the experiment of pre-sowing electromagnetic treatments.

MATERIAL AND METHOD

An object of study was the laboratory germination of tomato seeds from variety Milyana – namely, determinate, large fruited variety suitable for mid-early field production. The seed germination is within (92…92.50)%.

Controlled factors of the pre-sowing electromagnetic treatment in the AC corona discharge field are: voltage U (kV) between the electrodes (edge-plane) and the duration of treatment τ (s). After treatment the seeds were left for stay T (days) till their set for germination. The pre-sowing treatment was conducted on the 31-st of March 2014.

The tomato seeds were set in Petri dishes with wet filter paper for germination in controlled conditions in thermostat at temperature 25°C and relative humidity 95%. In each variant were set 100 seeds in 4 replications after 4, 8 and 12 day stay in electromagnetic treatment (*International Seed Testing Association, 2004; Ganeva D. et al., 2014, 2015; Sirakov K. et al., 2015*).

The laboratory germination of the seeds was established for each experiment (4, 8 and 12 days) at 14th day of sowing. Data were given in percentage towards the controls (%/c).

The results were mathematically processed (*Mitkov, 2011*), and response surfaces and lines of response were obtained (*http://www.statsoft.com*).

RESULTS

The pre-sowing electromagnetic treatments were conducted by three factorial experiments according to symmetrical constructional plan from B_3 type (*Mitkov, 2011*). The values of the controlled factors and their corresponding levels of variation are shown in Table 1.

Table 1

Controlled factors

Factors		Level of controlled factors					
		high		medium		low	
Voltage, U	$\overset{\circ}{x}_1$	+1	12 kV	0	9 kV	-1	6 kV
Duration of impact, τ	$\overset{\circ}{x}_2$	+1	35 s	0	20 s	-1	5 s
Length of stay, T	$\overset{\circ}{x}_3$	+1	12 days	0	8 days	-1	4 days

The plan of the experiment with the results established for the laboratory seed germination is given in Table 2.

The reported average values of the laboratory germination (g) of the controlled seeds are the following: the germination in stay of the treated seeds for 4 days is g=92.25%, in stay of 8 days the germination is g=92.00%, and after stay of 12 days – g=92.50%. Towards them the obtained results for laboratory germination of the seeds $Y_{\kappa.}$ for each variant of treatment and relevant stay are given in %/c.

According to the results (Y_i), given in Table 2 for the established laboratory germination of the particular variants of treatment by plan B_3, and according (*Mitkov, 2011*) the equation for regression was found. This equation expresses the relation between the laboratory germination and the combination of the individual factors (voltage U of treatment – factor $\overset{\circ}{x}_1$, duration of treatment τ – factor $\overset{\circ}{x}_2$, length T of stay to set of the seeds for germination – factor $\overset{\circ}{x}_3$) and their interactions: $\overset{\circ}{x}_1\overset{\circ}{x}_2$, $\overset{\circ}{x}_1\overset{\circ}{x}_3$, $\overset{\circ}{x}_2\overset{\circ}{x}_3$, $\overset{\circ}{x}_1^2$, $\overset{\circ}{x}_2^2$ *and* $\overset{\circ}{x}_3^2$:

By the control (*Mitkov, 2011*) it was established that the equation (1) is adequate according to the comparison of the calculated criteria of Fisher with its critical value. On the basis of the critical value of the Student's criteria it was established that the coefficients of regression in the equation are significant.

Table 2

Experiment planning matrix

Variants	Controlled factors						Laboratory germination, $Y_{к.}$, %/c
	$\overset{\circ}{x}_1$		$\overset{\circ}{x}_2$		$\overset{\circ}{x}_3$		
	-	U, kV	-	τ, s	-	T, days	
1	+1	12	+1	35	+1	12	104.60
2	-1	6	+1	35	+1	12	100.54
3	+1	12	-1	5	+1	12	102.70
4	-1	6	-1	5	+1	12	100.81
5	+1	12	+1	35	-1	4	101.08
6	-1	6	+1	35	-1	4	102.17
7	+1	12	-1	5	-1	4	102.17
8	-1	6	-1	5	-1	4	100.54
9	+1	12	0	20	0	8	101.63
10	-1	6	0	20	0	8	99.73
11	0	9	+1	35	0	8	99.73
12	0	9	-1	5	0	8	100.00
13	0	9	0	20	+1	12	101.08
14	0	9	0	20	-1	4	100.54

$$\hat{Y}_{к.} = 99{,}764 + 0{,}839\,\overset{\circ}{x}_1 + 0{,}190\,\overset{\circ}{x}_2 + 0{,}323\,x_3 - 0{,}069\,\overset{\circ}{x}_1\,\overset{\circ}{x}_2 + 0{,}676\,\overset{\circ}{x}_1\,\overset{\circ}{x}_3 + 0{,}136\,\overset{\circ}{x}_2\,\overset{\circ}{x}_3 + 0{,}916\,\overset{\circ}{x}_1^2 + 0{,}101\,\overset{\circ}{x}_2^2 + 1{,}046\,\overset{\circ}{x}_3^2 \quad (1)$$

The response surfaces and lines of response are studied for evaluation of the influence and interaction between the factors on the laboratory germination. They are composed according (*Mitkov, 2011*), and the programme product Statistica 8 (*http://www.statsoft.com*). The response surfaces and lines of response are obtained as a result of consecutive elimination of each one of the factors $\overset{\circ}{x}_1$, $\overset{\circ}{x}_2$ and $\overset{\circ}{x}_3$, and the other two vary between the levels given in Table 1. Since the number of the controlled factors is 3, the obtained and analyzed response surfaces and lines of response are by 3. It is known the presence of correlation between the quadratic members itself $\overset{\circ}{x}_i^2$ of the equation (1). This forces to calculate the remaining coefficients of the model (*Mitkov, 2011*) again in elimination of some quadratic members. It should be mentioned that in this calculation, the values of the free member and non-eliminated members were only changed.

Variant 1: The factor $\overset{\circ}{x}_3$ – duration of stay T is eliminated. In that case, in interaction of the factors $\overset{\circ}{x}_1$ and $\overset{\circ}{x}_2$ the equation of the response surface is of the following kind:

$$\hat{Y}_{к.} = 100{,}166 + 0{,}839\,\overset{\circ}{x}_1 + 0{,}190\,\overset{\circ}{x}_2 - 0{,}069\,\overset{\circ}{x}_1\,\overset{\circ}{x}_2 + 1{,}157\,\overset{\circ}{x}_1^2 + 0{,}342\,\overset{\circ}{x}_2^2 \quad (2)$$

In use of the Statistica 8 *(http://www.statsoft.com*), it was built the response surface (Figure 1a) and lines of response (Figure 1b) – laboratory seed germination in function of the voltage applied between the electrodes $\overset{\circ}{x}_1$ (U) and time of electromagnetic treatment $\overset{\circ}{x}_2$ (τ), in case of elimination the influence of the factor duration $\overset{\circ}{x}_3$ (T) of stay from treatment to seeds sowing.

The values of $\hat{Y}_{к.}$, for model (2), in %/c, are given in numerical type on the ordinate of the drawings from Figure 1.

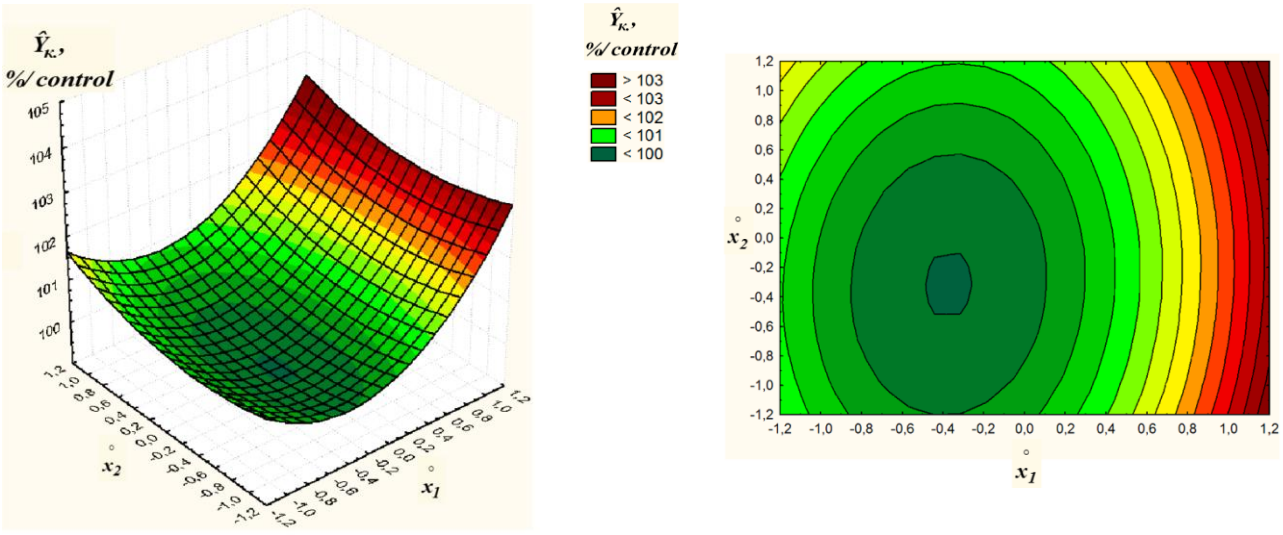

a) **b)**

Fig.1 – Response surface (a) and lines of response (b) – laboratory germination as a function of factors $\overset{\circ}{x}_1$ **(U) and** $\overset{\circ}{x}_2$ **(τ),** $\overset{\circ}{x}_3$ **(T) switched off factor**

The effect ($\hat{Y}_{\kappa.}$ in %/c) of the impact of the pre-sowing electromagnetic treatments of the seeds, obtained by the model (2), is shown in Figure 1a and Figure 1b by different colours (according to the legend of Figure 1) in the response surface and lines of response themselves. Moreover, where the dark green fields are, for example in $\overset{\circ}{x}_1$ =(+0.2…-0.9) and $\overset{\circ}{x}_2$ =(+0.8…-1.2), the pre-sowing impact should be depressing.

In case of accepting the values of the two factors in natural units it could be said that the depressing impact of the pre-sowing electromagnetic treatment on the laboratory germination should be expected in combination of the two factors in the limits U=(9.6…6.3) kV and τ=(32…2) s. Then the laboratory germination of the seeds will be smaller (i.e. <100%/κ) compared to the control/untreated seeds in electromagnetic field.

Bright green, yellow and etc. to dark brown areas, for example in $\overset{\circ}{x}_1$ =(+0.5…+1.2) and $\overset{\circ}{x}_2$ =(+1.2…-1.2) demonstrate that the selected values of the two controlled factors of pre-sowing treatment influence stimulating in a different degree on the observed parameter – laboratory germination which is expected to exceed to 3% that one of the controlled seeds.

When the values of the two factors are taken in natural units it could be said that the stimulating impact of the pre-sowing electromagnetic treatment on the laboratory germination is expected in combination of two factors in the limits U=(10.5…12.6) kV and τ=(38…2) s. The laboratory germination in this case will be over 103%/c towards that of the controlled/untreated in electromagnetic field seeds.

According to Figure 1a and Figure 1b it could be concluded that in the adopted upper levels of the controlled factors $\overset{\circ}{x}_1$ =1 (i.e. U=12 kV) and $\overset{\circ}{x}_2$ =1 (i.e. τ=35 s), a stimulating pre-sowing effect is obtained – the value of the laboratory germination will be over 103%/c. In these values of the controlled factors in (*Ganeva D. et al., 2014*) is described that the laboratory germination of the pre-sowing treated seeds was g = 104.60%/c towards the control.

According to Figure 1b it could be established that in increase of the values of the two factors which are studied, for example $\overset{\circ}{x}_1$ =+1.2 (i.e. U=12.6 kV) and $\overset{\circ}{x}_2$ =+1.2 (i.e. τ=38 s) it should be expected an increase of the laboratory germination of the seeds of over 103%/c.

In this respect experiments should be conducted for pre-sowing electromagnetic treatments of the seeds by using of risen values of the two controlled factors. It should take into considerations that the

excessive increase of the values of the applied voltage could not be achieved by technical reasons because probably the corona discharge between the two electrodes could develop in spark discharge and then in arc electric discharge which would results in damage – burning of the seeds.

On the basis of the Figure 1a and Figure 1b, it could be established that in decrease of the values of the two factors it should expect a stimulation of the seed laboratory germination up to 1% towards the controls. This could be obtained in voltage $\overset{\circ}{x}_1$ =-1.2 (i.e. U=5.4 kV) and duration of treatment $\overset{\circ}{x}_2$ =-1.2 (i.e. τ=2 s).

According to Figure 1a and Figure 1b, it could be established that an increase effect of stimulation of the laboratory germination (over 3% towards the control) could be also obtained in the following values of the two factors: $\overset{\circ}{x}_1$ =+1.2 (i.e. U=12.6 kV) and $\overset{\circ}{x}_2$ =-1.2 (i.e. τ=2 s).

Therefore, the treatment of the seeds in the above mentioned increased voltage of the corona electrical discharge should be short as an impulse (in this case for 2 seconds). On the other hand, this would contribute for greater increase of the voltage value applied for pre sowing treatment and decrease of the probability for electrical break between the electrodes.

Variant 2: The factor $\overset{\circ}{x}_1$ – applied voltage between the electrodes U is eliminated. The equation of the response surface in the interaction of the factors $\overset{\circ}{x}_2$ and $\overset{\circ}{x}_3$ is:

$$\hat{Y}_{\kappa.} = 100{,}116 + 0{,}190\,\overset{\circ}{x}_2 + 0{,}323\,\overset{\circ}{x}_3 + 0{,}136\,\overset{\circ}{x}_2\,\overset{\circ}{x}_3 + 0{,}312\,\overset{\circ}{x}_2^2 + 1{,}257\,\overset{\circ}{x}_3^2 \quad (3)$$

Figure 2a and Figure 2b demonstrate the response surface and lines of response – laboratory germination of the seeds in function of the duration of electromagnetic treatment $\overset{\circ}{x}_2$ (τ) and length of stay $\overset{\circ}{x}_3$ (T) from treatment to set of seeds for germination that are built by (3).

The impact of the pre sowing electromagnetic treatments of the seeds is shown in different coloured zones in Figure 2 as well as in Figure 1.

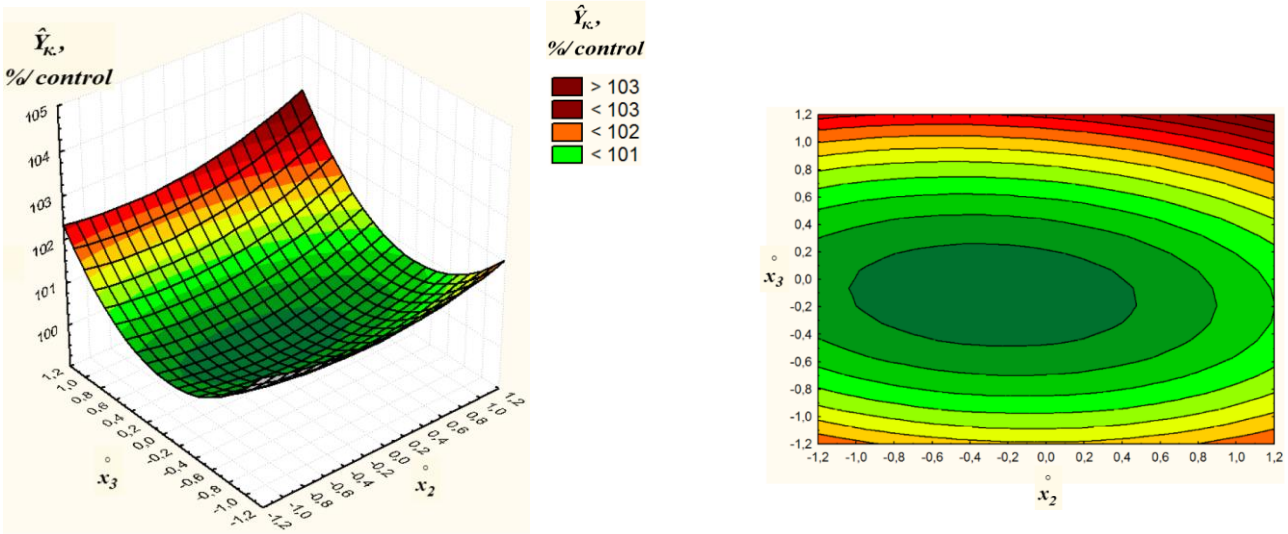

a) **b)**

Fig.2 – Response surface (a) and lines of response (b) – laboratory germination as a function of factors $\overset{\circ}{x}_2$ (τ) and $\overset{\circ}{x}_3$ (T), $\overset{\circ}{x}_1$ (U) switched off factor

The analysis of Figure 2a and Figure 2b demonstrates that in eliminated factor $\overset{\circ}{x}_1$ and in values of the controlled factors τ ($\overset{\circ}{x}_2$) and T ($\overset{\circ}{x}_3$) as follows: $\overset{\circ}{x}_2$ within (+1.2…-1.2) and $\overset{\circ}{x}_3$ – within (+0.6…-0.6), the pre sowing electromagnetic treatment will be with inhibiting effect.

When the values of the factors are in natural units the inhibiting effect of the pre sowing electromagnetic treatment on the laboratory germination is expected in combination of the two factors in the limits τ=(38…2) s and T=(10…6) days. The laboratory germination of the seeds in this case will be smaller (i.e. <100%/c) than that of the control/untreated seeds.

According to Figure 2a and Figure 2b could be concluded that an increase of the effect from pre sowing electromagnetic impact i.e. an increase of laboratory germination from 102%/c to over 103%/c could be obtained in combination of the values of the two controlled factors in the limits $\overset{\circ}{x}_2$ =(+1.2…-1.2) and $\overset{\circ}{x}_3$ =(+0.8…+1.2), respectively.

When the values are in natural units, the stimulation effect of the pre sowing electromagnetic treatment on the laboratory germination could be expected in combination of the two factors in the limits τ=(38…2) s and T=(11…13) days. Then the laboratory seed germination will be greater (over 103%/c) than that of the control/untreated seeds.

Variant 3: In this variant the factor $\overset{\circ}{x}_2$ – duration of the electromagnetic impact τ was eliminated. In this case in the interaction of the factors $\overset{\circ}{x}_1$ and $\overset{\circ}{x}_3$ the equation of the response surface is:

$$\hat{Y}_{\kappa.} = 99{,}803 + 0{,}839\,\overset{\circ}{x}_1 + 0{,}323\,\overset{\circ}{x}_3 + 0{,}676\,\overset{\circ}{x}_1\,\overset{\circ}{x}_3 + 0{,}939\,\overset{\circ}{x}_1^2 + 1{,}069\,\overset{\circ}{x}_3^2 \quad (4)$$

Figure 3a and Figure 3b show, respectively the response surface and lines of response – laboratory germination of the seeds in function of voltage $\overset{\circ}{x}_1$ (U) of the electromagnetic treatment and length $\overset{\circ}{x}_3$ (T) of stay from treatment to set the seeds for germination, built by the Model (4).

The analysis of Figure 3a and Figure 3b demonstrates that in eliminated factor $\overset{\circ}{x}_2$ and in values of the two controlled factors U ($\overset{\circ}{x}_1$) and T ($\overset{\circ}{x}_3$) as follows: $\overset{\circ}{x}_1$ within (+0.5…-1.2) and $\overset{\circ}{x}_3$ – within (+0.9…-1.1), the pre sowing electromagnetic impact will be inhibiting.

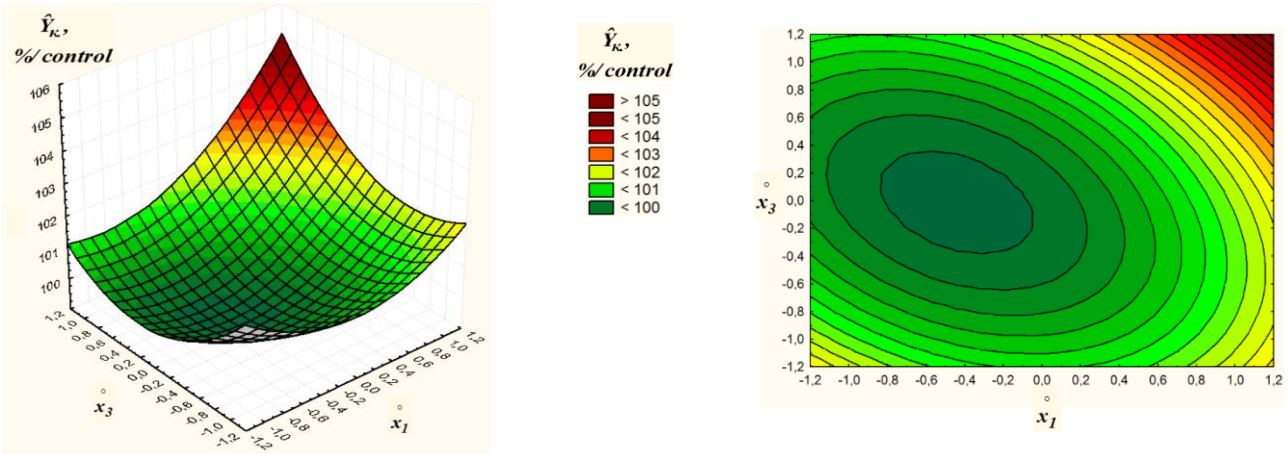

a) **b)**

Fig.3 – Response surface (a) and lines of response (b) – laboratory germination as a function of factors $\overset{\circ}{x}_1$ (U) and $\overset{\circ}{x}_3$ (T), $\overset{\circ}{x}_2$ (τ) switched off factor

When the values of the controlled factors are in natural units the inhibiting effect of the pre sowing electromagnetic treatment on the laboratory germination could be expected in combination of the factors duration of treatment τ=20 s with the remaining two factors in the limits U=(10.5…5.4) kV and T=approximately (11…3) days. In this case the laboratory germination of the seeds will be smaller (<100%/к) then that of the controls/untreated seeds.

The analysis of the Figure 3a and Figure 3b demonstrates that it is necessary the two controlled factors $\overset{\circ}{x}_1$ (U) and $\overset{\circ}{x}_3$ (T) to be with equal values or with greater values over the levels accepted as upper ones, i.e. $\overset{\circ}{x}_1 \geq 1$ and $\overset{\circ}{x}_3 \geq 1$ for stimulation of the laboratory germination with over 103%/c. Therefore if the factor $\overset{\circ}{x}_2$ is accepted at the mean level, i.e. $\overset{\circ}{x}_2 = 0$ (τ=20 s), the voltage of treatment $\overset{\circ}{x}_1$ should be accepted U≥12 kV and the length of stay $\overset{\circ}{x}_3$ – T 12 days.

The obtained theoretical results are confirmed by the presented in (*Ganeva D. et al., 2014*, 2015; *Sirakov K. et al., 2015*). Data demonstrates that as a result of the performed laboratory investigations after pre sowing electromagnetic treatments of the seeds from tomato variety Milyana by variant 1 – Table 2 (U=12 kV and τ=35 s) and length of the stay of the seeds to their set for germination T=12 days and T=365 days, the obtained results are the following:

- in T=12 days stay, the laboratory germination is stimulated to 4.6% over that of the control seeds, the root length of the germinated seeds – to 24.41%, of the hypo cotyledons – to 15.73%, of the cotyledons – 21.88% and the fresh plant weight – to 25.00%;
- in 365 days stay, the laboratory germination is increased over 9%, the root length – over 47%, the length of the hypo cotyledons – over 11.87% and that of the cotyledons over 16%.

According to that described above, it could be mentioned that by experimental (*Ganeva D. et al., 2014*, *2015*; *Sirakov K. et al., 2015*), and theoretical way is shown that in order to be obtained a stimulating effect of the pre sowing electromagnetic treatment of the seeds from tomato variety Milyana it is necessary that the controlled factor values to be higher – for voltage U≥12 kV, for duration of treatment τ≥35 s and length of stay to set of the seeds for germination T=(12 to 365) days, respectively. Similar stimulation effect could be expected when the pre sowing electromagnetic treatment is short/impulse with duration τ=2 s and voltage U≥12 kV, and T=(12 to 365) days from treatment to sowing.

CONCLUSIONS

1. On the basis of the performed laboratory investigations (*Ganeva D. et al., 2014*, *2015*; *Sirakov K. et al., 2015*), was established that the effective impact on the sowing properties of tomato seeds from variety Milyana could be obtained after pre sowing electromagnetic treatments in use of controlled factors with the following values: voltage of treatment U=12 kV, duration of treatment τ=35 s, length of stay from treatment to seed set for germination T=12 days. It was established that the positive effect as a result of pre sowing treatment is kept after 365 days from the treatment in U=12 kV and τ=35 s.

2. It is proved that after pre sowing electromagnetic treatment by extend plan of the experiment from B3 type and theoretical studies of the built response surfaces and lines of response – laboratory germination:

a) Positive results are obtained in the following values of the controlled factors: voltage of treatment U=12 kV, duration of treatment τ=35 s and length of stay from treatment to sowing T=12 days;

b) Efficient impact could be obtained in increase of the controlled factor values: voltage of treatment U over 12 kV, duration of treatment τ over 35 s and length of stay T of the seeds from treatment to sowing over 12 days;

c) Efficient impact should expect in combined increase of the values for controlled factor voltage of treatment and shortening of the duration of treatment to 2 s.

3. Theoretically established possibilities for efficient stimulation of the sowing properties and morphological characters of tomato seeds after pre sowing electromagnetic treatments should be examined in laboratory and field studies.

REFERENCES

[1] Danailov Zh., (2012), *Breeding and seed production of tomato (Solanum lycopersicum L.). History, methods, achievements, trends (Селекция и семепроизводство на домати* (*Solanum lycopersicum L.*). *История, методи, постижения, тенденции),* ISBN 978-954-322-502-6, "Prof. M. Drinov" Academic Publishing House, Sofia/Bulgaria;

[2] Ganeva D., Sirakov K., Mihov M., Martev K., Zahariev S., Palov I., (2014), Influence of pre-sowing electromagnetic treatments on propagating seed qualities of tomato variety Milyana (*Влияние на предсеитбените електромагнитни обработки и срока на съхранение върху кълняемата енергия и лабораторната кълняемост на семена от български сортове домати), Proceedings of the International Symposium ISB-INMA TEH`2014*, pp.646-653, Bucharest/Romania;

[3] Ganeva D., Sirakov K., Mihov M., Zahariev S., Palov I., (2015), Influence of pre-sowing electromagnetic treatments and duration of storage on germination energy and laboratory germination of seeds from Bulgarian tomato varieties (*Влияние на предсеитбените електромагнитни обработки и срока на съхранение върху кълняемата енергия и лабораторната кълняемост на семена от български сортове домати), INMATEH – Agricultural Engineering Journal*, vol.45, Issue 1, pp.43-50, Bucharest/Romania,;

[4] International Seed Testing Association, (ISTA), (2004), *International rules for seed testing*. Bassersdorf, Switzerland;

[5] Mitkov A., (2011), *Theory of experiment (Теория на експеримента), "*Dunavpress" Publishing House, Rouse/Bulgaria;

[6] Poryazov I., Petkova V., Tomlekova N., (2013), *Vegetable growing (Зеленчукопроизводство)*, "Dimi-99" Publishing Hause, Sofia/Bulgaria;

[7] Radevska M., Stoilova A., Palov I., Sirakov K., (2012), Impact of electromagnetic treatment and storage term on the pre-sowing properties of cotton seeds. I. Laboratory germination (Влияние на електромагнитната обработка и срока на съхранение върху посевните качества на семена от памук. I. Лабораторна кълняемост). *Plant Science*, vol.49, Issue 1, pp. 19-27, Sofia/Bulgaria;

[8] Sirakov K., (2006), Results of study after pre-sowing electromagnetic treatment of maize seed of Bulgarian and American hybrids (*Резултати от изследване след предсеитбени електромагнитни обработки на царевични семена от български и американски хибриди)*. Scientific works of "A. Kanchev" University of Ruse/Bulgaria, vol. 46, Issue 3.1, pp.87-91;

[9] Sirakov K., Ganeva D., Zahariev S., Palov I., Mihov M., (2015), Results of the investigation regarding the influence of pre-sowing electromagnetic treatment and storage period on sprouting of seeds of Bulgarian tomato varieties (Резултати от изследване влиянието на предсеитбените електромагнитни обработки и срока на съхранение върху прорастването на семена от български сортове домати)*, Ecology and Future*, vol. 14, Issue 1-2, pp. 65-71, Sofia/Bulgaria;

[10] TeKrony D.M., Egli D.B., (1991), Relationship of seed vigor to crop yield: A Review*, Crop Science,* Madison/WI, vol. 31, Issue 3, pp. 816-822;

[11] *** http://www.statsoft.com;

DETERMINATION OF THE RELAXATION PERIOD AT STATIC COMPRESSION OF GOLDEN DELICIOS APPLES VARIETY

/

DETERMINAREA PERIOADEI DE RELAXARE LA COMPRESIUNEA STATICĂ A MERELOR DIN SOIUL GOLDEN DELICIOS

Ph.D.Eng. Veringă D.[*1)], Ph.D.Eng. Vintilă M.[1)], Ph.D.Eng. Popa L.[2)], Phd.Eng.Ştefan V.[2)], Phd.Eng.Petcu A.S.[2)]

[1)] I.C.D.I.M.P.H. – HORTING Bucharest / Romania; [2)] INMA Bucharest / Romania

Tel: 0745 148.071; E-mail: veringa.daniela@yahoo.com

Keywords: *apples, storage, static compression*

ABSTRACT

The paper presents the Golden Delicious apples experimental researches, that aimed to emphasize apples behaviour at mechanical static or quasi-static compression stress and mechanical and rheological characteristics of fruits correlated to deficiencies determined (contusions, form distorsion), in order to anticipate their conduct in different practical situations.

REZUMAT

Lucrarea prezintă cercetările experimentale efectuate pe soiul de mere Golden Delicios care au urmărit să pună în evidență comportarea lor la solicitările mecanice de compresiune statică sau cvasistatică şi caracteristicile mecanice şi reologice ale fructelor în corelație cu defectele cauzate (contuzii, distorsionări ale formei), pentru a le putea anticipa în diferite situații practice

INTRODUCTION

During the long term storage the compression stress of apples located in the package bottom rows in boxes or containers should not be neglected, especially when the packages are not appropriate, determining the fruits defects, especially geometrical shape modifications (visible changes), which make them non marketable, thus leading to losses *(Ghergi A., Iordăchescu C., Burzo I., 1979; Gherghi A., 1994)*.

Experimental researches performed aimed to emphasize the Golden Delicious apple behaviour at mechanical static or quasi-static compression stress and rheological characteristics of fruits correlated to deficiencies (contusions, form modifications) determined in order to anticipate their conduct in different practical situations *(Abbott J.A., Lu R.,1996; Amir H., et al, 2008; Roudot A.C, 1991)*.

The apple compression resistance has determined as bio-flowing compression force and appropriate deformation and, at the same time, the specific hysteresis energy per cycle when loading-unloading, elasticity level (respectively plasticity level) to compression, Mayer hardness test (a measure of structure and tissue hardness) completed by resistance to penetration of a cylindrical rod and a suitable cone of shearing strain limit of flow (τc) of epicarp-pulp of whole fruits *(Căsăndroiu T., Ivănescu D., Vintilă M., 2009; Căsăndroiu T., Ivănescu D., 2009)* have found out.

It has aimed to find the rheological behaviour at compression between plane parallel rigid surfaces and a cylindrical punch, at constant load, followed by total unloading of fresh Golden Delicious apples, after harvesting *(ASAE recommendation, 1979)*.

MATERIAL AND METHOD

In order to perform the compression tests, The Golden Delicious apples were used, the fruits being grouped by three in each ripening class and coded as: A_1, A_2, A_3 representing the green apples; A_4, A_5, A_6 represent average ripe level apples and A_7, A_8, A_9 represent mature apples.

It has aimed to choose geoid shape fruits to be as close as possible to the spherical shape. Before being subjected to compression, the fruits were weighed, and their geometrical dimensions and radius of spherical surfaces in contact points with stress surfaces (by means of spherical shape meter) were measured, being shown in tab.1.

Table 1

Physical characteristics of fruits studied

Code	Ripe level	Mass m [g]	Height H [mm]	Equatorial Diam. D_e [mm]		Point 1	Point 2
				$D_{e\ max}$	$D_{e\ min}$	R_1 [mm]	R_2 [mm]
A1	green	140.3	66.54	71.13	65.47	41.76	48.46
A2		154.3	72.8	71.24	65.5	38.20	35.85
A3		153.1	68.41	70.32	66.63	42.26	44.40
A4	average	146.8	68.79	70.45	66.28	30.60	39.72
A5		145.8	67.58	72.87	69.68	33.66	38.62
A6		149.1	66.70	71.79	68.60	39.79	32.87
A7	ripe	177.3	71.75	74.49	71.18	31.84	39.53
A8		142.9	64.62	69.69	68.34	28.25	28.05
A9		154.4	75.80	69.53	67.67	34.72	39.05

Fruits were subjected to compression at a load rating between plane parallel rigid plates, using the universal apparatus of mechanical tests Hounsfield H25 KT.

After the compression, it aimed to test the firmness of fruit texture, sometimes called texture ‚rigidity" by using the method named « method of Magnes –Taylor pressing test", measuring the pressing force of a cylindrical rod calibrated of Φ 11.1 mm that penetrates into the fruit pulp to a certain depth, named ,,penetration resistance". Measurements were made with the Penetrometer FT 327 with a precision of 0.01 mm *(Manual of penetrometer presentation)*.

The fruit pulp texture resistance was determined in 12 points of each fruit, 4 points on every diameter (equatorial, apical and peduncle), according to fig. 1, in tab.2 being shown the data for the average penetration resistance between the 4 points on equatorial diameter.

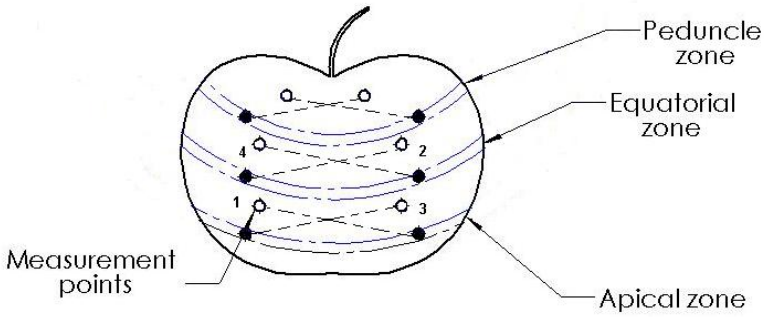

Fig.1 - Areas on fruit surface and points of measuring the penetration resistance

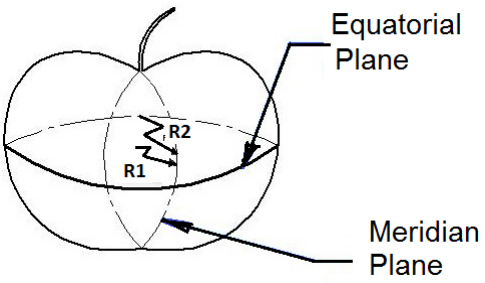

Fig.2 - Representation of radius measured in two plans

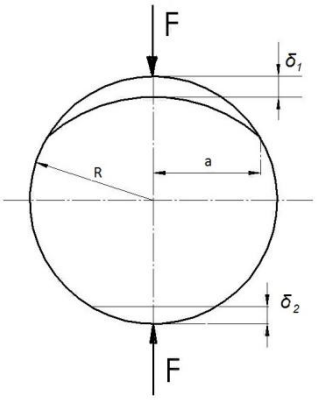

Fig.3 - Scheme for calculating the radius mark

There were calculated the elasticity module Young, *E* corresponding to bio-flow point and maximum normal tension $\sigma_{c\ max}$ of bio-flow, using the relations from the theory of elastic contact Hertz, *(Mohsenin M. N., 1986)*, ec. (1):

$$E = 0{,}749\frac{F\left(1-\upsilon^2\right)}{\delta^{3/2}}\left(\frac{1}{R_1^{1/3}}+\frac{1}{R_2^{1/3}}\right)^{3/2} \quad (1)$$

For the apples, it was considered υ=0,35; R_1 and R_2 representing the radius of curvature between the two contact points (fig.2), δ represents the total deformation (according to table 2), and F representing the force corresponding to bio-flow point (F_1 according to table 1).

After performing the calculations, the values from table 2 resulted.

Bio-flow tension was calculated by relation (2), where it represents the radius of track, in compliance with fig.3 *(Mohsenin M. N., 1986)*:

$$\sigma_c = \frac{3}{2}\frac{F}{\pi a^2} \quad (2)$$

RESULTS

Based on data obtained in tests one has aimed to research the possibility of establishing the correlations between the mechanical values measured and their compliance with the theoretical relations proposed for achieving the calculations.

After performing the compression tests with the apparatus Hounsfield H25 KT at 5 mm/min speed, using the cell of 1000 N, by processing the data gathered with Hounsfield Microsoft Windows Based program, graphics with force-deformation curves were obtained, from which were extracted the force and deformation values corresponding to the bio-flow point. These bio-flow point values are presented in table1.

From graphics and tables was extracted the value of force (F_1) corresponding to point C of bio-flow, displacement (total deformation up to bio-flow point) and slope corresponding to bio-flow point (table 2) and Figures 5-13 representing the force-deformation curve for each apple.

Data obtained from tests designed to determining fruit pulp texture resistance with Penetrometer FT 327 are given in table 3.

Table 2

Characteristics corresponding to bio-flow point (Hounsfield apparatus)

Code	Force F_1 [N]	Displacement (deformation) δ [mm]	Slope [N/mm]
A1	119.3	4.176	28.48
A2	64.0	2.616	24.43
A3	78.0	2.632	29.51
A4	42.0	2.120	19.69
A5	63.6	4.128	16.85
A6	120.4	5.300	22.72
A7	75.5	3.224	23.37
A8	35.0	2.392	14.60
A9	77.3	3.192	24.22

Noticing from graphics made by Hounsfield apparatus that deformation is delayed by certain quota, the correction of deformation δ, given in table 2 was made, using it in calculations

Table 3

Data of equatorial area referring to la R_{pmed}, E, E_{med}, σ_c, σ_{cmed}

Fruit	Force F [N]	Deformation δ corrected [mm]	$R_{p\,med}$ [N]	R_{pmed} [N]	E [Pa]	E_{med} [Pa]	σ_c [Pa]	σ_{cmed} [Pa]
A1	119.3	3.976	44.145	44.73	$4.19*10^6$	$5.426*10^6$	$0.352*10^6$	$0{,}374*10^6$
A2	64.0	2.276	44.120		$5.72*10^6$		$0.381*10^6$	
A3	78.0	2.292	45.910		$6.37*10^6$		$0.390*10^6$	
A4	42.0	1.720	47.995	42.66	$5.89*10^6$	$4.56*10^6$	$0.387*10^6$	$0.34*10^6$
A5	69.6	3.858	37.817		$2.85*10^6$		$0.264*10^6$	
A6	120.4	4.900	42.158		$3.44*10^6$		$0.371*10^6$	
A7	75.5	2.954	45.224	42.31	$4.66*10^6$	$4.15*10^6$	$0.393*10^6$	$0.31*10^6$
A8	35.0	2.052	39.534		$4.19*10^6$		$0.296*10^6$	
A9	77.3	2.792	42.183		$5.1*10^6$		$0.389*10^6$	

Graphically representing penetration resistance depending on the elasticity module in bio-flow point and penetration resistance depending on bio-flow resistance, the following graphics were obtained, fig.4.

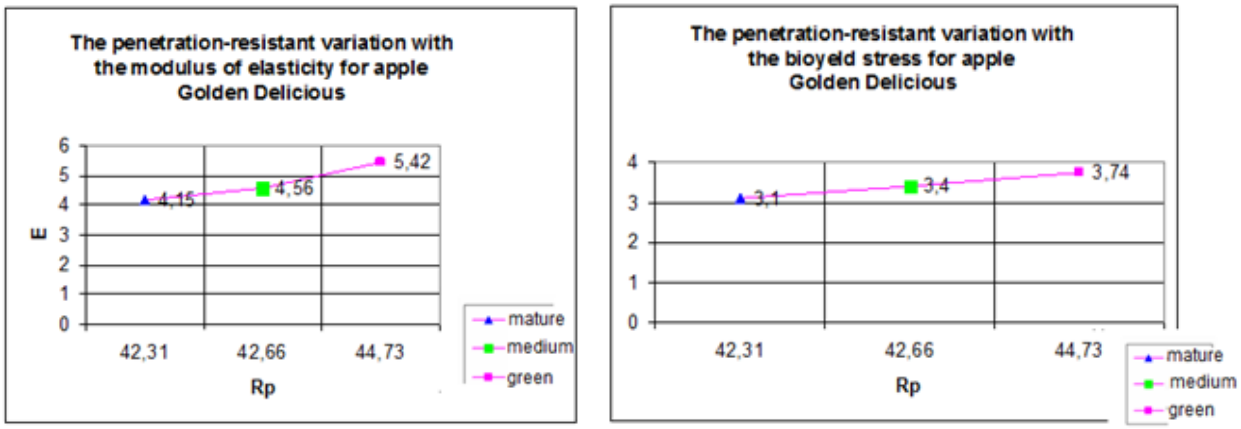

Fig.4 - Correlations (E, Rp) and (σc, Rp) for 3 degrees of ripening of Golden Delicious apple variety

From fig.4 it can observe that the correlations (E, R_p) and (σ_c, R_p), for Golden Delicious apple variety can be put in correlation with the apples ripeness.

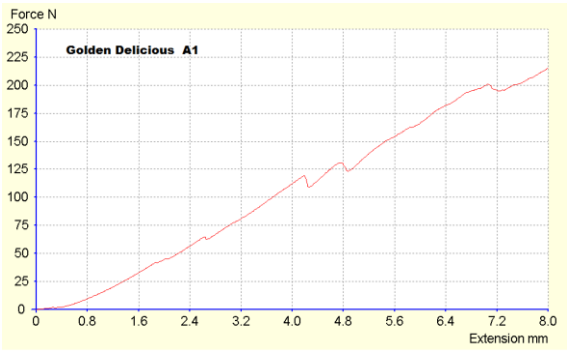

Fig.5 - Variation force - deformation for Delicious A1

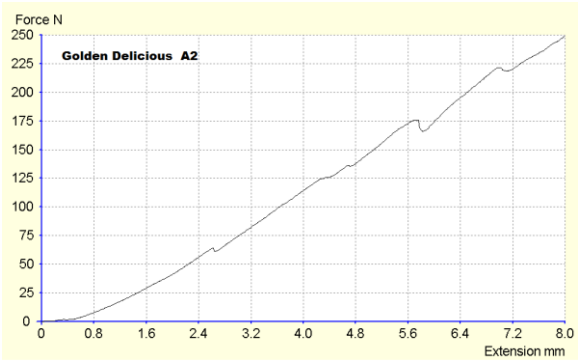

Fig.6 - Variation force - deformation for Delicious A2

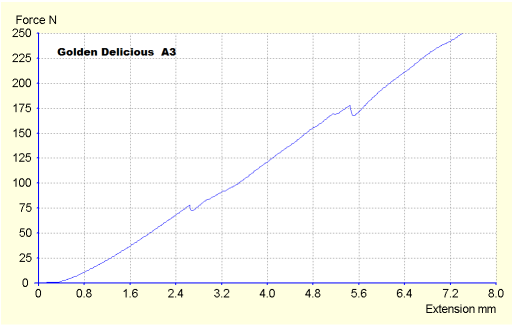

Fig.7 - Variation force – deformation for Delicious A3

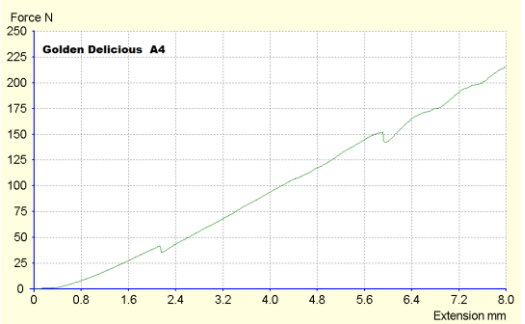

Fig.8 - Variation force – deformation for Delicious A4

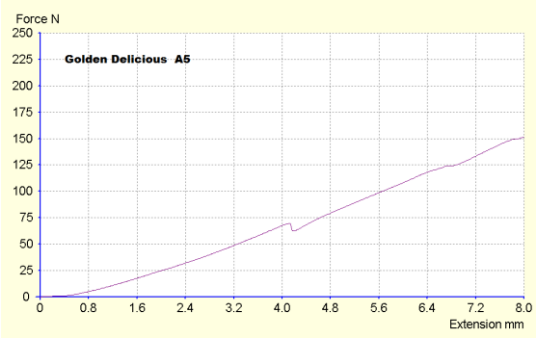

Fig.9 - Variation force – deformation for Delicious A5

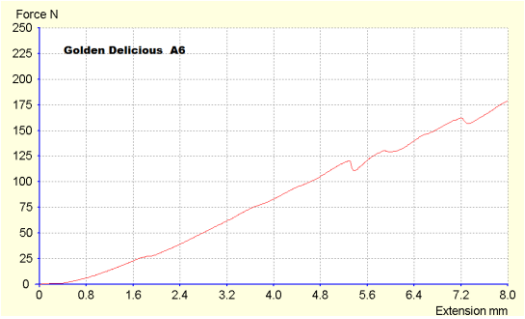

Fig.10 - Variation force – deformation for Delicious A6

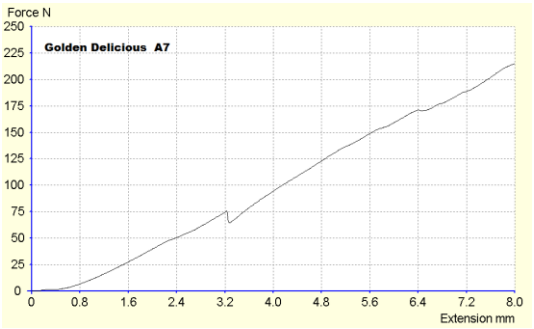

Fig.11 - Variation force–deformation for Delicious A7

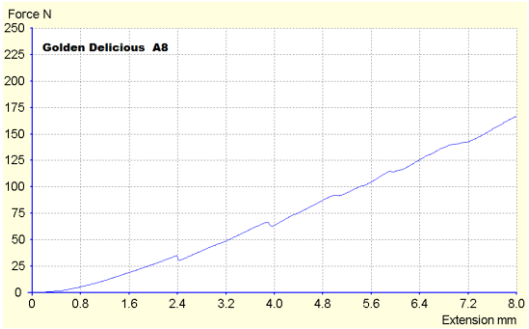

Fig.12 - Variation force–deformation for Delicious A8

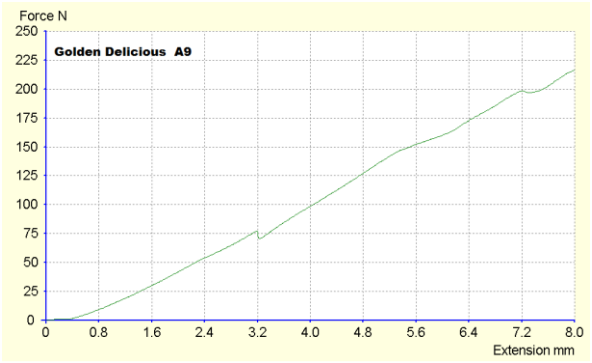

Fig.13 - Variation force-deformation for Delicious A9

CONCLUSIONS

Following the analysis of apple varieties existing in Romania, we have oriented towards the Golden Delicious study, because this variety is most demanded by market and presents technological features for a long storage period.

Losses and damages appearing during apples conservation are caused by static and quasi-static stress as well as, metabolic processes and diseases.

Considering the fruit as a viscous-elastic body, knowing the rheological parameters such as elasticity modules, viscosity parameters, relaxing time etc. allows to anticipate the fruit behaviour when is subjected to mechanical strain.

Experimental researches performed aimed to emphasize the apples behaviour at static and quasi-static compression and their mechanical characteristics related to their faults (contusions, modifications of shape) in order to anticipate their conduct in different practical situations.

The compression resistance was determined as bio-flow force and related deformation, between two plane parallel plates, the elasticity module Young and penetration resistance, a measure of firmness.

Elasticity module and penetration resistance, as well as bio-flow tension may be put into correlation with ripening level of Golden Delicious apples (these values increasing along with apple ripening degree).

REFERENCES

[1] Abbott J.A., Lu R., (1996), Anisotropic mechanical properties of apples, *Transactions of the ASAE*, vol.39(4), pp.1451-1459, USA;

[2] Amir H., Sayyah A., Behrooz Esmailpour, (2008), Apple firmness measurement based on viscous elastic properties, *Journal of Food Agriculture & Environment*, vol. 6(2), pp.276-279;

[3] Căsăndroiu T., Ivănescu D., Vintilă M., (2009), Experimental researches on homogenity of apple texture firmness (Cercetări experimentale privind omogenitatea fermității texturii pulpei merelor), *"Efficient use in agriculture and food industry of alternative energy and mechanizing-automation technologies, Scientific papers,* no*.27 INMATEH (Lucrări ştiinţifice,,Utilizarea eficientă în agricultură şi industria alimentară a energiilor alternative şi a tehnologiilor de mecanizare-automatizare, nr.27)*, pp.171-180 Bucharest/Romania;

[4] Căsăndroiu T., Ivănescu D., (2009), Theoretical aspects on mathematical modeling of the maximum allowable static compression received to no mechanical injury in apples (Aspecte teoretice privind modelarea matematica a compresiei statice maxime premise care sa nu prejudicieze merele din punct de vedere mecanic), *Modelling And Optimization In The Machines Building Field*, vol 15(2), Alma Mater Publishing House, pp.29-38, Bacău/Romania;

[5] Ghergi A., Iordăchescu C., Burzo I. (1979), *Maintaining the quality of fruits and vegetables in fresh state*, Ed.Tehnica Publishing House, Bucharest/Romania;

[6] Gherghi A. (1994), *Technology of horticultural products capitalization (Tehnologia valorificării produselor horticole)*, vol.I and vol.II, Publishing and Printing Workshops Metropol, Bucharest;

[7] Mohsenin M. N., (1986), *Physical properties of plant and animal materials*, Gordon and Breach Science Publishers, NY/USA;

[8] Roudot A.C., Duprat F., Weinian C., (1991), Modelling the response of apples to loads, *Journal of Agricultural Engineering Research*, vol.48, pp.249-259;

[9] *** ASAE recommendation, (1979), S-368.1, A-30, Compression tests of food materials of convex shape, *Agricultural Engineering Yearbook, ASAE,* St. Joseph, Michigan/USA;

[10] *** *Manual of penetrometer presentation* - Penetrometer Pénéfel FT 327.

SEGMENTATION OF RICE PLANTHOPPERS IN RICE FIELDS BASED ON AN IMPROVED LEVEL-SET APPROACH

/

基于改进水平集方法的农田稻飞虱图像分割

Ph.D. Yue Hongwei[1)], Assoc. Prof. Ph.D. Cai Ken[*2)], Assoc. Prof. Ms. Lin Hanhui[3)], Eng. Chen Zhihui[4)], Eng. Zeng Zhaofeng[5)]

[1)]School of Information Engineering, Wuyi University, Jiangmen / China;
[2)]School of Information Science and Technology, Zhongkai University of Agriculture and Engineering, Guangzhou / China;
[3)]Center for Educational Technology, Guangdong University of Finance and Economics, Guangzhou / China;
[4)]Faculty of Automation, Guangdong University of Technology, Guangzhou / China
[5)] Department of Mathematics and Computer Science, California State University, East Bay / U.S.A
Tel: +8602034172680; Email: icken@126.com

Keywords: *agricultural plant, rice planthopper, image segmentation, variation level set, steerable filter*

ABSTRACT

With the wide application of machine-vision technology in detecting agricultural plant diseases and insect pests in the field, this paper proposed an innovative approach for performing automatic segmentation of rice planthopper images. First, to weaken background interference, the Otsu approach was adopted to accomplish the preliminary segmentation. Then, a steerable filter was employed to improve the segmentation results of the feet and tentacles. Finally, by adding priori gray-level information, our proposed method improved the approximation capability of level-set-based evolution curves to targets. Results indicated that the approach adopted in this paper could clearly segment the contour of rice planthoppers.

摘要

随着机器视觉技术在农业病虫害识别领域的广泛应用,基于图像的稻飞虱害虫诊断成为有效地手段,本文提出一个新颖的方法来完成稻飞虱的自动分割问题。首先,为了消弱背景的干扰,利用大津法方法完成稻飞虱的初步分割。然后利用方向滤波器改善稻飞虱足和触角分割效果。最后融入先验灰度信息,提高了水平集演化曲线对于目标的逼近能力。结果表明,本文采用的方法可以清晰地分割稻飞虱的边缘轮廓,准确定位害虫区域。

INTRODUCTION

Rice planthoppers belong to Delphacidae, a kind of migratory pest that considerably damages rice. These planthoppers are the most serious pests of rice, and they inflict their harm by absorbing nutrients and releasing several destructive substances that substantially affect rice growth *(Gurr et al, 2011; Matsukawa et al, 2014; Zhou et al, 2013)*. Rice planthoppers have about 200 species. The three most common species are the white-backed planthopper, the small brown rice planthopper, and the brown planthopper. Given the great harm caused by these rice planthoppers, agricultural producers usually misuse pesticides and consequently cause concealed problems in food safety. Thus, rice has been requested to be sprayed on-site at appropriate times and amounts, and real-time diagnosis has been proposed. However, considering their small size and dark colour, rice planthoppers are difficult to identify and distinguish from one another.

The approaches used locally and abroad for identifying rice planthoppers and other agricultural pests currently include acoustic detection, trapping, and near-infrared technology *(Huynh et al, 2012; Selby et al, 2014)*. These methods essentially use manual detection. Normally, the recognition of infection depends on the inspector's practical experience. According to the current public literature, research on rice planthoppers has mainly focused on the relationship between the ecological environment and the insects' growth, as well as the prediction and forecast of future insect outbreaks *(Bottrell et al, 2012; Li et al, 2013; Otuka et al,* 2012*)*. With the wide application of machine-vision technology in agricultural fields, image-based pest diagnosis is becoming a fast and effective approach. However, related literature on rice planthoppers is rarely available. Our team collects rice planthopper images taken from the field as samples and studies the insects in terms of identification, diagnosis, and prediction. Given the complex background information on the collected samples, image pre-treatment is required before image identification to remove irrelevant information, strengthen relevant information detectability, and maximally simplify the data. Consequently, the reliability of feature extraction and matching identification can be improved. Thus, as an important link for pre-treatment, the image segmentation of rice planthoppers directly affects the following feature extraction and identification links.

Research on machine vision technology began late in agriculture. Attaining a high-efficiency, high-accuracy segmentation algorithm is a hot and difficult issue in obtaining the automatic identification. In recent years, the level-set approach has been widely used in image segmentation because of its good segmentation results and theoretical basis. Chan and Vese combined the level-set theory with the Mumford-Shah (M-S) model and generated a C-V level-set model *(Chan and Vese, 2001)*. This strategy adopted global information to extract target boundaries without relying on an image gradient. Therefore, images of no meaning to the gradient or those with weak edges can also be well segmented. At the same time, the improved algorithm *(Allaire et al, 2014; Bashir et al, 2014; Li et al, 2005; Zhang et al, 2013)* based on a C-V level set was achieved accordingly. Many improved level-set approaches demonstrate good performances in image segmentation. However, for cases with many complex images (e.g., background gray multilevel hierarchy), targets that are occluded or defected, and targets and background with similar gray levels, the segmentation results are hardly satisfactory without the support of priori information. Therefore, one important research direction for the level-set approach is to integrate targets' priori information into the level-set models and accordingly enhance the approximation capability of evolution curves to targets.

The remainder of this paper is organized as follows. Section 2 describes the traditional C-V level-set model and the main idea of an improved algorithm. Section 3 presents an actual experiment that evaluates the performance of the improved level-set approach. The conclusions are given in Section 4.

MATERIAL AND METHOD

The structure of the image acquisition device is designed based on the rice planthoppers' photo-axis feature of yellow and green. According to our preferences, 160 W self-ballasted fluorescent mercury lamps with high pressure are used as the background light source to trap rice planthoppers. A rice planthopper acquisition system is presented in Figure 1. Under the conditions of an open field environment, planthopper images are taken (Figure 2). The size of each captured image is 640 pixels by 480 pixels.

Fig.1 - Acquisition system of rice planthopper images

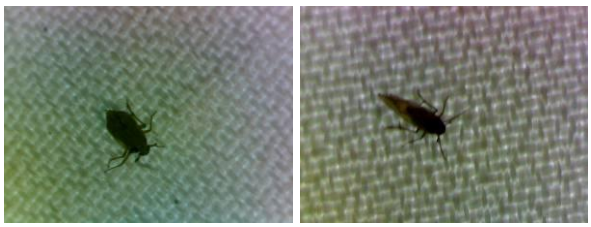

Fig.2 - Sample images of rice planthoppers

The C-V model assumes that the gray level of the homogeneous area is constant. The images are segmented into target area R_a (the average gray level is C_a) and background area R_b (the average gray level is C_b). The data smoothness item of the M-S models is removed, thus leaving the fidelity term and collective measurement item. The simplified fitting energy equation can be described as follows:

$$E(C) = E_a(C) + E_b(C) = \int_{inside(C)} |I - C_a|^2 dxdy + \int_{outside(C)} |I - C_b|^2 dxdy \quad (1)$$

In the process of curve evolution, Chan and Vese added length and area terms as bound terms and generated a general energy model for image segmentation as follows:

$$E(C, C_a, C_b) = \mu L(C) + \nu S_a(C) + \lambda_a \int_{inside(C)} |I - C_a|^2 dxdy + \lambda_b \int_{outside(C)} |I - C_b|^2 dxdy \quad (2)$$

In the formula, $\mu, \nu \geq 0$, $\lambda_a, \lambda_b > 0$ are the weight coefficients of each energy item, $L(C)$ is the length of evolving curve $C(x, y)$, and $S_a(C)$ is the acreage of the inner area. $L(C)$ and $S_a(C)$ are presented as follows:

$$L(C) = \int_\Omega |\nabla H(\phi(x, y))| dxdy = \int_\Omega \delta(\phi(x, y)) |\nabla H(\phi(x, y))| dxdy \quad (3)$$

$$S_a(C) = S[inside(C)] = \int_\Omega H(\phi(x, y)) dxdy \quad (4)$$

The C-V level-set model is based on the hypothesis of image piece-wise smooth functions. Therefore, the Heaviside and Dirac functions are introduced to cause the gradient descent flow equation to act at all level sets. As a result, the inner areas with hollow targets can be monitored automatically, and the energy function can be reduced to a global minimum. The discrete expression is:

$$H(z) = 0.5[1 + \frac{2}{\pi} \arctan(\frac{Z}{\varepsilon})], \ \delta(z) = \frac{d}{dz} H(z) \quad (5)$$

The abovementioned formula is then incorporated in equation (2) to yield the following energy function:

$$E(C, C_a, C_b) = \mu \int_\Omega \delta(\phi) |\nabla \phi| dxdy + \nu \int_\Omega H(\phi) dxdy + \lambda_a \int_\Omega |I - C_a|^2 H(\phi) dxdy + \lambda_b \int_\Omega |I - C_b|^2 [1 - H(\phi)] dxdy \quad (6)$$

After each iteration, the C_a and C_b values are expressed as:

$$C_a = \frac{\int_\Omega I(x, y) H(\phi(x, y)) dxdy}{\int_\Omega H(\phi(x, y)) dxdy}, \ C_b = \frac{\int_\Omega I(x, y)[1 - H(\phi(x, y))] dxdy}{\int_\Omega [1 - H(\phi(x, y))] dxdy}. \quad (7)$$

On the basis of the variation approach, we combine equations (6) and (7) to generate the E-L expression of equation (2) as:

$$\frac{\partial \phi}{\partial t} = \delta(\phi)[\mu k - \nu - \lambda_a [I - C_a]^2 + \lambda_b [I - C_b]^2] \quad (8)$$

$$k = \frac{\phi_{xx} \phi_y^2 - 2\phi_x \phi_{xy} \phi_y + \phi_{yy} \phi_x^2}{(\phi_x + \phi_y)^{3/2}} \quad (9)$$

where k represents the curvature. According to the above analyses and results, the curve evolution status for each moment can be identified through numerical methods by only giving the level-set function of the initial time. The advantages of C-V models are shown in two aspects. First, targets with undefined edge gradient can be detected. Traditional edge detection methods not only lead to segmentation failure but also cause edge crack problems. Second, internal contours can also be detected automatically. Some problems are also found apart from favorable aspects. For example, the image with intensity inhomogeneity cannot be detected. The domain of the image function $I(x, y)$, which is involved in the PDF equation, concerns the entire image data with global features. Consequently, the calculation of data processing in the whole domain is considerably heavy. The C-V level-set model uses global features to segment target images. Images are segmented into target area R_a and background area R_b to obtain the two-phase image segmentation. This strategy involves the use of same-level functions to segment two areas. In the natural environment, rice insect image acquisition in rice fields is degraded by uneven illumination. The corresponding gray-level histogram contains two or more troughs, or the background image gray level

contains two or more hierarchies. The two-phase image segmentation appears powerless. Therefore, rice planthopper images with similarities between targets and background or with intensity inhomogeneity cannot be effectively segmented by the C-V level set.

Accordingly, this paper considers two aspects to improve the C-V approach; initialization of the level-set function and priori information added to targets. In the traditional C-V approach, the level-set function is represented by a signed distance function generated from closed curves. Curve C divides the plane into internal and external areas. The signed distance function corresponds to $\phi(x,y)=\pm d$, where d represents the distance between point (x,y) and the curves on the plane. Normally, the signed distance function is defined as a circular conical surface, and the calculation is relatively complicated. In literature *(Wei, 2010)*, the radius of the closed curve C is set to infinite; therefore, curve C can be shown as a straight line on the plane and divides the plane into the upper area Ω_u, $y \geq y_0$ and lower area Ω_d, $y < y_0$. The initialization function ϕ_0 is defined as a discontinuous curved surface function expressed as:

$$\phi_0(x,y)=\begin{cases}\rho_u,(x,y)\in\Omega_u\\ \rho_d,(x,y)\in\Omega_d\end{cases},\ \rho_u\times\rho_d<0 \tag{10}$$

Given the improved initialization of level-set functions, this paper employs the closed curve C in dividing the plane into internal and external areas (Ω_{in} and Ω_{out}, respectively), where ϕ_0 is defined as:

$$\phi_0(x,y)=\begin{cases}\rho_{in},(x,y)\in\Omega_{in}\\ \rho_{out},(x,y)\in\Omega_{out}\end{cases},\ \rho_{in}\times\rho_{out}<0 \tag{11}$$

Furthermore, the recalculation of values C_a and C_b is required after each iteration. The computational process costs a substantial period of time that still cannot guarantee the target image to be the segmentation result. Other background areas may also be included, and thus some considerable discrepancies between segmentation result and the target are attained in certain features. If rough priori information, such as the gray level, is already known, the tough gray level can be directly given to C_a and C_b. Thus, the computation during the whole iteration process can be greatly reduced, and the differences in the gray level feature between the segmentation result and the target can also be narrowed. This paper adopts this algorithm. C_a and C_b are known in the whole computation process, thus making the curve evolution alternately rely on the image target and background gray-level information.

The energy function of the modified C-V level-set segmentation model is as follows:

$$E(C)=E_0+E_m(\phi) \tag{12}$$

where ϕ is the level-set function. Image similarity after segmentation is controlled by the first item E_0 on the right-hand side of the equation, which is used as the fidelity term. The specific form is:

$$E_0=\lambda_a\int_{inside(C)}\left|I-C_a\right|^2dxdy+\lambda_b\int_{outside(C)}\left|I-C_b\right|^2dxdy \tag{13}$$

In the formula, $\lambda_a,\lambda_b\geq 0$ .The second item $E_m(\phi)$ is the external energy term that prompts the evolution from the evolving curves to the target boundary. It is defined as follows:

$$E_m(\phi)=\mu L_g(\phi)+\nu A_g(\phi) \tag{14}$$

In the formula, $\mu,\nu\geq 0$ is the weight coefficient of each item. The definitions of $L_g(\phi)$ and $A_g(\phi)$ are:

$$L_g(\phi)=\iint_\Omega g\delta(\phi)\left|\nabla\phi\right|dxdy\ ,\ A_g(\phi)=\iint_\Omega gH(-\phi)dxdy \tag{15}$$

where g is the edge indication function. The external energy term is added to obtain a more accurate contour of the segmentation target. The rough contour can be obtained through the effect of E_0. For further refinement of the contour, we relied on the $E_m(\phi)$ item. Using the variation principle to achieve the minimum total energy equation (12), the E-L equation of the level-set function ϕ can be derived as:

$$\frac{\partial\phi}{\partial t}=\delta(\phi)[-\lambda_a(I-C_a)^2+\lambda_b(I-C_b)^2+\mu(gk+\nabla g\frac{\nabla\phi}{\left|\nabla\phi\right|})+\nu g] \tag{16}$$

RESULTS

The first strategy used determines a precise localization of the pest-infested area to adapt to the natural conditions in open rice fields. Otsu is an adaptive threshold determination method that is also called the maximum variance method. The basic concept of Otsu involves the use of a gray-level histogram to dynamically determine the image segmentation threshold based on the maximum variance between the target and the background. This method divides the image into the background and the target depending on the gray-level feature. The larger variance between the background and the target implies greater differences between the two parts of the image. Furthermore, the differences become smaller when part of the target is erroneously divided as the background or when part of the background is erroneously divided as the target. Using the Otsu method to apply image binarization to Figure 3 and eliminate small isolated areas through morphological operation, we obtain the rice planthopper binary image shown in Figure 4.
The corresponding edge contour can be used as the initial contour of the level set.

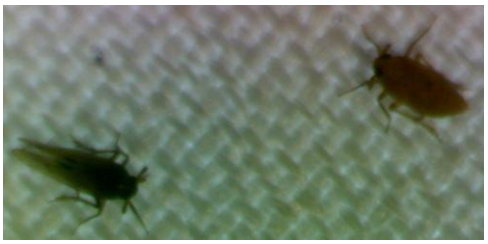

Fig.3 - Sample image of rice planthoppers

Fig.4 - Initial contour of the level set

In the experiment, the weight coefficient λ_a, λ_b, μ, and v are all set to 1, time step Δt is set to 0.5, the function parameter ε of H is set to 1.5, ρ_{in} and ρ_{out} are set to 2 and −2, respectively. Through the analysis of a large number of plant diseases and insect pest images, C_a can be set to 55 and C_b can be set to 110. The segmentation results achieved by the traditional C-V and modified level sets are separately illustrated in Figures 5 and 6. The final images of the rice planthopper obtained by eliminating small isolated areas through the morphological operation of Figures 5(a) and 6(a) are shown as Figures 5(b) and 6(b). The intensity of non-homogeneity of the acquisition background (intensity inhomogeneity is mainly caused by curtain textures) caused the images with similarity between targets and background to be ineffectively segmented by the traditional level-set approach (Figure 5(b); the background region is divided into plant diseases and insect pest region). The algorithm proposed in this paper uses priori information to set up C_a and C_b of the target and the background and obtains better segmentation results than the traditional one. Figures 5(b) and 6(b) indicates that the algorithm also generates better performance in highlighting details.

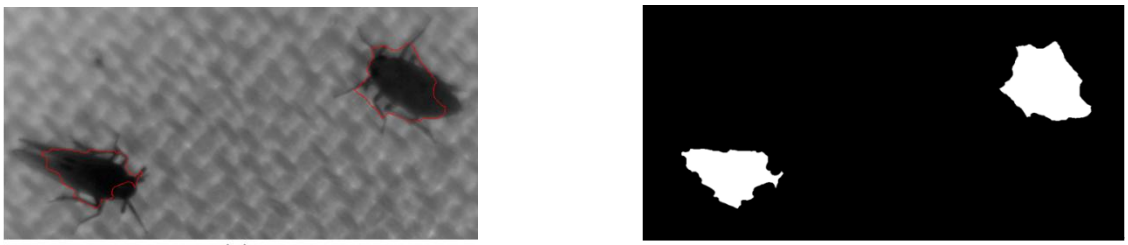

(a) (b)

Fig.5- Segmentation result attained by the traditional C-V

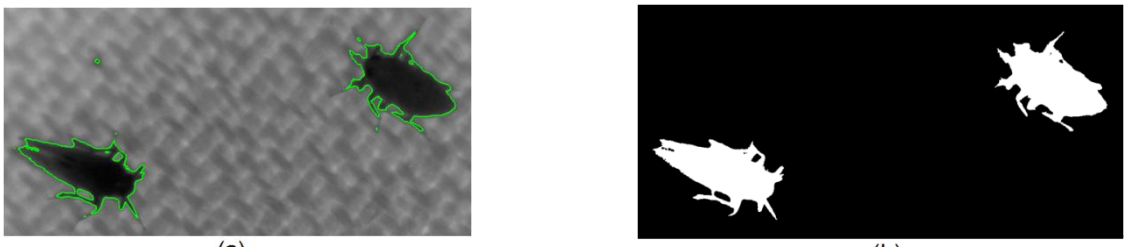

(a) (b)

Fig.6 - Segmentation result attained by the proposed C-V

To obtain good detailed segmentation, the feet and tentacles of the rice planthoppers must be enhanced before applying the contour evolution of the level set. The feet and tentacles of the rice planthoppers are not well segmented in the processing of insect pest image I (Figure 6(b)). In this paper, a steerable filter *(Freeman and Adelson, 1991)*, which is a kind of directional gradient operator, is used to enhance the image. Through the linear combination of a group of basis filters, the filter achieves the response to any direction. The second derivative of a two-dimensional Gaussian function is used as the basis filter. The related expression is as follows:

$$G(x,y)=\exp(-\frac{x^2+y^2}{2\sigma^2}) \tag{17}$$

The corresponding second derivative is expressed by the following basis filter:

$$G_\theta(\sigma)=k_a(\theta)G_{2axy}(\sigma)+k_b(\theta)G_{2bxy}(\sigma)+k_c(\theta)G_{2cxy}(\sigma) \tag{18}$$

$$G_{2axy}(\sigma)=(\frac{x^2}{\sigma^2}-1)\exp(-\frac{x^2+y^2}{2\sigma^2}),k_a(\theta)=\cos^2(\theta) \tag{19}$$

$$G_{2bxy}(\sigma)=\frac{xy}{\sigma^2}\exp(-\frac{x^2+y^2}{2\sigma^2}),k_b(\theta)=-\sin(2\theta) \tag{20}$$

$$G_{2cxy}(\sigma)=(\frac{y^2}{\sigma^2}-1)\exp(-\frac{x^2+y^2}{2\sigma^2}),k_c(\theta)=\sin^2(\theta) \tag{21}$$

where σ decides the scale of filters, and θ is the input direction. The decomposition angle θ of steerable filters can be set arbitrarily. For texture images, the angle at which the maximum variance of decomposition coefficient appears can be ascertained by increasing the decomposition angle from 0° to 180° by certain degrees. The result denotes that the texture images attain the most obvious gradient variation at such an angle. In the experiment, the direction angle is sampled as $0,\pi/N,\cdots,(N-1)\pi/N$ to obtain many different directional filters. The value of parameter N is 18. We assume that plant disease and insect pest image H can be obtained after filtering image I to yield the following expression:

$$N(I)=\min(H,I) \tag{22}$$

The equation means that with the minimum pixel number of images I and H, $N(I)$ attains the evolution segmentation of a level set by replacing I. The results before and after filtering by steerable filters are displayed in Figure 7. The feet and tentacles of the rice planthoppers are enhanced with stronger contrast effects and more outstanding edges in Figure 7(b). The level-set segmentation result achieved using the approach proposed in this paper is illustrated in Figure 8. By comparing Figures 6(b) and 8(b), we note that the feet and tentacles of the rice planthoppers achieved better segmentation after direction filtering.

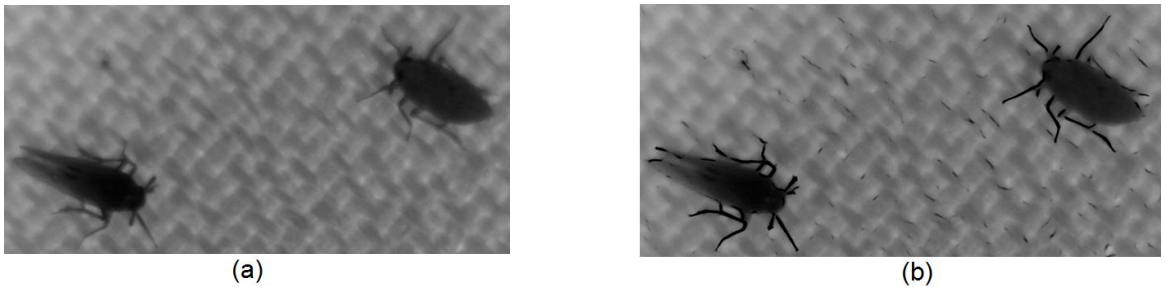

(a) (b)

Fig.7 - Results before and after filtering by steerable filters

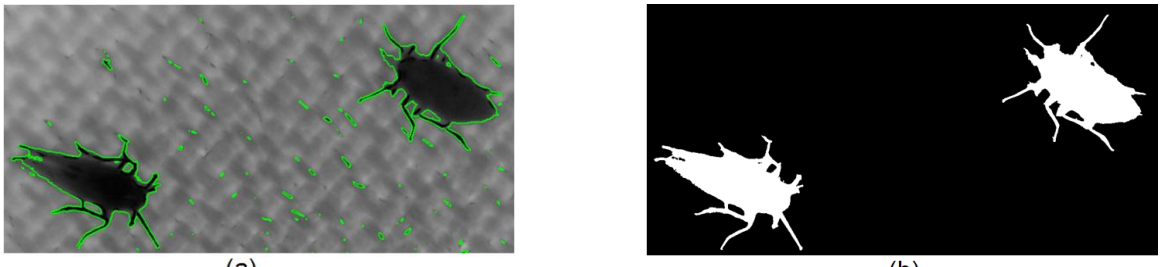

(a) (b)

Fig.8 - Segment results of the proposed C-V after filtering by steerable filters

The comparison of the minimum iterative step and the iterative operation time is presented in Table 1. The hardware environment of this contrast experiment is a computer with a CPU Intel Core2 E7500+2.93 GHz and 1.96 GB memory. As shown in Table 1, the proposed method also exhibited significantly improved efficiency relative to the traditional C-V method.

Table 1

Comparison of different methods

	Traditional method	Proposed method
Least number of iterations	263	4
Iteration time (ms)	807	312

CONCLUSIONS

The use of computer vision to recognize crop diseases has become a new development direction in precision agriculture. However, many disease and insect pest image segmentation algorithms are presently implemented in the laboratory environment. Under field conditions, the collected images of agricultural plant diseases and insect pests are more easily affected by noise, and thus a large number of false segmentations may occur. This paper discusses the improvement of image segmentation using the C-V level-set model from two aspects, namely, the initialization function and the target priori information. The study also reports an enhanced solution for the rice planthopper segmentation problem under open-field conditions. Using the proposed method, we further improved the segmentation results relative to those achieved by the traditional C-V level-set approach. This research also lays the foundation for succeeding feature extractions and identification. Rice planthoppers are a highly recognized natural disaster that considerably endangers rice production. Hence, multiple feature fusion of classification methods should be considered in future research to realize the remote real-time identification of the pest.

ACKNOWLEDGEMENT

This work was supported by the Features Innovative Program in Colleges and Universities of Guangdong (No.2015KTSCX069), the Pearl River S&T Nova Program of Guangzhou (No.201506010035), the State Scholarship Fund (CSC No.201408440326), the Project of Outstanding Young Teachers' Training in Colleges and Universities of Guangdong (No. YQ2015091), the National Spark Program of China(No.2014GA780009), the Natural Science Foundation of Wuyi University (No.2014zk10) and the PhD Start-up Fund of Natural Science Foundation of Wuyi University.

REFERENCES

[1] Allaire G., Dapogny C., Frey P., (2014), Shape optimization with a level set based mesh evolution method, *Computer Methods in Applied Mechanics and Engineering*, Vol.282, Elsevier Science SA., pp.22-53, Lausanne;

[2] Bashir S., Rees J. M., Zimmerman W. B., (2014), Investigation of pressure profile evolution during confined micro-droplet formation using a two-phase level set method, *International Journal of Multiphase Flow*, Vol.60, Pergamon-Elsevier Science LTD, pp.40-49, Oxford;

[3] Bottrell D. G., Schoenly K. G., (2012), Resurrecting the ghost of green revolutions past: the brown planthopper as a recurring threat to high-yielding rice production in tropical Asia, *Journal of Asia-Pacific Entomology*, Vol.15, Issue 1, Korean Society of Applied Entomology, pp.122-140, Suwon;

[4] Chan T. F., Vese L. A., (2001), Active contours without edges, *IEEE Transactions on Image Processing*, Vol.10, Issue 2, IEEE-INST Electrical Electronics Engineers INC., pp.266-277;

[5] Freeman W. T., Adelson E. H., (1991), The design and use of steerable filters, *IEEE Transactions on Pattern Analysis and Machine Intelligence*, Vol.13, Issue 9, IEEE Computer Society, pp.891-906;

[6] Gurr G. M., Liu J., Read D. M. Y., et al., (2011), Parasitoids of Asian rice planthopper (Hemiptera: Delphacidae) pests and prospects for enhancing biological control by ecological engineering, *Annals of Applied Biology*, Vol.158, Issue 2, pp.149-176, Wiley-Blackwell/Hoboken;

[7] Huynh V. K., Zucker J., Huynh H. X., et al.,(2012), Spatial estimator of brown plant hopper density from light traps data, *2012 IEEE RIVF International Conference on Computing and Communication Technologies, Research, Innovation, and Vision for the Future*, IEEE, pp.1-6, Ho Chi Minh;

[8] Li C., Xu C., Gui C, et al., (2005), Level set evolution without re-initialization:a new variational formulation, *IEEE International Conference on Computer Vision and Pattern Recognition*, IEEE, pp.430-436, San Diego;
[9] Li Ma, Huaming Liao, Chuanhong Feng, et al., (2013), Anylysis of the unusual occurrence of rice planthopper in Sichuan Province in 2012*, Chinese Agricultural Science Bulletin*, Vol.29, Issue 33, pp.337-340, Chinese Agricultural Science Bulletin Press/Peking;
[10] Matsukawa M., Ito K., Kawakita K., et al., (2014), Current status of the occurrence and farmer perceptions of rice planthopper in Cambodia, *Japan Agricultural Research Quarterly*, Vol.48, Issue 2, pp.167-173, Japan International Research Center for Agricultural Sciences/Tsukuba;
[11] Otuka A., Zhou Y., Lee G. S., et al., (2012), Prediction of overseas migration of the small brown planthopper, Laodelphax striatellus (Hemiptera: Delphacidae) in East Asia, *Applied Entomology and Zoology,* Vol.47, Issue 4, Springer, pp.379-388 Tokyo/Japan;
[12] Selby R. D., Gage S. H., Whalon M. E., (2014), Precise and low-cost monitoring of plum curculio (Coleoptera: Curculionidae) pest activity in pyramid traps with cameras, *Environmental Entomology*, Vol.43, Issue 2, pp.421-431, Oxford University Press/Cary;
[13] Wei Z., Bi D., Ma S., (2010), Improved fast C-V level set infrared image segmentation, *Journal of Data Acquisition and Processing*, Vol.25, Issue 3, pp.347-352, Data Acquisition and Processing Press/Nanjing;
[14] Zhang K., Zhang L., Song H., et al., (2013), Reinitialization-free level set evolution via reaction diffusion, *IEEE Transactions on Image Processing*, Vol.22, Issue 1, pp.258-271, IEEE-INST Electrical Electronics Engineers INC./Piscataway;
[15] Zhou G., Xu D., Xu D., et al., (2013), Southern rice black-streaked dwarf virus: a white-backed planthopper-transmitted fijivirus threatening rice production in Asia, *Frontiers in Microbiology*, Vol.4, pp.270, Frontiers Media SA./Lausanne.

RESEARCH AND APPLICATION OF THE EVAPORATION CAPACITY SPATIAL INTERPOLATION METHOD FOR AGRICULUTRAL ENVIRONMENT
/
面向农业环境的蒸发量空间插值方法研究和应用

Ph.D. Yinlong Jin [*1)], Prof. Ph.D. Eng. Jiesheng Huang[1)], Ph.D. Ben Li[1,2)]
[1)]State Key Laboratory of Water Resource and Hydropower Engineering Science ,Wuhan University, Wuhan / China;
[2)] College of Earth, Ocean, and Atmospheric Sciences, Oregon State University, Corvallis / U.S.A.
Tel: +86-138-71136226; E-mail:wrhjinyl@whu.edu.cn

Keywords: *Agricultural environment; Waterlogging field; Evaporation capacity; Spatial interpolation*

ABSTRACT

Waterlogging is a common agricultural disaster with complicated causes when agricultural environment changes, one of which is evaporation. Identifying waterlogging disasters requires evaporation data with continuous space–time distribution. Traditional spatial interpolation methods are based on the correlation between the interpolating point and observation station. By contrast, the present study develops a new method by conducting the following work: First, ground evaporation and air temperature are considered to be a field coupled with the atmospheric flow field, which is calculated through the spectral method. A new spatial interpolation method is proposed based on spherical harmonics and with the incorporation of temperature parameters into the calculation model. Second, the internal and external errors of the interpolation results are calculated under multiple temperature conditions, and precision evaluation and robustness analysis are conducted on the interpolation results of the daily evaporation capacity. Lastly, a comparative analysis is conducted on the calculation results of the monthly evaporation capacity and MOD16 data under multiple temperature conditions. This study provides selection methods and judging conditions for temperature parameters and also discusses the occurrence of the temperature accumulative effect in the interpolation of the monthly evaporation capacity. This study also explains the contracting phenomenon of the residual distribution and model precision, as well as the temperature accumulation phenomenon, in the interpolation of the monthly evaporation capacity. The experimental results show that the method proposed in this study is a feasible and effective spatial interpolation method for evaporation capacity and can provide scientific basis for the farming and water management.

摘要

农田环境变化时，涝渍灾害是常见的成因复杂的农业灾害，蒸发是重要的致灾因素．渍害的识别需要时空连续分布的蒸发量数据,传统的空间插值方法依据插值点与观测站之间的相关性，本文寻求新思路并进行了以下工作：首先，从大气运动场解算的谱方法，将地面蒸发和大气温度看做一个耦合场，提出一种基于球谐函数的空间插值新方法，同时将温度参数纳入解算模型．再者，计算多种温度条件下插值结果的内外符合精度，对日蒸发量插值结果进行精度评价和稳健性分析．最后，对多种温度条件下的月蒸发量计算结果和MOD16 数据进行对比分析，给出了温度参数选择方法判定条件，同时提出了月蒸发量插值计算中的温度累积效应．同时解释了残差分布与模型精度的相悖现象和月蒸发量插值中的温度累积现象．实验结果表明本文研究方法是一种可行且有效蒸发量空间插值算法，可为农业水管理提供科学依据。

INTRODUCTION

Many studies focus on agriculture environment, where the long-term saturation state of soil moisture in the crop root system restricts crop growth and reduces crop productivity *(Qian and Wang, 2015).* Field evaporation is a key link in the water circulation process and a significant component of water circulation. Along with rainfall and runoff, it determines the hydrologic balance in a region and directly influences farmland environment. Under certain topographic and rainfall conditions, a continuously low evaporation capacity results in long-term soil water saturation. This then leads to waterlogging disasters and causes crop failure, while a continuously high evaporation would result in droughts as well as crop failure. Hence, changing the process and features of evaporation capacity is the main basis for field water applications and management, and research on evaporation capacity is of great importance to agricultural production *(Su and Feng, 2015)*.

At present, many methods to calculate evaporation capacity are available. The most direct method is the instrument measurement method, which involves the use of an evaporation pan and land evaporator to

directly measure the evaporation capacity. In the case of insufficient or lack of measured data, the indirect method can also be used to estimate the evaporation capacity. The methods with the broadest application are the Penman–Monteith (P-M) formula, which is the only standard for calculating ET0 suggested by Food and Agriculture Organization of the United Nations (FAO), and the Hargreaves (H-S) formula, which can calculate the daily ET0; the former requires seven meteorological factors, and the latter needs four meteorological factors. Moreover, remote sensing technology, together with meteorological data, under a certain assumption, may employ the water-vapour balance equation, geostatistics theory, or all kinds of regression methods to conduct spatial interpolation and thereby estimate the evaporation capacity within a large scale *(Hassan, 2012)*. The aforementioned methods have their own advantages and limitations. When empirical methods, such as the P-M formula, are used, the physical conditions of various regions must necessarily be considered. Hence, such methods are quite difficult to apply when the evaporation capacity has a large variation. When remote sensing inversion or the water-vapour balance equation is used to estimate the evaporation capacity, the model needs multiple parameters with a complicated model structure. The development of remote sensing and GIS technology can realize the acquisition of large-scale evaporation capacity data; however, such acquisition remains very difficult to realize given continuously changing large-scale evaporation capacity data and the restrictions imposed by ground data and meteorological conditions *(Raghuveer et al., 2011; Paul et al., 2012).*

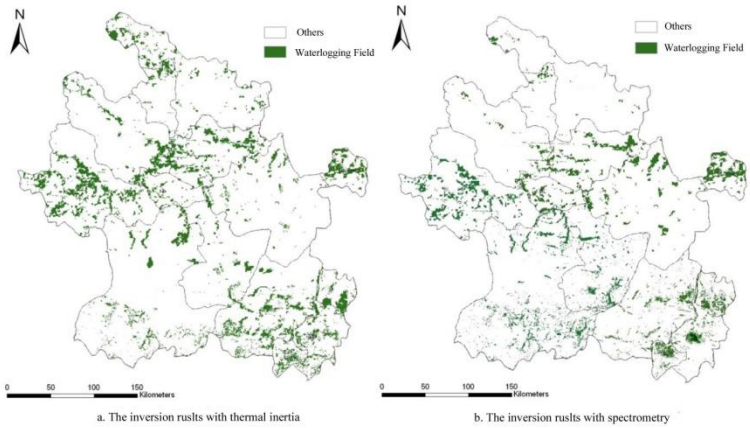

Fig.1 - Distribution diagram of the inversion results for the waterlogging field

Waterlogging control, drought resistance, and disaster reduction have always been important in the field of agricultural production research. Fig.1 shows the inversion results of using evaporation data with continuous space–time distribution and other multi-source data on waterlogging fields in Anhui Province *(Jin et al, 2014)*. Many spatial interpolation methods exist, such as the Thiessen polygon, spline function method, inverse distance weighted (IWD), Kriging, spatial interpolation model of artificial neural network (BPNNSI), and so on. The relevant assumptions of the aforementioned methods are based on the spatial distribution and location of evaporation capacity, which is then solved by the methods by considering the other factors that influence it *(Cha, 2011).* The results obtained are limited to some data of observation stations near the interpolation point with obvious uncertainty. The present study proposes a spatial interpolation method based on the spherical function, which considers evaporation capacity as a field covering the whole interpolation area, and the using spectral method to solve the overall parameters. It also integrates temperature data to further reduce the uncertainty of the calculation results *(Tian, 2012).* Anhui is located in a transitional area of warm temperature zone with an average annual temperature of 14–16 °C and a temperature difference of 2 °C between the south and north.

MATERIAL AND METHOD

Data source

The temperature dataset “China daily surface air temperature value 0.5°×0.5°grid point dataset (V2.0)” was downloaded from the Chinese meteorological data shared service network, and the basic meteorological element data from 2,472 open sea stations (i.e., excluding Xisha and Coral Island) and from the latest national-level surface meteorological stations reorganized on the basis of special database. The evaporation capacity data were derived from two sources. The first source was the daily evaporation capacity data from 26 meteorological stations in Anhui Province downloaded from the Anhui drought

severity information network. The second dataset, the MOD16 data (transpiration product) provided by MODIS with a spatial resolution of 1 km for a period of months, could be directly downloaded from the website provided by MODIS. The MOD16 data from May to August of 2013 were selected for the experiment in this study.

Data preprocessing

The downloaded temperature data consisted of ASCII coded documents, which could directly be read. The transformation of the format and spatial data had to be conducted, and the internal grid data files (*.img) supported by the ARCGIS platform were generated. The MOD16 data were also subjected to file format transformation, reprojection, and splicing, and clipping work, depending on the ARCGIS platform. The spatial datum was introduced for the convenience of analysis in this study. The spatial datum involved in this paper consisted of GCS_WGS_1984.

Spatial interpolation method based on spherical harmonic function

The research on evaporation began with bare land evaporation, using the empirical and mechanism method. The development of this line of research showed, that the evapotranspiration problem of crops was closely related to bare land evaporation. Researchers introduced the energy balance method and water vapour diffusion theory to the research on evapotranspiration. The evapotranspiration quantity of crops is considered to indicate the process of energy consumption; the water yield consumed by crop evapotranspiration is calculated through energy balance (*Li et al., 2013; Yang, 2011*).

Based on the aforementioned analysis, various corresponding transpiration formulas are available for different phases of crop evapotranspiration. Under normal conditions, the calculation of evaporation on bare soil uses the formula similar to that of crops:

$$E = k(e_1 - e_2) \tag{1}$$

where E is the crop evapotranspiration quantity, [mm]; k is a constant, [mm/hPa]; e_1 is the saturation vapour pressure and e_2 is the actual vapour pressure, [hPa].

Based on the Magnus formula (2), e_1 is a function of temperature:

$$e_1 = 6.1 \times 10^{\frac{7.45t}{t+273.16}} \tag{2}$$

where t is the daily average temperature in ^{o}C. Within the variation range of the meteorological temperature, the Magnus formula can be replaced by a straight line, and Equation (2) is transformed into

$$e_1 = Ct + D \tag{3}$$

where C is a constant, [hPa/K] and D is a constant, [hPa].

In Equation (1), the variation of the absolute value of e_2 is smaller than that of e_1, and its absolute value can be expressed with a constant. The above equation is substituted into (1), and the following can be obtained:

$$E = mt + n \tag{4}$$

where m is a constant, [mm/K] and n is a constant, [mm].

As shown above, the direct factors that influence the calculation of transpiration involve air pressure and temperature, so that atmospheric factors, such as temperature, should be considered in the spatial expansion of the transpiration data. The models used to predict evapotranspiration are divided into two types: The first involves direct calculation, such as the air humidity method, temperature wind speed method, and others; the second involves the determination of the total evapotranspiration quantity and crop factors of the reference crop, such as the P-M formula, complementary correlation theory, SPAC theory, evapotranspiration method for the reference crop, remote sensing method, and so on *(Lagos et al., 2013; Seitz, 2008)*. This study considers evaporation to consist of a field covering the surface of the earth and uses the spherical function model to solve the parameters of this field to realize the expansion of the evaporation data from a single observation station to continuous coverage.

The spherical function has been widely applied to the resolution of field equations, such as earth physics and atmospheric motion, among others. Compared with the classical grid method, the spectral method of the spherical function features high precision, good stability, and simple resolution *(Tolk, 2015; Seitz, 2008)*. The spherical function is adopted in this study to establish the basic model. By considering the relationship between evaporation and temperature, spatial distribution models (with or without consideration of temperature) are established, and the resolution results are then analyzed.

When the influence of temperature is not considered, the evaporation calculation model can be called a purely spherical function model and is expanded into the following form:

$$ET(\beta,s)=\sum_{n=0}^{n_{\max}}\sum_{m=0}^{n}\tilde{P}_{nm}(\sin\beta)(a_{nm}\cos(ms)+b_{nm}\sin(ms)) \quad (5)$$

where $ET(\beta,s)$ is the evapotranspiration in the observation station, [mm]; $n_{\max}$ is the order of the spherical harmonic function; $\tilde{P}_{nm}=\Lambda(n,m)P_{nm}$ is the normalized Legendre polynomial; Λ is the normalized function; P_{nm} is the normalized Legendre function; (β,s) is the geographic latitude and longitude of the observation station; and a_{nm} and b_{nm} are the coefficients to be resolved.

$$\Lambda(n,m)=\sqrt{2\frac{2n+1}{1+\delta_{nm}}\cdot\frac{(n-m)!}{(n+m)!}} \quad (6)$$

In the equation, δ_{nm} is the Kronecker function.

Considering the influence of temperature factors on evapotranspiration and the relationship expressed in Equation (4), the influence of temperature is integrated into Equation (5), and it can be called the expandable spherical function model, as shown in the following equation:

$$ET(\beta,s)=\sum_{n=0}^{n_{\max}}\sum_{m=0}^{n}\tilde{P}_{nm}(\sin\beta)(a_{nm}\cos(ms)+b_{nm}\sin(ms))+\mu T \quad (7)$$

where T is the temperature of the observation station, [K]; and μ is the coefficient to be resolved, [mm/K]. The other symbols are also found in Equation (5).

Model resolution

The specific flow of the model resolution flow is shown in Fig.2.

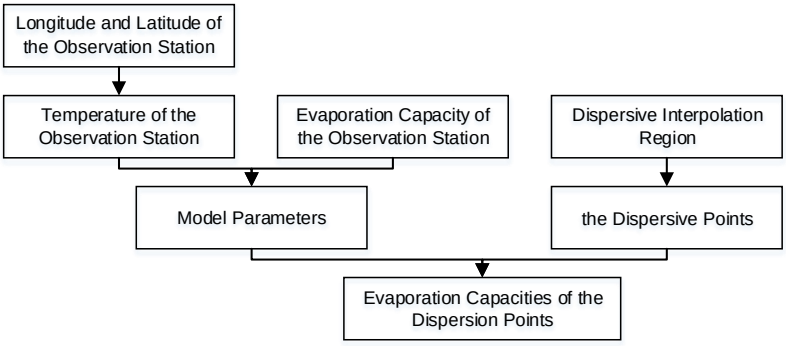

Fig.2 - Flow chart of the model resolution

The specific steps of the model resolution are as follows: First, the spatial analysis function of ARCGIS software is used to extract the temperature data. Second, the parameters in Equation (5) and (7) are re-resolved with the combination of the longitude and latitude and the measured value of evaporation. One group of parameters corresponds to one day. A total of nine coefficients are used when the temperature is not considered, and ten when the temperature is considered. The administrative region in An'hui Province is then dispersed, and the longitudinal and latitudinal coordinates and temperature values at the dispersed point are obtained. The evaporation capacity at this point is determined according to the parameters.

RESULTS

Model precision analysis

To evaluate the effectiveness of this model, the data from 23 observation stations, which are evenly distributed among the 26 observation stations in Anhui Province, are adopted to conduct mathematical modelling and calculation. The other three are used to conduct externally coincident inspections and to measure the precision of the model. Considering five day's worth of data from August 25 to 29, 2013, the compensating computation of the two models is established. The statistical information of the residual absolute error value is shown in Table 1, which compares the externally coincident precision of the inverse distance weighting (IDW) and Kriging methods under the same resolution conditions.

The internal error is the precision obtained through the compensating computation under optimal estimation is also called the mean square error $\hat{\sigma}$ of the unit weight:

$$\hat{\sigma} = \sqrt{V^T PV / (n_s - t_s)} \tag{8}$$

Where V is the residual error of the evaporation capacity in the observation station involved in the adjustment calculation, n_s is the number of observed values and is set as 23, and t_s is the observed quantity and is set as 10. The externally coincident precision is obtained by calculating the data in the observation station of the externally coincident inspection. The calculation formula is as follows:

$$\hat{\sigma}_{EAA} = \sqrt{\frac{\sum_{k=1}^{3}(ET_{ass} - ET_{real})}{3}} \tag{9}$$

Where $\hat{\sigma}_{EAA}$ is the externally coincident precision; ET_{ass} is the estimated model value of the evaporation capacity in the observation station; and ET_{real} is the known observed value in the observation station.

Table 1

Statistical table of the absolute values of the residual error and precision indexes (unit: mm)

Spherical Function	Time	$v \le 1$	$1 < v \le 1.5$	$1.5 < v \le 2$	$v > 2$	$\hat{\sigma}$	$\hat{\sigma}_{EAA}$	OM	$\hat{\sigma}_{EAA}$
Temperature Not Considered (SHTNC)	1st day	82.6%	13.0%	4.4%	0.0	0.92	1.45	IDW	1.82
	2nd day	78.3%	21.7%	0%	0.0	0.99	0.90		1.79
	3rd day	87.0%	4.4%	4.4%	4.2%	1.01	0.48		1.81
	4th day	87.0%	13.0%	0%	0.0	0.83	0.53		1.73
	5th day	82.6%	8.7%	8.7%	0.0	0.97	0.94		1.77
Temperature Considered (SHTC)	1st day	95.6%	0%	4.4%	0.0	0.94	1.43	Kriging	1.85
	2nd day	73.9%	26.1%	0%	0.0	1.03	1.07		1.72
	3rd day	91.3%	0%	4.4%	4.3%	1.04	0.77		1.79
	4th day	91.3%	8.7%	0%	0.0	0.88	0.49		1.63
	5th day	82.6%	8.7%	8.7%	0.0	1.04	0.96		1.75

Note: v: the absolute value of the residual error; OM: other method; Kriging: the Kriging model for spatial interpolation

The v represents the absolute value of the residual error after the compensating computation of the model. Table 1 shows the statistics of the percentage of the absolute values of the residual error and the number of those involved in the calculation of the model. Based on Table 1, most of the absolute values of the residual error are superior to 1 mm; those over 90% are less than 1.5 mm; and those consisting of only several data points are greater than 1.5 mm. Generally speaking, both the two models can satisfy the requirements of the spatial interpolation of the evaporation capacity. Regardless of the adjustment and residual error of the model, or the internal and external errors, the numerical values are quite close to one another. The data from columns 8 and 10 in Table 1 are also compared. The external coincident precisions of the two models adopted in this paper are superior to the corresponding values of the IDW and Kriging methods.

Careful analysis shows that an inconsistency exists between the distribution laws of the residual error and the precision of the two models. As shown in Table 1, among the continuous five-day interpolation results, with the exclusion of the two-day results, the results from the other four days do not conform with the law that a good residual error distribution corresponds to good model precision. The residual errors with absolute values of less than 1 mm correspond to the spatial interpolation model that considers the temperature and appear more frequently. The model precision indexes are low, and the highest proportion of the residual errors with absolute values of less than 1 mm of the model that considers the temperature is 95.6%. By contrast, the corresponding value of the model that does not consider temperature is 82.6%. Thus, the difference between the values of the two is 13.0%. For the internal error, the former is 0.94, and the latter is 0.92. For the external error, the former is 1.43, and the latter is 1.45. What is worth mentioning is that the residual error distribution corresponds to two interpolation models that are consistent, while the precision index of the model that considers temperature is slightly lower.

Model precision and reliability are two significant indexes for evaluating the interpolation model. Aside from being influenced by their own functional precision, the resulting interpolation precision is also influenced by the precision of the adopted parameters. Generally speaking, the more parameters the model involves, the lower the interpolation results precision are. However, adopting reasonable parameters can enhance model reliability. Temperature parameters are introduced to the spatial interpolation model that considers temperature. Although this slightly lowers the model precision, it optimizes the distribution laws of the residual error, thereby improving model reliability. In terms of the interpolation results of the daily evaporation capacity, the influence of temperature cannot be highlighted because of the small daily evaporation capacity.

Analysis of the precision of the monthly evaporation data and selection of temperature data

The spherical model is used to conduct the spatial interpolation of the daily evaporation capacity from May to August, 2013. The monthly evaporation capacity is then calculated. When the expanded model is used to conduct spatial interpolation, three kinds of temperature data are selected: the daily average temperature, daily maximum temperature, and mininum temperature. By contrast, when the temperature is not considered in the calculation, four kinds of interpolation results can be obtained.

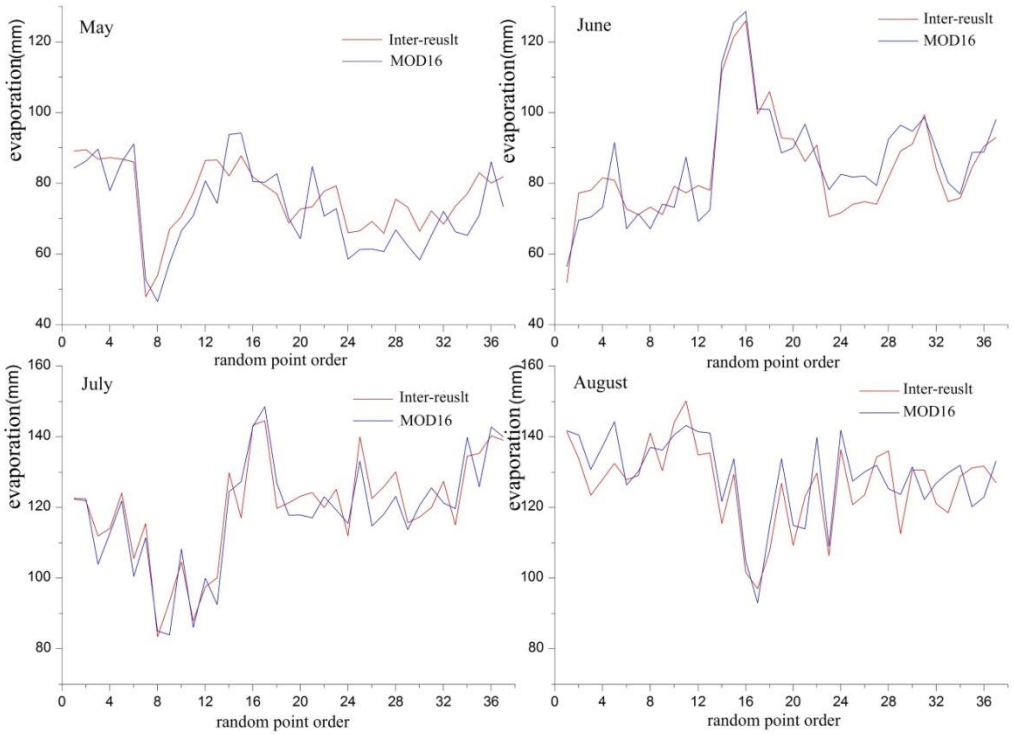

Fig.3 - Comparative diagram of the average temperature interpolation results and MOD16

For 50 randomly generated inspection points, four kinds of interpolation data corresponding to the inspection points are extracted. With the MOD16 data corresponding to the inspection points as the truth value of the evaporation capacity, 37 inspection points data are reserved after the abnormal points on the water surface and urban and town areas are excluded; the variances are calculated and listed in Table 2. A correspondence diagram between the monthly evaporation capacity and MOD16 data, which are obtained by adopting the daily average temperature interpolation, is shown in Fig.3. A comparative diagram between the expanded model and purely spherical function model under the four situations is shown in Fig. 4.

As shown in Fig. 3, the comparison of the monthly evaporation capacities is resolved by expanding the model, which adopts the daily average temperature and MOD16 data. The red line represents the interpolation results, and the blue line represents the MOD16 data. The variation tendencies of the two are consistent, and the interpolation results only jitter up and down the MOD16 data. The maximum error is less than twice the variance. Fig. 4 compares the monthly evaporation capacities of the spherical function models under the four situations. The graph entities for May and July are consistent, but some inspection points exhibit large deviation in June. A large fluctuation with opposite change tendencies occurs in August *(Bezborodov et al. 2010, M.P. Gonzalez et al. 2009)*. Combining the variance data of the evaporation capacities at the inspection points in Table 2, the interpolation data variance in the expanded model, which

uses the daily average temperature, remains stable and small. By contrast, the variances in the interpolation data in other forms are not stable enough. Thus, adopting the daily average temperature as the parameter of the interpolation model can result in relatively ideal interpolation results.

Table 2

Statistical table of the variance in the monthly evaporation data (unit: mm)

Month	DMaxT	DAvgT	DMinT	TE	EMaxError	MOD16
5	6.10	5.98	6.37	6.91	-12.30	93.8
6	4.94	5.05	5.25	7.72	12.25	72.5
7	5.01	5.18	5.47	5.98	-11.72	127.3
8	6.64	5.74	7.51	9.16	14.44	115.0

Note: D: daily; A: average; T: temperature ; TE: temperature excluded; EMaxError :evaporation max error

Given the major hopping position in Fig.4, it is necessary to analyze the characteristics of the temperature data at the test point to study whether the model is practicable for the temperature data. The variance of the model, which takes the average temperature in Table 2 as parameter, is considered to be the threshold value. The inspection point with an error smaller than the threshold value follows a consistent trend, and the inspection point with an error larger than the threshold value is deviation positions. And then the calculation of the statistics of the consistent and deviant positions of the trend corresponding to each month is needed.

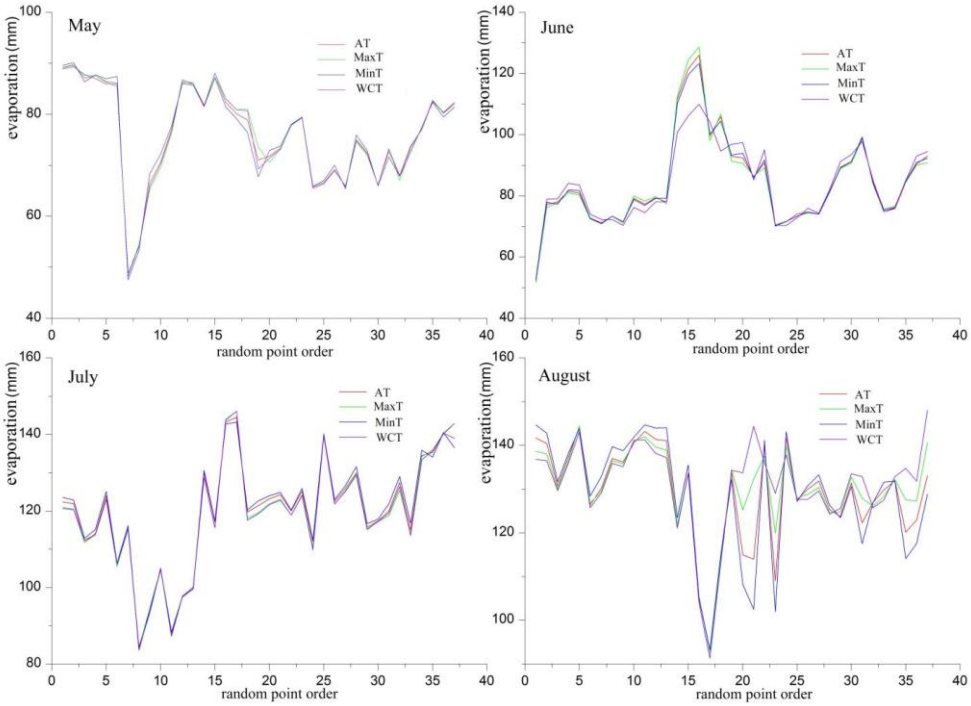

Fig.4 - Comparative diagram of the interpolation results under the four situations

The average maximum temperature, average temperature, average minimum temperature, difference between the average maximum and average minimum temperatures, difference between the average maximum and average temperatures, maximum temperature difference at consistency, and minimum temperature difference at deviation are listed in Table 3.

Table 3

Statistical table of the temperature data characteristics at the inspection points (unit: °C)

M	MAMaxT	AMT	MAMinT	MaxTD	MaxATD	MaxTDC	MinTDD
5	26.71	21.59	17.21	9.50	5.12	4.98	6.47
6	28.45	24.27	20.98	7.47	4.18	3.12	8.58
7	33.99	32.73	30.12	3.87	1.26	4.10	6.23
8	34.29	31.65	25.41	8.88	2.64	3.69	8.98

Note: M: month; A: average; T: temperature; D: difference; DC: difference at consistency; DD: difference at deviation

The data volume matrix in Table 3 is established, and its correlation coefficient matrix is solved. The correlation between columns 7 and 8 in Table 3 with the proceeding columns is observed, and the maximum correlation coefficient is 0.42. Hence, the model interpolation effect does not have any significant linear correlation with the overall variation range of the temperature data or with the temperature. The correlation coefficient between columns 7 and 8 is -0.76, which is a significantly negative correlation. Hence, the data in columns 7 and 8 in Table 3 are combined and taken as the indexes of the model's resistance capability to temperature variations; that is, the interpolation effect is good when the temperature variation is within 3.12 °C, but is poor when the temperature variation is above 6.23°C.

The monthly evaporation interpolation is calculated by transforming the multiple temperature parameters. Through the comparative analysis of the interpolation results and the continuous space–time distribution features of the MOD16 data, the adoption of the daily average temperature can obtain the optimal solution of the model. The variance in the optimal value is taken as the threshold value to classify the interpolation results. The maximum temperature difference at consistency (TDC) and minimum temperature difference at deviation (TDD) can also be obtained. These two are correlated with the interpolation results and can serve as the indexes to evaluate the temperature difference resistance capacity and the applicability of the model.

Accumulation effect of the daily evaporation capacity with consideration of the temperature

The expanded spherical function model, which considers the temperature, produces the accumulation effect of the daily evaporation capacity *(Jiménez-Bello et al. 2011).* The comparation and analysis of the MOD16 data in August with the accumulation effect had been made. As shown in Fig.5, A represents the accumulated monthly value of the spatial interpolation of the daily evaporation without consideration of the temperature, B represents the value with consideration of the temperature, and C represents the MOD16 data.

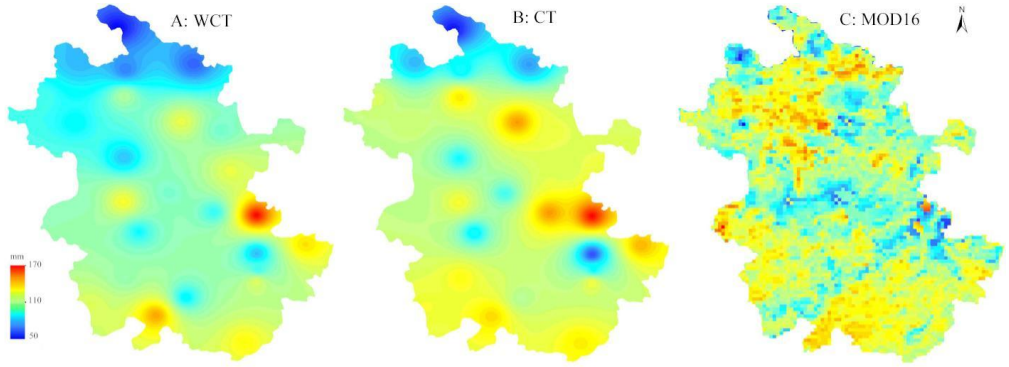

Fig.5 - Monthly cumulative comparison of the spatial interpolation of the evaporation capacity

The overall evaporation data in Fig. 5A are low. Meanwhile, the evaporation distribution in Fig. 5B more closely approaches the data in Fig. 5C than those in Fig. 5A, the evaporation data to the east and west of Anhui Province are higher than those in the corresponding areas in Fig. 5A, which embody the accumulation effect of the spherical function model that considers the temperature. Based on the statistical data of the monthly evaporation capacity during the 4-month spatial expansion in 37 inspection points examined in this study, the temperature accumulation effect may indicate that the sum of the monthly evaporation capacities in the inspection points obtained by the model resolution corresponds to each temperature parameter minus those obtained by the model resolution that does not consider temperature. The difference values are listed in Table 4; column 1 represents the month, columns 2 to 4 represent the difference values of the evaporation capacity, column 5 represents the sum of the evaporation capacities of the inspection points of the model that does not consider temperature, and column 6 represents the MOD16 data.

Table 4

Statistical table of the difference values of the monthly evaporation capacity and relevant data (unit: mm)

M	maxT	AvgT	minT	TE	MOD16
5	5.48	4.32	0.09	2338.568	2346.4
6	22.60	19.48	19.30	2550.447	2591.9
7	35.25	18.49	16.27	4292.903	4263.4
8	9.23	49.67	77.67	3976.740	3998.2

Note: M: month; Avg: average; T: temperature; E: excluded

Based on Table 4, the sum of the monthly evaporation capacities in all the months under all the temperature parameters are greater than the sum of the monthly evaporation capacities resolved by the model that does not consider temperature.

This indicates that the model that considers temperature has a temperature accumulation effect. The difference value matrix of the evaporation capacities from columns 2 to 4 in Table 4 and the temperature data matrix from columns 2 to 4 in Table 3 are established.

The correlation coefficient between the two matrices is 0.251, which indicates that the linear correlation between the temperature accumulation effect and temperature is not obvious.

The correlation coefficient between columns 5 and 6 in Table 4 is 0.997, which indicates that the resolution of the function model has a significant correlation with the MOD16 data.

The temperature accumulation effect exists in the interpolation of monthly evaporation data. However, it is restricted by the spatial density of temperature, observed evaporation value, and data precision. Moreover, given the complicated relationship between temperature and evaporation capacity, this study does only little to reveal the temperature accumulation phenomenon, which should be the focus in future studies.

CONCLUSIONS

To satisfy the requirements of the agricultural environment study for continuous space–time distribution, the calculation of the evaporation spatial interpolation should not be limited to traditional methods, and relevant multi-source information must necessarily be integrated.

This study proposes a new method for the spatial interpolation of the evaporation capacity. It then uses actual measured data in Anhui Province and national temperature field distribution to verify the proposed method and at the same time analyses the influence of the temperature field on the interpolation results.

The following conclusions can be drawn from the study:

- Error analysis indicates that this method has high precision and is superior to the pure IDW and KRIGING methods. The introduction of temperature parameters results in inconsistencies between the distribution law of the residual error of the interpolation results and the internal and external errors. This occurs because, after the temperature parameters are introduced to the spatial interpolation model, the errors of the temperature parameters are propagated and affect the model precision. However, the interpolation results lead to a more optimal distribution, thereby enhancing the reliability of the model;
- Based on the analysis, the TDC and TDD are correlated with the interpolation results. They can serve as indexes for the model temperature difference resistance ability and evaluation of the model applicability. Taking the MOD16 monthly evaporation capacity with continuous space–time distribution features as the control, this paper analyses the monthly evaporation interpolation results under multiple temperature values and adopts the daily average temperature to conduct model resolution and obtain the optimal solution;
- In the calculation of the spatial expansion of the monthly evaporation capacity, the model that considers temperature exhibits the temperature accumulation effect phenomenon, and it has a more complicated relationship with the daily evaporation data.

This study satisfies the required evaporation data for agricultural environment and provides a reference and basis for the calculation of field evaporation data and analysis of the relationship between temperature and field evaporation. This promotes farmland water management and utilization, as well as relevant progress in agricultural production. However, evaporation, which is a complicated natural phenomenon, has a complex relationship with factors, such as altitude, wind speed, and temperature. Further analysis must be conducted on the influence of all these factors on the method proposed in this study.

ACKNOWLEDGEMENT

The work was supported by the National Science and Technology Pillar Program during the 12th “Five-Year Plan” Period (Project No.: 2012BAD08B03-4)

REFERENCES

[1] Bezborodov G. A., Shadmanov D. K., Mirhashimov R. T., et al., (2010), Mulching and water quality effects on soil salinity and sodicity dynamics and cotton productivity in Central Asia, *Agriculture, Ecosystems & Environment,* Elsevier B.V./ America, Vol.138, Issue.1-2, ISSN 0167-8809, pp.95-102;

[2] Cha Weiwei, Liu Yu., Liu Yulong. etc., (2013), Regional evaporation and transpiration simulation and verification and remote sensing based on SWAT model, *Journal of China Institute Water Resource and Hydropower Research,* Vol.11, Issue 3, pp.167-175, ISSN 1672-3031, China Institute of Water Resources and Hydropower Research, Beijing;

[3] Gonzalez-Dugo M. P., Neale C. M. U., et al., (2009), A Comparison of Operational Remote Sensing-based Model for Estimating Crop Evapotranspiration. *Agricultural and Forest Meteorology*, Elsevier B.V., Vol.149, Issue 11, pp.1843-1853, ISSN 0168-1923;

[4] Hassan M., (2013), Evaporation estimation for Lake Nasser based on remote sensing technology, *Ain Shams Engineering Journal*, Vol.4, Issue 4 , pp.593-604, Ain Shams University, Cairo;

[5] Jin Y. L., Huang J. S., Wang X. G, (2014), Identification of waterlogged field based on multi-source data, *Engineering Journal of Wuhan University*, Vol.47, Issue 3, pp.289-293, ISSN 1671-8844, Wuhan University, Wuhan / China,;

[6] Jiménez-Bello M. Á., Alzamora F. M., Castel J. R., et al.,(2015), Validation of a methodology for grouping intakes of pressurized irrigation networks into sectors to minimize energy consumption. *Agricultural Water Management*, Elsevier B.V./ America, Vol.102 , Issue 1, pp.46-53; ISSN 0378-3774,

[7] Lagos L. O., Martin D. L., Verma S.B., et al., (2013), Surface energy balance model of transpiration from variable canopy cover and evaporation from residue-covered or bare soil systems: model evaluation, *Irrigation Science*, Springer- Verlag, Berlin/Germany, Vol.31, Issue 2 , pp.135-150, ISSN 0342-7188;

[8] Li Xianghu, Zhang Qi, Ye Xuchun, (2013), The effects of spatial distribution of Different soil physical properties on hydrological processes modelling, *Journal of Soil and Water Conservation*, Vol.33, Issue 05, pp.190-195, ISSN 0022-4561, Soil Water Conservation Society, Ankeny;

[9] Paul D. C., William P.K., Martha C. A., et al., (2012), Two-source energy balance model estimates of evapotranspiration using component and composite surface temperatures, *Advances in Water Resources*, Vol.50, Issue 3, pp.134-151, ISSN 0309-1708, Loughborough University, Leicestershire;

[10] Qian Long, Wang Xiugui, Luo Wenbing, (2015), Yield reduction analysis and determination of drainage index in cotton under waterlogging followed by submergence, *Transactions of the Chinese Society of Agricultural Engineering*, vol.31, Issue 13, pp.89-97, ISSN 1002-6819, Chinese Society of Agricultural Engineering, Beijing;

[11] Raghuveer K. V., Eric F. W., Craig R. F., et al., (2011), Global estimates of evapotranspiration for climate studies using multi-sensor remote sensing data: Evaluation of three process-based approaches, *Remote Sensing of Environment*, Elsevier B.V./America, vol.115, Issue 3, pp.801-823, ISSN 0034-4257;

[12] Seitz F., Schmidt M., Shum C. K., (2008), Signals of extreme weather conditions in Central Europe in GRACE 4-D hydrological mass variations, *Earth and Planetary Science Letters*, Elsevier B.V./America, vol. 268, Issue1-2, pp.165 -170, ISSN 0012-821X;

[13] Su T., Feng G. L., (2015), Spatial-temporal variation characteristics of global evaporation revealed by eight reanalyses, *Science China Earth Sciences*, Science China Press , Beijing, vol.58, Issue 2, pp.255-269, ISSN 1674-7313;

[14] Tian F., Qiu G. Y., Yang Y. H., et al., (2013), Estimation of evapotranspiration and its partition based on an extended three-temperature model and MODIS products, *Journal of Hydrology*, Elsevier B.V./ America , Vol. 498, Issue1-4, pp.210- 220, ISSN 0022-1649;

[15] Yang D.J., (2011), *Soil water dynamics model and its application on SPAC system modelling*, vol.1, pp.78-110, ISBN 9787308092746,, Zhejiang University Press, Hangzhou.

THE ROOT-ZONE SOIL WATER AND HEAT DYNAMICS OF BEANS OF PROTECTED AGRICULTURE IN COLD REGIONS OF NORTH CHINA
/
中国北方寒地设施农业中豆角根区土壤水热变化规律研究

Senior Engineer Teng Y.[1, 2)], Prof. Ph.D. Zhang Z.X.[1)], Prof. Tao Y.H.[2)], Prof. Ph.D. Si Z.J.[2)], Senior Engineer Liu S.Y.[2)], Senior Engineer Yu Z.L.[2)], Ph.D. Principal Scientist Zhao Y.L.[3)]
[1)] College of Hydraulic & Architecture, Northeast Agricultural University, Harbin/China; [2)] Heilongjiang Hydraulic Research Institute, Harbin/China; [3)]Independent researcher, West Palm Beach/United States
Tel:+86013936031311; E-mail:hljskyty@126.com

Keywords: *soil water; soil water suction; greenhouse; drip irrigation; water-use efficiency*

ABSTRACT

This study aims to explore the effects of different irrigation quotas on the root-zone soil water and heat dynamics, water-use efficiency, and yield of cold-region beans in protected agriculture at different growing stages. To identify the optimal water-saving irrigation scheme, field plot experiments were conducted at Heilongjiang Hydraulic Science and Technology Experimental Research Center No. 1 Greenhouse from 2014 to 2015 in Harbin, north China. An orthogonal experimental design was used for the experiments. The growing period of beans comprised four stages, and three irrigation quota levels (6, 12, and 24 mm) were set for each growing period. The greenhouse drip irrigation experiment results showed that variations in soil water suction (SWS) were negatively correlated with irrigation level. SWS varied more substantially with less irrigation but revealed a smaller change at a higher level of irrigation. When the temperature changed at the same gradient, the changing rate of soil potential was larger during the temperature-rise period than that at the cooling stage. The change in soil potential slowed when the temperature decreased. In cold regions, greenhouse beans could bear moderate water deficits during harvest time, and the optimal schemes for water-saving irrigation were as follows: 12 mm for planting, 12 mm for flowering, 24 mm for fruiting, and 6 mm for harvesting. Our research findings on the root-zone SWS dynamics of beans and the optimal water-saving irrigation scheme would serve as a reference for the precise and highly efficient irrigation of an automatic irrigation system for greenhouse crops.

摘要

为了探明滴灌条件下，寒地设施农业豆角不同生育期不同灌水定额对豆角根区土壤水热变化规律和豆角水分利用效率、产量的影响，并筛选出最佳的节水灌溉模式。于 2014—2015 年在中国北方哈尔滨市的黑龙江省水利科技试验研究中心 1 号日光温室中进行小区试验，采用正交试验设计，将豆角生育期划分为 4 个阶段，每个生育期灌水定额设 3 个水平，分别为 6 mm、12 mm、24 mm，温室滴灌试验研究结果表明：土壤水吸力变化幅度与灌水量水平呈负相关，灌水量越少土壤水吸力变化幅度越大，灌水量越大土壤水吸力变化幅度越小。在相同的温度变化梯度下，土壤水势变化的速率在升温过程中比降温过程中要快，并且土壤水势变化的速率随着温度的降低而变缓。寒地温室秋豆角在采收期可适度亏水，最佳的节水灌溉模式为灌水定额定植期 12 mm，开花期 12 mm，结荚期 24 mm，采收期 6 mm。豆角根区土壤水吸力变化过程的研究结果及优选的节水灌溉模式将为温室作物自动控制灌溉系统进行精准及节水灌溉提供灌溉指标参考依据。

INTRODUCTION

Greenhouse vegetables in protected agriculture are becoming increasingly prevalent in north China. Given the large water demand of vegetables, frequent irrigation is needed during the cultivation process. It will cause high interior temperature and humidity, which differ from the natural moisture and heat environment of the land. Water shortage is already a global issue. Therefore, water-saving irrigation schemes have great implications for the conservation and efficient use of water resources *(Maraseni et al., 2012)*. Studies have already been made on deficit irrigation for greenhouse crops *(Kuşçu et al., 2014; Lima et al., 2015)*. This sets high expectations on the water management of greenhouse vegetation cultivations.

Suitable soil water and heat conditions are important for the favourable growth of crops *(Moraru et al., 2012)*. The moisture and thermal condition for crop growth can be improved with no doubt by using drip irrigation in a greenhouse environment. The proper monitoring and control of indoor soil water and heat conditions have also become important approaches for promoting good quality and high yielding crops.

However, soil water and heat affect each other in a sophisticated manner. The literature shows that demonstrated the impact of temperature on soil moisture for the first time by using quantitative methods, and temperature distribution was related to soil water movement. This result was further validated in detail by other researchers *(Baoping et al., 2002)*. Their studies showed that several days are needed to achieve a constant value of soil water content after its evolution resulting from the change in soil temperature gradient. The main factors that affected soil moisture gradient included the initial soil water content, bulk density, temperature gradient, and mean temperature. Furthermore, a large number of studies indicated that water moves from the high-temperature end to the low-temperature end whether in unsaturated or saturated soil *(Sanjit et al., 2011)*. By contrast, water movement would cause temperature changes, which in turn affect moisture movement. Soil water and heat movement was mainly analyzed in studies on soil freezing and thawing *(Yuanming et al., 2014; Jiazuo and Dongqing, 2012)*, whereas the moisture–heat relationship under greenhouse conditions was rarely investigated.

So far, a number of studies have been conducted on the water consumption and water-use efficiency (WUE) of field crops, particularly for corn *(Ahmadi et al., 2015; Qianqian et al., 2011)*, cotton *(Minxian et al., 2011; Pettigrew, 2004)*, and wheat *(Fan et al., 2005; Qinglin et al., 2012)*. These works revealed that the characteristics of water consumption for field crops were different during different growing stages. By properly reducing irrigation during a certain growing stage, water could be saved while maintaining yield *(Patel et al., 2013)*. However, only a few studies analyzed water consumption, WUE, and irrigation parameters for greenhouse vegetables *(Al-omrana et al., 2005)*. Furthermore, such studies focused only on tomatoes, cucumbers, etc., and not on beans *(Dejie et al., 2011; Guobao et al., 2012)*. Snap bean is a well-known, good-quality local vegetable in north China and is an important export product *(Guofu et al., 2010)*. Snap bean has high protein content (up to 20% of its dry mass) and contains 18 types of amino acids, particularly lysine. Given the increasing demand for snap beans, greenhouse cultivation is experiencing widespread use.

In recent years, state-of-the-art irrigation techniques and approaches (e.g., drip irrigation and deficit irrigation *(Feng et al., 2010; Yancong et al., 2012)* have been adopted in greenhouse cultivation. However, these techniques exhibit unsatisfactory performance due to blindness in water management. Considering the historical issues in greenhouse vegetation cultivation, research on the characteristics of water consumption at different stages for different growing periods, as well as their impacts on crop growth, yields, and quality, is still at the early stages *(Brevedan and Egli, 2003; Guobao et al., 2012)*. This study uses beans as the research object and investigates the movements of soil water and heat and their interactions under different irrigation treatments throughout four stages from planting to harvesting. This study used greenhouse field plot experiments and drip irrigation scheme, which is commonly used in greenhouse cultivation in northern cold regions. The results of this study will provide evidence on the proper monitoring and scientific adjustment of soil water and heat environment for the drip irrigation of greenhouse crops. Furthermore, this study will serve as a reference for the rational establishment of irrigation indices.

MATERIAL AND METHOD

Study Site Description

The experiments were conducted at Heilongjiang Hydraulic Science and Technology Experimental Research Center (N45° 43′ 09″ , E126° 36′ 35″ , and altitude of 156 m) No. 1 Greenhouse from 2014 to 2015. The study site is located at the cold temperate zone with a semi-humid continental climate, which has four distinctive seasons. The average temperature is 4.6 °C in spring, 21.3 °C in summer, 4.1 °C in autumn, and −17.2 °C in winter. The average annual rainfall is 500–600 mm, 70% of which occurs in July, August, and September. The frost-free season lasts for 130–140 days. Two stubble vegetables could be cultivated in the greenhouse. The experimental greenhouses were arranged east–west (length of 50 m, width of 6 m) and were 8 m apart from other greenhouses. The greenhouses were covered with anti-fogging polyethylene film and were not overshadowing each other. The experimental soil was loam, with a bulk density of 1.26 g/cm^3 for the cultivated layer, field capacity of 36% (gravimetric water content), and water table of >8 m.

Material and Experimental Design

The crop type selected for our experiments was snap bean (or Jiangjun bean). The whole vegetable bed was cultivated from south–north, with a length of 5 m, width of 0.8 m, and interval of 30 cm × 40 cm between plants. Each vegetable bed was equipped with a drip irrigation pipe that supplies water to 2 rows

of crops. The distance between the drip irrigation emitters was the same as the spacing in the rows. The experimental field was sown on 27th July 2014, planted on 6th August 2014 and harvested on 14th November 2014 (total of 100 days from planting to harvesting). In the next year, the field was sown on 5th July, planted on 16th July, and harvested on 28th October (104 days from planting to harvesting). All the experimental field plots were under unified management before planting before, and then implementing different irrigation schemes. Drip irrigation was adopted, and the irrigation volume was measured by the water meter. For each plot, the fertilizing, weeding, and controlling of diseases and pests all complied with the green-vegetable-cultivation standards.

An orthogonal experimental design was used. The growing period of beans comprised 4 stages: seedling stage (from planting to flowering), flowering stage (from flowering to fruiting), fruiting stage (from fruiting to the start of harvesting), and harvesting stage (from the start to the end of harvest time). A total of 3 irrigation levels were set for each growing period: 6, 12, and 24 mm, with an additional level of sufficient water supply for the control group. A total of 10 irrigation treatments were applied (Table 1). To reduce natural and human disturbances to the field experiments, each treatment was repeated 3 times, resulting in 30 plot experiments arranged in order (see figure 1 of field experiments).

Table 1

Irrigation treatments for the experiments

Treatment	Factor Level(Irrigation volume mm)			
	Seedling A	Flowering B	Fruiting C	Harvesting D
T1	1 (6)	1 (6)	1 (6)	1 (6)
T2	1 (6)	2 (12)	2 (12)	2 (12)
T3	1 (6)	3 (24)	3 (24)	3 (24)
T4	2 (12)	1 (6)	2 (12)	3 (24)
T5	2 (12)	2 (12)	3 (24)	1 (6)
T6	2 (12)	3 (24)	1 (6)	2 (12)
T7	3 (24)	1 (6)	3 (24)	2 (12)
T8	3 (24)	2 (12)	1 (6)	3 (24)
T9	3 (24)	3 (24)	2 (12)	1 (6)
CK	3 (24)	3 (24)	3 (24)	3 (24)

a)

Fig.1 – Field experiments

b)

c)

Fig.1 – Field experiments

Measurements and Methods

Plot irrigation was measured using water meters. Soil water suction (SWS) was measured using the soil suction sensors of an automatic data-acquisition system (measurement range of 0–100 kPa). The plot yield of the beans was recorded and then converted into yield per hectare.

The observation point for each plot was placed below the drip irrigation belt 5 cm apart from the drip irrigation emitter horizontally at the surface layer and root zone (20 cm). Continuous SWS and temperature under different irrigation treatments were monitored and recorded by WP-3 Greenhouse Environment Monitoring System (internally developed via “948” project).

Data Analysis

Data were processed and plotted in EXCEL. The ANOVA and significant tests (Duncan’s multiple range test) of the experimental results were conducted using SPSS.

RESULTS

Impact of Varied Irrigation Treatments on Production and WUE

Nowadays, improvement on both crop yield and water use efficiency is a main goal of water-saving agriculture. Yield and WUE of beans under different irrigation treatments are shown respectively in Table 2.Compared with the CK treatment, percentages by which the production and WUE are increased or decreased for the 2-year experiments are calculated. Reduced production and improved WUE are observed for most of the treatments. Therefore, it is necessary to further analyse the irrigation scheme that results in the optimal production and WUE.

Table 2

Yield and WUE of beans under different irrigation treatments

Treatment	2014				2015			
	Yield (t/hm^2)	Compared to control group (%)	WUE (kg/m^3)	Compared to control group (%)	Yield (t/hm^2)	Compared to control group (%)	WUE (kg/m^3)	Compared to control group (%)
T1	24.03ab	−23.70	39.73g	205.20	22.35a	−23.84	39.59g	204.66
T2	23.64ab	−24.94	23.45ef	80.14	24.18b	−17.61	26.07e	100.59
T3	22.27a	−29.28	12.27a	−5.71	21.43a	−26.97	12.96a	−0.25
T4	30.65b	−2.68	19.00cd	45.98	27.29cde	−7.00	18.80c	44.66
T5	29.90b	−5.05	26.49f	103.47	31.58g	7.63	29.01f	123.24
T6	27.76bc	−11.84	21.52de	65.30	28.32def	−3.47	23.42d	80.18
T7	26.93abc	−14.49	15.90bc	22.16	25.81c	−12.04	16.00b	23.14
T8	27.72bc	−11.97	13.75ab	5.63	28.84ef	−1.72	15.55b	19.65
T9	26.61abc	−15.51	17.37c	33.40	26.73cd	-8.89	17.92c	37.89
CK	31.49b		13.02ab		29.34f		13.00a	
A1	23.31a				22.65a			
A2	29.44b				29.07c			
A3	27.09b				27.13b			
B1	27.21a				25.15a			
B2	27.09a				28.20b			
B3	25.55a				25.50a			
C1	26.51a				26.28a			
C2	27.00a				26.07a			
C3	26.37a				26.51a			
D1	26.85a				26.89b			
D2	26.11a				26.10ab			
D3	26.88a				25.85a			

Table 2 displays the results of the orthogonal experiments and ANOVA, as well as the multiple comparisons of WUE. Results showed that different irrigation treatments influenced the production and WUE of cold-region greenhouse autumn beans in different ways. During various growing periods, reduced irrigation led to a decrease in bean yield and to a significant increase in WUE. Irrigation Treatment 5 (T5) in 2015 increased the yield by 7.63%, and Treatment 3 (T3) resulted in reductions in WUE by 5.71% and 0.25% in 2014 and 2015, respectively. By analyzing the two-year experiments, we found that the impact of reduced irrigation on crop yields was the largest for the seedling stage A, followed by the flowering stage B, harvesting stage D, and fruiting stage C. The results of the multiple comparisons revealed that the optimal irrigation combination in 2014 was A2B1C2D3 and A2B2C3D1 (i.e., T4 treatment and T5 treatment); this approach not only showed the lowest reduction in yield of 2.68% and 50.05% but also enhanced WUE by 45.98% and 103.47%. In 2015, the optimal combination was A2B2C3D1 (i.e., T5 treatment); this approach increased production and WUE by 7.63% and 123.24%, respectively. Therefore, T5 was the optimal irrigation scheme. The results also indicated that cold-region greenhouse beans could bear moderate water deficits during harvest time. Thus, water could be saved substantially without affecting yield. Our analyses demonstrated that WUE increased significantly even though the yield of beans increased to a small extent or decreased slightly, thus achieving unity of guaranteed production and highly efficient water utilization.

On the basis of the two-year experimental results, T1 treatment was selected for its noticeable improvement on WUE regardless of its impact on yield. T5 treatment was the optimal choice because of its significant enhancement of WUE without affecting the production. CK treatment was applied to analyze the root-zone soil moisture dynamics of greenhouse beans in cold regions.

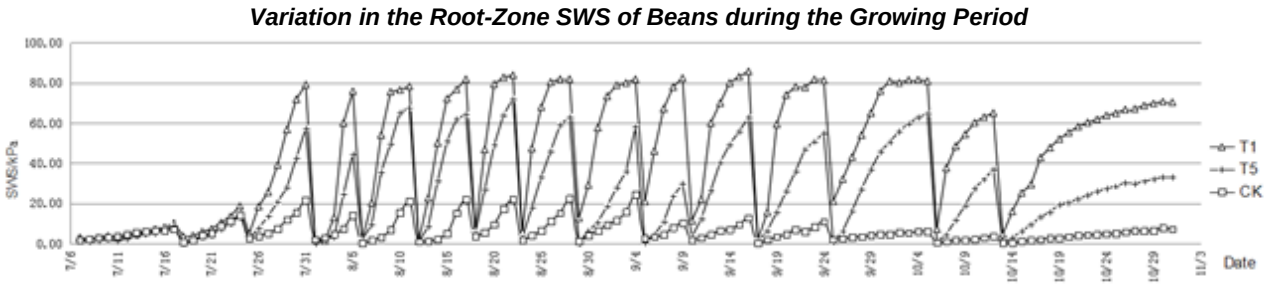

Fig.2 - Time series of SWS

Figure 2 shows the evolution of the root-zone SWS throughout the whole growing period for cold-region greenhouse autumn beans under T1, T5, and CK irrigation treatments. The ladder-shaped variations of the soil water potential could be seen under T1 treatment from the start of the irrigation to the beginning of the next, with the highest reaching approximately 80 kPa. Under T5 and CK treatments, a roughly triangle-shaped evolution was observed in SWS. However, the peak was approximately 60 kPa for the T5 treatment and less than 25 kPa for CK. A smaller amount of irrigation led to the wider wave curve of SWS, larger range of the enveloping line, more rapid and substantial SWS increase after irrigation, and vice versa). This result implied that a larger irrigation volume corresponded to the slow increase of SWS. From the end of the irrigation till the start of the next, less irrigation resulted in the faster and slower increase of SWS for the earlier and later stages, respectively, and vice versa.

In order to quantify the temporal dynamics of root-zone SWS, we distinguished between the former and latter periods of irrigation intervals, during which the average daily changes in SWS of beans between two irrigations at different growing stages are shown respectively in Table 3. Due to relatively long time span of the planting and harvesting periods, each of them was also divided into the earlier and later stages.

Table 3

Diurnal changes in SWS (kPa)

Growing period	T1		T5		CK	
	Three days after irrigation	Three days later after irrigation	Three days after irrigation	Three days later after irrigation	Three days after irrigation	Three days later after irrigation
Earlier stage of seedling	6.3	8.6	4.5	9.4	1.5	3.8
Later stage of seedling	22.6	7.4	18.6	10.5	1.8	7.4
Flowering stage	25.1	0.9	16.9	8.3	3.9	5.1
Fruiting stage	19.6	3.6	6.9	9.6	2.2	3.6
Earlier stage of arvesting	18.2	4.0	9.8	6.5	1.1	1.1
Later stage of harvesting	12.0	2.9	4.6	2.3	0.4	0.4

As shown in Table 3, by ignoring a few growing periods, SWS changed significantly within three days after irrigation and revealed gentle trends of variations afterwards. The average daily changes in SWS within three days after T1 irrigation treatment were between 6.3–25.1 kPa; after the three days, the average daily changes were only 0.9–8.6 kPa. Moderate variations could be observed for the CK treatment. SWS was altered by 0.4–3.9 kPa per day within the three days after irrigation and then became 0.4–7.4 kPa. The mean diurnal change in the suction was 4.6–18.6 kPa within three days after T5 irrigation treatment and 2.3–10.5 kPa thereafter. This result indicated that with a lower amount of irrigation water moved faster in soil within three days after irrigation, i.e., soil moisture was depleted more rapidly and vice versa. Table 3 shows that diurnal changes in SWS were the largest during the later stages of planting and flowering for the beans, implying that water consumption was significant during these two stages. This result was consistent with the findings from our previous analyses on crop production, i.e., the influence of irrigation volume on the bean yields was the highest during the seedling and flowering periods. Therefore, the growth of beans was relatively sensitive to moisture when at the seedling and flowering stages. This conclusion was again reinforced.

Impact of Irrigation Volume on SWS Dynamics

Statistical analyses were conducted on the daily root-zoom SWS dynamics of beans for each growing period after irrigation under T1–T9 treatments. The average daily SWS at different irrigation levels for each growing stage was obtained (Figure 3).

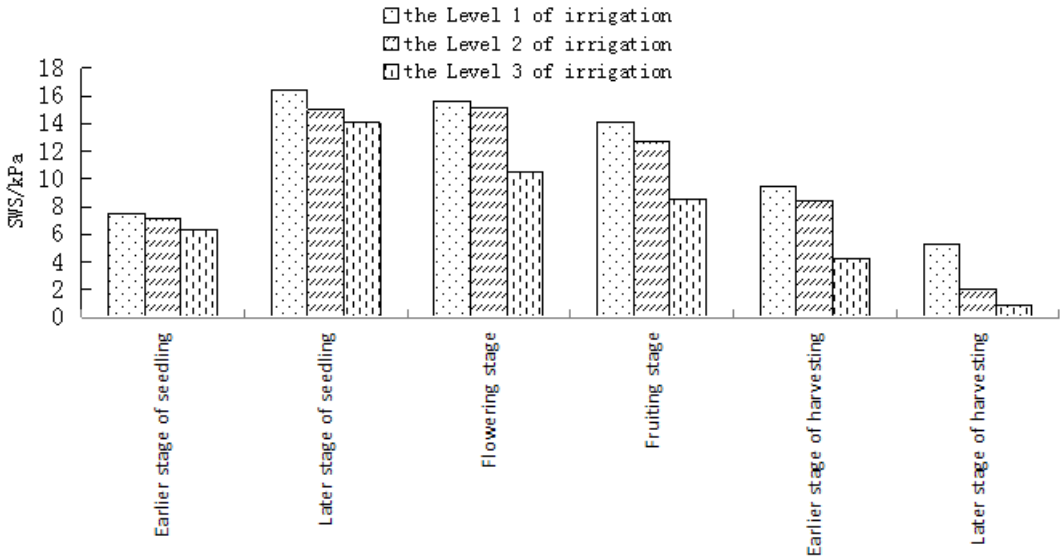

Fig.3 - Average daily SWS

As seen in Figure 3, daily SWS decreased gradually with increasing irrigation levels in different growing stages. A larger amount of irrigation led to a more significant decrease in daily SWS change. Throughout the whole growth period of beans (from planting to the end of harvesting), daily SWS initially increased and then decreased, with the peak being reached during the later planting stage at 14.06–16.41 kPa. The flowering stage showed the second largest daily SWS, which became the smallest during the later harvesting stage at merely 0.9 kPa under level 3 irrigation. This result was consistent with the water consumption evolution for the entire growth period of beans, thus indicating that daily SWS dynamics were able to reflect the water consumption law of the whole growing period (i.e., a general trend of an increase followed by a decrease). The highest, second highest, and lowest water consumptions were observed at the later planting stage, flowering stage, and harvesting stage, respectively.

Impact of Variation in Temperature on SWS

We analyzed the root-zone SWS variations of beans within a whole day (the third day after CK irrigation in the middle of July, August, September, and October; Figure 4).

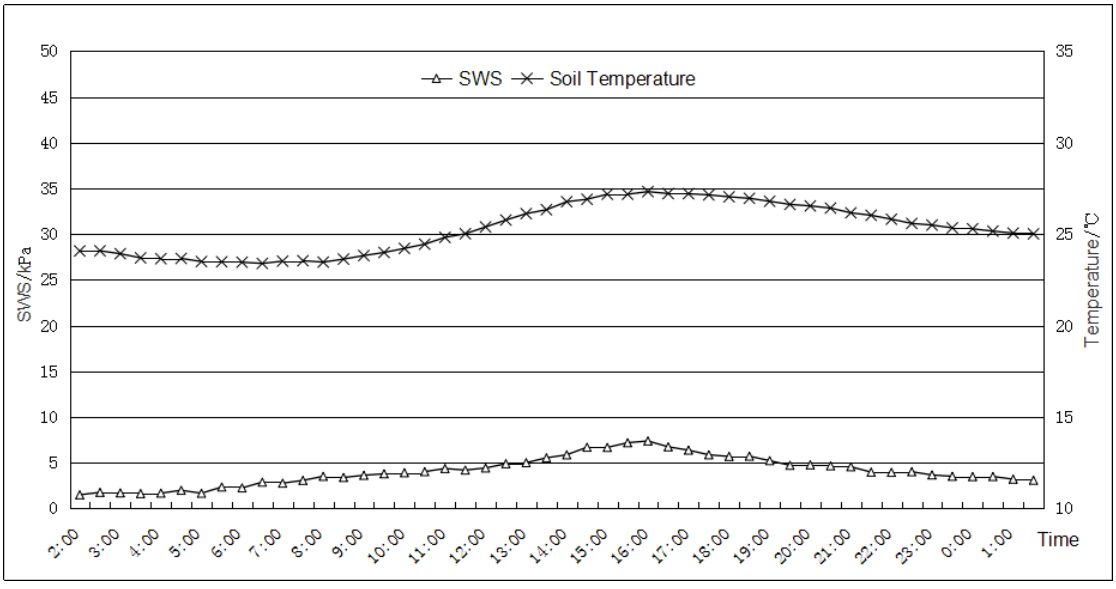

a) July, average temperature of 25.3 °C

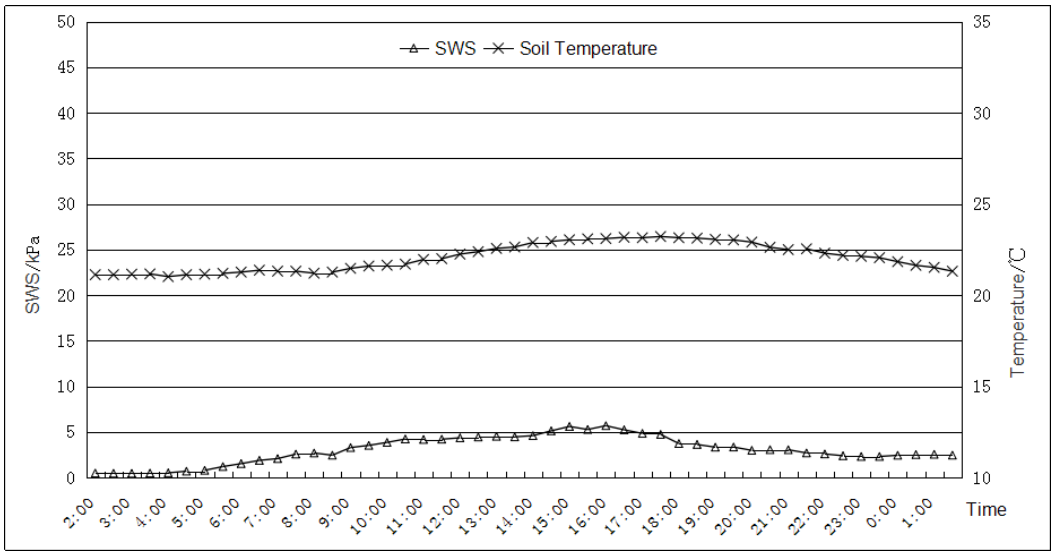

b) August, average temperature of 22.1 °C

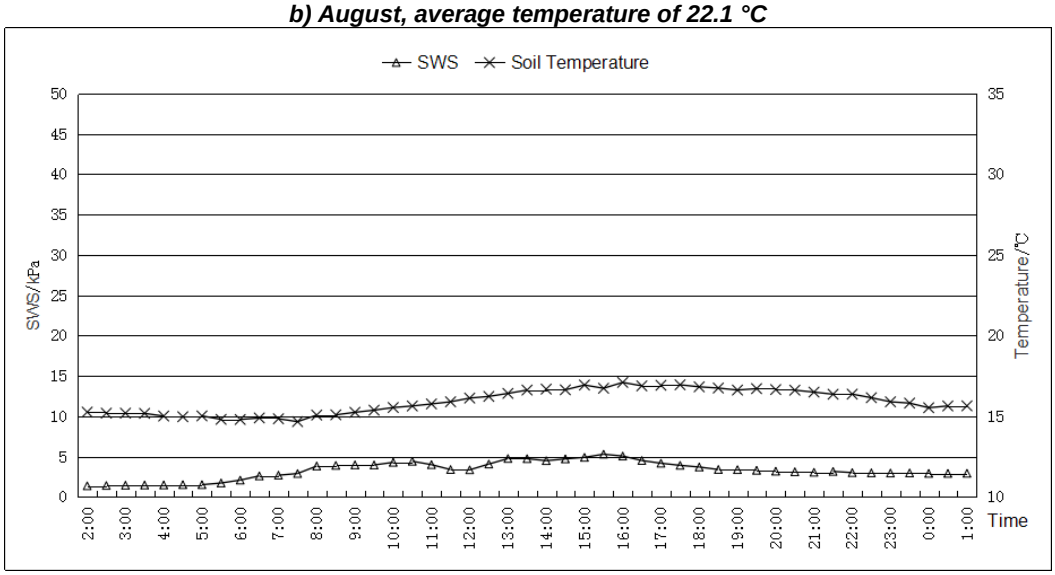

c) September, average temperature of 15.9 °C

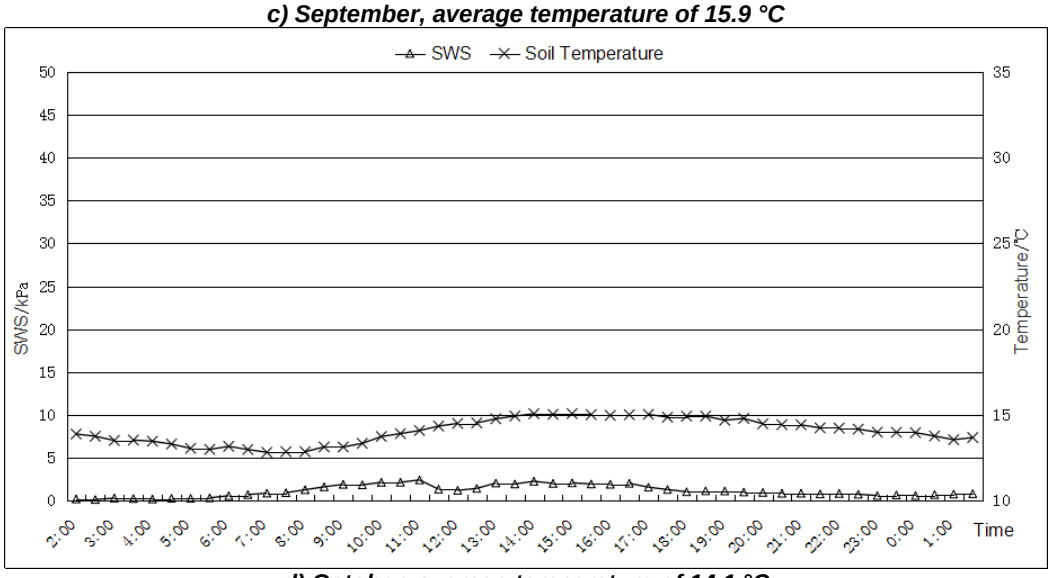

d) October, average temperature of 14.1 °C

Fig.4 - SWS variations within 24 hr in the 3rd day after irrigation

Figure 4 shows that SWS did not increase with time after the same and adequate irrigation in different months over various growing stages. On the contrary, suction varied with temperature at similar trends. Positive linearity between temperature and soil water potential on the basis of Capillary theory *(Dexter et al., 2010)*. Both the soil temperature and SWS reached the maximum at 4 pm rather than at 2

pm when air temperature was the highest. We accordingly divided the process of soil water redistribution into two parts: the temperature-rise period from 2 am to 4 pm, and the temperature-fall period from 4 pm to 2 am the next day. In July, with a temperature increase of 0.1 °C on average, SWS increased by 0.18 kPa; when the temperature decreased by 0.1°C on average, suction decreased by 0.20 kPa. In August, SWS increased by 0.26 and 0.18 kPa when the temperature increased and decreased by 0.1 °C, respectively. In September, SWS increased and decreased by 0.20 and 0.15 kPa upon a 0.1 °C increase and decrease in temperature, respectively. In October, temperature increased or decreased by 0.1 °C, thus increasing and decreasing SWS by 0.16 and 0.09 kPa, respectively. Except for July, the increase in SWS with temperature was more substantial than the decrease. This result implied that, with the same gradient in temperature change, the change rate of soil potential was larger in the temperature-rise period than that at the cooling stage. Moreover, with a drop in the average temperature from July to September, the range of variation in SWS upon a 0.1°C change in temperature showed a descending trend, thus indicating a slowing down of the changing rate of soil potential because of a decrease in temperature.

CONCLUSIONS

Two-year drip irrigation experiments were conducted for greenhouse autumn beans in cold regions. We analyzed the impacts of irrigation volume on the yields, WUE, and root-zone SWS at different growing periods under various irrigation treatments.

In terms of maintaining production and saving water at the same time, T5 irrigation treatment was the optimal scheme of water-saving irrigation for cold-region greenhouse autumn beans , i.e., irrigation quotas were 12 mm for planting, 12 mm for flowering, 24 mm for fruiting, and 6 mm for harvesting. The irrigation volume affected the bean yields significantly during the planting and flowering stages.

For different growing periods, daily variations in root-zone SWS decreased gradually with increasing irrigation levels.

With the same gradient in temperature change, the changing rate of soil potential was larger in the temperature-rise period than that at the cooling stage and slowed down when temperature decreased.

ACKNOWLEDGEMENT

This research was supported by science and technology key project of Heilongjiang Province of China (GZ08B103)

REFERENCES

[1] Ahmadi S. H., Mosallaeepour E., Kamgar-Haghighi A. A., et al., (2015), Modeling maize yield and soil water content with aquacrop under full and deficit irrigation managements, *Water Resources Management*, vol. 29, Issue 8, Springer, pp.2837-2853, Dordrecht/Netherlands;

[2] Al-Omran A. M., Sheta A. S., Falatah A. M., et al., (2005), Effect of drip irrigation on squash (cucurbita pepo) yield and water-use efficiency in sandy calcareous soils amended with clay deposits, *Agricultural Water Management*, vol. 73, Issue 1, Elsevier, pp.43-55, Amsterdam/Netherlands;

[3] Baoping F., Zhangyu Z., Jianfeng Z., et al., (2002), Review of effect of temperature on soil water movement. *Advances in Water Science,* vol.13, Issue 5, pp.643-648, Nanjing Hydraulic Research Institute, Nanjing/China;

[4] Brevedan R. E., Egli D. B., (2003) , Short periods of water stress during seed filling, leaf senescence, and yield of soybean, *Crop Science*, vol.43, Issue 6, pp.2083-2088, Crop Science Society of America, Madison/USA;

[5] Dejie K., Guobao Z., Yuanpei Z., et al., (2011), Research of Water Consumption Regularity with Drip Irrigation under Mulch of Greenhouse Tomato in Ningxia, *Acta Agriculturae Boreali-occidentalis Sinica*, vol. 20, Issue 1, pp.19-123 Northwest A&F University, Yangling/China;

[6] Dexter A. R., Richard G., Czyz E. A., et al., (2010), Changes in the matric potential of soil water with time and temperature, *Soil Science,* vol. *175*, Issue 175, pp.320-328 Springer, Philadelphia/U.S.A.;

[7] Fan T., Stewart B. A., Payne W. A., et al., (2005), Supplemental irrigation and water-yield relationships for plasticulture crops in the loess plateau of china, *Agronomy Journal*, vol.97, Issue 1, pp.177-188 America Society Agronomy, Madison/U.S.A.;

[8] Feng W., Taisheng D., Rangjian Q., et al., (2010), Effects of deficit irrigation on yield and water use efficiency of tomato in solar greenhouse, *Transactions of the Chinese Society of Agricultural Engineering*, vol. 26, Issue 9, pp.46-52 Chinese Society of Agricultural Engineering, Beijing/China;
[9] Guobao Z., Yuanpei Z., Dejie K., et al., (2012), Effect of different irrigation amount on water requirement rule and water use efficiency of cucumber in greenhouse, Issue 1, *Water Saving Irrigation*, pp.22-24 Chinese National Committee on Irrigation and Drainage, Wuhan/China;
[10] Guofu H., Yun Z., Chengyan L., et al., (2010), Scanning electron microscope and cluster analysis of cold area Phaseolus vulgaris L.var.chinensis Hort, *Journal of Northeast Agriculture University*, vol.41, Issue 7, pp.79-83 Northeast Agricultural University, Harbin/China;
[11] Jiazuo Z., Dongqing L., (2012), Numerical analysis of coupled water, heat and stress in saturated freezing soil, *Cold Regions Science & Technology*, Issue 72, pp.43-49 Elsevier, Amsterdam/Netherlands;
[12] Kuşçu H., Turhan A., Demir A. O., (2014) , The response of processing tomato to deficit irrigation at various phenological stages in a sub-humid environment, *Agricultural Water Management*, vol.133, Issue C , pp.92-103 Elsevier, Amsterdam/Netherlands;
[13] Lima R. S. N. D., Martins A. O., Deus B. C. D. S. D., et al., (2015), Partial root zone drying (PRD) and regulated deficit irrigation (RDI) effects on stomatal conductance, growth, photosynthetic capacity, and water-use efficiency of papaya, *Scientia Horticulturae*, Issue 183, pp.13-22 Elsevier, Amsterdam/Netherlands;
[14] Maraseni T. N., Mushtaq S., Reardon-Smith K., (2012), Integrated analysis for a carbon- and water-constrained future: an assessment of drip irrigation in a lettuce production system in eastern Australia, *Journal of Environmental Management,* vol.111, Issue 1, pp.220-226 Elsevier, London/England;
[15] Meixian L., Jinsong Y., Xiaoming L., et al., (2011), Effects of irrigation amount and frequency on soil water distribution and water use efficiency in a cotton field under mulched drip irrigation, *Chinese Journal of Applied Ecology*, vol.22, Issue 12, pp.3203-3210, Ecological Society of China, Shenyang/China;
[16] Moraru P. I., Rusu T., (2012), Effect of tillage systems on soil moisture, soil temperature, soil respiration and production of wheat, maize and soybean crops, *Journal of Food Agriculture & Environment,* vol.10, Issue 2, pp.445-448 WFL Publisher, Helsinki/Finland;
[17] Patel N., Rajput T. B. S., (2013), Effect of deficit irrigation on crop growth, yield and quality of onion in subsurface drip irrigation, *International Journal of Plant Production*, vol.7, Issue 3, pp. 417-436, Gorgan University, Agricultural Sciences & Natural Resources, Gorgan/Iran;
[18] Pettigrew W. T., (2004), Physiological consequences of moisture deficit stress in cotton, *Crop Science*, vol.44, Issue 4, pp.1265-1272 Crop Science Society of America, Madison/USA;
[19] Qianqian C., Yangyang F. Yingbin H. et al., (2011), Effects of different soil water content on stomata development and water consumption of maize, *Agriculture Research in the Arid Areas*, vol.29, Issue 3, pp.75-79 Northwest A&F University, Yangling/China;
[20] Qinglin L., Enhe Z., Qi W., et al., (2012), Effect of irrigation and nitrogen supply levels on water consumption, grain yield and water use efficiency of spring wheat on no-tillage with stubble standing farmland, *Acta Prataculturae Sinica*, vol.21, Issue 5, pp. 169-177 Chinese Grassland Society, Lanzhou/China;
[21] Sanjit K., Shukla, Manoj K., et al., (2011), Coupled liquid water, water vapor, and heat transport simulations in an unsaturated zone of a sandy loam field, *Soil Science,* vol. *176*, Issue 8, Springer, Philadelphia/U.S.A., pp. 387-398;
[22] Yancong W., Hao L., Jingsheng S., et al., (2012), Effects of regulated deficit irrigation on quality and water consumption of solar greenhouse green eggplant, *Journal of Irrigation and Drainage*, vol.31, Issue 1, pp.75-79, Farmland Irrigation Research Institute, Ministry of Water Resources & CAAS, Xinxiang/China;
[23] Yuanming L., Wansheng P., Mingyi Z., et al., (2014), Study on theory model of hydro-thermal–mechanical interaction process in saturated freezing silty soil, *International Journal of Heat & Mass Transfer*, vol.78, Issue 5, pp.805-819 Elsevier, Oxford/England.

CHARACTERIZATION OF HEAVY METAL POLLUTION IN VEGETABLE FIELD SOILS AND HEALTH RISK ASSESSMENT IN DAYU COUNTY, CHINA

/

中国大余县菜田土壤重金属污染特征及潜在生态风险评价

Ph.D. Chen Ming, B.S. Yang Tao, B.S. Yang Quan, B.S. Xu Hui, A.P. Nie Jinxia
Jiangxi Key Laboratory of Mining and Metallurgy Environmental Pollution Control,
Jiangxi University of Science and Technology, Ganzhou / China
Tel: +86-797-8312762; E-mail: just168@163.com

Keywords: *ground vegetable soil; heavy metals; pollution assessment; ecological agriculture*

ABSTRACT

The content of seven heavy metals (Cd, Pb, Cu, Cr, Zn, As, and Hg) in soil samples that collected from vegetable fields surrounding sewage irrigation district in Dayu County of China were detected and analyzed. The purpose of the analysis is to determine the harmful effects of heavy metal pollution to agricultural development through characterize the heavy metal pollution characteristics of soil. This study evaluated the heavy metal pollution index and the results show that, except for Pb, Cr, and Zn, the amount of majority heavy metals in most sites exceeded the Soil Environmental Quality Standard grade II level. In particular, the Cd pollution is the most serious with its contents exceed the standard level by 18.3 times. The nemerow comprehensive pollution index (NCPI) analysis shows that 90% of the sampling points are under moderate or severe pollution. In particular, NCPI is maximized to 13.22 in S-6. According to potential ecological risk (PER) assessment, the single-factor PER (Er) is Cd > Hg > As > Cu > Pb > Cr > Zn. The Er of Cd is maximized to 1,833.33 in S-6, indicating that Cd pollution in this site is extremely serious. Results of the comprehensive PER index (RI) indicats that all sites are under strong ecological risks. Therefore, soil pollution caused by heavy metals can severely harm the local agro-ecological environment.

摘要

通过对大余县污灌区周围菜田土壤样品中 Cd、Pb、Cu、Cr、Zn 和 As、Hg 等七种重金属含量的分析检测，目的在于通过分析土壤重金属的污染特征来表明当前重金属污染对农业发展带来的危害。结果表明，菜田土壤重金属除 Pb、Cr、Zn 外，其他重金属含量大部分超过《土壤环境质量标准》二级标准值，以 Cd 污染超标 18.3 倍最为严重。从内梅罗综合污染指数看，90%的采样点 P 综值达到中度或重度污染，以 S-6 的 P 综值达 13.22 最为严重。从潜在生态风险评价结果表明，单个元素潜在生态风险值 Er 按大小排序为：Cd> Hg> As> Cu> Pb> Cr> Zn，其中以 S-6 中 Cd 的 Er 值达到最大值为 1833.33，说明该区域受 Cd 污染极为严重，其次 RI 值说明所有采样点都处于强生态风险程度以上。因此，由重金属引起的菜田土壤污染已严重危害当地农业生态环境。

INTRODUCTION

The rapid economic development has currently triggered a series of pollution problems, particularly the heavy metal pollution (*Zhang Wei, et al., 2015*). The content of several heavy metals in soils have exceeded allowable levels or even the background levels because of human production and living activities. These heavy metals cannot be decomposed or utilized by microorganisms *(Dou Zhiyong, et al., 2015*), but will be enriched by organisms. These heavy metals in soils have a long retention time and poor mobility *(Ma Jianhua et al., 2014; Zheng Hongyan et al., 2015)*. In recent years, many reports on soil heavy metal pollution have been published *(Olawoyin R., et al., 2012)*. Soil heavy metal pollution mainly originates from farmland sewage irrigation and pesticide application. In April 2015, the Ministry of Agriculture stated that wastes from mines and industrial plants are discharged into agriculture lands, which leads to the decrease in agricultural production and environmental quality. Long-term and excessive use of fertilizers and pesticides and improper waste disposal caused serious agricultural non-point source pollution.(*An Jing, et al., 2016*) The primary source of heavy metals, according to the Department of Environmental Protection, was irrational exploitation mining (*Liu Shuo et al., 2016*), which is also one of the main causes of serious pollution in agricultural lands.

Dayu County in Jiangxi Province, China has many large-scale tungsten mines and is called the “world capital of tungsten”. Accompanied by the rapid economic development, tungsten mining also causes

severe pollution, as the disorder mining produces large amounts of waste water that containing heavy metals. It has jeopardized the farmland soil, water and other agricultural resources. China is a large agricultural country, which primarily relies on irrigation and agricultural development; therefore, agricultural pollution affects not only the GDP of the country but also the life and health of people. However, only a few studies on heavy metal pollution in the farmland fields surrounding sewage irrigation district in Dayu County have been conducted. Thus, in this study, we selected the vegetable soil heavy metal pollution as one of the representatives in farmland pollution and characterized the heavy metal contents in vegetable soils surrounding sewage irrigation district in Dayu county. On this basis, we assessed the potential ecological risks (PERs) in the area which will provide a good reference and theoretical basis for better management of the agricultural environment in Dayu.

MATERIAL AND METHOD

Study area

Dayu County (E 114°–114°44′, N 25°15′–25°37′) is located in the southwest of Jiangxi Province and the upstream of Zhangjiang River, which passes through Dayu from west to east. The northern part of Dayu is adjacent to Luoxiao Mountains and Chongyi County, the eastern part is adjacent to Nankang County, the southern part is adjacent to Nanxiong City of Guangdong Province, and the western part is adjacent to Renhua County of Guangdong. Xihuashan Tungsten Mine (6.48 km^2), which is located in the north-western part of Dayu. Samples of vegetable field soils and vegetables were collected from the tailing southward along riverbanks surrounding sewage irrigation district.

Sample collection and analysis

Samples of vegetable field soils were collected in June 2015. In particular, samples were collected in a quincunx manner, according to the Technical Specification for Soil Environmental Monitoring (HJ/T166-2004) and terrain characteristics of the area. The point positions were recorded by a Global Positioning System (GPS). Surface soils (0–20 cm) in good condition were selected. In total, 10 soil samples were collected. The soil samples were packed into clean and marked sampling bags and transported to our laboratory for analyses and tests. The sampling sites were shown in Fig.1

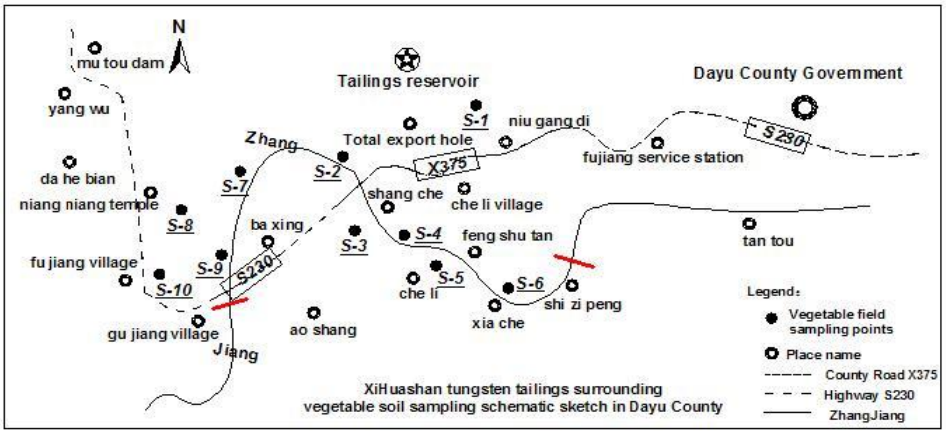

Fig.1 - Vegetable field soil sampling sites

After natural drying, impurities, including small stones and plant residues, were removed from the soil samples. Approximately 1kg of soil was collected from each sample by using the quartation method. Then, the samples were ground and screened by using a 100 mesh nylon screen. Table 1 showed the soil sample pretreatment methods.

Table 1

Soil sample pretreatment methods

Item	Soil sample				
	pH	SOM	CEC	Cu, Pb, Zn, Cr, Cd	As, Hg
Method	Water–soil ratio 2.5:1	Potassium dichromate–volumetric method	$BaCl_2$–H_2SO_4 method	HNO_3–HF–$HClO_4$ digestion[1]	Aqua regia digestion[2]
Equipment	PHS-3C mine magnetic pH meter	Acid titration	Acid titration	AAS	AFS-8220 meter

Note: AAS: atomic absorption spectrophotometer; AFS: atomic fluorescence spectrophotometer; SOM: soil organic matter; CEC: cation exchange capacity

[1]:Liu Yan, et al., 2013; [2]:Zhao Ximei, et al., 2014

All samples were tested by using the Chinese National Standard Soil References (GBW07405). The reliability of data was analyzed through spiked recovery control (80%–120%) and parallel control (relative standard deviation <10%) *(He Yusheng et al., 2015)*; therefore, the measured data were controlled within permissible error ranges.

Data processing

Statistical processing and plotting were conducted on Origin 7.5 and Excel 2013. Statistical analysis was conducted on SPSS 20.0. Correlations between heavy metals and soil physicochemical properties were analyzed by using Pearson's method.

Evaluation methods

Pollution indices are used to characterize heavy metal pollution in vegetable field soil in agriculture. The single-factor pollution index (SFPI) *(Wang Youqi et al., 2014; Liu Yan et al., 2013)* reflects the pollution degree of a single pollutant. For a more comprehensive and integrated evaluation of soil pollution, the Nemerow comprehensive pollution index (NCPI) *(Wang Lixia et al., 2005)*. PERs in this region were also assessed.

(1) The SFPI is used to evaluate the pollution degrees of single pollutants. The SFPI is computed as follows:

$$Pi = \frac{Ci}{Si} \tag{1}$$

where P_i is the SFPI of pollutant i in soil, C_i is the measured content of pollutant i (mg·kg^{-1}),S_i is the evaluation standard of pollutant i (mg·kg^{-1}) from the Soil Environmental Quality Standard grade II level (GB 15618-1995).

(2) The NCPI can comprehensively reflect the soil pollution degree of all pollutants. The NCPI is computed as follows:

$$P_{com} = \sqrt{\frac{\left(Ci/Si\right)^2_{\max} + \left(Ci/Si\right)^2_{ave}}{2}} \tag{2}$$

where P_{com} is the NCPI of pollutants in a soil sample, $(C_i / S_i)_{max}$ is the maximum value of NCPI in this region (mg·kg^{-1}),$(C_i/S_i)_{ave}$ is the average NCPI of pollutants in this region (mg·kg^{-1}). The evaluation criteria are listed in Table 2.

Table 2

Grading criterion of soil heavy metal pollutions

Grade	SFPI grading criterion			NCPI grading criterion		
	Pollution index	Pollution grade		Pollution index	Pollution grade	
1	$P_i < 1$	Clean	I	$P \le 0.7$	Safe	I
2	$1 \le P_i < 2$	Slight	ii	$0.7 < P \le 1$	Warn	II
3	$2 \le P_i < 3$	Medium	iii	$1 < P \le 2$	Slight	III
4	$P_i \ge 3$	Heavy	iv	$2 < P \le 3$	Medium	IV
5				$P > 3$	Heavy	V

Assessment of soil potential ecological risk (PER), The PER index *(Gao Peng, et al., 2015; Xu Zhongyi et al., 2014)* is used to evaluate the potential risk of a single heavy metal or the comprehensive risk of several heavy metals in a region. The PER index is computed as follows:

$$E_r^i = T_r^i \times \frac{Ci}{Si} \tag{3}$$

$$RI = \sum E_r^i \tag{4}$$

where C_i is the measured content of heavy metal i (mg·kg^{-1}), S_i is the background level of heavy metal i (mg·kg^{-1}), E_r^i is the single PER index of heavy metal i, RI is the comprehensive PER index of heavy metals in a region. The toxicity response coefficients of heavy metals used in this research are (T_r^i) *(Lars H., 1980)*: Cd = 30; Pb = Cu = 5; Cr = 2; Zn = 1; As = 10; Hg = 40. The relevant PER assessment grades are listed in Table 3.

Table 3

Potential ecological risk division level

E_r^i	RI	Pollution degree	Grade
$E_r^i < 40$	$RI < 150$	Slight PER	I
$40 \le E_r^i < 80$	$150 \le RI < 300$	Medium PER	II
$80 \le E_r^i < 160$	$300 \le RI < 600$	Severe PER	III
$160 \le E_r^i < 320$	$RI \ge 600$	Very severe PER	IV
$E_r^i \ge 320$		Extremely severe PER	V

RESULTS

Distribution of heavy metal contents in vegetable field soils

As shown in Table 4, soil samples S-1, S-2, S-3, S-7, S-9, and S-10 are below pH 6.5, and other samples are within pH 6.5–7.5, which are consistent with the characteristic of partial acid vegetable field soil in south Jiangxi and corresponding to grade II of the national standards. Except for S-4, the Cd contents in other sample sites are within 0.5–5.5, which all exceed the grade II level, particularly in S-6, which is 18.3-fold higher. No sample exceeds the grade II levels of Zn, Cr, or Pb. As for Cu, except for S-5, other samples exceed the grade II level, particularly in S-9, which is 3.32-fold higher. As for As, 80% samples exceed the grade II level, particularly in S-2, S-6, and S-8. As for Hg, except for S-5, S-6, S-9, and S-10, other sites exceed the grade II level of Hg, particularly in S-1 and S-3, which exceed the level by more than 3-fold.

Table 4

Statistical description of soil heavy metal contents

Site	pH	SOM ($g \cdot kg^{-1}$)	CEC ($cmol \cdot kg^{-1}$)	Heavy metal ($mg \cdot kg^{-1}$)						
				Cd	Pb	Cu	Cr	Zn	As	Hg
S-1	6.45	31.8	14.5	1.2	59.8	116.9	76.4	75.9	79	1.2
S-2	6.3	45.79	17.6	2.8	92.9	100.5	67.7	88.3	103.5	0.49
S-3	4.8	31.28	13.5	1.2	88.8	82.1	63.3	65.3	23	0.97
S-4	7.21	22.61	10.5	0.2	80.5	122.7	45.9	98.5	35.6	0.71
S-5	6.5	22.54	11.8	1.2	88.8	92.8	50.2	82.6	8.8	0.12
S-6	6.68	21.53	9.6	5.5	84.6	179.7	37.1	139	92.4	0.2
S-7	5.99	21.89	10.2	1.9	84.6	112.1	59	81.9	50.9	0.65
S-8	6.65	34.56	16.5	3.5	142.7	192.3	72.1	122.2	112.2	0.8
S-9	5.38	22.36	11.2	0.5	126.1	166.2	72.1	98.5	55.6	0.1
S-10	4.91	27.11	12.8	1.9	167.6	83.1	102.6	70.6	49	0.24
Mean	–	–	–	2	101.64	124.84	64.64	92.28	61	0.55
SD	–	–	–	1.58	33.03	40.4	18.41	23.19	34.68	0.38
CV/100%		–	–	79	32	32	28	25	57	69
Chinese grade II		pH	<6.5	0.3	250	50	150	200	40	0.3
			6.5–7.5	0.3	300	100	200	250	30	0.5
			>7.5	0.6	350	100	250	300	25	1
Background in Jiangxi			–	0.1	32.1	20.8	75	69	10.4	0.08
Background in Ganzhou			–	0.09	34.19	15.17	34.56	58.05	8.85	0.06

Note: CV: variation coefficient; SD: standard deviation

The majority of tested heavy metals significantly exceed the soil background levels in Jiangxi or Ganzhou. The contents of Cd, Pb, Cu, Cr, Zn, As, and Hg exceed the background levels in Ganzhou by 2.22–61.11, 1.75–4.90, 5.41–12.68, 1.07–2.97, 1.12–2.39, 0.99–12.68, and 1.67–20 times, respectively. In particular, the Cd content in site S-6 exceeds by 61.11-fold. S-6 is located downstream of Zhangjiang River and is affected by rainwater erosion because of the low terrain, which probably brought heavy metals from the tailing. The variation coefficient reflects the discrete degree of samples, with a large value indicating a more severe artificial disturbance or more serious pollution. The distribution of Cd content shows significant geographical difference or significant external interference (mainly intense human activities). The variation coefficients of Zn, Cr, Pb, and Cu are similar at 25%, 28%, 32%, and 32%, respectively, indicating that none of the four heavy metals show significant geographical difference and have uniform external influence. The distributions of these heavy metals might be homologous in this region, according to the variation coefficients of vegetable field soil heavy metals in Taicang City *(Zhang Xiaolan, et al., 2007)*. As shown in Fig. 1, S-3 and S-5 are located in the other bank opposite to the ailing and are less affected by the tailing, which probably led to the large differences in As contents. Therefore, in terms of heavy metal content in soil, long-term exploration activity have resulted in extremely serious pollution of agricultural land, which is one of the factors that restrict agricultural production activities.

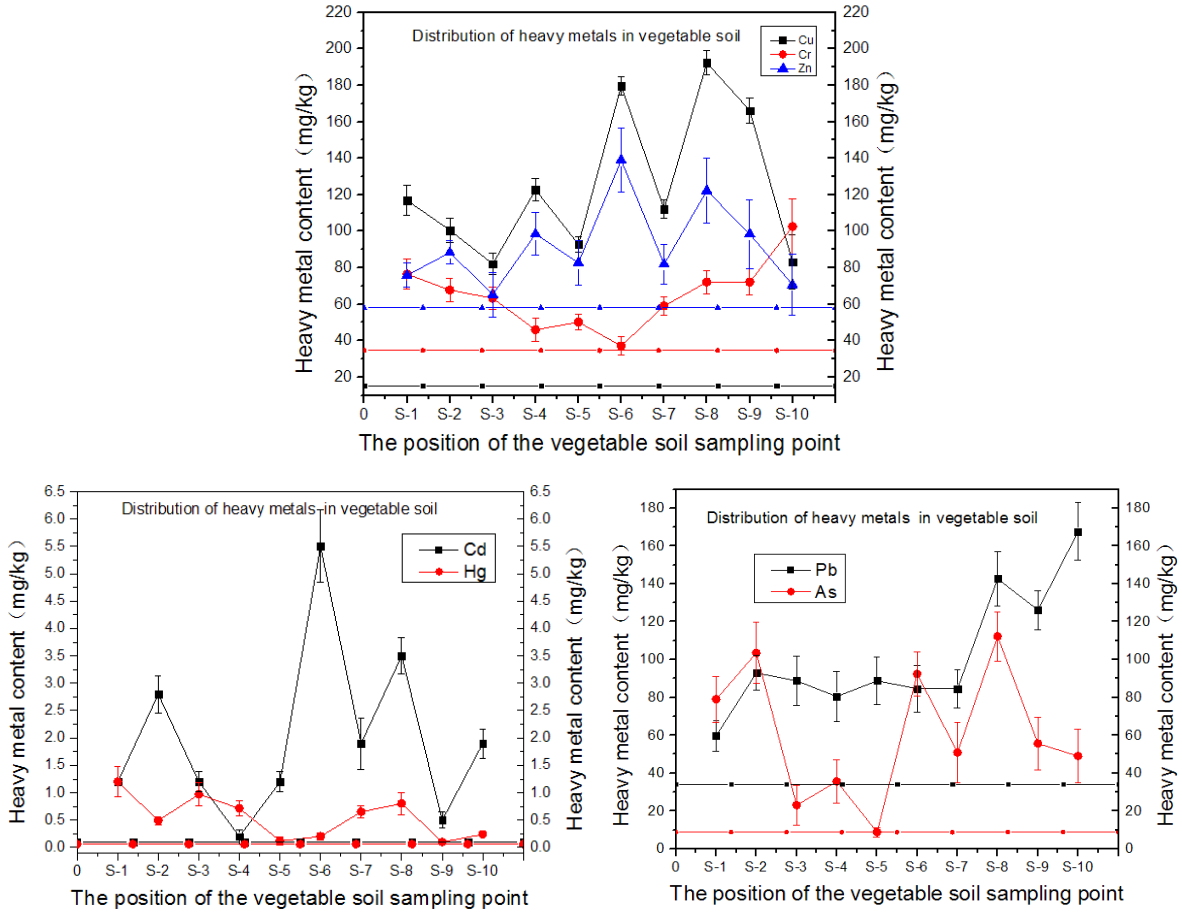

Fig.2 - Distribution of heavy metal contents in vegetable field soils

Note: Dash indicates Ganzhou soil background value

Fig.2 shows the histograms of heavy metal content distribution at all sampling sites. As shown in the figure, the soil heavy metal contents in S-2, S-6, and S-8 are generally higher than that in other sites. In particular, soil heavy metal pollution is extremely severe in S-2 probably because of the influence of the nearby tailing and its location in the sewage irrigation area. Soil heavy metal pollution is very severe in S-6 because S-6 is located downstream of Zhangjiang River and is affected by rainwater erosion, which probably brought heavy metals from the tailing because of its low terrain. Soil heavy metal pollution is extremely severe in S-8, because insecticide use and geological conditions, including its location in upper river, original state without mining, high background value of heavy metal content within the geological strata structure.

Correlation analysis in vegetable field soils

The correlations between heavy metals and soil physicochemical properties in vegetable fields by using Pearson's correlation method. Thereby, we preliminarily determined the correlations between heavy metals and physicochemical properties and whether the sources were similar among different heavy metals. This analysis of agricultural production activities as source pollution had a certain reference value. The results are listed in Table 5.

Table 5

Correlation analysis (Pearson) between heavy metals and soil physiochemical properties

	Cd	Pb	Cu	Cr	Zn	As	Hg	pH	SOM	CEC
Cd	1									
Pb	0.097	1								
Cu	0.499	0.155	1							
Cr	−0.229	0.665*	−0.272	1						
Zn	0.697*	0.057	0.896**	−0.501	1					
As	0.677*	0.134	0.615	0.122	0.586	1				
Hg	−0.185	−0.414	−0.126	0.094	−0.284	0.156	1			

	Cd	Pb	Cu	Cr	Zn	As	Hg	pH	SOM	CEC
pH	0.23	−0.459	0.42	−0.614	0.581	0.322	0.106	1		
SOM	-0.152	-0.172	-0.199	0.207	−0.269	0.282	0.117	−0.204	1	
CEC	0.1	0.188	0.084	0.468	−0.163	0.524	0.396	−0.035	0.691*	1

Note: *p < 0.05; **p < 0.01 (two-sided).

As shown in Table 5, significant positive correlations are observed among Cd, Zn, As, and Cu, together with the characteristics of regional heavy metal pollution. The contaminants from the sewage irrigation district are dominated by Cd, accompanied by As, Cu, and Zn. Pb and Cr contents are also significantly and negatively correlated with pH In particular, a higher pH lead to lower Pb or Cr content, and vice versa. However, the changes are different from Cu and Zn. Hg is not significantly correlated with other heavy metals, whether Hg originated from atmospheric precipitation should be further investigated. As and Cr contents are significantly and positively correlated with CEC, indicating that CEC promoted the absorption of As and Cr. Thus, long-term mining or heavy metal accumulation in soil from chemical fertilizers, pesticides, and other changes in soil physical and chemical properties can be inferred as the sources of heavy metal contaminants in agricultural soil.

Assessment of soil heavy metal pollution

- ***Pollution indices***

SFPI and NCPI, with grade II of the national standards as reference, were used to evaluate the vegetable field soils surrounding the sewage irrigation district (Table 6).

Table 6

Assessment of soil heavy metal pollutions

Metal	Site																			
	S-1		S-2		S-3		S-4		S-5		S-6		S-7		S-8		S-9		S-10	
	P	GRD	P	GRD	P	GRD	P	GRD	P	GRD	P	GRD	P	GRD	P	GRD	P	GRD	P	GRD
Cd	4	iv	9.3	iv	4	iv	0.67	i	4	iv	18.3	iv	6.33	iv	11.67	iv	1.67	ii	6.33	iv
Pb	0.2	i	0.4	i	0.36	i	0.27	i	0.36	i	0.34	i	0.34	i	0.57	i	0.5	i	0.67	i
Cu	2.3	iii	2	iii	1.64	ii	1.23	ii	1.86	ii	3.59	iv	2.24	iii	3.85	iv	3.32	iv	1.66	ii
Cr	0.5	i	0.5	i	0.42	i	0.23	i	0.33	i	0.25	i	0.39	i	0.48	i	0.48	i	0.68	i
Zn	0.4	i	0.4	i	0.33	i	0.39	i	0.41	i	0.**7**	i	0.41	i	0.61	i	0.49	i	0.35	i
As	2	ii	2.6	iii	0.58	i	1.19	ii	0.22	i	2.31	iii	1.27	ii	2.81	iii	1.39	ii	1.23	ii
Hg	4	iv	1.6	ii	3.23	iv	1.42	ii	0.4	i	0.67	i	2.17	iii	2.67	iii	0.33	i	0.8	i
NCPI	3.1	V	6.8	V	2.52	IV	1.14	III	2.93	IV	13.2	V	4.67	V	8.56	V	2.49	IV	4.63	V

Table 6 shows that the SFPIs of Pb, Cr, and Zn in all samples, SFPIs of a part of Hg and As, and SFPI of Cd in S-4 are marked “clean,” whereas the SFPIs in other cases are marked “slight,” “medium,” or even “severe” pollution. The most aggressive pollutant is Cd. 80% of the sites are severely polluted largely, because these areas are located near the tailing and significantly affected by the tailing. Cu pollution in S-6, S-8, and S-9 and Hg pollution in S-1 and S-3 are severe. Results of the NCPI indicate that all sites are polluted. In particular, S-4 has the smallest NCPI and is slightly polluted mainly because Cd pollution at S-4 is at the “clean state.” The NCPIs of approximately 60% of the sampling sites are severely polluted, which are ranked as S-6 > S-8 > S-2 > S-7 > S-10 > S-1. The highest NCPI in S-6 (P = 13.22) is attributed to the largest contribution of Cd pollutant and severe pollutions of Cu and Hg.

- ***Assessment of potential ecological risk***

With the background levels in Ganzhou as references, the *Er* of seven heavy metals and the RI in each sampling site in this sewage irrigation district were computed. Based on relevant PER assessment grades listed in Table 3, the PERs in the study area were estimated. The results are listed in Table 7.

Table 7

Potential ecological risk of heavy metals in vegetable soils in the study area

Site	E_r^i							*RI*	Risk grade
	Cd	Pb	Cu	Cr	Zn	As	Hg		
S-1	400	8.75	38.53	4.42	1.31	89.27	800	1,342.27	IV
S-2	933.33	13.59	33.13	3.92	1.52	116.95	326.67	1,429.09	IV
S-3	400	12.99	27.06	3.66	1.13	25.99	646.67	1,117.09	IV

S-4	66.67	11.77	40.44	2.66	1.7	40.23	473.33	1,117.49	IV
S-5	400	12.99	30.59	2.91	1.42	9.94	80	537.84	III
S-6	1,833.33	12.37	59.23	2.15	2.39	104.41	133.33	2,147.22	IV
S-7	633.33	12.37	36.95	3.41	1.41	57.51	433.33	1,178.33	IV
S-8	1,166.67	20.87	63.38	4.17	2.11	126.78	533.33	1,917.31	IV
S-9	166.67	18.44	54.78	4.17	1.7	62.83	66.67	375.25	III
S-10	633.33	24.51	27.39	5.94	1.22	55.37	160	907.75	IV

As shown in Table 7, the PERs of Pb, Cr, and Zn in vegetable soils are at a “slightly polluted” level, indicating that this area is not significantly harmed by these three heavy metals. Cu contents in 60% of the sites and As contents in 20% of the sites show slight PER; As contents in 40% of the sites show medium PER, but the remaining 40% of the sites show heavy PER (Fig. 1), indicating that As pollution in these areas are significantly affected by human disturbance and geological structure disturbance. As for Cd, S-4 and S-9 is not higher than high PER, and the remaining sites are at very high PER, with up to 1,833.33 as the highest *Er*. As for Hg, S-9, S-6 and S-5 are not higher than high PER, S-10 is at high PER, and the remaining sites are at very high PER, with up to 800 as the highest *Er*. Hg pollution might originate from the dusts due to mining, which then precipitate through air ash onto vegetable soils. Then, according to the RIs, 80% of the sites are at very high PER, indicating that these areas are at a bad eco-environment state largely. because of the eco-environmental risk causes. Therefore, based on the evaluation of heavy metal pollution in vegetable soil, local agricultural production activities are inhibited by heavy metal pollution and long-term mining significantly affects the sustainable development of agriculture.

CONCLUSIONS

Use of the heavy metal pollution index to characterize the soil contaminated by heavy metals to determine the harmful effects of heavy metal pollution to agricultural development. shows the following:

- Except for Pb, Cr, and Zn, the contents of the rest of the heavy metals exceed the Soil Environmental Quality Standard grade II level. Cd pollution is the most severe. The seven heavy metals all cause serious pollution according to the Ganzhou soil background levels, which indicate a significant accumulation of heavy metals in the field of ecological agriculture.
- .Cd, Zn, As, and Cu are significantly and positively correlated, but other heavy metals are not significantly correlated. Pb and Cr contents are significantly and negatively correlated with pH, or the acid conditions improve the activities of Pb and Cr. The amounts of As and Cr in soil are significantly and positively correlated with CEC, indicating that CEC promotes the absorption of As and Cr.
- The SFPI analysis shows that heavy metal pollution in vegetable soil is similar to (1), because Cd pollution is the most severe and approximately 80% of the sampled points .The NCPI analysis shows that S-4 was slightly polluted, whereas the other sites are moderately or severely polluted. The NCPI of S-6 is the largest (13.22). The *Er* of the single-element PER ranking is Cd > Hg > As > Cu > Pb > Cr > Zn, As for Cd, 80% sites are at very high PER, with up to 1,833.33 as the highest *Er*. All RIs show strong ecological risk, or it has already a serious harm to the ecological agriculture.

In a word, Cd pollution is the serious pollution in the sampling areas, and it has strong potential ecological risk, causing a bad influence upon the development of agriculture. Or this study shows that long-term mining exploration activities caused serious heavy metal pollution to surrounding agricultural areas .Heavy metal pollution in agricultural soil is one of the factors that significantly restrict agricultural development, which affects the economic development and GDP growth of the area. Meanwhile, the potential risks of heavy metal soil contaminants on human health should be further investigated.

ACKNOWLEDGEMENT

The work was supported by the National Science and Technology Pillar Program during the 12th “Five-Year Plan” Period (2012BAC11B07) and by the Jiangxi International Science and Technology Cooperation Plan (20133BDH80027) and by the Jiangxi Graduate Innovative Special Fund Project (YC2015-S295).

REFERENCES

[1] An Jing, Gong Xiaoshuang, Chen Hongwei, et al., (2016), Temporal and spatial characteristics and health risk assessments of heavy metal pollution in soils of Shenfu irrigation area. *Journal of Agro-Environment Science*, Vol.35, Issue 1, pp.37-44;

[2] Dou Zhiyong, Chen Jianhua, Zhou Ping, et al., (2015), Ecological Risk Assessment of Heavy Metals in Soil and based on the total effective state Tongling mining, *Environmental Pollution and Control*, Vol.37, Issue 11, pp.6-10, Environmental Pollution and Control magazine/Zhejiang;
[3] Gao Peng, Liu Yong, Su Chao, (2015), Distribution and Risk Assessment of Soil Heavy Metals in Area Surrounding Taiyuan City, *Journal of Agro-Environment Science*, Vol.34, Issue 5, pp.866-873 Agro-Environment Protection Institute/Tianjin;
[4] He Yusheng, Liao Xiangjun, Ni Qian, et al., (2015), Distributive characteristics and pollution evaluation of heavy metals in soils and vegetables from vegetable bases in Haikou City. *Chinese Journal of Soil Science*, Vol.46, Issue 3, pp.721-726, Science Press Ltd./Shenyang;
[5] Lars H., (1980), An ecological risk index for aquatic pollution control - A sedimentological approach. *Water Research*, Vol.14, Issue 8, pp.975-1001, Pergamon Elsevier Science LTD./Oxford;
[6] Liu Shuo, Wu Quanyuan, Cao Xuejiang, et al., (2016), Soil Heavy Metal Pollution Assessment and spatial distribution of Longkou Coal Mining Area, *Environmental Science*, Vol.37, Issue 1, pp.270-279, Science Press/Bei Jing;
[7] Liu Yan, Gan Guojuan, Zhu Xiaolong, et al., (2013), Heavy metal pollution and health risk in vegetables and soils in a industrial and mining area in Hunan Province. *Environmental Chemistry*, Vol.32, Issue 9, pp.1737-1742, Science Press Ltd./Peking;
[8] Long Jiahong, Tan Ju, Wu Yinju, et al., (2013), A Comparative Study on the Detection of Heavy Metal in soil with Different Digestion Methods. *Environmental Monitoring in China*, Vol.29, Issue 1, China pp.123-126, National Environmental Monitoring Centre/Peking;
[9] Ma Jianhua, Ma Shiyuan, Chen Yunzeng, (2014), Mirgration and accumulation of heavy metals in soil-crop-hair system in a sewage irrigation area, Henan, China, *Acta Scientiae Circumstantiae*, Vol.34, Issue 6, pp.1517-1526, Science Press Ltd./Peking;
[10] Olawoyin R., Oyewole S. A., Grayson R. L., (2012), Potential risk effect from elevated levels of soil heavy metals on human health in the Niger delta. *Ecotoxicology and Environmental Safety*, Vol.85, Issue 3, pp.120-130, Academic Press Inc. Elsevier Science/America,;
[11] Wang Lixia, Guo Zhaohui, Xiao Xiyuan, et al., (2008), Heavy metal pollution of soils and vegetables in the midstream and downstream of the Xiangjiang River, Hunan Province. *Journal of Geographical Sciences*, Vol.18, Issue 3, pp.353-362, Institute of Geographic Sciences and Natural Resources Research, CAS/Peking;
[12] Wang Youqi, Bai Yiru, Wang Jianyu, (2014), Distribution of Soil Heavy Metal and Pollution Evaluation on the Different Sampling Scales in Farmland on Yellow River Irrigation Area of Ningxia: A Case Study in Xingqing County of Yinchuan City. *Environmental Science*, Vol.35, Issue 7, pp.2714 -2720, Science Press Ltd./Peking;
[13] Xu Zhongyi, Chen Jin'an, Zhang Yang, et al., (2014), On Speciation Distribution and Potential Ecological Risk Assessment of Heavy Metals in Sediments of Aha Reservoir. *Journal of Southwest China Normal University (Natural Science Edition)*, Vol.39, Issue 3, pp.71-76, Southwest China Normal University Press/Chongqing;
[14] Yi Min, Rong Xuejun, Deng Dongmei, (2015), Characteristics analysis and potential ecological risk assessment of heavy metals in agricultural soil around Yuan baoshan Mine of Guangxi, China. *Journal of Guangxi University of Science and Technology*, Vol.26, Issue 2, pp.93-98, Guangxi University of Science and Technology Press/Liuzhou;
[15] Zhang Wei, Ge Jiantuan., (2015), Contamination by Heavy Metal and Evaluation on Potential Ecological Risks in an Antimony Mine. *Agricultural Science& Technology*, Vol.16, Issue 3, pp.600-602, Hunan Institute of Agricultural Information & Engineering/Hunan;
[16] Zhao Ximei, Lu Chunyan, Liu Qing, et al., (2014), Using Atomic Fluorescence Spectrometry to Study the Distribution of As and Hg in Orchard Soils. *Spectroscopy and Spectral Analysis*, Vol.34, Issue 20, pp.538-541, Peking University Press/Peking;
[17] Zheng Hongyan, Yao Xiurong, Hou Yanlin, et al., (2015), Establishment of Heavy Metal Bio-accumulation Model of Soil Pattern-Crop System in China. *Journal of Agro-Environment Science*, Vol.34, Issue 2, pp.257-265, Agro-Environment Protection Institute/Tianjin;

APPLICATION RESEARCH ON THE DUAL-SPOOL VALVE CONTROL SYSTEM IN A HYDRAULIC –FARM-ORIENTED LOAD TRACTOR
/
双阀芯液压控制系统在农用装载机中的应用研究

A.P. Wenhua Jia*[1)], Prof. Chenbo Yin[2)], Dr. Binghui Jia[1)] , Dr. Guo Li[1)], A.P. Dasheng Zhu[1)], Song Zhang[3)]
[1)] School of Mechanical Engineering, Nanjing Institute of Technology, Jiangsu / China;
[2)] School of Mechanical and Power Engineering, Nanjing University of Technology, Jiangsu 211800 / China;
[3)] IPEK – Institut für Produktentwicklung, Karlsruher Institut für Technologie (KIT), Karlsruher / Germany
Tel: +13505177950; E-mail: geovrml@163.com

Keywords: *Dual spool; Stress response; Power consumption; Farm-oriented load tractor*

ABSTRACT

To cope with the increasingly severe working environment confronting agricultural load tractors, load tractor design must consider the comprehensive influences of noise immunity, control precision, and power loss, among others, of hydraulic systems. A SY235 load tractor and a dual-spool multi-way valve-based prototype were applied as research objects in this research. The antisymmetric data processing function of AMESIM software was employed to update and replenish point data, while a cubic interpolation method was adopted to process the data. In addition, the displacement characteristics, inlet and outlet pressures, and energy consumption of each cylinder in the hydraulic systems of both load tractors equipped respectively with the dual-spool multi-way valve and single-spool multi-way valve were investigated. Meanwhile, a single action experiment was performed on the booms, bucket rods, and buckets of the two load tractors. A comparison of the real test with the simulation model demonstrated that the cylinder controlled by the dual-spool valve exhibited small pressure and power consumption and quick displacement response. Therefore, the cylinders controlled by the dual-spool multi-way valve system had quicker pressure response, smaller pressure and overshoot, and superior overall manipulability. Finally, retraction and external swinging experiments of the buckets were performed on the dual-spool experimental prototype. Experimental results demonstrated that the dual-spool multi-way valve system exhibited faster displacement response and more superior overall performance compared with the single-spool control system. The simulation model combined with the real vehicle experiment is of great significance to the further study of the static and dynamic characteristics and energy-saving performance of the dual-spool agricultural load tractor.

摘要

为应对越来越恶劣的农用装载机工作环境，挖掘机设计需综合考虑液压系统的抗干扰性、控制精度、功率损失等的影响。论文以以 SY235 型号装载机和双阀芯多路阀原型为依据，利用 AMESIM 的反对称数据处理功能更新补充点数据和三次方插值方法处理数据，研究了双阀芯多路阀和单阀芯多路阀装载机液压系统中各油缸的位移特性、进出口压力特性以及能耗情况。通过实车实验与仿真模型进行对比，结果表明双阀芯多路阀控制的油缸压力小，功率消耗小，在位移响应上也是双阀芯系统稍快。通过整机工况实验，得出了双阀芯多路阀控制系统的油缸压力响应较快，压力较小，超调量较小，整体操作性能占优，用双阀芯试验样机做铲斗内收和外摆实验，双阀芯控制系统在位移响应上比单阀芯控制系统快，双阀芯多路阀整体性能占优。仿真模型结合实车实验对深入研究双阀芯农用装载机的静动态特性和节能性能具有重要意义。

INTRODUCTION

Farm-oriented load tractors are widely used in the fields of basic construction, agricultural facilities, construction of new rural areas, and other aspects. These equipments are important in the basic construction of rural areas. Consequently, increased performance requirements of the hydraulic system of the load tractor are needed. The dual-spool system can independently control the inlet oil pressure and return oil pressure under the premise that all working conditions of executive mechanisms are satisfied. Various combinations of the ratio between two spool displacements, accompanied by sensor technology, can better deal with the matching relation between pressure and load, as well as realize the functions that traditional single-valve spool systems can not.

The performance of a hydraulic farm-oriented load tractor depends on whether the match among various subsystems is reasonable *(Casoli Paolo, Anthony Alvin, 2013; Yi Yuan and Yu Tu, 2013; Choi*

Kyujeong et al, 2015; Kumar A, 2013). In recent years, researchers from many universities and institutions in China and abroad have conducted extensive research on the static and dynamic behaviours of the main pump, the matching performances of engine power, and the orifice area of the throttling groove in the multiple directional control valve spool *(Xiong Y et al, 2015; Barreto CEAG and Schiozer DJ, 2015; Lisowski E et al, 2014)*, and have gained numerous achievements. The concept of independent control was proposed by the German professor, Bark, in the control theory of cartridge valve in 1987 *(Ye Y et al, 2014; Kumar A et al, 2013)*. Matti et al *(2015)* conducted an in-depth study on the principles of independent control, and then used multiple digital valves to replace traditional proportional valves to discuss the changes in system performance. Some researchers utilized multiple cartridge valves to replace traditional single-core valves and study the independent control strategy *(Claudio Alimonti et al, 2010; Feng C and Kamat V.R., 2013)*. Feng used double-valve core systems to independently control the executive mechanisms, as well as study the dynamics and energy-saving features of the systems. They concluded that the system oil pressure and energy consumption were reduced by the use of double-valve core control technology, realizing nearly 15% in energy saving *(Mattila J and Virvalo T., 2000)*. At CONEXPO Asia2007, American equipment manufacturers displayed a type of newly developed hydraulic load tractor. According to their data, this type of load tractor adopts independent control technology for load ports. Compared with traditional hydraulic load tractors, the newly developed hydraulic load tractors can reduce energy consumption by 25% and increase productivity by 10% *(Atik FA et al, 2005; Falck Tillmann, 2012)*. In the VT02 series of Linde Corp., Germany, double-core multi-control valves are used and pressure compensators are preserved in valve cores. American EATON Corp.'s Ultronics Corp. provides a series of electro-hydraulic control solutions, including a double-core electro-hydraulic valve control system that adopts independent control technology for use in load tractors, loaders, and aerial vehicles and other agricultural machineries. The remainder of this paper is organized as follows. Section 2 compares single-spool multi-control valves and dual-spool control technology. Section 3 analyzes the dual-spool multi-way valve farm-oriented load tractor hydraulic system characteristics. Section 4 analyzes the aforementioned system characteristics by adopting the method of combination simulation and experiment and comparing the single-core multi-way valve with the double-core multiplex valve. Section 5 summarizes the conclusions

MATERIAL AND METHOD

Mathematical Model of Dual-spool Valve-controlled Hydraulic Cylinder Systems

Compared with single-spool multi-control valves, dual-spool control technology is the combination of a number of technologies, such as electro-hydraulic proportional and sensor technology. Two valve cores are used in the main valve, and executive mechanisms are independently controlled by single-switching valves. The schematic structures of a single group of dual-spool valves are shown in Figures 1 and 2. The parameters of the vehicle operating device of this corresponding load tractor is shown in Table1.

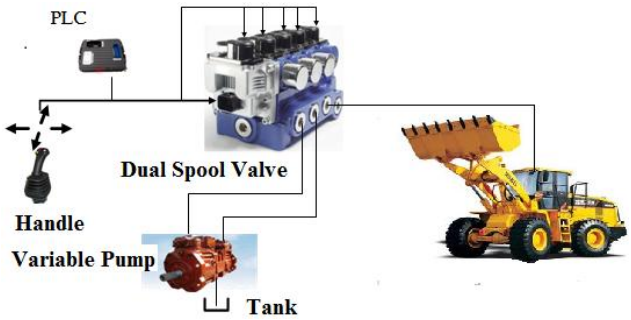

Fig.1 - Dual spool multi-way valve

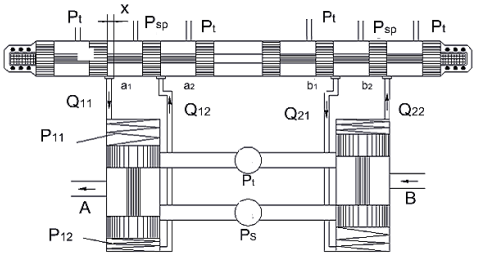

Fig.2 - Dual spool valve structure of an load tractor hydraulic system

Table 1

Parameters of the vehicle operating device

Definition of the parameter	Parameter values
A. Maximum digging depth	3.03 m
B. The horizontal distance between the bucket and the center of the front wheel	5.31 m
C. The horizontal distance between the bucket and the rotating center	4.11 m
D. The horizontal distance between the bucket on top and the rotating center	2.64 m
E. Maximum digging height	3.40 m
F. Maximum unloading height	2.85 m

In Figure 2, P_s is main pressure, P_{sp} is pilot oil pressure, P_t *is oil return pressure, A and B* is working oil port, P_{11} and P_{12} are pressure at both ends of the valve. a_1,a_2,a_3 *and* a_4 are ports of pilot valve. Q_{11}, Q_{12}, Q_{13}, *and* Q_{14} are flow at each intersection.

The dual-spool valve is symmetric, and its throttle area gradients are equal. The optimal displacement relationship between the two spools is obtained by adjusting the displacement ratio of the two main spools in order to adapt to all kinds of working conditions. Their displacement relationship can also be flexibly adjusted according to different working conditions. Assuming the positive direction of the piston movement is the positive direction of the Y coordinate, only the positive direction is studied because of the similarity of theories.

The displacement ratio of valve spools 2 and 1 is provided as $x_1 / x_2 = m_1$. The cylinder area ratio of the rod and rodless chambers is $A_1 / A_2 = n$. Q_1 is used as the load flow.

$$\begin{cases} P_L = F/A_1 = P_1 - nP_2 \\ Q_L = (Q_1 + nQ_2)/(1+n^2) \end{cases} \quad (1)$$

Where P_L is load pressure, F is load equivalent effect, A_1 is area of rod chamber, A_2 is area of rodless chamber, P_1 *is pressure of rod chamber,* P_2 *is pressure of rodless chamber.*

The characteristic equation of the system pressure and flow is as follow.

$$Q_L = C_d w_1 x_1 m_1 \sqrt{2/(\rho(m_1^2 + n^3))(P_S - P_L)} \quad (2)$$

Where C_d is the flow coefficient, ρ is the oil density, and $w_1 = w_2$ is the throttling area gradient.

Flow gain of valve 1:

$$K_{qp1} = \partial Q_L / \partial_{x1} = C_d w_1 m_1^3 / \left(m_1^2 + n^3\right) \sqrt{2/(\rho(m_1^2 + n^3))(P_S - P_L)} \quad (3)$$

Flow gain of valve 2:

$$K_{qp2} = \partial Q_L / \partial_{x2} = C_d w_1 n^3 / \left(m_1^2 + n^3\right) \sqrt{2/(\rho(m_1^2 + n^3))(P_S - P_L)} \quad (4)$$

Flow gain of the dual-spool valve:

$$K_{qp} = K_{qp1} + K_{qp2} m_1 = C_d w_1 m_1 \sqrt{2/(\rho(m_1^2 + n^3))(P_S - P_L)} \quad (5)$$

Flow pressure coefficient:

$$K_{cp} = -\partial Q_L / \partial_{P_L} = C_d w_1 x_1 m_1 \sqrt{2/(\rho(m_1^2 + n^3))(P_S - P_L)} / 2\left(P_S - P_L\right) \quad (6)$$

System linear equation of the pressure and flow characteristic:

$$Q_L = K_{qp} x_1 - K_{cp} P_L \quad (7)$$

Initial volume of the hydraulic cylinder is $V_{10} = V_{20} = (V_1 + V_2)/2 = V_0$, and Y is infinitesimal.

Flow continuity equation of the rodless chamber:

$$Q_1 = A_1\, dY/dt + V_0/\beta_e \cdot dP_1/dt + (C_{ec} + C_{ic})P_1 - C_{ic}P_2 \tag{8}$$

Flow continuity equation of the rod chamber:

$$Q_2 = A_2\, dY/dt - V_0/\beta_e \cdot dP_2/dt - (C_{ec} + C_{ic})P_1 + C_{ic}P_2 \tag{9}$$

Where V_1 and rodless V_2 are the volumes of the rodless and rod cylinder chambers respectively, β_e is the elastic modulus of the hydraulic oil, C_{ec} is the external leakage coefficient, and C_{ic} is the internal leakage coefficient. C_{tc}, C_{tc1} are calculating coefficient.

Equation (10) can be obtained by solving the preceding equations:

$$Q_L = A_1\, dY/dt + V_1 + V_2/2(1+n^2)\beta_e \cdot dP_L/dt + C_{tc}P_L + C_{tc1}P_S \tag{10}$$

$$C_{tc} = \frac{m_1^{\,2} + n^3}{(1+n^2)(m_1^{\,2} + n^3)} C_{ec} + \frac{(1+n)(m_1^{\,2} + n^2)}{(1+n^2)(m_1^{\,2} + n^3)} C_{ic} \tag{11}$$

$$C_{tc1} = \frac{(1+n)(n^3 - n^2)}{(1+n^2)(m_1^{\,2} + n^3)} C_{ic} \tag{12}$$

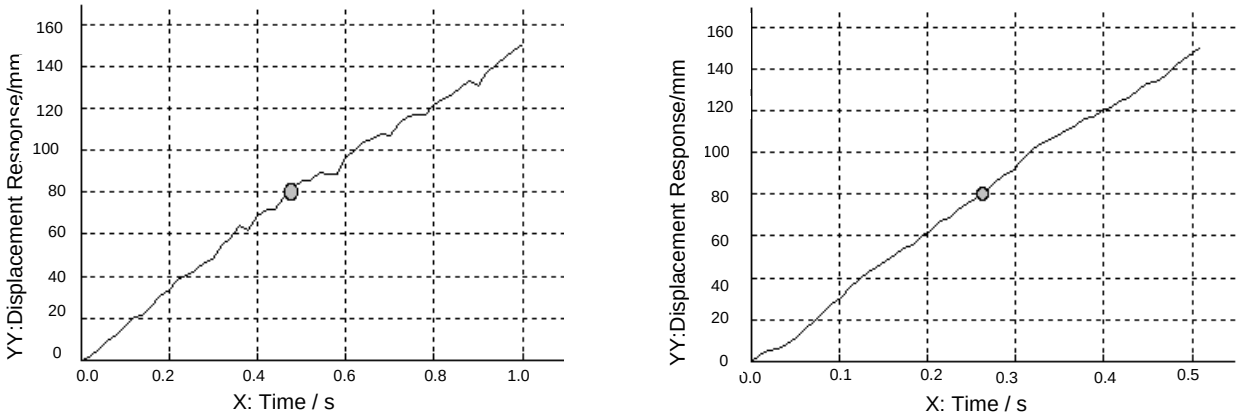

a) *m_1=0.01* ***b)*** *m_1=100*

Fig.3 - Cylinder displacement response curve with different *m_1*

The parameters of the Model SY235 load tractor manufactured are adopted. The effective area ratio between the rod and rodless chambers of the bucket cylinder is n=0.49. The cases where m1 equals 0.01, 0.49, 1, and 100 are studied. The experimental results are shown in Tables 2.

Table 2

Simulation schedule of cylinder displacement response

Definition of the parameter	Parameter values			
m_1	0.01	0.49	1	100
T_1	0.47	0.37	0.31	0.27

Note: T1 is the response time of different cases, and m_1 is the bucket cylinder displacement at 80 mm.

The displacement response time of the bucket cylinder decreases with the increase of *m1*, because if *m1* increases, the opening amount of the cylinder oil outlet will increase, thus reducing the back pressure and resistance.

Therefore, a large m1 affects pressure response, whereas a small *m1* affects displacement response. The figures and tables clearly show that the cylinder pressure and displacement responses are both relatively good when *m1* is approximately 0.49. Furthermore, 0.49 is exactly the effective area ratio between the rod chamber and the rodless chamber of the bucket cylinder, n. Therefore, when *m1* equals *n*, both the cylinder pressure response and displacement response are relatively good.

Working Device Model

To model the machine ADAMS and perform a combined study and verification from Fig.5, the Model AMESim is established, constituting of the farm-oriented load tractor main pump, dual spool multi-control valves, executive mechanisms, and so on.

The rotary conditions of the load tractor are temporarily not studied. The slewing platform, chassis, and track are viewed as a whole. The operation can be obtained by Boolean operation. The model contains 15 components, as shown in Fig.4. Translational joint motion is added in the mobile assistant of the boom, arm, and bucket cylinder.

The excavation trace curve of the bucket prong is obtained. The maximum excavation height and depth are 9616 and 6739 mm respectively. Although these values are slightly different from the sample values of 9640 and 6785 mm, they are basically consistent, which demonstrates that the established model is correct

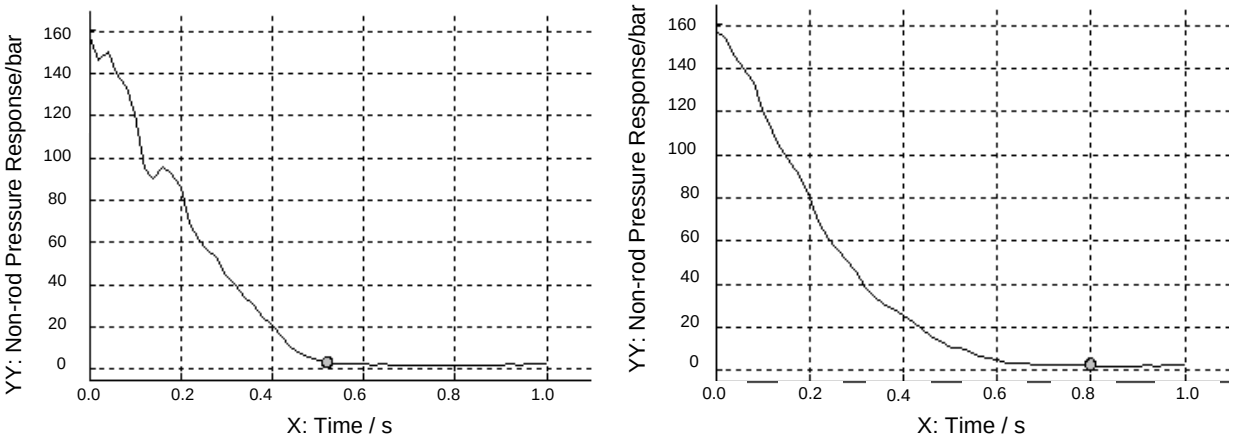

a) m_1=0.01 ***b)*** m_1=100

Fig.4 - Cylinder rodless chamber pressure response curve with different m_1

RESULTS

Distribution of heavy metal contents in vegetable field soils

The AMESIM model is established. The input speed of the engine is 2050 r/min, input power is 110 kW, and input torque is 512 N.M. Table 3 lists the main parameters of the hydraulic cylinder of load tractor.

Table 3

Main parameters of the farm-oriented load tractor

Hydraulic Cylinder		Diameter (mm)	Displacement (mm)
Boom	Piston	130	1332
	Rod Piston	90	
Bucket	Piston	120	1048
	Rod Piston	85	
Arm	Piston	135	1663
	Rod Piston	95	
Other	Whole (23,034 kg)	On-board platform	Gravity: 5705.48 kg, Density: 8278 kg/m^3
		Off platform	Gravity: 17,294.52 kg, Density:1548 kg/m^3

The co-simulation mode is adopted for the joint simulation module, which is shown in the table 3. Table 3 clearly shows that the ratio between the displacements of two valve cores is 2.02, which can be transformed into the spring setting of two main spools.

The spring coefficients of main valves 1 and 2 are set to k1=9.55 N/mm and k2=19.3 N/mm respectively. The flow area and displacement relation of the main spool and the pilot spool are shown in Figs. 6(a) and (b) respectively.

Figure 7 shows the cylinder pressure and displacement characteristic curve of the simulated working conditions of the load tractor bucket adduction action. To facilitate analysis, the pressure characteristic curve covers the 0th to 15th second, and the displacement covers the 15th to 25th second. When the fuel tank just extends out, the pressure of the rod chamber and rodless chamber dramatically increases. This increase is attributed to the opening amount of the valve, which is relatively small at first, and the impact

on the rod chamber. Therefore, the pressure of the rod chamber is significantly increased. With the constant inflow of pilot signals, the opening amount of the valve core reaches the maximum, and the pressure of two chambers decreases. However, Figure 7 clearly shows that within 15 seconds, the pressure of the rod chamber of the bucket cylinder is basically larger than that of the rodless chamber. This difference is related to the initial state of the load tractor set in the simulation. The gravity of buckets is always downward because the load tractor equipment is just lifted to a suitable height in the simulation setting. Based on the equation P1A1+f=P2A2, the area of rodless chamber A1 is larger than that of rod chamber A2. *f* represents the downward component of gravity. Therefore, the pressure of the rod chamber is large, and the displacement curve finally reaches 1048 mm. The whole process is consistent with the real working conditions of the farm-oriented load tractor prototype in agricultural production.

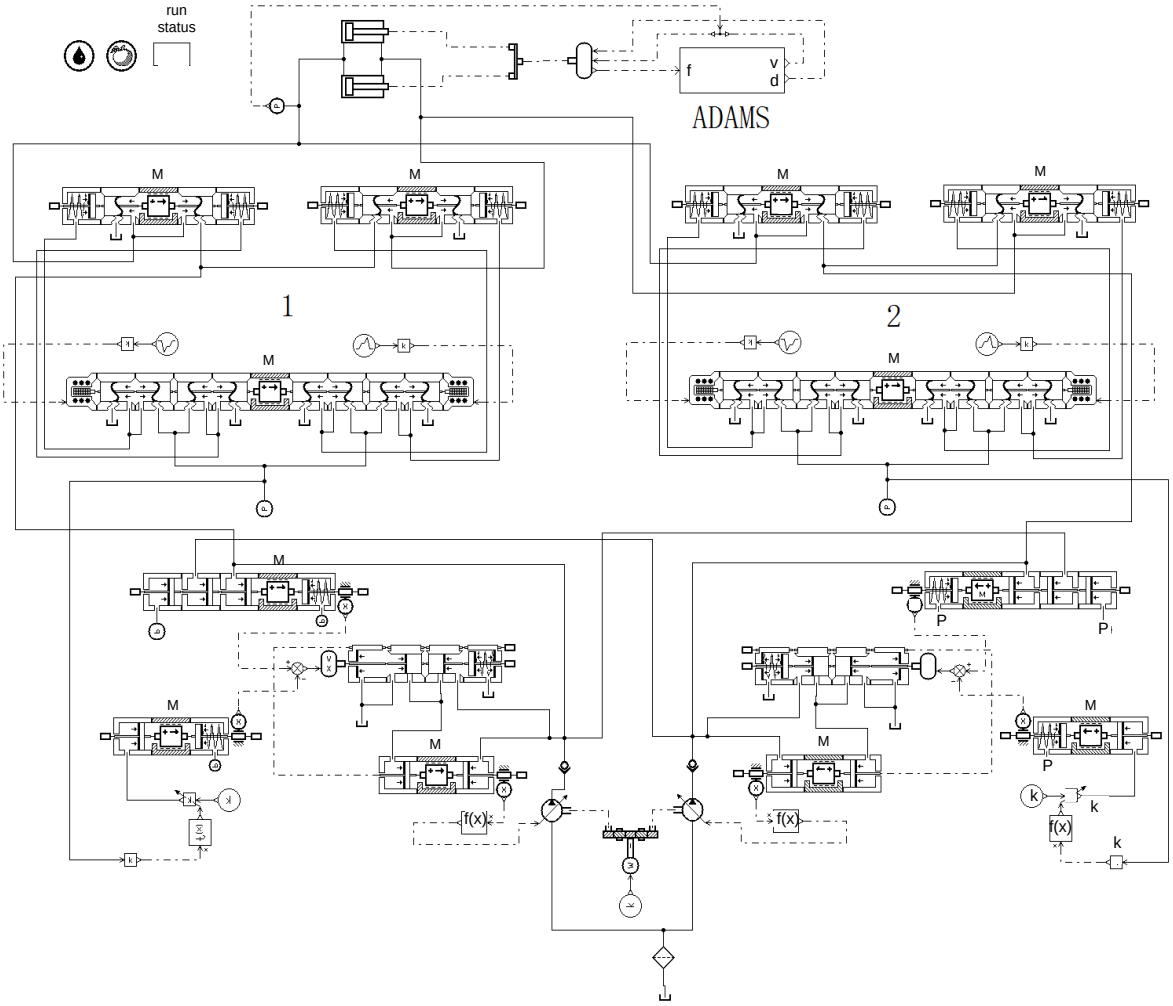

Fig.5 - Dual spool bucket joint AMESIM and ADAMS model simulation

In terms of the pressure of the cylinder rod chamber, and compared with the spool bucket circuit, the curve of dual spool valves varies faster than that of the single spool. At around the 13th second, the left and right cores become stable, faster than the single core. The average pressure of dual spool simulation is smaller than that of single core at 14 bar. In terms of cylinder rodless chamber pressure, the average curve of dual spool is smaller than that of the single core at 1.27 bar, with a maximum pressure difference of 4.1 bar. At around the 11th second, a small fluctuation occurs in the single core, whereas the dual spool remain smooth. At the 13th second, the dual spool reach a stable state, faster than the single core. In terms of displacement response, the dual spool are 2 seconds faster than the single core. In the aspect of energy consumption, both inlet oil pressure and return oil pressure are smaller than the single core. The following results can be obtained by using *P=pq* and *q=vA* to compute. The working power consumption of the load tractor stick with double-core multi-control valves within 15 seconds is 24.64 kW, while that for single-core multi-control valves is 30.61 kW. These values indicate that the single-core multi-control valve control system consumes more energy than the dual spool.

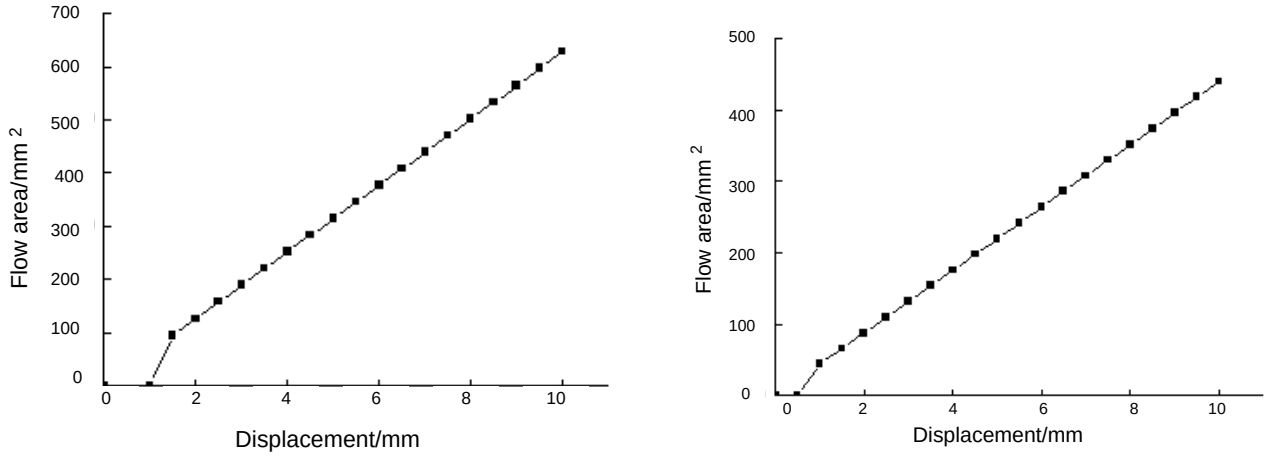

Fig.6 - Relation graph between flow area and spool displacement

a) main spool b) pilot spool

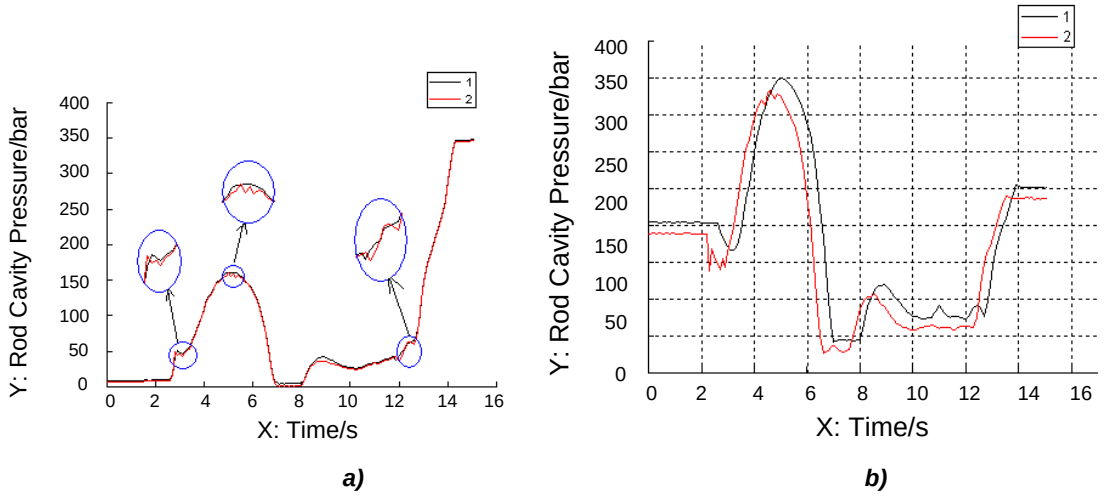

Fig.7 - Curve between pressure and time

a) Curve between rod cavity pressure and time b) Curve between chamber pressure and time

Experiments for this Farm-oriented Load tractor Prototypes with Dual-spool Multi-control Valve

A bucket circuit is used for verification. The load tractor handle is operated to perform bucket adduction and outward swing action. The bucket cylinder pressure and displacement curve are obtained, as shown in Figure 8.

A comparison of the first 9 seconds in Fig.8 with those in Fig.7 indicates that the general trend is that the pressure in simulation is smaller than that in experiments. The average of the rodless chamber is smaller than 2.3 bar, while the rod chamber is smaller than 20 bar. The displacement speed of the simulated cylinder is faster than that in experiments because the practical factors consistent with real situations are not considered in the simulation, such as leakage and resistance along the way. At the beginning, actions have not started and the engine is idling. The curves for simulation and experiments correspond to relatively small values and vary slow. At the moment of valve opening, the pressure of the two chambers will suddenly increase, which can be seen from the two pressure curves of the rodless chamber. This increase happens twice in the experiment curves because when the load tractor is operated, the handle will jitter, a factor that is not excluded in simulation. The two pressure curves of the rod chamber reveal that a sudden pressure change occurs. Moreover, overflow happens owing to the effect of impact, and the pressure reaches the maximum. With the increase in opening amount of the valve core, the pressure of the two chambers constantly decreases. Before the bucket extends to the maximum length, the pressure of the rodless chamber is also smaller than that of the rod chamber, which is the same as in the simulation. Clearly, the joint simulation of the established double-core system satisfies the requirements method.

Experimental Comparison of Dual-spool and Single-spool Multi-control Load tractors

The same operations on dual-spool and single-spool load tractors are performed, including boom lifting / lowering working conditions, arm adduction / outward swing working conditions, and bucket adduction / outward swing working conditions. The synchronization of the pilot handle is guaranteed. After handle operation, data are displayed in the PC software in real time. Fig. 9 shows the load tractor test site. The experimental data of the double-valve core and single-valve core load tractors are shown in Table 4.

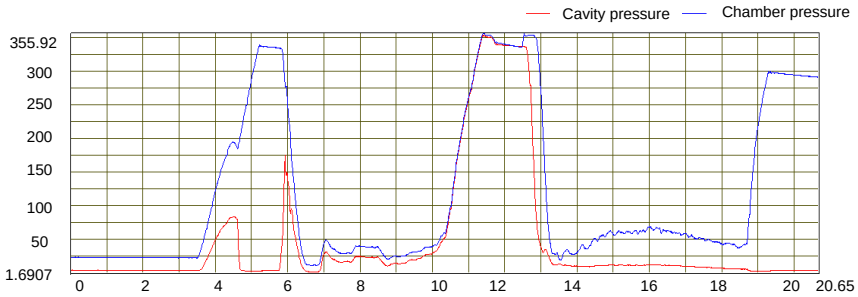

Fig.8 - Bucket cylinder pressure and displacement experiment curve

The data clearly show that the pressure of the double-core multi-control valve on the cylinder reaches the peak and stability faster than that of the single-core multi-control valve. The response of the double-core multi-control valve is faster. The pressure of the double-core multi-control valve on the cylinder is smaller, and the energy consumed within the same time interval is lower. The overshoot of the double-core multi-control valve is also lower than that of the single-core multi-control valve, which is another reason why the former reaches stable status faster. Moreover, due to the operation, overshoot fluctuates. As shown in the table, the pressure overshoot surpasses 100% in the cylinder rodless chamber of the bucket adduction working conditions and the rod chamber of the arm outward swing. This outcome indicates that the handle shakes in the two operations, thus causing shocks. Other working conditions are relatively smooth.

Fig.9 - Load tractor test site

Table 4

Farm-oriented load tractor experimental data of the dual-spool and single-spool valve (boom lift,varm adduction, bucket adduction)

Working conditions	Device		p_m /bar	p_w /bar	t_z /s	t_m /s	t_o /s	M_p /%
Boom lift	Chamber	Dual	118.758	117.2	50.22	1.01	7.9	2.6
		Singl	125.538	120.8	52.99	2.06	10.9	4.8
	Cavity	Dual	4.600	3.68	50.31	14.97	29.44	10.23
		Singl	6.632	5.45	53.41	17.85	32.86	11.98
Arm adduction	Chamber	Dual	124.58	80.081	10.50	5.74	7.92	54.9
		Singl	148.02	95.841	10.95	6.81	9.64	55.39
	Cavity	Dual	44.006	28.00	10.04	6.00	7.20	51.26
		Singl	46.546	31.83	10.91	6.57	8.73	55.4
Bucket adduction	Chamber	Dual	33	14.342	4.45	9.88	3.98	116.5
		Singl	35.1	15.742	7.74	1.37	5.31	123.7
	Cavity	Dual	48.795	28.2	4.05	1.06	1.49	66.9
		Singl	69.315	41.6	7.85	1.35	3.68	68.4

Note: The engine speed is 2050 r/min, p_m is the maximum pressure of the device in a corresponding working condition, p_w is the stable pressure of the device in a corresponding working condition, t_z is the time needed to complete the working condition, t_m is the time needed to reach the peak value of pressure, t_0 is the time needed to reach the stable pressure, and M_p is the overshoot. Rodless chamber refers to the rodless chamber of the cylinder, and rod chamber refers to the rod chamber of the cylinder.

CONCLUSIONS

The SY235 farm-oriented load tractor and a dual-spool multi-way valve-based prototype were applied for support. The electronic control improvements of the load tractor were completed. Oil capacity, power consumption, and displacement response capability of the dual-spool system were obtained. In addition, the performance of a single-spool system was comparative analyzed. The conclusions are shown as follows::

- Theories of double-core multi-control valves are analyzed. The conclusion drawn is that when the ratio between the displacements of the two valve cores in a double-core multi-control valve equals the ratio between the effective areas of hydraulic cylinder chambers, the pressure and displacement responses of the cylinder are relatively good.
- The experiments of bucket adduction and outward swing are carried out for a double-core load tractor prototype. The curves of experiment and simulation are compared and analyzed to verify that the joint simulation model of the double-core system is correct.
- The same single actions of boom, arm, and bucket are tested for two load tractors. The double-core control system is fast in pressure response and has more fluctuations at the beginning of actions, which is not very stable. The dual-spool control system reaches stable status first. The average pressure of the double-core multi-control cylinder is lower than that of the single-core system, which has low energy consumption. The double-core control system is faster than the single-core control system in displacement response. The overall performance of the double-core multi-control valves is better than the single ones. The SY235C-8S prototype can provide the test platform for further improvement of dual-spool multi-control valves.

Through the simulation research and prototype experiment, the power consumption of the dual-spool valve is found to be smaller and more energy saving in a farm-oriented load tractor. The study also found that the system has a certain internal leakage, which is the direction of further research for early rollover warning design in agricultural production.

ACKNOWLEDGEMENT

This work was supported in part by The National Natural Science Fund of China, Jiangsu Natural Science Foundation, University of Jiangsu Natural Science Foundation, and SANY Co., Ltd. in Jiangsu. Lecturer, Support Fund Nos. 51505211, 51505212, 51405222, 11302097, and BK20130741.

REFERENCES

[1] Casoli P., Anthony A., (2013), Gray box modeling of an excavator's variable displacement hydraulic pump for fast simulation of excavation cycles, *Control Engineering Practice*, Pergamon Press, Vol.21, Issue 5, pp.483-494, New York/U.S.A;

[2] Yi Yuan, Yu Tu, (2013), The Load Sensing Principle of Proportion Multi-channel Valve and its Application in Excavator, *2013-Third International Conference on Intelligent System Design & Engineering Applications*, Vol.1, pp.1469-1472, Brown University Psychopharmacology Update/Hong Kong;

[3] Choi Kyujeong, Seo Jaho, Nam Yongyun, Kim Kyeong Uk, (2015), Energy-saving in excavators with application of independent metering valve, *Journal of Mechanical Science and Technology,* Vol.29, Issue 1, pp.387-395 Korean Society of Mechanical Engineers, Seoul / Korean;

[4] Kumar A., Fitzsimons B., Trombetta C., (2013), Atrioventricular Groove Hematoma During Mitral Valve/Tricuspid Valve Repair: Transesophageal Echocardiography Characteristics, *Anesthesia and analgesia*, Vol.115, Issue 5, pp.986-988 International Anesthesia Research Society, New York / U.S.A;

[5] Xiong Y, Wei J.H, Feng R.L., (2015), Adaptive robust control of a high-response dual proportional solenoid valve with flow force compensation, *Proceedings of the institution of mechanical engineers part I-Journal of systems and control engineering*, Vol. 229, Issue.1, pp.3-26, University of Bath/UK;

[6] Barreto C., Schiozer D.J. (2015), Optimal placement design of inflow control valve using a dynamic optimization process based on technical and economic indicators, *Journal of petroleum science and engineering*, Vol.125, Issue.1, pp.117-127, Elsevier Science BV, Amsterdam/Netherlands;

[7] Lisowski E., Czyzycki W., Rajda J., (2014), Multifunctional four-port directional control valve constructed from logic valves, *Energy conversion and management*, Vol.87, Issue 10, pp.905-913, Pergamon Elsevier Science LTD , Oxford/England;

[8] Ye Y, Yin C.B., Li X.D., Zhou W.J., Yuan F.F., (2014), Effects of groove shape of notch on the flow characteristics of spool valve, *Energy conversion and management*, Vol.86, Issue 10, pp.1091-1101, Pergamon Elsevier Science LTD , Oxford/England;

[9] Kumar A., Fitzsimons B., Trombetta C., (2013), Atrioventricular Groove Hematoma During Mitral Valve/Tricuspid Valve Repair: Transesophageal Echocardiography Characteristics, *Anesthesia and analgesia*, Vol.116, Issue 5, pp.986-988, Cleveland, International Anesthesia Research Society, New York/U.S.A;

[10] Claudio Alimonti, Gioia Falcone, Oladele Bello, (2010), Two-phase flow characteristics in multiple orifice valves, *Experimental Thermal and Fluid Science*, Vol.34, Issue.8, pp.1324-1333, Elsevier Science INC, York/U.S.A;

[11] Feng C; Kamat V.R., (2013), Plane registration leveraged by global constraints for context-aware AEC applications, *Computer-Aided Civil and Infrastructure Engineering*, Vol.28, Issue.5, pp.325–343 Blackwell Publishers, Inc, Malden/U.S.A;

[12] Matti Linjama, Matti Vilenius, (2005), Improved digital hydraulic tracking control of water hydraulic cylinder drive, *International Journal of Fluid Power*, Vol.6, Issue 1, pp.29-39, TuTech Innovation, West Lafayette/U.S.A;

[13] Mattila J, Virvalo T., (2000), Energy-efficient motion control of a hydraulic manipulator, *Proceedings 2000 ICRA, IEEE International Conference on Robotics and Automation*, Piscataway, Vol.24-28, pp.3000-3006, NJ/USA;

[14] Atik FA., Pettersson G.B., Sigurdsson G., Gonzalez-Stawinski G.V., Sabik E.M., Kim A., Svensson, L.G., (2005), The ultimate development of mitral valve endocarditis: Atrioventricular separation, atrioventricular groove abscess and hemorrhagic pericarditis, *Journal of heart valve disease*, Vol.14, Issue 1, pp.29-32, Icr Publishers, Pinner/England;

[24] Falck Tillmann., Dreesen Philippe., De Brabanter Kris, (2012), Least-Squares Support Vector Machines for the identification of Wiener-Hammerstein systems. *Control Engineering Practice*, Vol.20, Issue 11, pp.1165-1174, New York/U.S.A, Pergamon Press.

STRUCTURAL INTENSITY METHOD APPLIED TO STUDY OF VIBRATIONS DAMPING
/
METODA INTENSIMETRIEI STUCTURALE APLICATĂ LA STUDIUL AMORTIZĂRII VIBRAȚIILOR

Assoc. Prof. Ph.D. Eng. Carp-Ciocârdia D.C.*[)], Prof. Ph.D. Fiz. Magheți I.
University POLITEHNICA of Bucharest, Faculty of Biotechnical Systems Engineering, Department of Mechanics / Romania
Tel: 0722461797; E-mail: craita.carp@upb.ro

Keywords: *structural intensity, energy flow, inter spectral density*

ABSTRACT

Article describes a practical method for determining the vibration damping of the material based on the use of structural intensity measurements of longitudinal vibrations. Structural intensity is grounded on the analogy with the concept of acoustic intensimetry that uses the correlation between the signals obtained from two accelerometers. The structural intensity method can be applied, by computation or by measurement, for identification of the vibration propagation trace and for vibration control. In this paper, after developing the theory on calculation of longitudinal vibration power flow, one proposes an experimental method for determining the attenuation of longitudinal vibrations of materials according to their nature, size and method of fixing the structure that takes the vibrations transmitted by means of a vibration absorber.

REZUMAT

Articolul descrie o metodă practică de detarminare amortizării vibrațiilor unor materiale pe baza măsurătorilor de intensimetrie structurală a vibrațiilor longitudinale. Intensimetria structurală se bazează pe analogia cu conceptul de intensimetrie acustică, care utilizează corelația dintre semnalele care provin de la două accelerometre. Metoda intensimetriei structurale se poate aplica, prin calcul sau prin măsurători, pentru identificarea căilor de propagare a vibrațiilor şi pentru controlul vibrațiilor. În această lucrare, după dezvoltarea teoriei privind calculul fluxului de putere al vibrațiilor longitudinale, se propune o metodă experimentală pentru determinarea atenuării vibrațiilor longitudinale a materialelor în funcție de natura lor, dimensiuni şi modul de fixare al structurii care preia vibrațiile transmise, prin intermediul unui absorbitor de vibrații.

INTRODUCTION

Acoustic intensimetry bases have grown substantially as theoretical fundamentals as well as applications *(Fahy, 1989)*. In recent years, a more attention was directed to develop the method of structural intensimetry with practical applications *(Noiseux, 1970; Orăşanu et al, 2013)*. Measurements of vibration energy flow can give information about identification of the positions of vibration sources, energy transmitted from source in different ways and different types of vibrations waves *(Verheij, 1990)*.

Unlike numerical methods, which are based on theoretical models that allow it to approximate the energy of the transmitted vibration, such as the method of discretization developed in references *(Craifaleanu and Dragomirescu, 2015; Orăşanu and Dragomirescu, 2015)*, the proposed method consists in the processing of the signals obtained from direct measuring.

MATERIAL AND METHOD

1. Structural intensity

For the study of power transmission characteristics of structural vibrations it is not enough to make simple measurements of vibration levels, but it is necessary to determine the distribution of energy flow through structural intensity measurements. This flow represents the instantaneous rate of energy transfer per unit area in a given direction and is called the structural intensity. For this purpose it shall determine inter spectral acceleration density in two closely related sections, similar to the technique of the two microphones in acoustic intensimetry technique.

In recent years, one has made great progress in measuring sound power. In the field of vibrations, practical measurements rise many and difficult problems.

Structural intensity of vibrations, $\bar{I}$, in a given direction, is obtained by the time-average of the product of force *F* and the vibration speed vector, $\bar{v}(r,t)$:

$$\left\langle \bar{I} \right\rangle_t = \frac{1}{T}\int_0^T F(r,t)\cdot\bar{v}(r,t)dt \quad \text{or in complex form:} \quad \left\langle \bar{I} \right\rangle_t = \frac{1}{2}\mathrm{Re}\left[\hat{F}\cdot\hat{\bar{v}}^*\right] \tag{1}$$

The complex shape from (1) is used when the force and the particle velocities are treated as complex harmonic variables. The direction of intensity is the same with the direction of the particle resultant velocity. The expression of intensity depends on the type of vibration of a structure, namely: longitudinal, bending and torsional. In the following, we will establish a theoretical expression for the longitudinal vibrations of the beams.

2. Longitudinal vibrations of the beams

One studies the vibrations of the homogeneous beam, with a constant cross section that is acted by a longitudinal force. For an element of length *dx* (fig.1), we can write Newton'law

$$m\frac{\partial^2 u}{\partial^2} = F + \frac{\partial F}{\partial x}dx - F \tag{2}$$

Where:

u(x,t) is the displacement of particles in section located at distance *x* and *F* is the normal force on the same section which it is assumed that varies linearly with the distance.

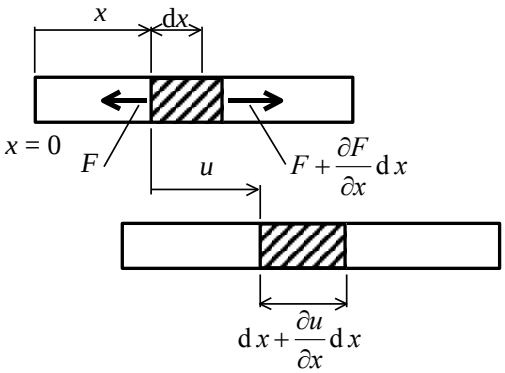

Fig.1 - Toolbar element during longitudinal vibration

Relative elongation, by definition, the ratio between the elongation Δ*l* and the original length *l*, it is written:

$$\varepsilon = \frac{\Delta l}{l_0} = \frac{dx + \frac{\partial u}{\partial x}dx - dx}{dx} = \frac{\partial u}{\partial x} \tag{3}$$

so that Hooke's law becomes:

$$\frac{F}{A} = E\frac{\partial u}{\partial x} \tag{4}$$

Where:

A is the area of the bar's section and *E* is the Young's modulus.

Using the last three relationships one can obtain:

$$\rho A dx\frac{\partial^2 u}{\partial t^2} = EA\frac{\partial^2 u}{\partial x^2}dx \ , \tag{5}$$

Where:

ρ is the density of the bar material.

The final relationship

$$\frac{\partial^2 u}{\partial t^2} = \frac{E}{\rho}\frac{\partial^2 u}{\partial x^2} \tag{6}$$

represents the equation of longitudinal vibrations of the beam. The report $\sqrt{E/\rho}$ is noted with c_L and has the dimensions of velocity. It is the speed of propagation of longitudinal vibrations and according to this, the transcribed form of equation (6) is:

$$\frac{\partial^2 u}{\partial t^2} = c_L^2 \frac{\partial^2 u}{\partial x^2} \ . \tag{7}$$

Structural intensity, for longitudinal vibrations in a beam, can be written successively

$$I_L = \langle F.v \rangle = \frac{EA}{c_L^2}\left\langle \frac{\partial^2 u}{\partial t^2} dx \int \frac{\partial u}{\partial t} dt \right\rangle = \frac{EA}{c_L^2}\Delta\left\langle (\frac{a_1 + a_2}{2}) \int (a_2 - a_1) dt \right\rangle \tag{8}$$

Where:

a_1 and a_2 are the accelerations at two nearby points 1 and 2, located at a distance Δ between accelerometers.

The relations (8) were obtained using the finite approximations *(Pavic, 1992)*:

$$a \cong \frac{1}{2}(a_1 + a_2) \text{ and } \int a dt \cong \int (a_2 - a_1) dt$$

$$F = \frac{EA}{\Delta r}(u_1 - u_2) \tag{9}$$

$$v = \frac{du}{dt} \cong \frac{v_1 + v_2}{2} = \frac{1}{2}\int (a_1 + a_2) dt$$

For harmonic wave, with angular velocity ω, the normal force is

$$F = \frac{EA}{i\omega\Delta}(a_1 - a_2) \tag{10}$$

and the vibration velocity of a particle will be written

$$v = \frac{a_1 + a_2}{2i\omega} \ . \tag{11}$$

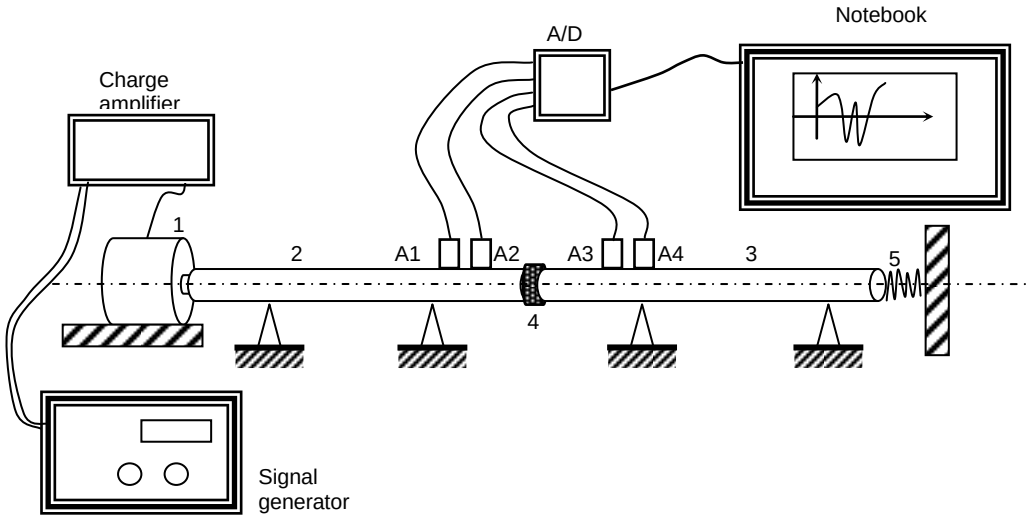

a)

Fig.2 - The block diagrams of the damped measurement

1 - Shaker; 2,3 - Beam ; 4 - Sample; 5 - Spring; A1-A4 - Accelerometers; A/D

Structural intensity can also be measured using cross-correlation method between the two acceleration signals. Here the vibration intensity vector component, in the direction of the two accelerometer will be

$$I_L(\omega) = -\frac{EA}{\omega^3 \Delta} \mathrm{Im}[G(a_1, a_2)], \quad (12)$$

where $\mathrm{Im}[G(a_1, a_2)]$ is the imaginary part of cross-spectrum between the two accelerometers signals.

For bending waves in a rod, the energy flow may be written as

$$I_B(\omega) = \frac{2\sqrt{Bm}}{\omega^2 \Delta} \mathrm{Im}[G(a_1, a_2)] 2\pi / \lambda, \quad (13)$$

where:

B is bending stiffness, *λ* is the wave length and *m* is mass per unit length *(Craifaleanu et al., 2014; Orăşanu and Craifaleanu, 2011; Zhao, 1988)*.

RESULTS

In the first experiment there were used two horizontal bars with an outer diameter of 20 mm. Between the two bars a sample of cork with the role of damping longitudinal vibration transmitted from the first to the second bar has been fixed. The connection between the second bar and the outside has been carried out by means of a spring (fig.2,a).

The second experiment was carried out by means of two vertical cylindrical bar with an outer diameter of 100 mm. Between the two bars was fixed too a sample of cork with the purpose of vibration damping, the second rod being rigidly fixed to the foundation (fig.2,b).

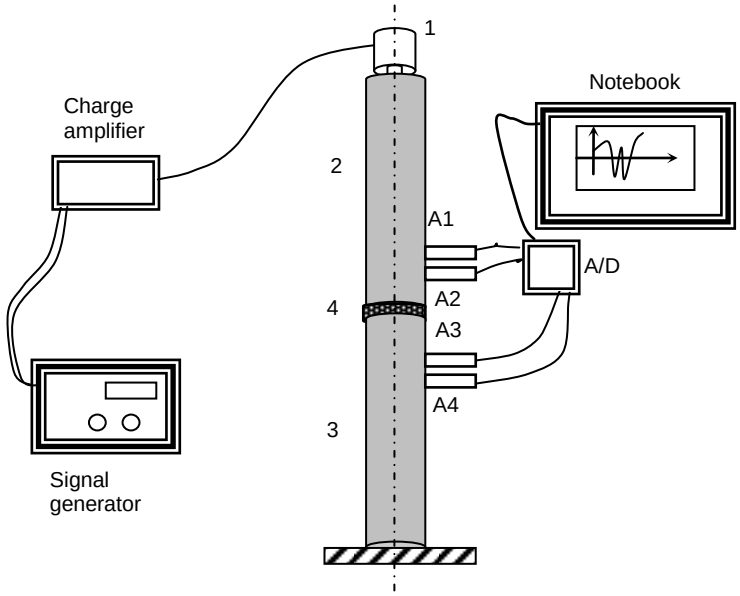

b)

Fig. 2 - The block diagrams of the damped measurement
1-Shaker; 2,3-Beam ; 4-Sample; 5-Spring; A1-A4 - Accelerometers; A/D

In both cases, the used accelerometers A1-A2 and A3-A4, of delta-share type (B&K 4507), having the phase difference of not more than 4°, were mounted so that their axes coincide with the axes of the bars and the mini shaker. The experiments were carried out also, for other types of material (rubber, felt) of different thickness (0.5 cm, 1 cm and 2 cm).

The signal generated by the mini shaker is a white noise signal. Vibration energy flow (vibration intensity) expressed by relation (12) as the cross-spectra density of two accelerometer signals is shown in fig.3 and fig.4, in the frequency range of 1-1000Hz, for a 1cm sample of cork.

Significant differences occur in the resonance frequencies of the bar that takes over the damped vibrations.

CONCLUSIONS

The measurements made on the flow of vibration energy can provide qualitative and quantitative information on vibration damping of longitudinal direction by a vibration damper. Differences between the two experimental devices (fig.3 and fig.4) are not significant where there are no resonance frequencies of the bar behind the damper. It might occur increases of vibration power at the resonance frequencies of the structure behind the damper.

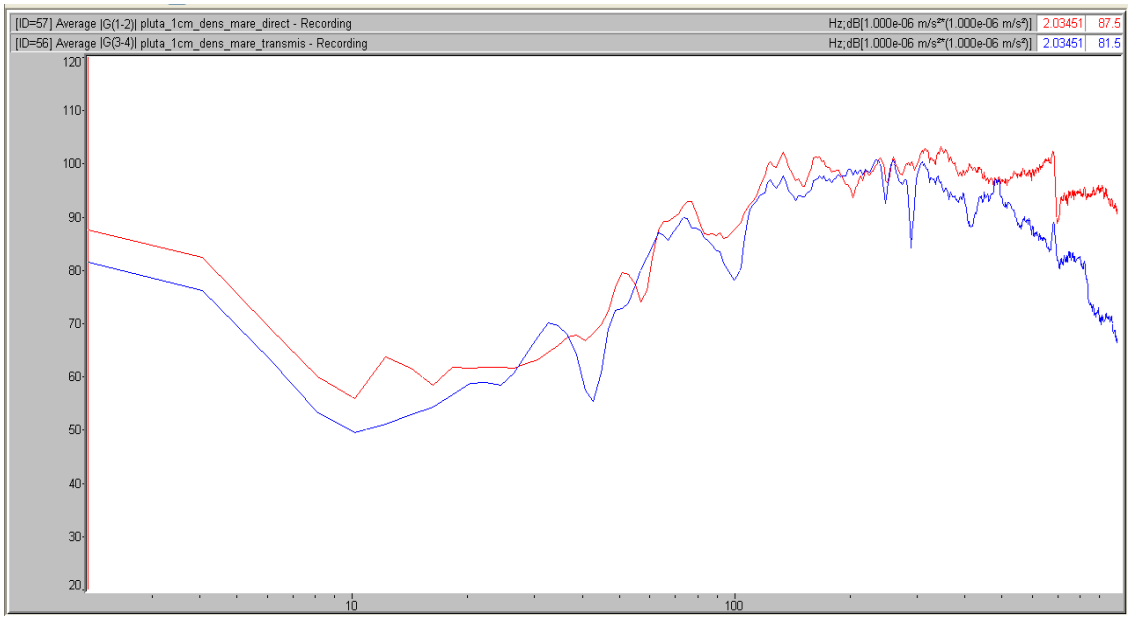

Fig.3 - Power flow vibration spectrum corresponding to the experiment from fig.2a, for sample of cork of 1 cm

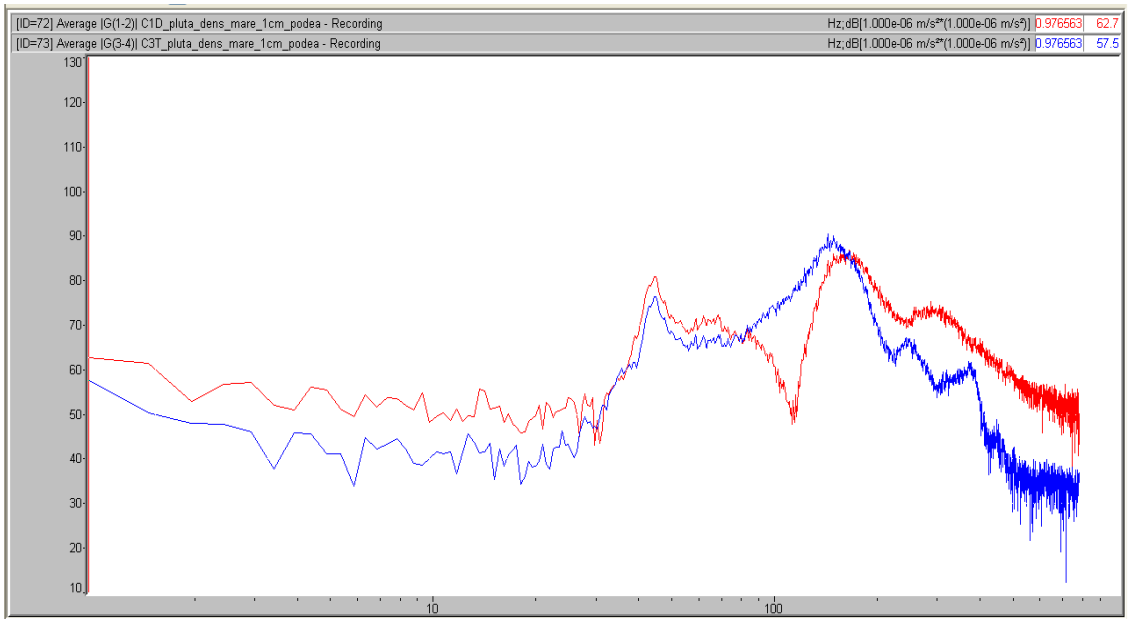

Fig.4 - Power flow vibration spectrum corresponding to the experiment from fig.2b, for sample of cork of 1 cm

Measurements of structural intensity depend on:

- errors of tools by the phase difference between the measured accelerations and corresponding electrical signals;
- the transducer mass must be much smaller than the structural apparent mass;
- the spacing between the accelerometers produces errors proportional with ($\frac{2\pi}{\lambda} \cdot \Delta$), where λ is the wave length.

For the study of bending vibration damping, the excitation and measurement direction of accelerations are chosen perpendicularly to bars.

For torsional vibrations, things are more complicated, both from the point of view of the excitation and of the transducer, which is specific for measurement of torsional vibrations.

REFERENCES

[1] Craifaleanu A., Orăşanu N., Dragomirescu C., (2014), Bending vibrations of a viscoelastic Euler-Bernoulli beam–two methods and comparison (Vibrațiile la îndoirea unei bare vâscoelastice Euler-Bernoulli-două metode de comparare), *The VI*th *International Conference on Robotics*, *ROBOTICS 2014*, *Applied Mechanics and Materials (Conferința internațională de Robotica, ROBOTICA 2014, Mecanici Aplicate şi Materiale)*, Vol.762, pp.47-54 ISSN 1660-9336;

[2] Craifaleanu A., Dragomirescu C., (2015), Numerical and experimental vibration analysis of the suspension system of an agricultural machine (Analiza numerică şi experimentală a vibrațiilor unui sistem de suspensie la o maşină agricolă), *INMATEH - Agricultural Engineering Journal*, Vol.47, No.3, pp.127-134, ISSN 2068-2239, Bucharest/Romania;

[3] Fahy F.J., (1989), Sound intensity, *Elsevier Applied Science*, London, New York;

[4] Noiseux D.U., (1970), Measurements of Power Flow in Uniform beams and plates, *The Journal of the Acoustical Society of America*, vol.47, pp.238-247;

[5] Orăşanu N., Craifaleanu A., (2011), Theoretical and experimental analysis of the vibrations of an elastic beam with four concentrated masses (Analiza teoretică şi experimentală a vibrațiilor unei bare elastic cu patru mase concentrate)*, Proceedings of the Annual Symposium of the Institute of Solid Mechanics*, SISOM 2011, pp.471-480, ISSN 1843-5459, Editors: Tudor Sireteanu & Vlad Gr. Laşcu, Bucharest/Romania;

[6] Orăşanu N., Craifaleanu A., Magheți I., (2013), Measurement of acoustical reflection waves by the correlation technique, *Proceedings of the Annual Symposium of the Institute of Solid Mechanics*, SISOM 2013, pp.262-267, ISSN 1843-5459, Editors: Tudor Sireteanu & Vlad Gr. Laşcu, Bucharest/Romania;

[7] Orăşanu N., Dragomirescu C., (2015), Study of the vibrations of a plow blade (Studiul vibrațiilor unei lame de plug) , *INMATEH Agricultural Engineering Journal*, Vol.47, No.3, pp.121-136, ISSN 2068-2239, Bucharest/Romania;

[8] Pavic G., (1992), Vibroacustical energy flow through straight pipes, *The Journal of Sound Vibrations*, vol.154, pp.411-429, ISSN 0022-460X, Bucharest/Romania;

[9] Verheij W.J., (1990), Measurements of structure-borne wave intensity on lightly damped pipes, *Noise Control Engineering Journal*, vol.35, no.2, Sept-Oct, pp.69-72, ISSN 0736-2501;

[10] Zhao Qichang, (1988), Measurement of power flow in vibrational structure*, Chinese Journal of Acoustics*, Vol.7, No 3, pp.201-213, ISSN 0217-9776.

DYNAMICS OF FLEXIBLE ELEMENTS OF DRIVE SYSTEMS WITH VARIABLE CONTACT POINT TO THE PULLEYS

/

ДИНАМІКА ГУЧКИХ ЕЛЕМЕНТІВ ПРИВІДНИХ СИСТЕМ ІЗ ЗМІННОЮ ТОЧКОЮ ДОТИКУ ДО ШКІВІВ

Lect. Ph.D. Eng. Sokil M.B.[1)], Prof. Ph.D. Eng. Lyashuk O.L.[2)], Eng. Dovbush A.P.[3)]
[1)]National University Lviv Polytechnic / Ukraine; [2)]Ternopil Ivan Pul'uj National Technical University / Ukraine;
[3)]National Scientific Center "Institute for Agricultureral Engineering and Electrification " / Ukraine
E-mail: Oleg-lashyk@rambler.ru

Keywords: *wave theory, dynamics, flexible elements, pulley, transportation*

ABSTRACT

The developed technique makes possible to investigate the impact on oscillations of flexible elements of drive systems and transportation of nonlinear forces, the speed of longitudinal movement and perturbations of boundary conditions. Based on the obtained results it is proved that even for the linear analogue system the slowly time-dependent variable of the distance between the flexible elements (SE) contact points and the pulleys causes the change of the basic parameters of the waves. The limits of applying the wave theory of motion in the case of nonlinear oscillations of flexible elements of drive systems under slowly varying boundary conditions are expanded. The basic computations to analyze the main parameters of the dynamic process depending on motion speed of flexible element, tension force, and the ratio describing the motion principle of the contact point of flexible element and the pulley, are made.

РЕЗЮМЕ

Розроблена методика дає можливість дослідити вплив на коливання гнучких елементів систем приводу та транспортування нелінійних сил, швидкості поздовжнього руху та збурень крайових умов. Отримані результати показують, що навіть для лінійного аналогу системи повільнозмінна в часі величина віддалі між точками контакту ГЕ та шківів спричиняє зміну основних параметрів хвиль. Розширено межі застосування хвильової теорії руху на випадок нелінійних коливань гнучких елементів привідних систем із повільно змінними крайовими умовами. Отримано базові співвідношення для описання визначальних параметрів динамічного процесу у залежності від швидкості руху гнучкого елементу, сили натягу, співвідношення, яке описує закон руху токи контакту гнучкого елементу та шківа.

INTRODUCTION

The wave theory of motion in recent decades has become a new development to describe the various processes and phenomena *(Goroshko O. O., 2012; Chen L. Q. et al, 2004; Chen L. Q., 2005; Dodd Ret al, 1988; Kharchenko Y.V., Sokil M.B., 2006; Mytropolskyi Y.A., 1995; Mytropolskyi Y. O., Sokil B.I., 1998; Mytropolskyi Y.A., 1998; Mytropolskyi Y.A., Lymarchenko O.S., 1998; S. Ponomareva W.T., van Horssen, 2004; Sokil M.B., 2012).* As for its application in the theory of oscillations, the research concerning the dynamics of nonlinear continuum should be mentioned primarily (*Chen L. Q. et al, 2004; Chen L. Q., 2005*; *Kharchenko Y.V., Sokil M.B., 2006; S. Ponomareva. W.T., van Horssen, 2004; Sokil M.B., 2012)*. The nonlinear continuum, which is widely used in engineering, includes the flexible elements (SE) of drive systems and transportation. The peculiarity of their operation is that they are characterized by longitudinal component of motion speed. Based on the wave theory of motion adapted to the dynamics of such systems, it is possible to explain many interesting phenomena that are not inherent in their simplified equivalents, i.e. SEs that do not account the longitudinal component of the motion speed and actually existing nonlinear power factors *(Mytropolskyi Y.A., 1998; Mytropolskyi Y.A., Ymarchenko O.S., 1998; Mytropolskyi Y.A., Moseenkov B. I., 1976).* In particular, even the SE motion speed constantly causes the change of the main parameters of this element's oscillations. At the same time, in many of the cited studies there was an assumption that the SE length *(Goroshko O. O., 2012)* or the distance between the contact points (for one-dimensional models) or correspondently the SE line of contact to the head and driven pulleys or drums is invariable (*Chen, L. Q., 2004; Chen L. Q., 2005*; *Kharchenko Y.V., Sokil M.B., 2006; S. Ponomareva. W.T., van Horssen, 2004; Sokil M.B., 2012*). This assumption, with reasonable accuracy, is true when the axes of

the head and driven pulleys or drums are stationary. This allows using classical boundary conditions in the appropriate mathematical models of the dynamics of the process. At the same time, while operating various kinds of mechanisms and systems in which SE carries out the transfer motion, the assumption requires clarification. This primarily concerns the mechanisms whose axes of head and driven drums (or one of them) are movable, i.e. spring loaded (see. Fig.1 and Fig.1.b).

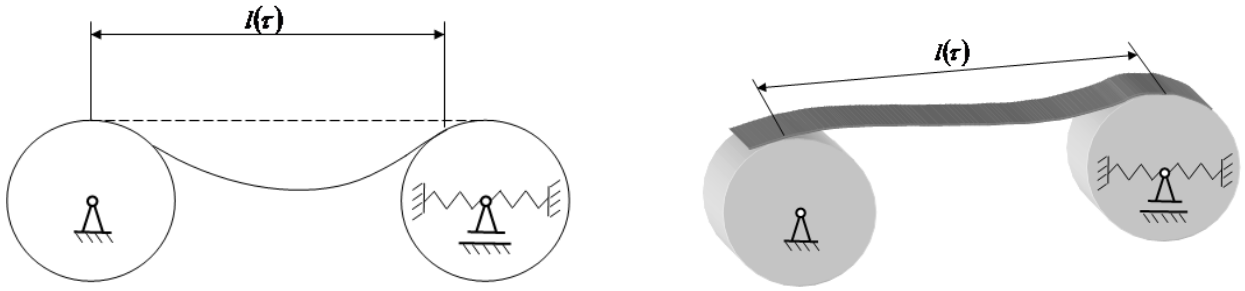

a) b)

Fig.1 - Driven gears with movable SE contact points to the pulley (a) or to the drum (b)

In this case, coordinates of the SE contact points and pulleys or drums and the distance between them are variable. The construction of mathematical models of the dynamics of SE and their solutions require refined formulation of the problem, a correct representation of boundary conditions and taking into account the variable tension force caused by the SE. The studies of this problem are carried out in such a context.

MATERIAL AND METHOD

It is known *(Chen L. Q., 2005, Sokil M.B., 2012)*, that the differential equation of SE oscillation of low bending stiffness, which is characterized by a constant component of speed V , can be represented as

$$u_{tt} + 2Vu_{xt} - \left((\alpha(\tau))^2 - V^2\right)u_{xx} = \varepsilon f\left(u, u_x, u_t, u_{xx}\right) \quad (1)$$

where:

ε - the small parameter;

$\alpha(\tau)$ - the slowly variable function, which is determined through a variable tension force $T(\tau)$ and the SE linear weight ρ : $(\alpha(\tau))^2 = T(\tau)/\rho$,);

$\varepsilon f\left(\tau, u, u_x, u_t, u_{xx}\right)$ - the known analytic function that describes the nonlinear forces, and the small parameter specifies the small value of the SEs in comparison with the linear constituent of restoring force.

In (1), the function $u(t, \tau, x)$ determines the deviation from the SE equilibrium position with Euler coordinate x *(S. Ponomareva. W.T., van Horssen, 2004)* at an arbitrary point of time t .

Here, for simplicity, we will consider the case for which the SE contact point and right pulley is a slowly varying function of time $l = l(\tau)$, $\tau = \varepsilon t$ - "slow" time. In this case, the boundary conditions for equation (1) take the form

$$u(t, \tau, x)_{|x=0} = u(t, \tau, x)_{|x=l(\tau)} = 0 \quad (2)$$

The task is to determine the influence of parameters $V, \alpha(\tau), l(\tau)$ and functions $\varepsilon f(\tau, u, u_x, u_t, u_{xx})$ on the dynamics of SE.

The solution of the formulated problem is associated with solving the boundary problem (1), (2). The maximum value of non-linear forces is small as compared to the maximum value of term $(\alpha(\tau))^2 u_{xx}$ (see Restrictions on nonlinear forces). Thus, for its development, the general ideas of perturbation methods can be used *(J. Cole., 1972)*. The SE can be most effectively used to describe the analytically undisturbed movement, i.e. to find solution of equation under the boundary conditions, which are analogous to (2).

$$u^0_{tt} + 2Vu^0_{xt} - \left((\alpha(\tau))^2 - V^2\right)u^0_{xx} = 0 \quad (3)$$

Even a relatively simplified mathematical model of the dynamic process of the researched object to build the solution does not allow the direct applying of the main backgrounds of classical Fourier and

d'Alembert methods for partial differential equations *(Mytropolskyi Y.A., Moseenkov B. I.,1976).* Despite the "non classicality" of boundary conditions (2), single-dynamic process of unperturbed problem with sufficient degree of accuracy can be interpreted as an imposition of different length of waves but the same frequencies. Thus, the solution of the boundary problem (3), (2) is assumed to have the form

$$u^0(t,\tau,x)=a\left(\cos\left(\kappa(\tau)x+\omega(\tau)t+\varphi_0\right)-\cos\left(\chi(\tau)x-\omega(\tau)t-\varphi_0\right)\right) \tag{4}$$

In the dependence (4) $\omega(\tau)$ - frequency, a - amplitude of direct and reflected waves, $\kappa(\tau),\chi(\tau)$ - their wave numbers, and φ_0 - initial phase of the waves. The formal difference of the given description of the dynamic process in SE with "no classical" boundary conditions in comparison with “classical” ones is the dependence of wave numbers $\kappa(\tau),\chi(\tau)$ and frequencies $\omega(\tau)$ on slow time τ. Through formal computations, which are similar to the case of classical boundary conditions *(Kharchenko Y.V., Sokil M.B., 2006; Sokil M.B., 2012)*, we get the value of specified parameters

$$\kappa(\tau)=\frac{k\pi}{\alpha(\tau)l(\tau)}(\alpha(\tau)+V),\ \chi(\tau)=\frac{k\pi}{\alpha(\tau)l(\tau)}(\alpha(\tau)-V),\ \omega(\tau)=\frac{k\pi}{\alpha(\tau)l(\tau)}((\alpha(\tau))^2-V^2), \tag{5}$$

where the constant $k=1,2,...$ points the wave mode.

Note 1. Based on the linear boundary problem describing the unperturbed motion, its multi-frequent solution can be recorded without much difficulty.

The nonlinear forces and boundary conditions simultaneous effect give the solution of specified approximated task of function $u(t,\tau,x)$, which can be represented in the form

$$u(t,x)=a\left[\cos\left(\kappa(\tau)x+\psi\right)-\cos\left(\chi(\tau)x-\psi\right)\right]+\varepsilon U_1(\tau,a,\psi,x) \tag{6}$$

where:

$\psi=\omega(\tau)t+\varphi$, $U_1(\tau,\psi,x)$ - unknown analytic periodic ψ function satisfying boundary conditions arising from (2), i.e.,

$$U_1(\tau,a,\psi,x)_{|x=0}=U_1(\tau,a,\psi,x)_{|x=l(\tau)}=0 \tag{7}$$

In addition, the nonlinear forces cause the change of the dynamic process’s amplitude and frequency. Laws of changing the given parameters, as in *(Mytropolskyi Y.A., Moseenkov B. I.,1976)*, will be set by differential equations

$$a_t=\varepsilon A_1(\tau,a)...\ \varphi_t=\varepsilon B_1(\tau,a). \tag{8}$$

Right parts of last ratio, that is, functions $A_1(\tau,a)$, $B_1(\tau,a)$ and $U_1(\tau,a,\psi,x)$ are arranged in such a way that the solution in the form of presentation (6) with the proposed degree of accuracy will satisfy the original boundary problem (1), (2). The above mentioned provides a dependence binding the desired function, that is, $A_1(\tau,a)$, $B_1(\tau,a)$ and $U_1(\tau,a,\psi,x)$

$$\begin{aligned}\omega^2(\tau)\frac{\partial^2U_1}{\partial\psi^2}+2V\omega(\tau)\frac{\partial^2U_1}{\partial\psi\partial x}-((\alpha(\tau))^2-V^2)\frac{\partial^2U_1}{\partial x^2}=F_1(\tau,a,x,\psi)-a\frac{d\omega(\tau)}{d\tau}\left(\sin\left(\kappa(\tau)x+\psi\right)+\sin\left(\chi(\tau)x-\psi\right)\right)+\\ +2\left\{A_1(\tau,a)\left(\omega(\tau)+\kappa(\tau)V\right)\left(\sin\left(\kappa(\tau)x+\psi\right)+\left(\omega(\tau)-\chi(\tau)V\right)\sin\left(\chi(\tau)x-\psi\right)\right)+\right.\\ \left.+aB_1(\tau,a)\left(\left(\omega(\tau)+\kappa(\tau)V\right)\cos\left(\kappa x+\psi\right)-\left(\omega-\chi V\right)\cos\left(\chi(\tau)x-\psi\right)\right)\right\}\end{aligned} \tag{9}$$

where:

$F_1(\tau,a,x,\psi)$ corresponds to the function $f(\tau,u,u_t,u_x,u_{xx})$ provided that function $u(t,\tau,x)$ and its derivatives accept only the main meanings in the equations arising from (6).

After uncomplicated transformations right parts of the differential ratio (6) take the form

$$\begin{aligned}&A_1(\tau,a)\left(\omega(\tau)+\kappa(\tau)V\right)\left(\sin\left(\kappa(\tau)x+\psi\right)+\left(\omega(\tau)-\chi(\tau)V\right)\sin\left(\chi(\tau)x-\psi\right)\right)+\\ &+aB_1(\tau,a)\left(\left(\omega(\tau)+\kappa(\tau)V\right)\cos\left(\kappa x+\psi\right)-\left(\omega-\chi V\right)\cos\left(\chi(\tau)x-\psi\right)\right)=\\ &=\left(A_1(\tau,a)\cos\psi-aB_1(\tau,a)\sin\psi\right)\left[\left(\omega(\tau)+\kappa(\tau)V\right)\sin\kappa(\tau)x+\left(\omega(\tau)-\chi(\tau)V\right)\sin\chi(\tau)x\right]+\\ &+\left(A_1(\tau,a)\sin\psi+aB_1(\tau,a)\cos\psi\right)\left[\left(\omega(\tau)+\kappa(\tau)V\right)\cos(\kappa(\tau)x)-\left(\omega(\tau)-\chi(\tau)V\right)\cos(\chi(\tau)x)\right]\end{aligned} \tag{10}$$

$$a\frac{d\omega(\tau)}{d\tau}\left(\sin\left(\kappa(\tau)x+\psi\right)+\sin\left(\chi(\tau)x-\psi\right)\right)=a\frac{d\omega(\tau)}{d\tau}\left(\left(\sin\kappa(\tau)x+\sin\chi(\tau)x\right)\cos\psi+\right.$$
$$\left.+\left(\cos\kappa(\tau)x-\cos\chi(\tau)x\right)\sin\psi\right).$$

For unambiguous definition the unknown functions $A_1(\tau,a)$ and $B_1(\tau,a)$ of differential equation (9) should be imposed on the function $U_1(\tau,a,\psi,x)$. The additional condition is stipulated: it cannot be one of the additions of proportional $\sin\psi$ and $\cos\psi$. The physical meaning of specified statements is as follows: the amplitude of the wave process coincides with the amplitude of its first mode. The above statements will come true in the following case

$$\int_0^{2\pi}U_1(\tau,a,\psi,x)\begin{Bmatrix}\sin\psi\\ \cos\psi\end{Bmatrix}d\psi=0\,. \tag{11}$$

The partial derivatives of specified function have similar properties. This allows deriving a system of linear algebraic equations and functions $A_1(\tau,a)$ and $B_1(\tau,a)$ from the differential equation (9)

$$\rho(\tau,x)A_1(\tau,a)+aq(\tau,x)B_1(a)=\frac{a}{2}\frac{d\omega}{d\tau}r(\tau,x)-\frac{\varepsilon}{2\pi}\int_0^{2\pi}F_1(\tau,a,\psi,x)\cos\psi d\psi\,,$$
$$q(\tau,x)A_1(a)-a\rho(\tau,x)B_1(a)=\frac{a}{2}\frac{d\omega}{d\tau}p(\tau,x)-\frac{\varepsilon}{2\pi}\int_0^{2\pi}F_1(\tau,a,\psi,x)\sin\psi d\psi\,, \tag{12}$$

where

$$\rho(\tau,x)=\left(\omega(\tau)+\kappa(\tau)V\right)\sin\kappa(\tau)x+\left(\omega(\tau)-\chi(\tau)V\right)\sin\chi(\tau)x)),\ p(\tau,x)=\left(\cos\kappa(\tau)x-\cos\chi(\tau)x\right),$$
$$q(\tau,x)=\left(\omega(\tau)+\kappa(\tau)V\right)\cos\kappa(\tau)x-\left(\omega-\chi(\tau)V\right)\cos\chi(\tau)x\,,\ r(\tau,x)=\left(\sin\kappa(\tau)x+\sin\chi(\tau)x\right).$$

Note 2: We consider the case for which nonlinear system forces cause the change only in time of the basic parameters of the wave process ("short systems"). A more general case for which the determinative parameters of waves also depend on the linear variable (the case of "long" systems) can be another subject of research.

RESULTS

The conducted research allows to use the averaging out device *(Mytropolskyi Y.A., 1972)* using the variable x in relation to the system of differential equations (12). Due to obtained results, the functions describing the basic parameters of the wave process can be defined by the following formula:

$$A_1(\tau,a)=\frac{1}{2\pi l(\tau)\left[\left(\omega(\tau)+\kappa(\tau)V\right)^2+\left(\omega(\tau)-\chi(\tau)V\right)^2\right]}\int_0^{l(\tau)}\left\{\rho(\tau,x)\left[a\frac{\pi d\omega(\tau)}{d\tau}r(\tau,x)-\varepsilon\int_0^{2\pi}F_1(\tau,a,\psi,x)\cos\psi d\psi\right]\cos\psi d\psi-\right.$$
$$\left.-q(\tau,x)\left[a\frac{\pi d\omega(\tau)}{d\tau}p(\tau,x)-\varepsilon\int_0^{2\pi}F_1(\tau,a,\psi,x)\sin\psi\,d\psi\right\}\right]dx$$
$$B_1(\tau,a)=\frac{1}{2\pi al(\tau)\left[\left(\omega(\tau)+\kappa(\tau)V\right)^2+\left(\omega(\tau)-\chi(\tau)V\right)^2\right]}\int_0^{l(\tau)}\left\{\rho(\tau,x)\left[a\frac{\pi d\omega(\tau)}{d\tau}p(\tau,x)-\varepsilon\int_0^{2\pi}F_1(\tau,a,\psi,x)\sin\psi d\psi\right]\cos\psi d\psi-\right.$$
$$\left.-q(\tau,x)\left[a\frac{\pi d\omega(\tau)}{d\tau}r(\tau,x)-\varepsilon\int_0^{2\pi}F_1(\tau,a,\psi,x)\sin\psi\,d\psi\right\}\right]dx. \tag{13}$$

A special case of specified dependencies at $V=0, l(\tau)\equiv l_0, \alpha(\tau)\equiv\alpha_0$ (α_0, l_0 - steel) are the known in literature results *(Mytropolskyi Y.A., Moseenkov B. I., 1976)* concerning nonlinear oscillations of flexible one-dimensional media with fixed ends.

Thus, in the first approximation the dynamic process of SE with its slowly varying contact point of right end and the pulley is described by dependence (6) in which the parameters a and ψ are determined in accordance with ratio (8) and (13).

The first improved approximation describes the impact of nonlinear forces on the form of waves; so the function $U_1(\tau,a,\psi,x)$ should be defined. Taking into account the imposed conditions, it can be represented as:

$$U_1(\tau,a,\psi,x)=\sum_m\sum_{n,n\neq 1}U_{1mn}(\tau,a)X_m(\tau,x)exp(in\psi) \tag{14}$$

where the system of functions $\{X_m(\tau,x)\}$ must be complete and materialize the boundary conditions (2). The system of functions $\{X_m(\tau,x)\}=\left\{\sin\frac{m\pi}{l(\tau)}x\right\}$ satisfies such conditions. In this case, the unknown coefficients $U_{1mn}(\tau,a)$ are linked by the system of linear algebraic equations:

$$\left\{n^2\omega^2-((\alpha(\tau))^2-V^2)\left(\frac{s\pi}{l(\tau)}\right)^2\right\}U_{1sn}(\tau,a)-2V\omega(\tau)\sum_{m=1}^{j}\frac{2s}{s^2-m^2}ni\frac{m\pi}{l}U_{1mn}(\tau,a)=-F_{1sn}(\tau,a),\ m+s-\text{the odd} \tag{15}$$

where $F_{1sn}(\tau,a)=\frac{1}{2\pi l(\tau)}\int_0^{2\pi}\int_0^{l(\tau)}F_1(\tau,a,x,\psi)\exp(-in\psi)X_s(x)dxd\psi.,1\le s\le j.$

As a rule, the first modes of oscillation greatly influence the dynamic process. Therefore, a system of algebraic equations (15) is sufficiently limited by the first few terms of the expansion. In this case, to find its solution is not difficult. In particular, if we use only the first two terms of the expansion of a function $U_1(\tau,a,\psi,x)$ in a series of system functions $\{X_m(\tau,x)\}$, we obtain:

$$U_{11n}(\tau,a)=-\frac{1}{\Delta}\left\{\left[n^2\omega^2-(\alpha^2-V^2)\left(\frac{2\pi}{l}\right)^2\right]F_{11n}(\tau,a)-\frac{8\pi ni}{3l}V\omega F_{12n}(\tau,a)\right\}$$

$$U_{12n}(\tau,a)=-\frac{1}{\Delta}\left\{\left[n^2\omega^2-(\alpha^2-V^2)\left(\frac{\pi}{l}\right)^2\right]F_{12n}(\tau,a)+\frac{8\pi ni}{3l}V\omega F_{11n}(\tau,a)\right\} \tag{16}$$

where $\Delta=\left[n^2\omega^2-(\alpha^2-V^2)\left(\frac{\pi}{l}\right)^2\right]\left[n^2\omega^2-(\alpha^2-V^2)\left(\frac{2\pi}{l}\right)^2\right]-\frac{64}{9}n^2\omega^2V^2$

CONCLUSIONS

The developed technique makes it possible to investigate the impact on oscillations of flexible elements of drive systems and transportation of nonlinear forces, the speed of longitudinal movement and perturbations of boundary conditions. Based on the obtained results it is proved that even for the linear analogue system the slowly time-dependent variable of the distance between the SE contact points and the pulleys causes the change of the basic parameters of the waves. In addition, under certain conditions, it can contain sustained dynamic process when SE is converted to unstable process. Thus, with decreasing SE tension force (at a constant speed and constant SE contact points and pulleys) the amplitude of oscillations increases. The process becomes unstable in a speed value. Simultaneously, the results can be the basis for developing methods of influence of periodic disturbance on SE oscillations with slowly varying distance between its points of contact to the pulleys.

REFERENCES

[1] Goroshko O. O., (2012), Forced oscillations of flexible pipe system of fluid flow and zero initial tension force at excitation. (Вимушені коливання гнучкого трубопроводу з потоком рідини та нульовим початковим натягом при силовому збудженні), *Bulletin of Kiev University. Series: Phys. mat. Sciences*, № 3, pp.67-70, Kyiv;

[2] Chen L. Q., Zu J. W., Wu J., (2004), Transverse vibrations of an axially accelerating viscoelastic string with geometric nonlinearity', *Journal of Engineering Mathematics 48*, pp.171–182;

[3] Chen L. Q., (2005), Analysis and control of transverse vibrations of axially moving strings, *Applied Mechanics Reviews*, Volume 58.2, pp.91–116;

[4] Cole J., (1972), Perturbation methods in applied mathematics (Методы возмущений в прикладной математике), *World*, p.272,Moscow;

[5] Dodd R., Black J., Gibbon J., Morris H., (1988), Solutions and nonlinear wave equations (Солитоны и нелинейные волновые уравнения), *World*, pp.694, Moscow;

[6] Kharchenko Y.V., Sokil M.B., (2006), Forced oscillations of mobile media and asymptotic method in their study (Вимушені коливання рухомих середовищ і асимптотичний метод у їх дослідженні) *Collection of scientific works "Science Bulletin of NLTU of Ukraine*" Vol.16.1, pp.134-139, Lviv;
[7] Mytropolskyi Y.A., (1995), On the construction of the asymptotic solution of the perturbed Klein-Gordon equation (О построении асимптотического решения возмущенного уравнения Клейна-Гордона), *Ukrainian Mathematical Journal*, 47, №9, pp.1209-1216, Lyiv;
[8] Mytropolskyi Y. O., Sokil B.I., (1998), On the use of Ateb-use functions for constructing the asymptotic solution of perturbed nonlinear Klein-Hordon equation (Про застосування Ateb-функцій для побудови асимптотичного розв'язку збуреного нелінійного рівняння Клейна – Гордона), *Ukrainian Mathematical Journal*, 50, №5, pp.665-670, Kyiv;
[9] Mytropolskyi Y.A., (1998), On the construction of the asymptotic solution of the Bretherton perturbed equation.(О построении асимптотического решения возмущенного уравнения Брезертона), *Ukrainian Mathematical Journal,* 59, №1, pp.58-71, Kyiv;
[10] Mytropolskyi Y.A., Lymarchenko O.S., (1998), On the question of the asymptotic approximation for the slow wave processes in nonlinear dispersive media.(К вопросу об асимптотических приближениях для медленных волновых процессов в нелинейных диспергирующих середах), *Ukrainian Mathematical Journal,* 59, №3, pp.357–371, Kyiv;
[11] Mytropolskyi Y.A., Moseenkov B. I., (1976), Asymptotycheskye solutions to equations in derivatives. (Асимптотические решения уравнений в частных производных), *High school*, p.592, Kyiv;
[12] Mytropolskyi Y.A., (1972), The method of averaging in nonlinear mechanics (Метод усреднения в нелинейной механике), *Scientific thought*, p.440, Kyiv;
[13] S. Ponomareva. W.T., van Horssen, (2004), On applying the Laplace transform method to an equation describing an axially moving string, *Proceedings in Applied Mathematics and Mechanics (PAMM)*, № 4, pp.107–108;
[14] Sokil M.B., (2012), Bending vibrations of flexible drive elements and structure solution of mathematical models.(Згинні коливання гнучких елементів систем приводів і структура розв'язку їх математичних моделей), *Scientific Bulletin of NLTU of Ukraine,* Ed. 22.1, pp.144-147, Lviv.

WRITING NORMS

Article Types

Three types of manuscripts may be submitted:

1. **Regular articles:** These should describe new and carefully confirmed findings, and experimental procedures should be given in sufficient detail for others to verify the work. The length of a full paper should be the minimum required to describe and interpret the work clearly (max.10 pages, even number);
2. **Short Communications:** A Short Communication is suitable for recording the results of complete small investigations or giving details of new models or hypotheses, innovative methods, techniques or apparatus. The style of main sections has not necessarily to be in accordance with that of full-length papers (max. 6 pages, even number);
3. **Reviews:** Submissions of reviews and perspectives covering topics of current interest are welcome and encouraged (max.10 pages, even number).

Manuscripts should be written in English (American or British usage is accepted, but not a mixture of these) and submitted **electronically** at the following e-mail addresses: ***inmatehjournal@gmail.com***
Please be sure to include your full affiliation and e-mail address (see Sample manuscript)
The authors are responsible for the accuracy of the whole paper and references.
There are allowed 2 papers by each first author.
The text layout should be in single-column format. To avoid unnecessary errors it is strongly advised to use the "spell-check" and "grammar check" functions of your word processor.

Review Process

All manuscripts are reviewed by 2 members of the Scientifically Review Office. Decisions will be made as rapidly as possible and the journal strives to return reviewers' comments to authors in approx.3 weeks.
The editorial board will re-review manuscripts that are accepted pending revision.

NOTE:

Submission of a manuscript implies: that the work described has not been published before (excepting as an abstract or as part of a published lecture or thesis) that it is not under consideration for publication elsewhere.

1. REGULAR ARTICLES

- Manuscripts should be concise, in ***1.15 line spacing***, and should have 2 cm all over margins. The font should be ***Arial 10 pt.*** Ensure that each new paragraph is clearly indicated, using **TAB at 1 cm**.
- Title will be ***Arial 12 pt***. and explicit figures will be ***Arial 9 pt***.
- Text will be written in English.
- Chapters' titles are written by ***Arial 10 pt, Bold, Uppercase*** (e.g INTRODUCTION, MATERIAL AND METHODS), between chapters is left a space for 10 pt. At the beginning of each paragraph, leave a tab of 1 cm.
- The paper body will be written in ***Arial 10 pt., Justify alignment***.

TITLE ***Arial 12 pt., Uppercase, Bold, Center*** *(in English language)* and ***Bold Italic*** *(in native language).*
Should be a brief phrase describing the contents of the paper. Avoid long titles; a running title of no more than 100 characters is encouraged (without spaces).

AUTHORS ***ARIAL 9, Bold, Centre alignment***
Under the paper's title, after a space (enter) 9 pt., write ***authors' names*** and ***affiliations (Arial 8 pt.-Regular)***
When the paper has more than one author, their name will be followed by a mark (Arabic numeral) as superscript if their affiliation is different.
Corresponding author's name (next row), ***(Arial 8 pt.)***. Should be added also: phone, fax and e-mail information, for the paper corresponding author (***font: 8 pt., Italic***).

KEYWORDS ***(In English)*** about 4 to 7 words that will provide indexing references should be listed (title: ***Arial 10pt, bold italic,*** text ***Arial 10 pt., italic***).

A list of non-standard *Abbreviations* should be added. In general, non-standard abbreviations should be used only when the full term is very long and used often. Each abbreviation should be spelled out and introduced in parentheses the first time it is used in the text. Standard abbreviations (such as ATP and DNA) need not to be defined.

ABSTRACT ***(in English and Native language, Arial 10 pt.)***, the title *bold*; the text of abstract: *italic*) should be informative and completely self-explanatory, briefly present the topic, state the scope of the experiments, indicate significant data, and point out major findings and conclusions. The Abstract should be max.250 words. Complete sentences, active verbs, and the third person should be used, and the abstract should be written in the past tense. Standard nomenclature should be used and abbreviations should be avoided. No literature should be cited.

INTRODUCTION (***Arial 10 pt.***) should provide a clear statement of the problem, the relevant literature on the subject, and the proposed approach or solution. It should be understandable to colleagues from a broad range of scientific subjects. We should refer to the current stage of researches performed in the field of the paper to be published, by quoting up-to-date specialty studies, preferably published after 2006, excepting certain referential specialty books/studies, especially papers issued in magazines/journals/conferences/ISI quoted symposia or in other international data bases, which are well known and available.

MATERIALS AND METHODS (***Arial 10 pt.***) should be complete enough to allow experiments to be reproduced. However, only truly new procedures should be described in detail; previously published procedures should be cited, and important modifications of published procedures should be mentioned briefly. Methods in general use need not be described in detail.

RESULTS (***Arial 10 pt.***) should be clarity presented. The results should be written in the past tense when describing findings in the authors' experiments. Results should be explained, but largely, without referring to the literature. Discussion, speculation and detailed interpretation of data should not be included in the Results, but should be put into the Conclusions section.

CONCLUSIONS (***Arial 10 pt.***) The main conclusions drawn from results should be presented in a short Conclusions section. Do not include citations in this section.

Formulae, symbols and abbreviations: Formulae will be typeset in Italics (preferable with the Equation Editor of Microsoft Office 2003) and should be written or marked as such in the manuscript, unless they require a different styling. They should be referred to in the text as Equation (4) or e.g. (4). The formulae should be numbered on the right side, between brackets ***(Arial 10 pt.)***:

$$P = F \cdot v \tag{1}$$

Terms of the equation and the unit measure should be explained, e.g.

P is the power, [W];
F – force, [N];
v – speed, [m/s]

SI units must be used throughout.

Tables should be self-explanatory without reference to the text. The details of the methods used in the experiments should preferably be described in the legend instead of in the text. The same data should not be presented both in table and graph form or repeated in the text.
Table's title will be typed ***Arial 9 pt, Bold, Centered***
In the table, each row will be written Arial 9 pt, single-spaced throughout, including headings and footnotes.
The table should be numbered on the right side, between brackets ***(Arial 10 pt)***:

Figure (Arial 9 pt., Bold, Center) should be typed in numerical order (Arabic numerals). Graphics should be high resolution (e.g.JPEG). Figure number is followed by what represent the figure or graph e.g.:

Fig.1 – Test stand

Legend: ***Arial 8 pt, Italic, Center,*** e.g.

1 - plansifter compartments; 2- break rolls; 3 – semolina machines; 4 – reduction rolls; 5 – flour

ACKNOWLEDGMENTS (***Arial 10 pt.***) of people, grants, funds etc should be brief (*if necessarily*).

REFERENCES (***Arial 10 pt.***)

(In alphabetical order, in English and in the original publication language).
Minimum 10 references, last 10 years, minimum 3 references from the last 2 years

It can be used "*References*" tool from the *Word Editor*.
References should be cited in the text in brackets as in the following examples:
(Babiciu P., Scripnic V., 2000)
All references must be provided in English with a specification of original language in round brackets.
Authors are fully responsible for the accuracy of the references.

References should be alphabetically, with complete details, as follows:
Examples:
Books: Names and initials of authors, year (between brackets), title of the book (Italic), volume number, publisher, place, pages number or chapter, ISSN/ISBN:
[1] Vlăduț V., (2009), *Study of threshing process in axial flow apparatus (Studiul procesului de treier la aparatele cu flux axial),* vol.1, ISSN/ISBN ……, "Terra Nostra" Publishing House, Iaşi/Romania;
Journal Article: Names and initials of authors, year (between brackets), full title of the paper, full name of the journal (Italic), volume number, publisher, place, ISSN, page numbers:
[1] Lizhi Wu, Yan Di., (2005), Demonstrational study on the land consolidation and rehabilitation (LCR) project of saline-alkali soil in arid areas: a case study of Lubotan LCR project in Pucheng County, Shaanxi Province（干旱区盐碱化土地整理工程实证研究-以陕西蒲城县卤泊滩土地整理项目为例）, *Transactions of the Chinese Society of Agricultural Engineering*, vol.21, no.1, ISSN ……, pp.179-182, Madison/Wisconsin;

[2] Leonov I.P., (1973), Basic machine theory for tobacco stringing. Post-harvest care of tobacco and rustic tobacco (Основы теории машин для закрепления табака на шнуры. Послеуборочная обработка табака и махорки), *Collection of scientific articles (сборник научно-исследовательских работ)*, pp.37-45;

Conference or Symposium: Names and initials of authors, year (between brackets), full title of the paper (Regular), full name of the conference/symposium (Italic), volume number, publisher, place, ISSN, page numbers

[1] Bungescu S., Stahli W., Biriş S., Vlăduț V., Imbrea F., Petroman C., (2009), Cosmos program used for the strength calculus of the nozzles from the sprayers (Program Cosmos folosit pentru calculul de rezistență la zgomot al aparatelor de distribuție), *Proceedings of the 35 International Symposium on Agricultural Engineering "Actual Tasks on Agricultural Engineering",* pp.177-184, Opatija / Croatia;

Dissertation / Thesis: Names and initials of authors, year (between brackets), full name of the thesis (Italic), specification (PhD Thesis, MSc Thesis), institution, place;

[1] Popa L., (2004), *Research on the influence of structural and functional parameters of the braking system on the braking performance of agricultural trailers (Cercetări privind influența caracteristicilor constructive şi funcționale ale sistemelor de frânare asupra performanțelor de frânare ale remorcilor agricole)*, PhD dissertation, Transylvania University of Braşov, Braşov / Romania.

Patents: Names and initials of authors, year (between brackets), patent title (Italic), patent number, country:

[1] Grant P., (1989), *Device for Elementary Analyses*. Patent, No.123456, USA.

Legal regulations and laws, organizations: Abbreviated name, year (between brackets), full name of the referred text, document title/type (Italic), author, place:

[1] *** EC Directive, (2000), Directive 2000/76/EC of the European Parliament and of the Council of 4 December 2000, on the incineration of waste, Annex V, *Official Journal of the European Communities*, L332/91, 28.12.2000, Brussels.

Web references: The full URL should be given in text as a citation, if no other data are known. If the authors, year, and title of the documents are known and the reference is taken from a website, the URL address has to be mentioned after these data:

The title of the book, journal and conference must be written in Italic, the title of the article, chapter of the book, must be written Regular.

Citation in text

Please ensure that every reference cited in the text is also present in the reference list (and vice versa). Do not cite references in the abstract and conclusions. Unpublished results, personal communications as well as URL addresses are not recommended in the references list.

Making personal quotations (one, at most) should not be allowed, unless the paper proposed to be published is a sequel of the cited paper. Articles in preparation or articles submitted for publication, unpublished, personal communications etc. should not be included in the references list.

Citations style

Text: All citations in the text may be made directly (or parenthetically) and should refer to:

- ***single author:*** the author's name (without initials, unless there is ambiguity) and the year of publication:
  "as previously demonstrated *(Brown, 2010)*".
- ***two authors:*** both authors' names and the year of publication: *(Adam and Brown, 2008; Smith and Hansel, 2006; Stern and Lars, 2009)*
- ***three or more authors:*** first author's name followed by "et al." and the year of publication: "As has recently been shown *(Werner et al., 2005; Kramer et al., 2000)* have recently shown ...."

Citations of groups of references should be listed first alphabetically, then chronologically.

Units, Abbreviations, Acronyms

- Units should be metric, generally SI, and expressed in standard abbreviated form.
- Acronyms may be acceptable, but must be defined at first usage.

Edited by: INMA Bucharest
6 Ion Ionescu de la Brad Blvd., sect. 1, Bucharest, ROMANIA
Tel: +4021.269.32.60; Fax: +4021.269.32.73
http://www.inmateh.eu
e-mail: ***inmatehjournal@gmail.com***